Numerical Simulations of Reactive Extrusion in Twin Screw Extruders

by

Estanislao Ortíz Rodríguez

A thesis
presented to the University of Waterloo
in fulfillment of the
thesis requirement for the degree of
Doctor of Philosophy
in
Chemical Engineering

Waterloo, Ontario, Canada, 2009

I hereby declare that I am the sole author of this thesis. This is a true copy of the thesis, including any required final versions, as accepted by my examiners.

I understand that my thesis may be electronically available to the public.

ABSTRACT

In this work, the peroxide-initiated degradation of polypropylene (PP) in co-rotating intermeshing twin-screw extruders (COITSEs) is analyzed by means of numerical simulations. This reactive extrusion (REX) operation is simulated by implementing (i) a one-dimensional and (ii) a three-dimensional (3D) modeling approach.

In the case of the 1D modeling, a REX mathematical model previously developed and implemented as a computer code is used for the evaluation of two scale-up rules for COITSEs of various sizes. The first scale-up rule which is proposed in this work is based on the concept of thermal time introduced by Nauman (1977), and the second one is based on specific energy consumption (SEC) requirements. The processing parameters used in testing the previously referred to scale-up approaches are the mass throughput, the screw rotating speed, and the peroxide concentration, whereas the extruder screw configuration and the barrel temperature profiles are kept constant. The results for the simulated operating conditions show that when the REX operation is scaled-up under constant thermal time, very good agreement is obtained between the weight-average molecular weight (Mw) and poly-dispersity index (PDI) from the larger extruders and the values of these parameters corresponding to the reference extruder. For the constant SEC approach, on the other hand, more significant variations are observed for both of the aforementioned parameters. In the case of the implemented constant thermal time procedure, a further analysis of the effect of the mass throughput and screw speed of the reference device on the scaled-up operation is performed. It is observed that when the lower mass throughput is implemented for the smaller extruder keeping a constant screw speed, the predicted residence times of extrusion for the larger extruders are lower, in general terms, than

those corresponding to the reference device, and a converse situation occurs for the higher implemented value of the mass throughput. Also, in general terms, the higher increase of the reaction temperature on the scaled-up operation corresponds to the lower mass throughputs and higher screw speeds specified for the reference extruder.

For the 3D modeling approach, two different case studies are analyzed by means of a commercial FEM software package. The REX simulations are performed under the assumption of steady-state conditions using the concept of a moving relative system (MRS). To complement the information obtained from the MRS calculations, simulations for selected conditions (for non-reactive cases) are performed considering the more realistic transient-state (TS) flow conditions. The TS flow conditions are associated to the time periodicity of the flow field inside the conveying elements of COITSEs. In the first case study, the peroxide-initiated degradation of PP is simulated in fully-filled screw elements of two different size COITSEs in order to evaluate scale-up implications of the REX operation. In the second case, the reacting flow is simulated for a conventional conveying screw element and a conveying screw element having a special design and corresponding to the same extruder size. For both of the analyzed cases, the effects of the initial peroxide concentration and mass throughput on the final Mw and PDI of the degraded resin are studied. The effect of the processing conditions is discussed in terms of the residence time distribution (RTD), the temperature of reaction, and the distributive mixing capabilities of the REX system.

When analyzing the scale-up case, it is found that for the implemented processing conditions, the final Mws and PDIs are very close to each other in both of the analyzed flow geometries when the specified flow is close to that corresponding to the maximum conveying capabilities of the screw elements. For more restrictive flow conditions, the final Mws and

PDIs are lower in the case of the screw element of the larger extruder. It is found that the distributive mixing ability of the reactive flow is mainly related to the specified mass throughput and almost independent of the specified peroxide concentration for a particular extruder size. For the analyzed screw elements, the conveying element corresponding to the small size extruder shows a slightly better distributive mixing performance. For this same case study, a further evaluation of the proposed scale-up criterion under constant thermal time confirms the trend of the results observed for the 1D simulations.

In the second case study, the special type of screw element consists of screws rotating at different speeds which have different cross sections. In this case, the outer and inner diameters of both the special and the conventional type of screw elements are specified to be the same. As in the previous case study, the distributive mixing capabilities appear to be independent of the specified peroxide concentrations but dependent on the mass flow rate. It is speculated from the simulation results, from both the transient- as well as the steady-state flow conditions, that the screw element with the special design would yield lower final values of the PDI and Mw. Also, this screw element appears to have improved distributive mixing capabilities as well as a wider RTD.

ACKNOWLEDGMENTS

I would like to acknowledge the Mexican National Council for Science and Technology (CONACYT) for being the primary source of funding for this research study. I am also thankful to the Natural Sciences and Engineering Research Council of Canada (NSERC) for having funded this project in several different ways.

I express my profound gratitude to my supervisor, Prof. Costas Tzoganakis, for his generous support and guidance throughout this research project. I greatly appreciate his insight in the selection and analysis of the case studies addressed in this work.

I am thankful to Dr. David Strutt for his assistance in the implementation of the 1D simulations presented in this work.

I would like to take the opportunity to thank all of my family members, especially my parents, for their continuous love, encouragement, and support during the different steps of my academic journey.

I am grateful to professors and friends at Univesidad Autonoma de San Luis Potosi, in Mexico, who inspired and encouraged me to pursue a PhD degree.

I want to thank all of my colleges in the Polymer Processing Lab as well as my Mexican and International friends. Undoubtedly, your friendship and support have made my stay in the graduate program a very pleasant one.

I would like to thank all the administrative and technical staff at the University of Waterloo for their helpful assistance.

TABLE OF CONTENTS

LIST OF FIGURES

LIST OF TABLES

1 INTRODUCTION AND OBJECTIVES

1.1 Introduction

Reactive extrusion (REX) is a continuous processing operation for the synthesis or modification of polymeric materials. Nowadays, a very common device used in the achievement of such an operation is the closely intermeshing self-wiping co-rotating twin screw extruder (COITSE). The self-wiping action of the extruder screws, which implies that one screw completely wipes its mate during the extrusion process, is a very desirable feature in the processing of materials susceptible to temperature degradation, as it is the case of thermoplastic materials. Another important characteristic of COITSEs is the fact that these machines generally present a modular design. This feature allows attaining different mixing and heating/cooling conditions along the extruder, providing a better control of the REX process.

As in any other engineering operation, it is desirable to rely on mathematical models for dealing with REX operations. However, the description of these operations, especially in COITSEs, is a difficult process due to the coupling of complex mathematical models and due to the complexity of the geometry of the extruder system. Nevertheless, in recent years, using reasonable simplifications, different models referred to as macroscopic or one dimensional (1D) models have been developed. These models yield average values for the variation of process parameters along the axial direction of the extruder, from hopper to die. Also, due to the improvement of computational power, three-dimensional (3D) simulations have been implemented, mainly for the case of non-reactive systems. When compared to 1D models, 3D models provide a more realistic description of the flow system, however, the applicability of such models is restricted to specific flow conditions.

1.2 Objectives

The present research study deals with the description of an important industrial REX process, which is the peroxide-initiated controlled degradation of polypropylene (PP). The extruder system being analyzed is a COITSE. Particularly, the goal of this work is to contribute to a better understanding of this process from an engineering perspective. For such a purpose, 1D as well as 3D computer simulations are implemented. The former simulations are performed with a computer code previously developed in this research group, while the latter is implemented by means of POLYFLOW® which is a computational fluid dynamics (CFD) package based on the finite elements method (FEM). For the 1D simulations, emphasis is given in evaluating two different scale-up rules. The first one of these rules corresponds to the scale-up theory for conventional non-reactive extrusion, and the second one is a scale-up approach proposed in this study. This effort is novel since most development REX work is done on smaller size laboratory extruders. These extruders operate under well controlled isothermal conditions. However, production extruders operate mostly adiabatically due to the low thermal conductivity of polymer melts. For the 3D simulation approach, also scale-up considerations are evaluated, but in this case more specific information, for instance, the mixing abilities of the extruders under different peroxide-feeding protocols and mass throughputs is sought. As an additional contribution of this study, 3D simulations are performed to evaluate the REX process in screw elements corresponding to a fixed extruder size, but in this case two different designs for the screw elements are evaluated. The first one of such screw designs corresponds to that of conventional conveying screw elements. The second design, on the other hand, corresponds to a special design of a variable speed extruder (currently being experimentally studied in this research group) where the speed of rotation of each one of the screws is different.

1.3 Outline of the Dissertation

A summary of the information presented and analyzed in this dissertation is outlined in the following paragraphs.

Chapter 2: A general background on both single- and twin screw extrusion is presented. Relevant aspects discussed regarding the extruders are their flow behavior, the identification of different operating zones, and the description of the main geometrical parameters of the extruder screws. At the end of this chapter, the COITSE which is the type of extruder addressed in this study is presented.

Chapter 3: The REX being analyzed in this work is presented as well as the reaction kinetics model to be implemented followed by a review on extrusion scale-up theory. Considerations regarding the implementation of 1D and 3D models in the simulation of both conventional and REX in COITSEs are addressed. Then, a review is presented of studies on residence time distributions (RTD) and distributive mixing analysis for this same type of extrudes. Also, a brief description of the 1D model implemented for the REX simulations is addressed.

Chapter 4: A numerical scale-up analysis is presented. An in-house previously developed

1D model is implemented for simulating the REX operation being described, for different size extruders. Two scale-up rules are tested in terms of the obtained final values of the weight-average molecular weights (Mws) and the polydispersity indexes (PDIs). The first scale-up rule corresponds to conventional scale-up theory, and it is based on constant specific energy consumption (SEC). The second scale-up approach is proposed in this work, and it takes into consideration the reactive nature of the system. The processing parameters used as independent variables in this case are the mass throughput, the screw rotating speed, and the concentration of the peroxide-feed stream.

Chapter 5: 3D simulations are implemented for describing the REX of interest in screw elements of two different size extruders. The effect of the mass throughput and the peroxide concentration on the final values of the Mws and PDIs of the reacting resin are addressed. From the 3D simulation results, also a complementary analysis of the RTDs and distributive mixing abilities of the different size extruder elements is presented.

Chapter 6: A similar analysis to that of the previous chapter is presented. In this case, however, the size of the extruder is fixed, but two different designs for conveying screw elements of the COITSE are analyzed. The first one of such designs corresponds to that of a conventional double-flighted screw element, whereas the second one corresponds to a variable speed extruder where the speed of the extruder screws is different from each other.

Chapter 7: A summary of the conclusions of this study is presented. Also, some recommendations for future work are addressed.

2 REVIEW ON REACTIVE EXTRUSION OPERATIONS

In this chapter, a general overview of conventional single- and twin screw extrusion is presented. This review is intended to provide the reader with a general background of conventional screw extrusion operations. Such a background is thought to be essential in better understanding the material to be presented in this research work which deals with a particular case of a REX process.

2.1 Single Screw Extrusion

Single screw extruders (SSEs) are the most important type of extruders in the polymer industry. This is due to some of the characteristics exhibited by these machines, as its straightforward design and lower cost (Rauwendaal, 2001). SSEs operate in a continuous fashion and they essentially consist of a rotating Archimedean screw housed in a cylindrical barrel, which may provide a means of heating, or cooling, for the extrusion operation.

2.1.1 The Plasticating Extruder

In the thermoplastic polymers industry, two types of operating modes can be identified in single screw extrusion, depending on the physical state of the material being loaded to the extruder. When the polymer load is in the solid state (solid granules), the operation is referred to as plasticating extrusion, whereas if the polymer is in the molten state the operation is termed melt extrusion. In what follows in this section, an overview of the former operating way will be addressed.

2.1.1.1 General Operating Considerations

In plasticating extrusion achieved in SSEs, three main operating sections can be identified. These operating zones are often referred to as (i) feed, (ii) compression/plastication and (iii) metering zones, and they are indicated in Figure 2.1. In the feed section, the polymer is mainly in the solid state, although some melting can also occur in this zone (Tadmor and Gogos, 1979). In the compression section, the channel depth is gradually reduced, and most of the melting of the polymer occurs in this zone. The reduction of the channel depth within the compression zone provides a means for pressure build-up, and this reduction also represents an improvement in the heat transfer from the extruder walls to the polymer. In general terms, the length of the compression zone depends upon the melting behavior of the polymer being processed. For a gradual melting, as in the case of low density polyethylene, long lengths are used; conversely, for materials exhibiting a sharper melting behavior short lengths are needed, as in the extrusion of nylon. In Figure 2.2, a schematic of the extruder screws corresponding to

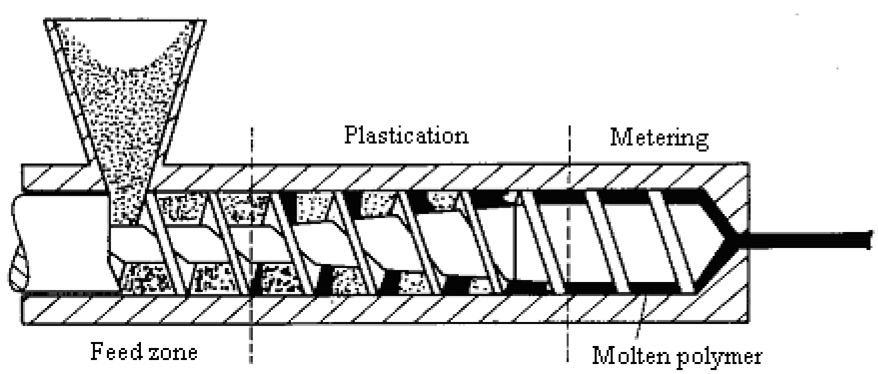

Figure 2-1 Operating zones in a single screw extruder [After Agassant et al., 1991].

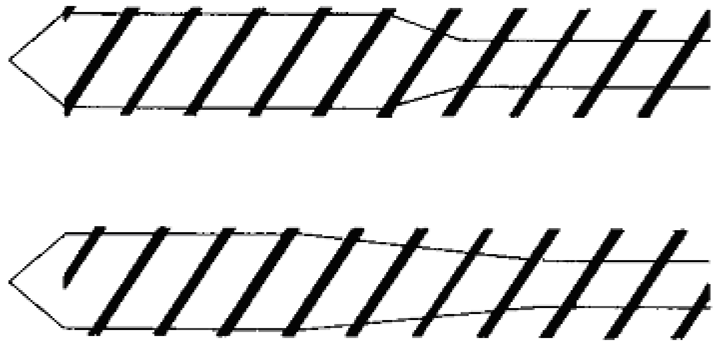

Figure 2-2 Different screw designs in single screw extrusion [After Morton-Jones, 1989].

the previously discussed cases is outlined. Finally, in the metering zone a further homogenization of the molten polymer and its pumping across the extruder die takes place.

The operation of single screw extrusion has been traditionally achieved in a flood-fed mode. In this operating condition, the polymer is loaded to the extruder hopper in such a way that the screw channels in the feed section of the screw are completely filled with the granulated polymer (see Figure 2.3a). Nevertheless, more recently a starve-fed operating condition has also been implemented in this type of machines (Rauwendaal, 2001). In the starve-fed operation mode, metering units are used to load the polymer into the hopper, as it is shown in Figure 2.3b. A drawback in this operating mode is that the effective length of the extruder is reduced, as a consequence of the fact that the starting turns of the screw are only partially-filled. However, the mixing capability of devices operated in this way is superior to that of extruders operating under a flood-fed mode. The latter is due to the fact that pressures developed along the extruder are lower to those corresponding to flood-fed

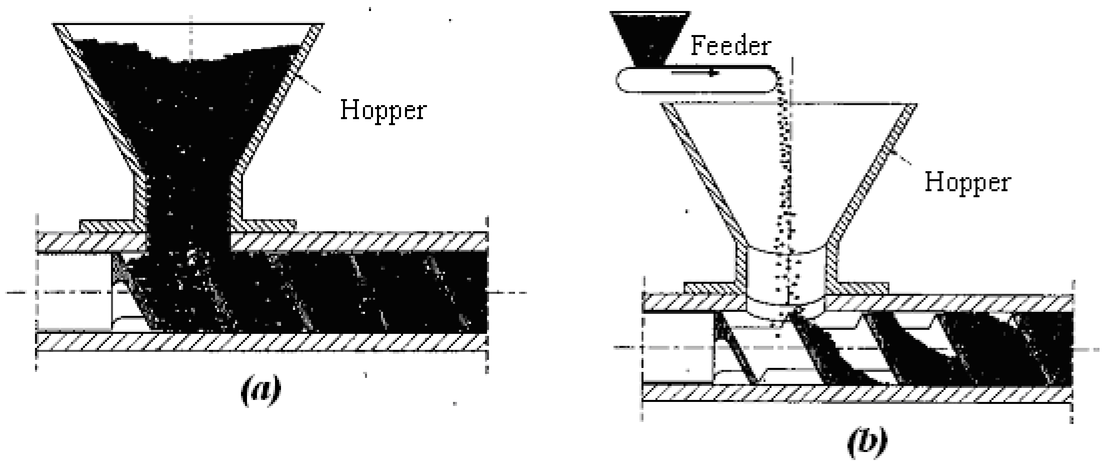

Figure 2-3 Schematics showing (a) flood-fed and (b) starve-fed operating conditions in single screw extruders [After Rauwendaal, 2001].

operation, and hence the agglomeration of material is reduced resulting in a better mixing performance (Rauwendaal, 2001).

2.1.1.2 Screw Geometry

The description of the screw geometry in the case of a SSE can serve two purposes. Firstly, the geometrical parameters are essential information in the models describing the conveying mechanisms taking place within the extruder. Secondly, it facilitates the understanding of the geometry of the screws in other extruder screw systems, as in the case of twin screw extruders which will be discussed later on in this work.

The geometry of a single extruder screw is presented by means of Figure 2.4. In this figure, t stands for the screw pitch, or screw lead, that corresponds to the axial length of a complete turn of the screw thread; ϕ_S is the helix angle; b and H represent the width and height of the screw channel, respectively; e is the flight thickness; D_R, the screw root diameter;

and S_R is the radial flight clearance. One should be reminded, however, that in the case of plasticating extrusion the geometry of the screw is not constant along the whole length of the screw. This is indicated by means of Figure 2.5 where the screw of a plasticating extruder is depicted indicating its different sections.

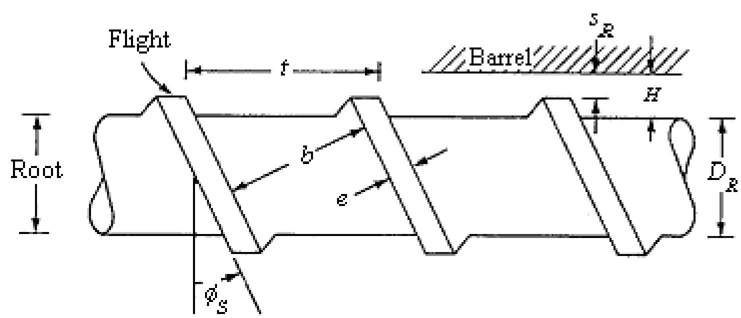

Figure 2-4 Extruder screw geometry of a single screw extruder [After Middleman, 1977].

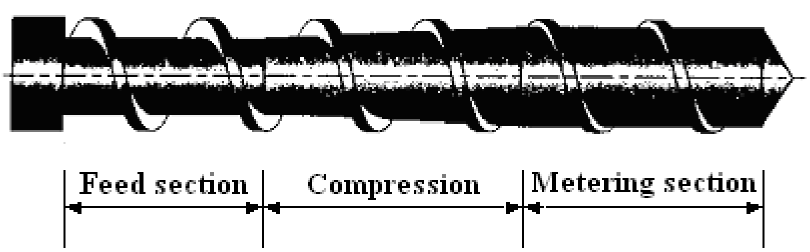

Figure 2-5 Different sections of the extruder screw used in placticating single screw extrusion [After Rauwendaal, 2001].

2.1.1.3 Flow Considerations

For a given screw geometry and screw rotating speed, only one value of throughput can be obtained for a specific die. This value can be determined when the flow rate capacities of the die and the extruder are simultaneously analyzed. The flow rate in both cases is a function of the pressure, and it can be represented by means of a curve known as the “characteristic” curve of the die and the extruder, respectively. In equations 2.1 and 2.2, the corresponding relationships for the flow rate and pressure build-up for both the metering zone and the die (for a cylindrical-shaped die) of the extruder, respectively, are presented.

$$Q = Q_d + Q_p = \frac{1}{2}\pi^2 D^2 NH \sin\phi \cos\phi - \left(\frac{\pi DH^3 \sin^2 \phi P}{12\eta l}\right) \qquad (2.1a)$$

$$Q = \alpha N - \left(\frac{\beta P}{\eta}\right), \text{ or } P = \frac{\eta}{\beta}\left(\alpha N - Q\right) \qquad (2.1b)$$

Where Q stands for the flow rate and the sub-indexes d and p refer to the drag and pressure flows, respectively. D stands for the screw diameter; N is the screw rotating speed; H, the height of the screw channel; ϕ, the helix angle; l, the length of the metering section of the extruder; η, the viscosity of the system; and P is the pressure build-up.

$$Q = \pi \frac{n}{3n+1}\left[\frac{1}{2K}\frac{P}{L}\right] R^{\left(1/n\right)+3} \qquad (2.2a)$$

$$P = \frac{2KL}{R}\left[\frac{Q(3n+1)}{\pi n R^3}\right]^n \qquad (2.2b)$$

In equation 2.2, K and n represent the power-law consistency index and the power-law index, respectively, and R is the radius of the die.

As a means of illustration of the interaction between the extruder and the die flow capacities, in Figure 2.6 the characteristic curves for two different screw geometries, as well as for two different cylindrical dies, for a Newtonian flow system are presented. From this figure, it can be noticed that for the open die the greater value of the throughput corresponds to the screw with the deeper channels. On the other hand, for the restricting die the greater throughput corresponds to the screw with the shallower channels. In the case of a non-Newtonian material, the characteristic curve of the die does not correspond to a straight line, as can be seen in Figure 2.7. In this figure, the characteristic curves for different dies and the curves corresponding to the operation of an extruder under different screw rotating speeds are represented.

An illustrative analysis of the flow occurring in the melt conveying section of the extruder can be achieved assuming an isothermal Newtonian flow. Under these circumstances, the flow field can be considered to be composed of independent down and cross channel contributions, as shown in Figure 2.8. In both of the two cases depicted in this figure, the flow field results from a combination of a pressure and a drag flows. Figure 2.8a also illustrates the influence of the pressure gradient over the down channel velocity profile. Here, an extreme case is that of a very high value of the pressure gradient (maximum flow resistance), where no net flow occurs.

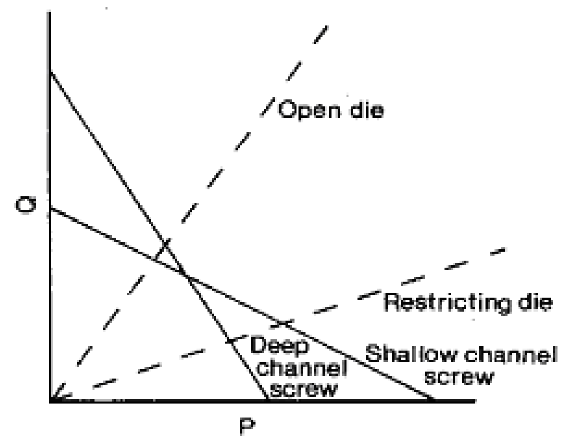

Figure 2-6 Operating conditions for a combination of different extruder screw geometries and dies [After Morton-Jones, 1982].

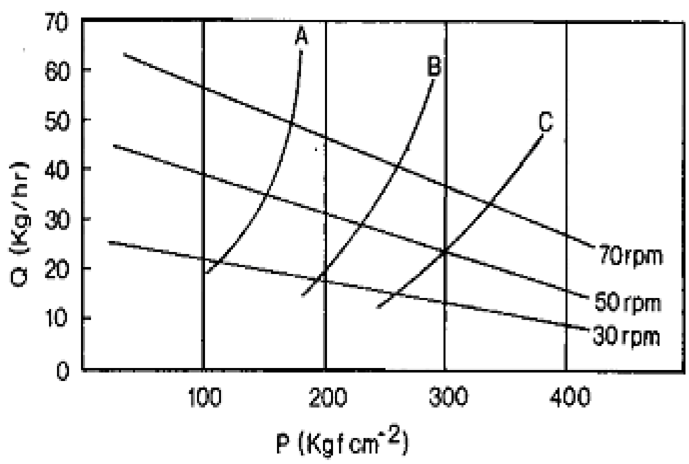

Figure 2-7 Operating conditions for a fixed extruder screw geometry and different screw rotating speeds, and different dies [After Morton-Jones, 1982].

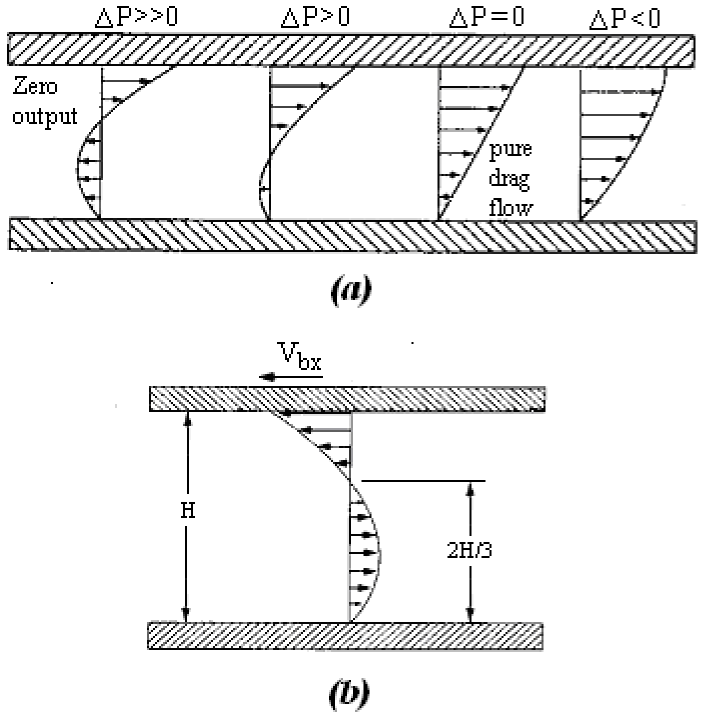

Figure 2-8 (a) Down channel and (b) cross channel velocity profiles for an isothermal Newtonian flow [After Rauwendaal, 2001].

In the preceding analysis, the effect of the transversal component of the velocity has been neglected. However, the actual flow within the extruder is a recirculating one, as shown in Figure 2.9, and such a flow pattern results from the interactions with the flights of the screw. Finally, the actual three-dimensional flow through the screw channel which is of a helical type is illustrated in Figure 2.10.

2.2 Twin Screw Extrusion

Twin screw extrusion is a continuous processing operation in which a material is extruded by means of the action of two Archimedean screws. The generic term for the devices achieving such an operation is “twin screw extruders”. When referring to twin screw

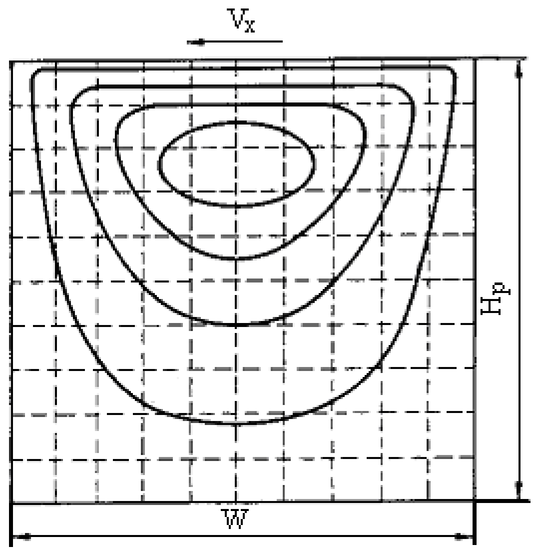

Figure 2-9 Recirculating flow in the melt conveying region of the SSE extruder [After Agassant et al., 1991].

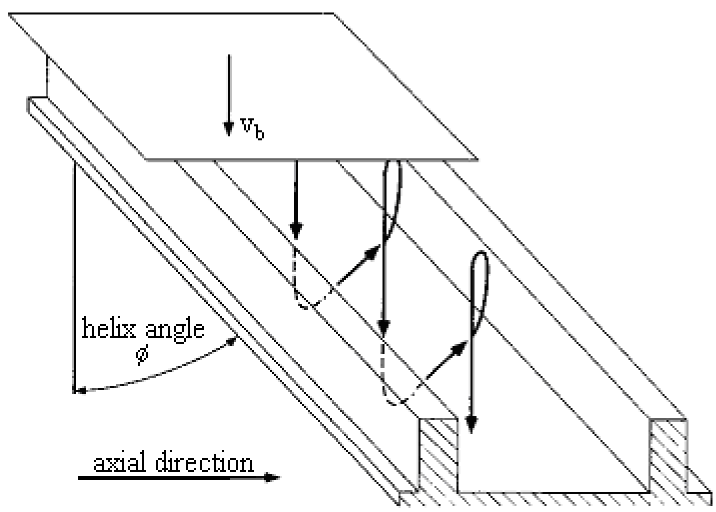

Figure 2-10 Illustration of the 3D flow within the screw channels [After Rauwendaal, 2001].

extruders one not only deals with a specific machine but rather with a variety of processing devices possessing different design characteristics. This fact, which will be discussed later, justifies in part the use of this type of extrusion in different polymer processing applications such as compounding, profile extrusion as well as reactive extrusion (Rauwendaal, 2001).

It is important to say that a lot of similarities arise between twin screw extrusion and the well known process of single screw extrusion. In this context, the operation of twin screw extrusion may be, in a very general way, divided in three main operating zones, that is, a feed zone, a main conveying zone, and a pumping zone. Figure 2.11 corresponds to a schematic of an extruder showing these different operating zones. The operating conditions and functional characteristics, e.g., pressure build-up and temperature, do vary from zone to zone and also along the whole axial length of the extruder.

2.2.1 Classification of Twin Screw Extruders

As previously stated, there is a variety of twin screw extrusion machinery exhibiting different mechanical designs (which makes a specific extruder suitable for a particular processing operation). Accordingly, these devices can be classified considering (a) the direction of rotation of the screws and (b) the contact between them. As a result of these classifications, different categories of twin screw extruders are obtained as indicated in Figure 2.12.

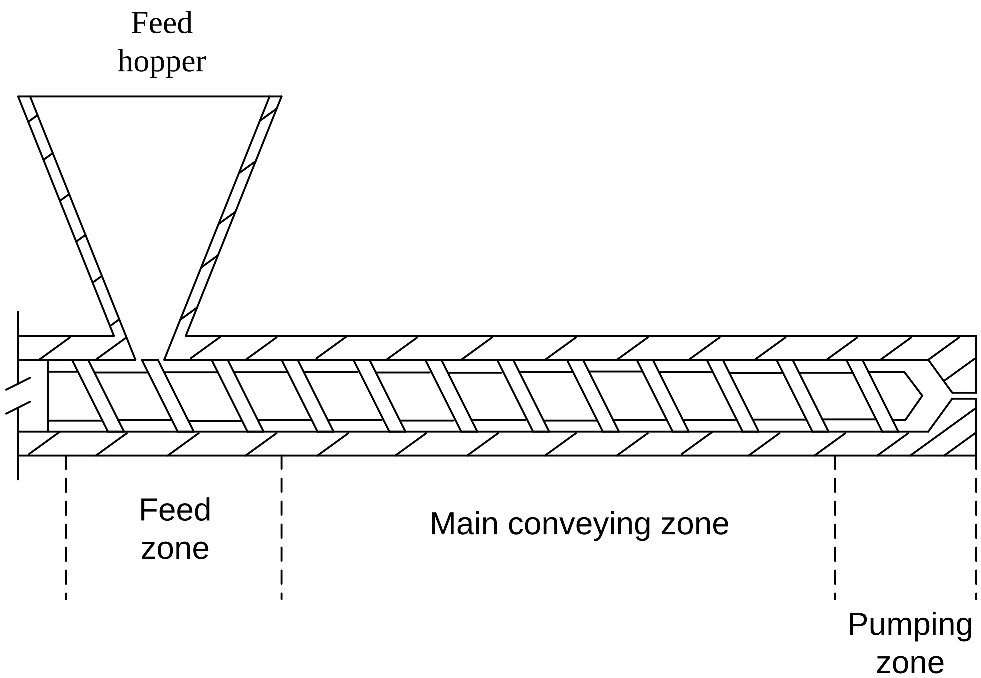

Figure 2-11 Identification of different operation zones in a twin screw extruder.

2.2.2 Closely Intermeshing Self-Wiping Co-rotating Twin Screw Extruder (COITSE)

COITSEs are a special type of the fully-intermeshing twin screw extruders previously described (see Figure 2.12). The screws of these devices feature a special screw root self-wiping profile as shown in Figure 2.13.

2.2.2.1 General Operating Considerations

The already addressed special design in a COITSE provides the screw system with a self-cleaning effect, due to the fact that the screws wipe each other during the extrusion operation. This self-wiping action is especially relevant when stagnation and accumulation leads to undesirable side effects, such as the degradation of the material being processed. The

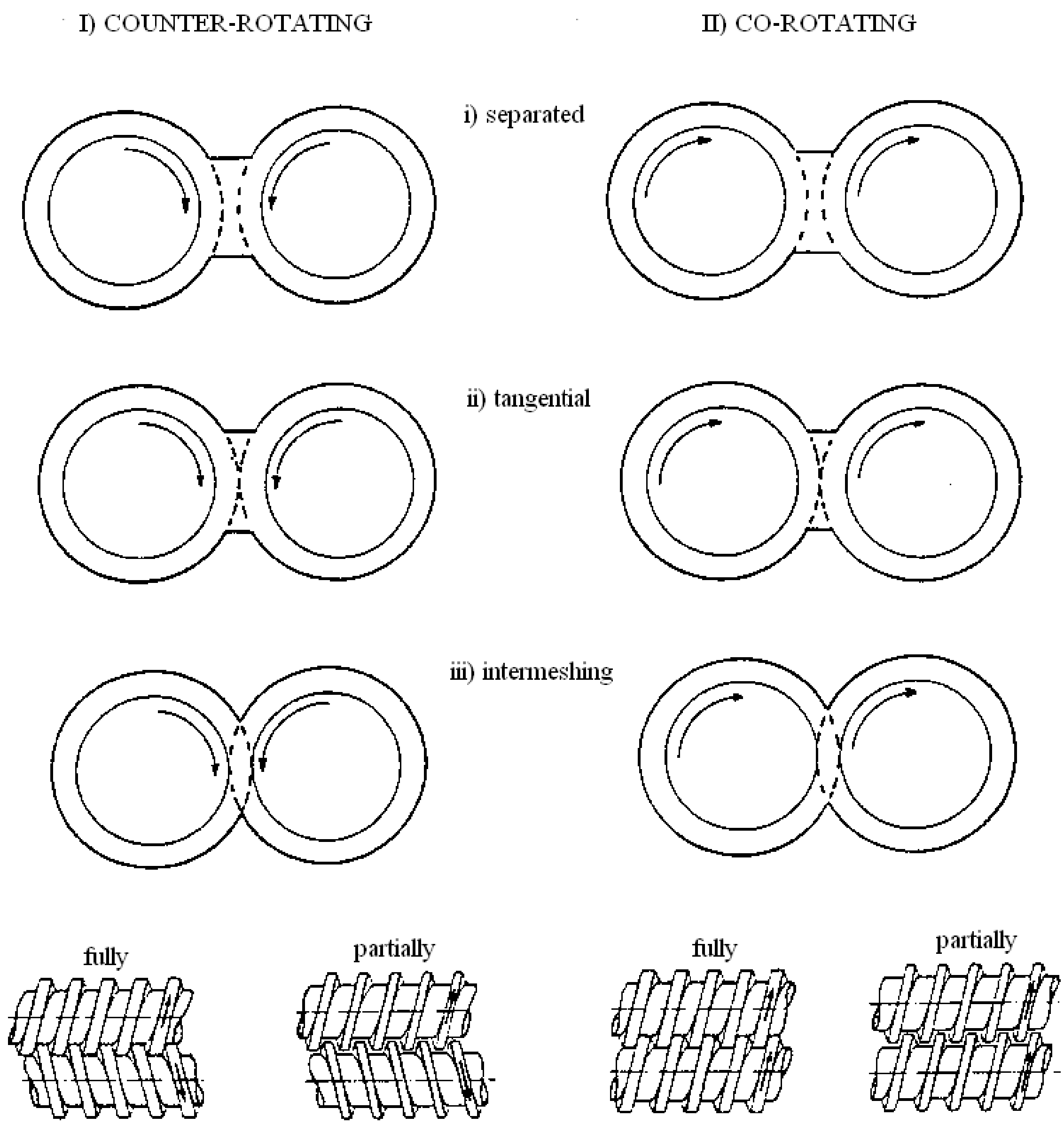

Figure 2-12 Classification of twin screw extrusion machinery considering the direction of rotation and contact between the screws [After White, 1991].

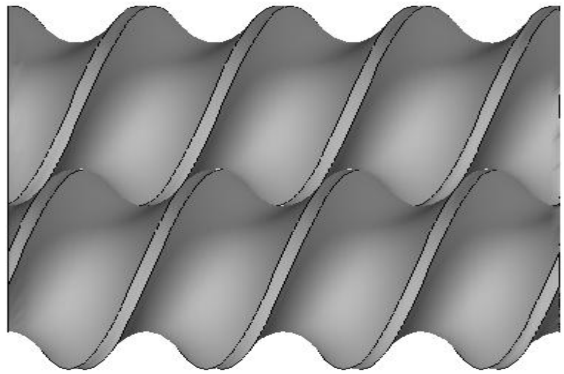

Figure 2-13 Screws assembly in a COITSE showing their special screw root profile.

latter may occur in polymer processing as well as in food processing operations. Some applications of the COITSE, in the polymer industry, are in the areas of polymer compounding, devolatilization, and reactive extrusion (Rauwendaal, 2001). In many applications, this type of extruder presents a modular design. In these cases, the configuration of the screw along the screw shaft is not uniform but may consist of different types of screw and mixing elements. Depending upon whether their pumping effects are forward or backward, screw elements are referred to as right- or left-handed screw elements, respectively. On the other hand, mixing elements consisting of blocks of kneading discs can also induce forward and backward pumping effects. Although kneading blocks are not the only mixing elements available for COITSEs, their use is very extended and these are the only elements to be considered in this work.

The feed hopper, in many instances, may provide a throughput that not necessarily matches the conveying capacity of the extruder (the machine is fed with metering units). Therefore, COITSEs generally operate in a starve-fed mode. The phenomena occurring in the main conveying zone depend upon the load being fed to the extruder. In the case of plasticating extrusion, the polymer, firstly in the solid state, is gradually melted while being transported along this zone. Finally, the pumping zone of the extruder must be fully-filled to allow the molten polymer to be pumped across the extruder die.

2.2.2.2 Conveying and Kneading Block Elements

The geometrical parameters described in Figure 2.4, for the case of a single extruder screw, are also useful to describe the geometry of the conveying elements (screw elements) in a COITSE. Nevertheless, it should be noted that in the latter case both the width and the screw channel height are not constant as in the case of Figure 2.4. Another important consideration when dealing with the screw geometry is the fact that in general terms the screws are multi-flighted (White, 1991). That is, the material within the extruder is transported along two or more parallel flights. In Figure 2.14, the corresponding cross sections for single-, double- and triple-flighted screw elements (also known as monolobal, bilobal and trilobal conveying elements) is illustrated. Finally, besides the radial flight clearance also a flight gap between the top of the flight of one screw and the root of its mate may be present for practical engineering reasons (Potente et al., 1994).

In the case of the COITSE, a precise description of the screw geometry was presented by means of kinematics considerations in a work by Booy (Booy, 1978). According to Booy, the cross section of a twin screw in a COITSE is determined from the diameter, centerline distance, and number of tips (number of parallel flights) of the screws, and when both screws rotate at the same speed their cross sections are identical. In Figure 2.15, the geometrical parameters describing the cross section of a double-flighted system of screws is presented. Equations 2.3 and 2.4 indicate the relationship between such parameters.

$$\alpha_i = \frac{\pi}{2n} - \frac{\alpha_t}{2} \tag{2.3}$$

$$C_L = D_S \cos(\alpha_i) \tag{2.4}$$

Here, C_L represents the center line distance; D_S is the external screw diameter; and n is the number of tips. α_i and α_t, which are angles in a plane perpendicular to the screw axis, stand for the intermeshing and tip angle, respectively.

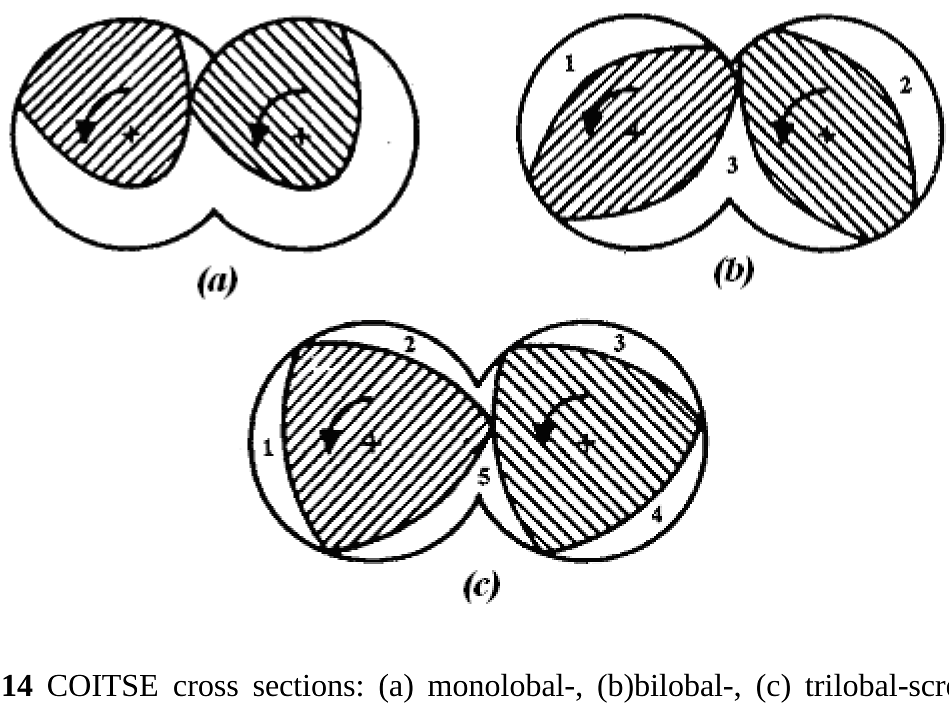

Figure 2-14 COITSE cross sections: (a) monolobal-, (b)bilobal-, (c) trilobal-screws [After Dreiblatt and Eise, 1991].

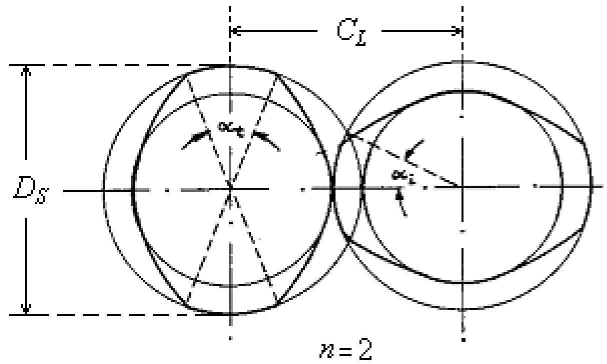

Figure 2-15 Cross section for a double-flighted COITSE system [After Booy, 1978].

The flow occurring in the conveying elements of a COITSE follows a characteristic "figure-eight" pattern, as shown in Figure 2.16. This is a consequence of the relative motion of the screws and of the tight intermeshing between them. The aforementioned flow pattern provides a means for the interchange of material from one screw to the other, and it is related to a good mixing efficiency presented by the conveying elements of this type of devices (Morton-Jones, 1989). In the case of bilobal screw elements, this characteristic fluid motion is reflected as the transport of the material along three independent flow channels, each one comprising both of the two screws, as indicated in Figure 2.17.

At this point, we address the already mentioned mixing elements, i.e., kneading blocks. These elements consist of an arrangement of individual kneading discs staggered at an angle from one to the other, as illustrated in Figure 2.18. Kneading blocks can have a forward or reverse staggering which results in positive or negative pressurization capacities, respectively. Neutral staggering results from a stagger angle of 90°. Kneading blocks generally operate in a fully-filled mode, and they possess very suitable mixing capabilities. In fact, most of the

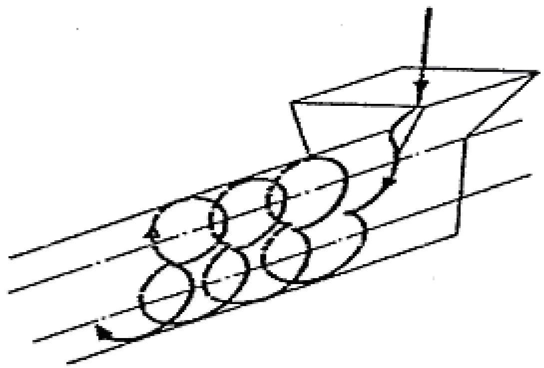

Figure 2-16 Characteristic “figure eight” flow pattern in a twin screw extruder [After Erdmenger, 1964].

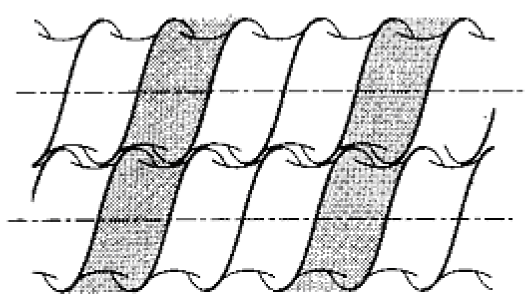

Figure 2-17 Flow pattern in the screw elements of a COITSE extruder [After Rauwendaal, 2001].

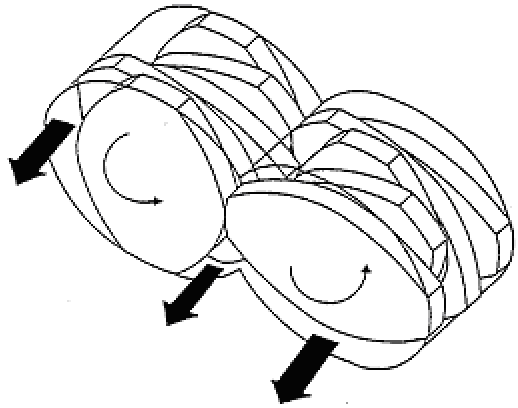

Figure 2-18 Kneading discs arrangement for a kneading block with a stager angle of 45° [After Yang and Manas-Zloczower, 1992].

melting occurring in an extruder takes place in these elements, due to their already mentioned mixing features. The cross section of the discs corresponds to that of a screw conveying element with the same tip angle (see Figure 2.15). The fully-filled conditions in a kneading block element are obtained by the action of a reverse conveying screw element, located downstream of the former element.

3 LITERATURE REVIEW

3.1 Reactive Extrusion (REX)

Reactive extrusion (REX) is a continuous process for the synthesis or modification of polymeric materials. In this process, two different engineering operations, which are polymer reaction engineering and polymer extrusion, are brought together into a single and unique operation.

3.1.1 Overview of the Reactive Extrusion Process

In reactive extrusion, an extruder is used as a chemical reactor to perform different kinds of polymerization or polymer modification reactions. Particularly, COITSEs are the most widely used devices in the performance of this type of reactions due to some of their operating characteristics, such as modular configuration and excellent mixing capacity (Sherrington, 1985; Tzoganakis, 1989). The latter mentioned feature allows reactions of polymers of high viscosity to be performed in this type of devices, and as a result the use of solvents is avoided. In fact, this represents one of the major advantages of REX over those conventional polymerization reactions where the use of a solvent is needed to achieve the reaction. Regarding its modular configuration, most extruders possess a segmented barrel whose sections can be individually heated or cooled. Also, by varying the type or design specifications of the elements present in each screw section different degrees of mixing can be attained along the screw. Due to these facts, an extruder can be transformed in a chemical reactor with controlled reaction zones (Sherrington, 1985).

In REX, the polymers are mainly fed into the extruder through the feed hopper. After this step, however, different reacting agents may also be added via injection ports specifically located along the extruder barrel. Also, any volatile byproducts can be eliminated through ventilation ports located towards the end of the extruder. Finally, the reacted polymer is extruded and processed in a very conventional way. Typical operating conditions for reactive extrusion operations are 70-500 °C, with a temperature differential between adjacent segments <100°C; residence times around 10-600 s; and pressure ranges of about 0-50 MPa (Sherrington, 1985). Also, it is important to note that for an optimum operation the extruder to be used as a chemical reactor must be designed having the knowledge of the specific reaction to be achieved.

3.1.2 Reactions Performed in Extruders

The range of applicability of REX processes is rather extended, starting from basic synthesis reactions (both step-growth and chain polymerization) all the way to polymer modification as well as copolymer formation reactions. In Table 3.1 a classification of reactions that have been carried out in extruders is presented. A summary of specific reactions detailed at some extent can be found in the literature (Sherrington, 1985; Brown, 1992).

3.2 Controlled Degradation of Polypropylene

Polypropylene resins produced industrially by conventional Ziegler-Natta polymerization reactions possess high weight-average molecular weights (Mws) and broad molecular weight distributions (MWDs). The rheological behavior exhibited by these materials limits their applicability in certain thermoplastic applications. To modify this behavior, these resins are

Table 3-1 Chemical Reactions Performed in Reaction Extruders [After Brown, 1992].

Type	Description
Bulk Polymerization	Preparation of high molecular weight polymer from monomer or low molecular weight prepolymer, or from a mixture of monomers or monomers and prepolymers.
Graft Reactions	Formation of grafted polymer or copolymer from reactions of polymers and monomers.
Interchain Polymer Formation	Reaction of two or more polymers to form random, graft, or block copolymer either through ionic or covalent bonds
Coupling/Crosslinking Reactions	Reaction of polymer with polyfunctional coupling or branching agent to build molecular weight by chain extension or branching, *or* reaction of polymer with condensing agent to build molecular weight by chain extension , or reaction of polymer with crosslinking agent to build melt viscosity by crosslinking
Controlled Degradation	Controlled molecular weight degradation of high molecular weight polymer (controlled rheology), or controlled degradation to monomer.
Functionalization/ Functional Group Modification	Introduction of functional groups into polymer backbone, endgroup, or sidechain, or modification of existing functional groups.

further subjected to a REX process. In this process, controlled molecular weight degradation is achieved to obtain materials with improved processing characteristics. The obtained materials, referred to as controlled-rheology polypropylenes (CRPPs), have reduced viscosity and elasticity and can be processed at lower melt processing temperatures. Some of their processing improvements include higher speeds in melt spinning of very thin fibers, extrusion of thin films and thin walled injection molded articles (Xanthos, 1992).

The basic reaction mechanisms involved in the REX degradation of PP can be described as follows. Firstly, the reaction is initiated by the action of very reactive peroxide free radicals. These radicals attack the polymer chains abstracting hydrogen preferentially from tertiary carbon atoms. Subsequently, a β-scission occurs in the previously formed polymer radical producing shorter polymer chains. Finally, the generated polymer undergoes a termination reaction. In Figure 3.1, a simplified reaction scheme for this reaction is outlined.

3.2.1 Modeling of the Peroxide-Initiated Degradation of PP

Along the years, several mathematical models have been proposed to describe the reaction kinetics of the peroxide-mediated degradation of PP. Among such models, one can refer for instance to those presented by Suwanda et al. (1988), Tzoganakis et al. (1988), Triacca et al. (1993), and Oliveira et al. (2003). In the derivation of these models, two distinctive features can be noted. Firstly, the moments technique is often applied to the kinetic mechanisms derived from the mass balance equations (Tzoganakis et al., 1988; Triacca et al., 1993). Secondly, the steady state assumption for the peroxide radicals is implemented to further simplify the obtained set of mass balance equations, whether or not the moments technique

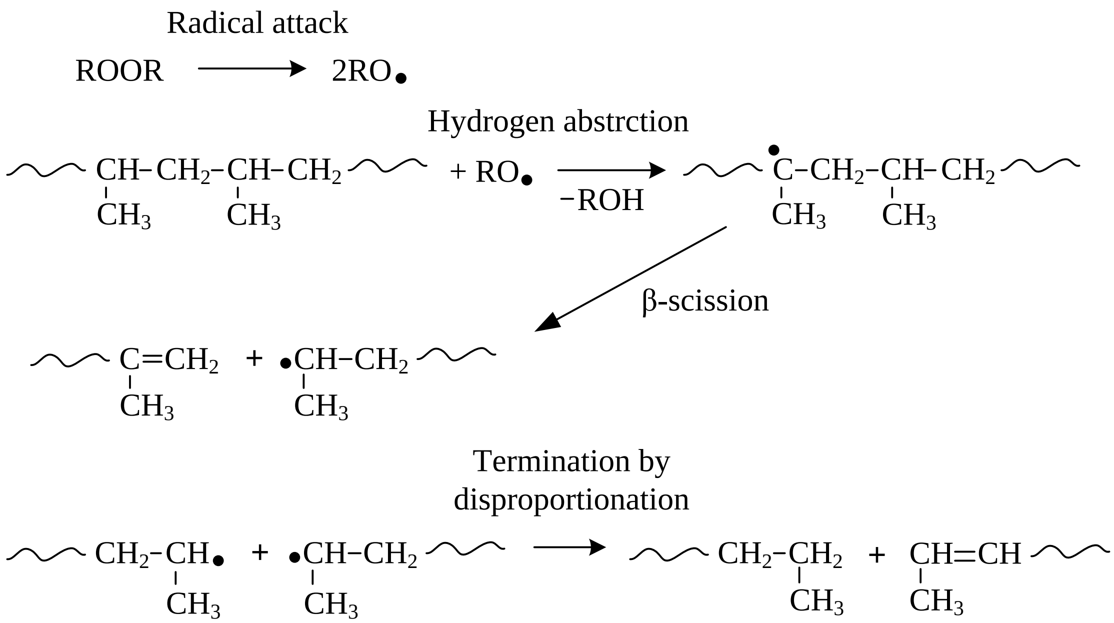

Figure 3-1 Basic mechanisms involved in the chemical degradation of PP [After Xanthos, 1992].

has been previously implemented. In the following paragraphs, a brief description of these models as well as some of the assumptions used in their derivation will be provided. The organic peroxide used in the works to be addressed is the 2,5-dimethyl-2,5-bis(t-butylperoxy)hexane.

The model proposed by Suwanda et al. (1988) considers that the dominant reactions occurring during the peroxide-initiated degradation of PP are the following ones: (1) initiation (one-step radical decomposition), (2) chain scission, and (3) termination by disproportionation. In the work presented by these researchers, the reaction was performed in a SSE. Relevant experimental conditions in their work were constant screw speed equal to 44 rpm; operating temperatures of 200 and 220 ^{o}C; and the peroxide concentrations varied from 0 to 0.04 wt %.

The model presented by Suwanda et al. (1988) predicts the variation of the MWD during the reaction starting from the MWD of the unreacted polymer. For the calculations, only the peroxide efficiency needs to be known in advance. The final kinetic expressions are presented by means of the set of equations 3.1 - 3.5. Because of its simplicity, this model has been used in studies dealing with the degradation of PP either in COITSEs or batch operation devices (Dickson et al., 1997; Alaugner et al., 2000).

$$[P_n]_2 = -\frac{\lambda_3}{\lambda_2} + \frac{(\lambda_2 [P_n]_1 + \lambda_3)}{\lambda_2}\left(\exp \lambda_1 \lambda_2 (t_2 - t_1)\right) \quad (3.1)$$

$$\lambda_1 = \frac{2 f_p k_D [I] m_0}{\rho} \quad (3.2)$$

$$\lambda_2 = 1 - n \quad (3.3)$$

$$\lambda_3 = 2 \sum_{r=n+1}^{\infty} [P_r] \quad (3.4)$$

$$[I] = [I]_0 \exp - (k_D t) \quad (3.5)$$

In equations 3.1-3.5, $[P_n]_1$ and $[P_n]_2$ stand for the concentrations of polymer molecules with chain length n at times t_1 and t_2, respectively. $[I]$ and $[I]_0$ represent the peroxide concentrations at time t and time 0, respectively; f_P and k_D are the peroxide decomposition efficiency and rate constant, respectively; m_0, the monomer molecular weight; and ρ is the polymer density.

In the model proposed by Tzoganakis et al. (1988 a), the following steps of the reaction mechanisms are considered: (1) initiation, (2) chain scission, (3) polymer chain transfer, (4) thermal degradation, and (5) termination by disproportionation. With these considerations, a set of equations in terms of the moments of the polymer and polymer radicals chain distributions was derived. From this point, a further simplification was made by considering that only steps 1, 2, and 5 are present in the overall reaction mechanism (Tzoganakis, et al. 1988 a). The final expressions proposed by these authors are presented here by means of equations 3.6 and 3.7. It can be noticed that from the information yielded by these equations the characteristic molecular weights of the polymer can be calculated, as indicated by means of equation 3.8.

$$\begin{aligned}
\frac{dI}{dt} &= -k_D I \\
\frac{dQ_0}{dt} &= 2 f_p k_D I \, \frac{Q_1 - 3Q_0}{Q_1 - Q_0} \\
\frac{dQ_1}{dt} &= -2 f_p k_D I \, \frac{2Q_0}{Q_1 - Q_0} \\
\frac{dQ_2}{dt} &= 2 f_p k_D I \, \frac{-(Q_3/3) + (Q_1/3) - 2Q_0}{Q_1 - Q_0}
\end{aligned} \tag{3.6}$$

$$Q_3 = \frac{2Q_2}{Q_1 Q_0}\left(2Q_2 Q_0 - Q_1^{\,2}\right) \tag{3.7}$$

$$\begin{aligned}
\bar{M}_n &= m_0 \left(Q_1 / Q_0\right) \\
\bar{M}_w &= m_0 \left(Q_2 / Q_1\right) \\
\bar{M}_z &= m_0 \left(Q_3 / Q_2\right)
\end{aligned} \tag{3.8}$$

In equations 3.6-3.8, I represents the peroxide concentration; f_p and k_D, are the peroxide decomposition efficiency and rate constant of decomposition, respectively. t represents time; and Q_i is the *ith* moment of the molecular weight distribution. M_n, M_w and M_z stand for the number-, weight- and z-average molecular weights, respectively; and m_0 is the monomer molecular weight.

The rheokinetic parameters in the model proposed by Tzoganakis et al. (1988 a) were determined from ampoule experiments and predictions of the model were tested from samples degraded in a SSE. Operating conditions in this case were screw speed 20 – 60 rpm; peroxide concentration 200 – 400 ppm; and an average barrel temperature of 207 ^oC. No mechanical or thermal degradation were observed by the authors. A similar result regarding the thermal degradation was reported in the case of the model presented by Suwanda et al. (1988), as can be seen in Balke et al. (1988). The proposed model has been implemented in numerical calculations of the REX of PP in both SSE and COITSEs (Tzoganakis et al., 1988 b; Strutt, 1998; Strutt et al., 2000; Vergnes and Berzin, 2004).

Triacca et al. (1993) presented a more complete analysis of the mechanisms taking place in the peroxide-initiated degradation of PP regarding the mechanisms involved in the reaction. An important difference of this model with respect to previous ones is the fact that it assumes that structural units possess equal reactivity regardless of their location on the polymer chain. Under this consideration, the overall reaction mechanism occurs under random chain scission. The proposed model, which has to be solved numerically, predicts the MWD in terms of the degree of chain scission, u**(** u being the fraction of broken C—C bonds). In the work by Triacca et al. (1993), the degradation experiments were carried out in a differential scanning calorimeter set-up. The results of this model were compared with previously reported results. Some of such results were from the works by Tzoganakis (1988) and Suwanda et al. (1988).

Using a very interesting approach, Oliveira et al. (2003) proposed an analytical solution for the variation of the MWD of the degraded PP during the REX process. In this work, the authors performed a mathematical analysis using the kinetic mechanisms reported by Suwanda et al. (1988), Tzoganakis et al. (1988 a), and Triacca et al. (1993). A parameter defined as the degree of degradation was introduced in this study. When this parameter was used as the independent variable, the same set of differential equations was obtained for each one of the analyzed models. This, according to the authors, means that it is not possible to discriminate among the proposed kinetic mechanisms based on molecular weight data only. The proposed model was tested with previously reported experimental results, and the predictions showed good agreement with the results used for comparison.

3.2.2 Operating Considerations in the REX of Polypropylene

Regarding some operating considerations for this REX operation, it can be said that this process resembles that of plasticating extrusion, in the sense that the polymer is fed to the extruder in the solid state. Especially in lab-scale experiments, the peroxide injection port is located at an axial length where the polymer has already been melted (Strutt at. al. 1998; Vergnes and Berzin 2004), although industrially the peroxide may also be added into the feed hopper. Because the configuration of the extruder plays a very important role in both the average residence time and RTD of the reacting PP, a proper configuration must be determined in order to obtain the target values of Mws and PDIs. Important components in the configuration of the extruder are kneading blocks which, due to their already addressed mixing capabilities, are used to disperse and homogenize the peroxide added into the flow system. Finally, towards the end of the extruder, when the prefixed degradation has been achieved, some ventilation port may be also needed to remove any volatile byproducts.

3.3 Modeling of Reactive Extrusion

Mathematical modeling of a REX process involves the simultaneous consideration of momentum, energy and mass balances, along with the kinetics of the reactions involved. There exists interdependency between the mechanisms described by the aforementioned equations. For instance, when mechanical energy is transmitted to the polymer, this energy is transformed into thermal energy via viscous dissipation which affects both the flow behavior and the progression of the reaction. Also, with the progression of the reaction, the rheology of the system is affected. In Figure 3.2, a classification of the mechanisms involved in a REX process is presented. In the rest of this section, two different approaches in the modeling of REX will be addressed.

3.3.1 Macroscopic (1D) Models

Macroscopic models are simplified models intended to yield a reasonable description of the REX process from hopper to die. These models are also described as 1D models, because the process variables are considered to vary only along the axial direction of the extruder. A very important simplification in a macroscopic modeling approach is the applicability of the principle of the "lubrication approximation". Under this consideration, the velocity field within the screw channels is simplified as a two dimensional (2D) field similar to that occurring between flat plates where the velocity component perpendicular to the surface of a

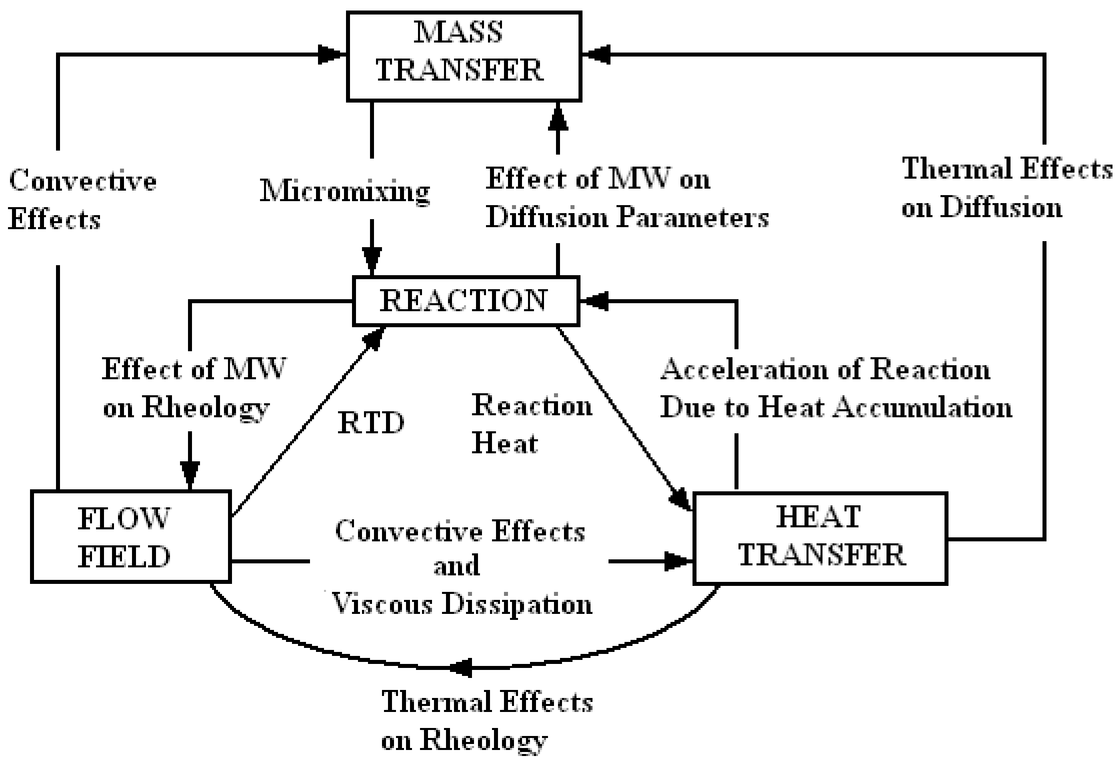

Figure 3-2 Mechanisms present in a reactive extrusion operation and their interaction [After Lindt, 1984].

reference plate is neglected. The lubrication approximation is a more general principle used in different polymer processing and other type of mechanical operations. To illustrate this principle, consider the hypothetical flow geometry outlined by means of Figure 3.3. Under the lubrication approximation approach, the local flow at any point of this flow geometry can be approximated by a fully developed flow, where the local gap represents the separation of the hypothetical parallel plates (Lee and Castro, 1989).

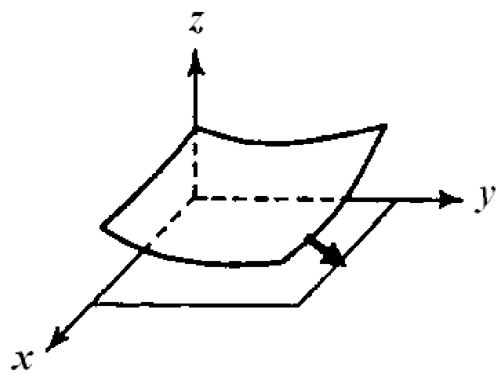

Figure 3-3 Hypothetical flow geometry for describing the lubrication approximation.

Another simplification implemented in the modeling of the flow in COITSEs is to represent the flow geometry as that obtained by unwinding the screws and the extruder barrel. This way, a grooved model is obtained as depicted in Figure 3.4a. In the case of a double-flighted geometry, three independent flow channels are obtained as indicated in this figure (Michaeli, 1995; Rauwendaal, 2001). Another approach in the simplification of the flow through the screw channels is to represent the channel, except for the intermeshing region, as a succession of “c-shaped” chambers (see Figure 3.4b). In both of the former models, the screws are considered to be motionless while the extruder barrel slides on top of the screw channels (kinematic reversal approach).

In the preceding discussion, very general considerations regarding the simplifications taken into account in the modeling of the flow in COITSEs have been discussed. In actual modeling, however, other important number of considerations and assumptions need to be made for the description of the physical and chemical phenomena taking place within the extruder system. During recent years, different global models dealing with conventional

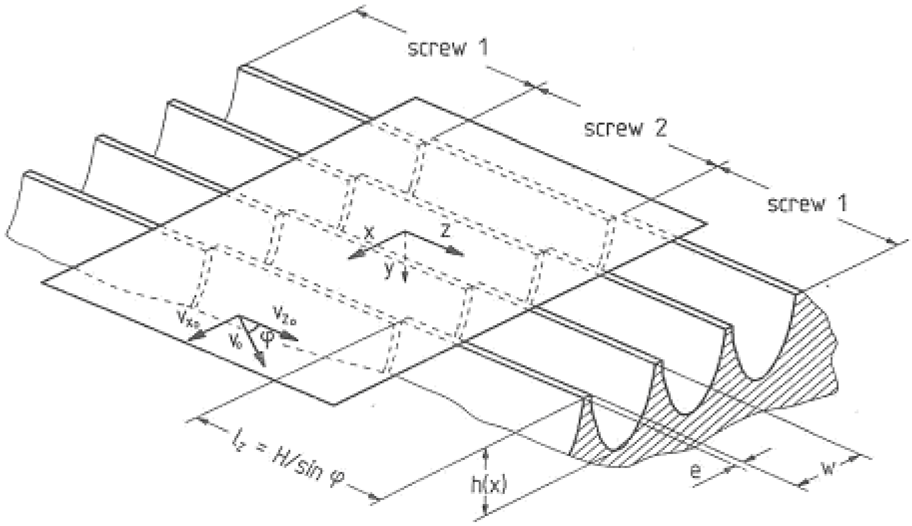

(a)

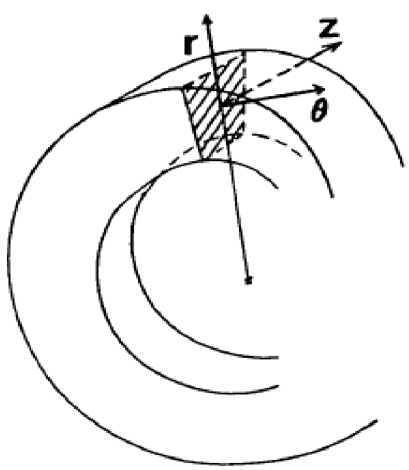

(b)

Figure 3-4 Simplified geometries used for the modeling of the flow in the screw elements of a COITSE. (a) Description with parallel channels [After Michaeli and Greffestein, 1995]. (b) Description with "c-shaped elements" [After Vergnes et al., 1998].

extrusion and REX in COITSEs have been published in the open literature (Meijer and Elemans, 1988; Chen and White, 1991; Potente et al., 1994; Michaeli et al., 1995; Vergnes et al., 1998; Zagal et al., 2005). In some cases, these models have been developed in the form of commercial computer software (Markarian, 2005). In the following paragraphs, some general remarks concerning published models will be made.

One of the first works to address with an integral approach the modeling of the flow phenomena within the melt section of COITSEs was presented by Meijer and Elemans (1988). In this study, an extension of equations developed for SSE was implemented for describing the flow in the COITSE. This was justified by the authors in terms of the similitude of the flow in these two types of extruders. In this work, several scenarios both hypothetical and real ones were analyzed, including the comparison of the predicted fully-filled length along the axial direction of the screws to that observed in an extruder with transparent plastic walls.

In 1990, Chen and White presented a study on the modeling of a COITSE. In this case, a non-Newtonian isothermal flow model was used to simulate the flow of the molten polymer in the extruder. The calculations presented by these researchers were focused on the determination of the screw characteristic curves of double- and tripled-flighted screw elements. An extension of this model was used later on (White and Chen, 1994) to deal with the description of the non-isothermal flow in the same type of extruders, with special emphasis in scale-up considerations.

Potente et al. (1994) published a macroscopic model which, in contrast with most of the published models, included the description of the plasticating zone of the COITSE. On the basis of this model, Strutt et al. (1997, 1998) developed a model for the controlled degradation of PP which was validated with experimental data from a previous work by Wang (1996). The chemical kinetics in this case were based on the model proposed by Tzoganakis et al. (1988 a).

A very complete study on the modeling of REX in COITSEs was presented by Michaeli et al. (1995). In this work, supported with experimental residence time distributions (RTDs), these researchers analyzed the effects, over the length of the polymerization zone, of modeling polymerization reactions with a cascade of: (i) continuous stirred tank reactors (CSTRs) and (ii) plug flow reactors. It was concluded by the authors that the implementation of a cascade of CSTRs in the global model yielded better results, especially for high degrees of mixing. Predictions of this model were compared with experimental data for different reactions like anionic bulk polymerization of nylon and polystyrene (Michaeli et al. 1995; Michaeli and Grefenstein, 1995).

An interesting approach in the modeling of extrusion in COITSEs was presented by Vergnes et al. (1998). In this work, the screw geometry was approximated by means of "c-shaped" chambers (in contrast with the previous discussed models where the grooved model was used, see Figure 3.4). This approach seems to be a good simplification in the calculation procedure. In this model, in which the plasticating zone was omitted, as in that one by Michaeli et al. (1995), the process is modeled after the first restrictive flow element where the material is assumed to be fully melted. An extension of this model has been used by the group of Vergnes in the description of several REX systems (Vergnes et al., 1998; Vergnes and Berzin, 2004; Berzin et al., 2006).

More recently, based on the work by Vergnes et al. (1998), Zagal et al. (2005) proposed a REX model for the description of the polymerization reaction of methyl methacrylate (MMA). In this model, the reaction was modeled by a series of CSTRs. The validation of the model was achieved with experimental data from Balke and Hamielec (1973). However, such a validation was to some extent limited because only one operating condition was analyzed. Also, as stated by the authors, the experimental reaction kinetic constants used in the model were obtained at temperatures below the usual temperatures of this REX system.

3.3.1.1 Outline of the 1D Model to be Implemented

The 1D model to be implemented in this work is the one developed by Strutt (1997, 1998). This model describes the REX operation under steady-state conditions in a COITSE, and it is comprised of different individual models describing different physical and chemical phenomena occurring in the COITSE. In what follows, a summary of the modeling approach implemented for the present 1D REX model is briefly outlined.

(a) Solids melting: The resin pellets are assumed to be spheres of equal radius. The size of the pellets is then reduced as melting take place.

(b) Melt conveying and pressurization: The flow in the screw elements is described by means of the lubrication approximation. The melt pumping capacity of the screw elements is dealt with by means of algebraic equations that approximate families of screw characteristic curves. Some considerations are made in order to approximate the flow behavior of the kneading discs to that of conveying screw elements. For both kneading blocks and screw elements, the leakage flows are taken into account.

(c) Material distribution in the extruder channels: An evaluation is made of whether an element is fully- or partially-filled. In the latter case, the degree-of-fill (DOF) of the element is calculated.

(d) Melt temperature change: An energy balance on the channel flow is performed considering heating from the barrel and viscous dissipation from the melt. The flow is considered as 1D plug flow in the direction of the channel, and the value of the shear rate is calculated for pure drag flow. In the plastication section, the heat and temperature of melting are taken into account in the prediction of the corresponding temperature.

(e) Reaction: A pure stream of peroxide is added at atmospheric pressure (in a zone of the extruder which is partially-filled). The reaction is simulated from the point where fully-filled conditions are detected downstream of the peroxide injection port.

The simulation of the REX process is performed by implementing a computer code which takes as input variables the material properties of the polymer and the operating conditions and screw configuration of the extruder. An important characteristic of the 1D model is that the extruder is divided in an integer number of calculations zones, dependent upon the length of the extruder. The outputs of the model are, along some other relevant information, the profiles of average pressure, filling level, melt temperature, and Mw along the axial distance of the extruder.

There are two loops for the calculations: an inner and an outer loop. The sequence of the calculations in the inner loop is as follows. First, the average melt pressure and DOF profiles are calculated, the direction of the calculations being from die to hopper. In this stage, the position of the start of melting (PSM) is calculated which corresponds to the beginning of the calculation zone. Secondly, the average melt temperature profile is calculated, starting from the PSM and proceeding towards the die. Here, it is assumed that the heat of reaction is negligible, and that the thermodynamic properties of the polymer do not change because of the reaction. Finally, the solid volume fraction profile is updated. The convergence criteria in the inner loop are based on the first position of the PSM and the summation of the absolute values of the changes of the average melt pressure. For the outer loop, the Mw is computed from the converged temperature and DOF profiles previously calculated in the inner loop. The calculations are performed downstream of the peroxide injection port. In this case, the convergence criterion is based on the summation of the absolute values of the changes in the Mw.

3.3.1.2 Improvements to the Simulation Program

For the present study, two changes were implemented in the previously developed simulation program. The first one consisted in specifying the calculation of the PDI profile. This profile is not considered in the original computer code, but it can be readily implemented in the calculation procedure of the original code. The second change consisted in actually improving the calculation program with respect to one of its reported drawbacks. The calculation problem in the original code consists of the existence of a mass throughput threshold below which no convergence is attained for the PSM. The solution to such a problem consisted of the implementation of an under-relaxation factor in the equation corresponding to the update of the pressure from its value in the previous iteration. This numerical strategy is used for improving the convergence of non-convergent systems (Chapra, 2008). In the case of different numerical algorithms implemented for solving coupled velocity-pressure equations, the general form of the correction of the pressure equation using the under-relaxation factor takes the form of equation 3.9 (Ferziger, 2002).

$$p^i = p^{i-1} - \alpha p^{'} \qquad (3.9)$$

In equation 3.9, p stands for the pressure; the superscripts i and $i-1$ indicate the present and previous iterations, respectively; α (where $0 \leq \alpha \leq 1$), is the under-relaxation factor; and p' is the pressure gradient or pressure correction.

3.3.2 3D Models

Previous to the implementation of 3D models, 2D and 2.5D models had been implemented for describing the flow phenomena in COITSEs. In 2.5D modeling, the simulations of a 2D model are advanced in an additional dimension to approach the 3D flow behavior. Some examples of both 2D and 2.5D simulations are available in the open literature, of which one can refer, for instance, to the works by Fukuoka (2000) and Potente and Fleke (1998). When 3D simulations were first implemented to the simulation of COITSEs, the geometry of the flow system was simplified by neglecting the radial gap of the screws (Goffart et al., 1996, Strutt et. al. 2000). Also, as it can be seen in the just addressed works, the geometry of the intermeshing region is still a simplified one. An important consideration in the latter simulation approach was to assume that the barrel was rotating and the screws were fixed (the kinematic reversal approach).

In recent years, the improvement in computational capacity, along with the development of very efficient computational fluid dynamics (CFD) algorithms, has allowed the implementation of more realistic 3D models for the description of complex flow systems. In the case of COITSEs, some publications on 3D simulations where few simplifications are made, especially in regards to the flow geometry, have appeared mostly describing non-reactive systems (Bravo et al., 2000, 2004; Avalosse and Rubin, 2000; Shah and Gupta, 2003; Wünsch et al., 2003). However, Zhu et al. (2005 a and b) have addressed the polymerization of ε-caprolactone in fully-filled screw elements of a COITSE by means of 3D simulations. In most of the previously described cases, the simulations have been performed with commercial CFD software (Avalosse and Rubin, 2000; Shah and Gupta 2003; Wünsch et al., 2003), which is generally based either on the finite element method (FEM) or in the finite volume method (FVM).

3.3.2.1 Non-Reactive Systems

An important consideration in the modeling and simulation of the flow in a COITSE is the fact that the flow field, and hence the variables of the system, present a special type of "transient flow". This condition is related to the time dependency of the flow field, associated to the rotation of the screws. To take into account the former situation, it is common practice to simulate a series of instantaneous positions of the screws and to recombine them to describe the overall effect of the screws motion. Some of the published works include the complete remeshing of the system for each individual position of the screw elements being simulated (Yang and Manas-Zloczower, 1992; Bravo et al., 2000). When approaching the transient behavior of a COITSE system by means of the aforementioned calculation procedure, the path of specific particles can be tracked by integrating the Eulerian velocity field according to the relationship given as equation 3.10 (Yao and Manas-Zloczower, 1997; Bravo et al. 2004).

$$\mathbf{X}(t) = \mathbf{X}(t_0) + \int_{t_0}^{t} \mathbf{V}(t)dt \qquad (3.10)$$

here $\mathbf{X}(t)$ and $\mathbf{X}(t_0)$ are the positions of a particle $\mathbf{X}$ at times t and t_0, respectively, and $\mathbf{V}(t)$ is the velocity vector of the particle.

More efficient ways to deal with the transient behavior of the COITSE have been implemented later on (Bertrand et al., 1997; Avalosse and Rubin, 2000; Gupta, M., 2008). In particular, the so called “mesh superposition technique, MST, (Avalosse and Rubin, 2000) will be briefly addressed here. With this approach, a fixed FEM mesh is generated for the inner part of the screw barrel (flow mesh) and a moving mesh for each screw. At each time step, the screw meshes are updated to their current position and superimposed on the flow mesh. Then, for all nodes of the flow mesh laying within the screws a penalty formulation is applied to impose a velocity value matching the rotation speed of the screws (Avalosse and Rubin, 2000; POLYFLOW® user’s guide, 2008).

3.3.2.2 Reactive Systems

As described above, up to date very few works have been presented on 3D simulations of REX in COITSEs. Also, the fact that in some cases the flow system still needed several simplifications, like the kinematic reversal principle, has already been discussed. One work in this category was presented by Strutt et al. (2000). In this study, the peroxide-initiated degradation of PP was simulated in conveying elements of a COITSE, and the effects of processing variables, among them the peroxide concentration, on the mixing characteristics of the reactive flow of the molten PP were analyzed. Additional information regarding this study as well as that by Zhu at al. (2005 b), discussed in the paragraph below, will be further addressed in Section 3.5.2 “Mixing Analysis”.

In a more recent study, Zhu et al. (2005 a) analyzed the polymerization of ε-caprolactane in screw elements of a COITSE. This study was focused on the comparison of the simulation predictions from 1D and 3D models for the aforementioned REX system. To further illustrate the differences in the prediction of the two implemented modeling approaches, simulations for screw elements of two different size extruders were performed. It was concluded from this study that the 3D model provided a better description of the REX system over a wider range of operating conditions than the 1D model. For the same REX system, Zhu et al. (2005 b) analyzed the effects of processing variables on the progression of the polymerization reaction. The results of this study were discussed in terms of mixing mechanisms and the energy balance of the system.

3.3.2.3 Overview of the Implemented REX Simulation

A general procedure regarding modeling considerations of the 3D REX simulations implemented in this work is discussed in the following paragraphs. As it has already been stated, the analysis of a reactive flow system implies the simultaneous solution of the equations of conservation of mass, momentum, energy, and reaction kinetics. The first three of these equations are written as equations 3.11-3.13. The species conservation can be modeled by equations 3.14 and 3.15. Assumptions implied in equations 3.11-3.15 are incompressible non-Newtonian flow, pseudo-steady state conditions, constant thermal properties of the melt flow, negligible heat of reaction, and neglected molecular diffusion of peroxide.

$$\nabla \cdot \bar{v} = 0 \qquad (3.11)$$

$$\nabla \cdot \rho \bar{v}\bar{v} = -\nabla P + \nabla \cdot \bar{\bar{\tau}} \qquad (3.12a)$$

$$\bar{\bar{\tau}} = \eta \left[\left(\nabla \bar{v} \right) + \left(\nabla \bar{v} \right)^T \right] \qquad (3.12b)$$

$$\rho C_p \bar{v} \cdot \nabla T = k \nabla^2 T + \bar{\bar{\tau}} : \nabla \bar{v} \qquad (3.13)$$

$$\bar{v} \cdot \nabla I = \frac{dI}{dt} \tag{3.14}$$

$$\bar{v} \cdot \nabla Q_i = \frac{dQ_i}{dt}, \; i = 0,1,2 \tag{3.15}$$

In equations (3.14 and 3.15), Q_i stands for the *ith* moment of the molecular weight distribution, and I is the peroxide concentration.

The equations of reaction kinetics are described by the model proposed by Tzoganakis (1988, 1988 a), presented in this work as equations 3.1 and 3.2. Here, the relationship for the weight-average molecular weight (equation 3.3) has been rewritten as equation 3.16. Considering the flow to be described by a power-law fluid model, the viscosity can be expressed by means of equation 3.17.

$$\bar{\bar{M}}_W = m_0 \left(Q_2 / Q_1 \right) \tag{3.16}$$

$$\eta = \begin{cases} \dfrac{K}{\dot{\gamma}_0^{\,1-n}}, & \dot{\gamma} < \dot{\gamma}_0 \\ \dfrac{K}{\dot{\gamma}^{\,1-n}}, & \dot{\gamma} > \dot{\gamma}_0 \end{cases} \tag{3.17}$$

where the power-law consistency index, K, and the power-law index, n, are expressed as $K = K(\bar{\bar{M}}_W, T)$ and $n = n(\bar{\bar{M}}_W, T)$ (Strutt, 1998, Strutt et al. 2000).

Regarding the implemented boundary conditions, non-slip on solid walls is assumed. For the inlet section of the screw elements, fully developed conditions for the velocity field are implemented, and for the outlet section zero normal and tangential forces are specified. On the other hand, constant inlet as well as barrel temperatures are specified, and at the outlet section of the flow domain a vanishing heat flux is imposed. Also, the screw surface is considered to be adiabatic. For the velocity field, an interpolation of the mini-element type (Fortin, 1981) is adopted whereas for the temperature field linear interpolation is implemented. With respect to the reacting species, a fixed concentration is defined at the entrance of the flow geometry, and a zero mass flux is specified at the barrel wall and at the exit section of the flow domain. After the boundary conditions have been specified, solving the basic set of governing equations of the system (equations 3.11-3.15) requires the simultaneous solution of equations 3.16 and 3.17 as well as equations 3.1 and 3.2. In the simulations performed in this study, equations 3.14, 3.15 and 3.17 are declared in POLYFLOW® as user defined functions.

In closing this section, it is pointed out that due to the few assumptions and simplifications made in their implementation, 3D models yield a more realistic description of a flow system than that provided by 1D models. However, the application of 3D models is restricted to specific locations and conditions prevailing within the COITSE. More specifically, conventionally, only fully-filled sections of the extruder have been simulated (Pokriefke, 2007). For this reason, it is expected that a more complete description of a complex system, as it is the case of COITSEs, be provided by the simultaneous implementation of both types of models.

3.4 Scale-up Considerations

3.4.1 Overview on Scale-up of Processing Operations

When dealing with the scale-up of a physical or chemical operation, one needs to be aware of the fact that, in general terms, both the scale of the equipment where the process is performed as well as the production rate are increased. However, the term scale-up is more restricted to the change in scale of the production rate (associated with the change in scale of the process equipment). Also, it should be noted that the target of any scale-up criterion is to keep constant values of predefined process parameters, for instance, the extent of reaction, mixing quality, and maximum process temperature.

A term often used in the open literature (Carley and McKelvey, 1953; Bird et al., 1960; Valentas et al., 1991) regarding the scale or size of the equipment where a process is performed, and which therefore deserves some attention, is geometric similarity. This expression means that any length of the larger device is equal to the corresponding length of the smaller device times a scalar value. In scaling-up chemical or physical operations, dimensional analysis is a very important tool. Dimensional analysis is related to the use of equations where dimensionless variables are implemented, and according to Valentas et al. (1991) there are two main categories of this type of analysis. These categories are (i) normalization and scaling of the differential equations describing the process and (ii) application of the Buckingham *pi*-theorem.

When dimensional analysis of the differential equations is applied, general differential equations that apply to both the smaller and larger devices are obtained. These equations as well as their corresponding boundary conditions are written in dimensionless forms, and they can be further simplified by inspection of the order of magnitude of the terms appearing in the dimensionless equations (Lee and Castro, 1989). The Buckingham *pi*-theorem essentially states that the relationship between **N** dimensional variables that contain **M** fundamental dimensions may be represented through the use of **N-M** dimensionless groups. A more detailed analysis of this theorem can be found in the book by Zlokarnik (1991). Another approach when scaling-up, as can be seen in the work by Valentas et al. (1991), is a type of semi-empirical method where no dimensional analysis is used, but in this case the physics of the process is well understood.

Some dimensionless numbers of common use in polymer processing are the Reynolds, Capillary, Deborah, Nusselt, Peclet, and Weissenberg numbers. All of these numbers stand for relationships between physical parameters and are, therefore, useful in the analysis of non-reactive processes. For operations where chemical reactions are involved, the Damköhler numbers I, III and IV can be applied. A summary of these and other dimensionless parameters has been presented by Lee and Castro (1989).

3.4.2 Scale-up of Extrusion Operations

Scale-up procedures are of crucial importance when a specific process which has been successfully achieved in the lab has to be transferred to the industrial level. In the case of extrusion processes, key variables to be considered when scaling-up are the degree of mixing, and the temperature and residence time of the material being processed.

3.4.2.1 Overview and General Considerations

Scaling-up in twin screw extrusion is different from that achieved in single screw extrusion, especially in the sense that while in the former case the screw configuration can be modified to match specific processing requirements, e.g., different degrees of dispersive and distributive mixing, in the latter case the screw configuration is fixed. However, a great deal of the extrusion scale-up theory has been developed for single screw extrusion. One of the pioneer studies in extruder scale-up was presented by Carley and McKelvey (1953). This study deals with the scale-up analysis of a melt-fed SSE. Works related to the scale-up analysis of polymer extrusion operations, most of them including the derivation of specific mathematical relationships, for SSEs as well as COITSEs and counter-rotating twin screw extruders (CRTSEs) have been presented by different authors (Chung, 1984; Rauwendaal 1986, 1987; Ganzeveld and Jansen, 1990; Potente 1981, 1991; Christiano, 1994; Colbert, 1997). Two features can be distinguished regarding the previously addressed works. Firstly, in general terms, the scaling-up is approached by means of a simplified dimensional analysis. Secondly, such an analysis in the case of TSEs is an extrapolation of the theory developed for SSEs.

Rauwendaal (1986, 1987, 2001) has presented an interesting summary of different scale-up approaches in the case of the SSEs. These publications address some special considerations to be taken into account when scaling-up this type of devices. One such important consideration, in the case of plasticating extrusion, is that the melting capacity of the scaled-up machine must match its pumping capacity. Nevertheless, Colbert (1997) has argued that the scale-up of a COITSE is not as critical as that of a SSE. According to this researcher, this is due to both the modular design and the starve-fed condition of the former type of extruder which can be changed to modify the performance of the process.

In an extrusion operation, the scaled-up geometrical and operating parameters are related to those of the machine being scaled-up by a power of the diameter ratio (Rauwendaal 1986, 1987; Potente 1991; Christiano, 1994). In this work, this power will be referred to as the scale-up index. The scaled-up parameters are classified into primary and secondary variables. The primary variables are the maximum channel depth (H), the screw length (L), the helix angle (ϕ) and the screw rotational speed (N). In equation 3.18, the relationship between the original and the scaled-up values for these variables is shown.

$$\begin{aligned} H_2 &= H_1 d^h \\ L_2 &= L_1 d^l \\ \phi_2 &= \phi_1 d^\beta \\ N_2 &= N_1 d^\nu \\ d &= \left(D_2 / D_1\right) \end{aligned} \tag{3.18}$$

Here, D_1 and D_2 are outer diameters of the screws of the scaled-up and reference extruders, respectively.

Secondary variables are, among others, power consumption, residence time, shear rate, and average residence time. The scale-up relationship for a secondary variable is obtained by analyzing its mathematical expression in terms of the primary variables involved in such an expression. For instance, equation 3.19 corresponds to the relationship of the shear rate for a Newtonian fluid (V_b is the barrel velocity), and in equation 3.20 the corresponding scale-up relationship is shown. In this case, the scale-up index results from a combination of those ones of the primary variables (see equation 3.18).

$$\dot{\gamma} = \frac{v_b}{H} = \frac{\pi DN}{H} \tag{3.19}$$

$$\dot{\gamma}_2 = \dot{\gamma}_1 d^{1+v-h} \tag{3.20}$$

3.4.2.2 Heat Transfer

In order to get an estimation of the heat transfer requirements in an extrusion process, an energy balance of the system needs to be performed. In equation 3.21 (After Davis, 1992), the more general case for a REX process is outlined. In this equation, a positive sign on the left hand side implies an input of energy through the heat barrel, whereas a negative sign means that heat needs to be removed from the system.

$$q_b = mC_p\left(T_p - T_f\right) + \Delta H_t - E + q_r \tag{3.21}$$

Here, q_b represents the heat transferred through the barrel; m, the mass considered for the energy balance; and C_p is the heat capacity. T_p and T_f stand for the product and feed temperatures, respectively; ΔH_t is the latent heat of melting; E, the drive motor energy; and q_r is the heat of reaction.

From the energy balance, it can be seen that the scaled-up process may be constrained by the heat transfer capacity of the system. Furthermore, when increasing the size of the extruder, the heat removal capacity decreases significantly due to the low thermal conductivity of the melt and the smaller transfer area per unit volume of the extruder barrel. This can be seen in equation 3.22 where the corresponding scale-up relationships for power consumption, heat transfer area, and conveying capacity are presented. It should be stated here that equations 3.22a and 3.22c correspond to the case of a Newtonian fluid.

$$E_2 = E_1 d^{2v+3} \qquad (3.22a) \qquad \text{Power consumption}$$

$$A_2 = A_1 d^2 \qquad (3.22b) \qquad \text{Heat transfer area}$$

$$Q_2 = Q_1 d^{v+3} \qquad (3.22c) \qquad \text{Conveying capacity}$$

Here, Q_1 and Q_2 stand for the volumetric flow rate of the reference and the scaled-up extruders, respectively.

Equation 3.22 applies to geometrical scale-up, i.e., when all the geometrical parameters of the extruder are scaled-up proportionally to d^1.

Except for any heat losses, the power consumption is essentially transformed into a heat source by means of viscous dissipation, and, for a constant screw rotating speed the scale-up index v is equal to 0. Then, it can be noticed that if the velocity is kept constant the heat generated by viscous dissipation increases by a power of 3, whereas the heat removal capacity increases only by a power of 2. For this reason, in the case of non-reactive systems, it is common practice to scale-up the throughput of COITSEs by a power of 2.65-3.0 (Colbert, 1997). For the case of reactive systems and for a more detailed analysis of heat transfer in REX the reader is referred to the book by Xanthos (Xanthos, 1992) for general guidelines.

In the preceding discussion, the effect of the heat of reaction has been omitted but this should be an additional restriction to the scale-up process. Zhu et al. (2004, 2005 a) have addressed the effects of this additional variable by means of computer-aided simulations, as will be discussed below in this document.

3.4.2.3 Case Studies

In an experimental work by Christiano (1994), three different approaches in the scale-up of a compounding operation in COITSEs were compared. The cases analyzed involved (i) constant heat conduction, (ii) constant specific power consumption and (iii) constant average residence time. The former restrictions imposed certain scale-up relationships, which are described here by means of equation 3.23.

$$\frac{A}{M} \propto d^{1+l-h-2-v} \qquad (3.23a)$$

$$\bar{t} \propto d^{l-1-v} \qquad (3.23b)$$

$$M \propto d^{2+h+v} \qquad (3.23c)$$

$$SEC \propto d^{n+nv-nh+l-h} \qquad (3.23d)$$

Here, A represents the heat transfer area of the extruder barrel; M is the mass throughput; n, the power law index of the system; SEC, the specific power consumption; and $\bar{t}$, the average residence time.

In this study, the performance of two extruders with diameters of 69 mm and 96.5 mm, operating under the conditions described by equation 3.23, was compared to that of a small extruder with a diameter equal to 47 mm. In both cases the L/D radio for the small and the larger extruders was kept constant. As stated by Christiano (1994), when scaling-up a compounding operation, the target is to maintain the degree of mixing and the final polymer melt temperature. The obtained results were analyzed in terms of the melt temperature and the calculated and experimental specific energy consumption. Also, electron microscopy micrographs were obtained to analyze the mixing performance. The best results in this study corresponded to the operation under constant specific energy. On the other hand, the worst results were obtained when operating under constant average residence time.

In a 1D simulation study, Chen and White (1991) simulated the flow behavior in double and triple-flighted conveying screw elements of commercial COITSEs and presented scale-up considerations regarding the operation of the analyzed machines. The simulations were performed for both Newtonian and a non-Newtonian flows assuming isothermal conditions. One characteristic of the analyzed extruders was that they presented similar values of the ratio of the center line distance to the screw outer radius, φ_c. It was argued by the authors that, because of the fact that the analyzed extruders presented very similar φ_c values, these machines would yield similar screw characteristic curves regardless of their size (under the assumed isothermal conditions). That is, that the mass throughput could be scaled from one machine to another.

In an extension of the implemented 1D model used by Chen and White (1991), these same authors (White and Chen, 1994) analyzed the scale-up implications of the non-isothermal operation of a COITSE. In this case, two extruders were simulated by means of the 1D model. Some conditions considered here were same L/D ratio, a power law index of 0.25, and a screw rotational speed of 250 rpm for both screws. The corresponding throughputs were 30 and 515 kg/h, respectively (corresponding to the same dimensionless throughput), and the barrel temperature was set to 200 ºC. It was shown in this study that the overall temperature rise was 20ºC and 50ºC for the small and the large extruders, respectively. Then, it was concluded that in the case of the larger extruder a lower rotational screw speed to decrease the heat generated by viscous dissipation, or a better cooling system, should be implemented.

Zhu et al. (2004, 2005 a) analyzed the scale-up of the REX of ε-caprolactone in fully-filled elements of two size COITSEs by means of 1D and 3D simulations. These authors found that for identical residence times in the screw elements, the polymerization reaction was accelerated when the screw diameter was increased. The latter meaning that the polymerization requires a short screw length (L/D) to be completed in the larger extruder. On the other hand, it was also found that when increasing the screw dimensions and screw rotational speed, the differences between the predictions of the 1D and the 3D models became very significant. These researchers pointed out that the rules applied to the scale-up of non-reactive systems might not be applicable to the reactive process, especially for polymerizations with very high reaction heat. Some considerations in this study were to double the screw diameter, and to keep an L/D ratio constant. In order to maintain the same average residence time while keeping the screw speed constant, the axial velocity was also doubled at the entrance which means that the throughput was increased by a factor of 8, i.e., proportionally to the cubic of the diameter ratio of the extruders. For the simulations, the same barrel temperature was used for both the small and the large extruders, and adiabatic conditions were considered to apply on the screw surface. Besides the already mentioned results, some simulations were conducted for the same extruder for screw elements having different pitches. It was found that when increasing the screw pitch the conversion was increased which was attributed to a better axial mixing.

3.5 Mixing and Residence Time Distributions

Both mixing and residence time are critical factors for a successful REX operation. Furthermore, these parameters need to be considered when scaling-up an extrusion process as discussed in the previous section. In this section, some aspects regarding the numerical evaluation of both residence time and mixing from a numerical point of view are presented.

3.5.1 Residence Time Distributions

In the case of residence time, the residence time distribution (RTD) function *f(t)* is defined such that *f(t)dt* is the fraction of fluid leaving the reactor with a residence time between *t* and *t+dt*. After integration of *f(t)*, the cumulative residence time distribution *F(t)* is obtained (see equation 3.24). *F(t)* stands for the fraction of flow at the exit of the reactor with a residence time equal or less than *t*.

$$F(t) = \int_0^t f(t)\,dt \qquad (3.24)$$

Numerical RTD evaluation requires the previous determination of the flow field of the system. In the case of COITSEs, the RTD is defined by the configuration of the extruder (Tzoganakis, 1989; Gao et al., 1999). Experimentally, the RTD is usually determined by using tracers. Different methods have been reported for the experimental determination of the RTD for polymer applications in COITSEs, for instance the use of TiO_2 as a tracer (Gao et al., 1999; Kruijt at al. 2001).

Although the COITSE system is being analyzed in this work, some exceptions will be made to address relevant work related to the peroxide-initiated degradation of PP in SSEs, which is the reaction being analyzed in this work. One of such works is the one presented by Tzoganakis et al. (1988 b). In this work, a mathematical model was presented for the REX system which included the determination of the RTD. The calculation of the RTD was based on the study by Pinto and Tadmor (1970) on this subject. The predicted RTD values were compared with experimental data, finding good agreement between the calculations and the experimental data. Relevant operating conditions for the experiments were barrel temperature of 220 ^{o}C, screw speed of 60 rpm, and peroxide concentrations of 0.01, 0.02 and 0.05 wt %. In their study, Tzoganakis et al. (1988 b) reported that as a result of increasing the peroxide concentration the RTD curves broadened. Similar results were also presented by Suwanda et. al. (1988), and according to Tzoganakis et al. (1988 b) this behavior is related to an increase in the pressure driven back flow as the peroxide concentration increases (which causes the viscosity to decrease).

In 1998, Potente and Flake presented a 2.5D numerical analysis on the RTD distributions in COITSEs in which the viscosity was modeled by a power-law model. In this work, the authors performed a comparison of the results obtained from their numerical analysis to those yielded by applying the model proposed by Pinto and Tadmor (1970), in which the flow in the screw channels is addressed as that occurring between two plates. It was argued by Potente and Flake that the assumption that the stream line of minimum residence time was located at a position where there is no traverse flow, as stated in the work by Pinto and Tadmor (1970), was not correct. This discrepancy was associated with the fact that at this specific location negative velocities could develop, whose magnitude depended on the flow rate and screw speed. The results from both of the analyzed models were tested with experimental data. A significantly better agreement was obtained when the experimental data were compared to the predictions of the 2.5D model.

In an experimental and theoretical work of non-reactive polymeric flow in a COITSE, Gao et al. (1999) analyzed the effect of processing operating conditions on the RTD of the extruder. These researchers reported that the dominant factor determining the characteristics of the RTD curve for a given screw configuration was the volumetric throughput. The time delay in the curve was reduced when the volumetric throughput or the screw speed increased. For a given mass throughput with different screw speeds, RTDs with similar shapes were obtained.

In a work presented by Avalosse and Rubin (2000), the flow in a conveying screw element and in an extruder element consisting of alternating sections of a conveying screw element and a kneading block section was simulated by means of a 3D model. The flow was considered to be Newtonian and isothermal and a constant pressure was specified for both of the analyzed flow geometries. In this case, as explained before, the transient nature of the flow was accounted for by means of the MST. The results of this work showed that the volumetric throughput was higher for the pure conveying screw element, and that the RTD was narrower for this same element.

Kruijt et al. (2001) presented a work on the 3D simulation of a Newtonian non-isothermal flow in fully-filled sections of a COITSE. In this work, the so called mapping method was adopted for the calculations, and as in recent studies regarding non-reactive systems, the time dependency of the flow was taken into account. Among other processing information of interest, the RTD was calculated. According to the authors, the obtained RTD curves showed good agreement with what is experimentally observed for polymer flows in COITSEs. The calculation approach implemented in this study is elegant but computationally expensive.

Ishikawa et al. (2002) presented a numerical 3D transient study of a non-Newtonian non-isothermal flow in different screw elements of a COITSE. The analyzed elements were a standard conveying element, a kneading block section, and a special screw element. The latter element corresponded to a standard conveying element with slots across the flight tip which were aimed to promote leakage flow. To validate their calculations, the authors carried out a comparison between the predicted and experimental pressure and temperature profiles. In this study, a constant flow rate was specified. For a set of operating conditions, the shape of the RTD curves obtained for the conveying and kneading block elements was similar, showing a high peak at short times. For the same set of operating conditions, the RTD of the special mixing element did not show the high peak at short times and was broader than the one obtained for the aforementioned elements.

Bravo et al. (2004) implemented a FEM 3D analysis for the description of the flow in the kneading disk region of a COITSE. In this work, the flow was assumed to be isothermal and the viscosity was described by a Carreau model. In this study, the effect of the ratio of the disc length to the disc diameter on the RTD, for a given number of discs and fixed stagger angle, was analyzed. From the simulation results, it was observed that as the L/D ratio was increased, the RTD broadened and the back flow in the system increased. The back flow in this case was related to the number of seeded tracking particles, at the flow inlet plane, moving backwards.

The RTD results in this case exhibited a scattered behavior, which according to the authors was related the low number of tracked particles, and the non-diffusive nature of such particles.

Very recently, Zhu et al. (2008) presented an experimental and 3D numerical simulation study of a variable speed COITSE. In this special type of extruder, the screws have a different number of flights and rotate at different speeds. Experimental visualization experiments were performed in a transparent wall extruder. A comparison was made between the performance of a conventional two-flighted screw element and a screw element having a two- and one-flighted screws (the special extruder). The simulations were performed under non-isothermal conditions for a PP whose viscosity was described by means of a Cross-Carreau model. A constant mass throughput was specified for both of the simulated extruders. For the analyzed conditions, the RTDs exhibited a similar shape, but in the special extruder the average residence time was about 60 % of that obtained for the conventional extruder design.

3.5.2 Mixing Analysis

Mixing occurring in high viscosity fluids such as molten polymers is known to occur by convective laminar flow. In polymer extrusion, two mixing mechanisms, i. e., dispersive and distributive mixing, can be identified. In general terms, the former one refers to the process of breaking up a dispersed phase by the action of fluid stresses at the interface. The latter mixing mechanism refers to spatial redistribution where a real interface may, or may not, be present (Biesenberger, 1992).

In distributive mixing analysis, the evaluation of mixing in terms of the deformation experienced by fluid elements along their journey through the flow system is performed. In Figure 3.5, the deformation of an infinitesimal filament as well as that of a surface element are outlined. A convenient way of determining the deformations experienced by fluid elements, in a particular flow situation, is the use of the Lagrangian reference frame. In such a reference frame, the position of a material element is described as a function of time and its initial position, as indicated in equation 3.25. From equation 3.25, the deformation tensor can be obtained. According to Ottino (1989), this tensor is the basic measure of deformation with respect to the reference configuration, **X.** The relationship between **x**, **X** and the deformation tensor has been written as equation 3.26.

$$\mathbf{x} = \mathbf{x}(\mathbf{X}, t) \qquad (3.25)$$

Here **x** is the position of a particle **x** at a time *t* and **X** is the initial position of **x**.

$$\mathbf{F} = \left(\nabla_{\mathbf{X}}\mathbf{x}\right)^{\mathbf{T}}$$
$$F_{ij} = \left(\frac{\partial x_i}{dX_j}\right) \qquad (3.26)$$

where **F** is the deformation tensor, and $\nabla_{\mathbf{X}}$ indicates differentiation with respect to **X**.

Generally, the solution of the flow field is numerically determined and, then, the deformation tensor is calculated as the fluid element travels through the flow field. In order to perform such a calculation, numerical differential equation solution techniques are used (Bigio and Conner, 1995). Two measures of strain which are the length stretch, λ, and the area stretch, η, ratios are derived for the type of the deformations depicted in Figure 3.5. These parameters are defined in equations 3.27 and 3.28, and they can be calculated from equations 3.29 and 3.30.

$$\lambda = \lim_{|d\mathbf{X}| \to 0} \left(\frac{|d\mathbf{x}|}{|d\mathbf{X}|} \right) \tag{3.27}$$

$$\eta = \lim_{|d\mathbf{A}| \to 0} \left(\frac{|d\mathbf{a}|}{|d\mathbf{A}|} \right) \tag{3.28}$$

$$\lambda = (\mathbf{C} : \mathbf{MM}) \tag{3.29}$$

$$\eta = (\det \mathbf{F})(\mathbf{C}^{-1}\mathbf{NN})^{1/2} \tag{3.30}$$

In equations 3.29 and 3.30, $\mathbf{C} \equiv (\mathbf{F}^T \cdot \mathbf{F})$, and **M** and **N** (the orientation vectors) are defined by

$$\mathbf{M} \equiv d\mathbf{X}/|d\mathbf{X}| \qquad \mathbf{N} \equiv d\mathbf{A}/|d\mathbf{A}|$$

Alternative measures of mixing efficiency have been proposed by others (Ottino et al., 1981; Zerafati and Bigio, 1994; Bigio and Coner, 1995). For the case of an infinitesimal area element, Zerafati and Bigio (1994), based on the analysis of the eigenvalues and principal directions of the rate of deformation tensor (**D)**, derived two efficiency parameters. These parameters are the energy efficiency index, η_{Fa}, and the area growth efficiency index, η_{La} (see equations 3.32 and 3.33), and they can be derived from the ratio of the instantaneous area growth to the total area stretch whose relation is shown in equation 3.31. Equation 3.32 indicates that the optimal area growth occurs when the orientation vector (**n)** is parallel to the direction of the minimum eigenvector (**n**$_3$), whereas equation 3.33 is a measure of the efficiency of the flow field to convert the input energy to the optimal eigenvalue, $\lambda_{3.}$ The

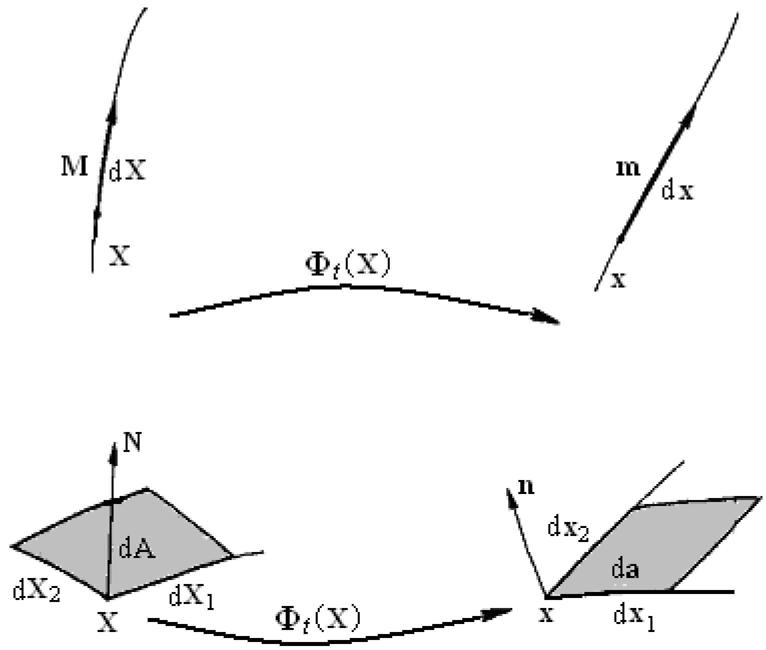

Figure 3-5 Schematic illustrating the deformations of an infinitesimal filament and a surface element [After Ottino, 1989].

previous analysis is very similar to that one presented by Bigio and Coner (1995), where mixing was described in terms of an infinitesimal filament. As noted by Zerafati and Bigio (1994), the analysis of the deformation of an infinitesimal area element is more suitable for a 3D flow, as that of an infinitesimal filament is a better approach when dealing with 2D flows.

$$\frac{\dot{\eta}}{\eta} = -\mathbf{D} : \mathbf{nn} \qquad (3.31)$$

In equation 3.31, $\dot{\eta} = \frac{\mathrm{d}\eta}{\mathrm{d}t}$, and $\mathbf{D} = \frac{1}{2}\left(\nabla\mathbf{v} + (\nabla\mathbf{v})^T\right)$, $\mathbf{v}$ being the instantaneous velocity vector. Equation 3.31 is a simplification, for the case of incompressible materials, of a more general equation.

$$\eta_{Fa} = \frac{-\lambda_3}{\sqrt{\mathbf{D}:\mathbf{D}}} = \frac{-\lambda_3}{\sqrt{II_D}} \tag{3.32}$$

$$\eta_{La} = \frac{\mathbf{D}:\mathbf{nn}}{\lambda_3} = \frac{\mathbf{n}^T\mathbf{Dn}}{\lambda_3} \tag{3.33}$$

where λ_3 stands for the minimum eigenvalue of **D**, and $\mathbf{n} = \mathrm{d}\mathbf{a}/|\mathrm{d}\mathbf{a}|$ (see Figure 3.5).

The more direct evaluation of mixing is that of distributive mixing, and the parameters discussed in the above paragraphs refer also to this type of mixing analysis. In the case of dispersive mixing, some proposed parameters for characterizing this type of mixing are based on the shear stress and more complex relationships derived from the flow field analysis. The primary goal of this work is not to analyze the dispersive nature of the flow, whose analysis is more common for kneading blocks and other types of mixing elements. However, in the paragraphs below, the description of the mixing index, λ, which has been used as indicative of dispersive mixing (Yeng and Manas-Zloczower, 1992; Avalosse at al., 2000) will be addressed. The mixing efficiency index, λ, is defined in terms of the magnitude of the rate of deformation and the vorticity tensors. The definition of this parameter is shown in equation 3.34. The limits of this equation are 0 for a purely rotational flow and 1 for a purely elongational flow, and in the case of a simple shear flow the mixing index is equal to 0.5. In dispersive mixing analysis, it is assumed that elongational flows provide better dispersive mixing capabilities. In the paragraphs below, some works regarding mainly distributive mixing analysis are addressed.

$$\lambda = \frac{|\gamma|}{|\gamma| + |\omega|} \qquad (3.34)$$

In equation 3.34 $|\gamma|$ and $|\omega|$ stand for the magnitudes of the rate of deformation and the vorticity tensors, respectively.

In 2000, Avalosse and Rubin presented a study on mixing and RTD characteristics of a standard conveying screw element and an element consisting of a kneading block section intercalated between conveying screw elements. In this study, it was observed that the element consisting of both standard conveying elements and the kneading block section presented the higher increase of the area stretch ratio. Also, Avalosse and Rubin concluded that this same element presented a larger dispersion of the mixing quality than that of that of the standard conveying screw element.

Strutt et al. (2000) presented a 3D study of the PP REX in forward screw elements of a COITSE. In this case, two screw speeds, 100 and 250 rpm, were analyzed. The increase in screw speed was related to a reduction in the peroxide conversion, and, hence, to higher molecular weights obtained at the exit of the flow element. For the implemented screw speeds, the temperature and pressure profiles of the molten resin as well as the conversion of initiator and relative weight-average molecular weight profiles presented similar shapes. In this study, also the evolution of the area stretch mixing efficiencies was evaluated. This parameter showed fluctuations in the intermeshing region of the screw elements, but everywhere else its value remained around 0.707, which is very close to the value of this parameter for two-dimensional shear flows. The peroxide concentration and screw speeds were found to have little effect on the values of the mixing efficiencies for the specified REX conditions. The higher mixing efficiencies (ability to convert the input fluid power to the maximum specific area of stretch ratio) were found in the translation region of the screw elements.

Yoshinaga et al. (2000) analyzed the flow behavior of a trilobal kneading block array under forward, backward, and neutral conveying conditions. In this case, the flow was simulated under isothermal conditions, and the viscosity was described by the Bird-Carreau model. In this work, the distributive mixing was analyzed in terms of the RTD and the nearest distance between flow markers. Under the simulated conditions, the neutral kneading block exhibited the best distributive mixing capabilities. This was concluded, among other facts, by considering the increase in the distribution of the nearest distance between flow markers for this element, when compared to the other types of analyzed kneading blocks.

Kruijt at al. (2001) implemented the mapping method to evaluate the concentration distribution in conveying elements of a COITSE. To perform the analysis of the distribution of concentration, two different zones having a different concentration (identified by different colors for visualization purposes) were specified at the entrance of the flow domain at t=0 s. The concentration profile was examined taking into account the motion of the screws, and then the intensity of segregation was obtained. It was observed, as expected, that the values of this latter parameter decreased as the axial distance in the direction of the flow increased.

Ishikawa et al. (2002) analyzed the mixing characteristics of different types of screw elements. In this case, the distributive mixing was analyzed in terms of the ratio of back to total flow (G value), the RTD, and the area stretch ratio as well as the distribution of this latter parameter. For the simulations, a fixed value of the flow rate was implemented. The authors justified the use of the RTD in evaluating distributive mixing highlighting the fact that this parameter can be experimentally evaluated. It was found that the special type of mixing element presented the gratest values of G, which increased when the screw rotating speed was increased. This element also exhibited the broader RTDs.

In their work, Bravo et al. (2004) discussed the mixing capabilities of kneading blocks consisting of kneading discs having different L/D ratios. These researchers related the RTD of the studied kneading block arrays to distributive mixing, associating broader RTDs with better distributive mixing. Also, the “axial distribution” of tracked particles was analyzed, again relating a broader axial distribution with better distributive mixing capabilities. In this study, the back flow was evaluated by means of the number of particles initially seeded at the entrance of the corresponding kneading block with velocities in the upstream conveying direction. Here, the increase in back flow was associated with better distributive mixing. Overall, it was concluded by the authors that the increase in the L/D ratio resulted in better distributive mixing, for the simulated processing conditions.

Zhu et al. (2005 b) studied the polymerization of e-caprolactane in screw elements of a COITSE. In this study, the effects of the screw speed, screw pitch, and initial inlet conversion on the REX system were analyzed. A fixed value for the mass flow rate was specified for the simulations. The authors reported that, when increasing the screw pitch of the elements, higher conversions were found for a given axial distance, and that this effect was associated with a better mixing intensity. This was concluded from higher values of the axial velocity obtained when the pitch of the elements was increased, and taking this fact as an indication of a broader distribution of the axial velocity. This same effect was also associated to a broader RTD.

Kajiwara et al. (2006) performed a mixing analysis for three different types of kneading block elements: conventional kneading blocks, and kneading blocks with (i) a grooved barrel and (ii) multi-clearance. Distributive mixing analysis was performed by the tracking of particles injected in three different zones of the entrance of the flow geometries. This analysis was performed by visual examination of colored markers at specific axial distance along the flow domains. According to this study, the best distributive mixing characteristics were obtained for the kneading block having the grooved barrel.

When analyzing the flow in screw elements with the same and different cross section geometries (same and different screw rotations, respectively), Zhu et al. (2008) reported that for a given flow rate the latter set of screw elements presented a higher average area stretch ratio than that of the former element. Thus, a better mixing capability was associated with the screw elements having the different cross section geometry. In this case, the viscosity of the system was described by means of a Cross-Careau model, and the flow was assumed to be non-isothermal.

3.5.3 Overview on Tracking Analysis Fundamentals

There are three types of lines that are used for visualization purposes: streamlines, pathlines and steaklines (Ottino, 1989; Broadkey, 1967). Streamlines are lines which are tangent to the velocity vectors corresponding to flow particles moving under steady-state flow conditions. Therefore, these lines can be interpreted as the trajectories of particles moving in a steady-state flow. Pathlines are similar to streamlines, but in this case there are no constraints in the time dependency of the flow, i.e., the flow can be either steady or non-steady. Streaklines are the loci of fluid particles that have previously passed through specific locations of the flow geometry. It is interesting to note that for steady-state flow conditions there is only one trajectory per particle that describes all of the aforementioned lines. According to the previous discussion, the trajectory of particles initially seeded at specific locations of the flow geometry are described as streamlines and pathlines, for steady-state and non-steady state flow conditions, respectively. In this work, the latter two definitions, applying to the specific type of flow that they describe, are extensively used.

3.6 Additional Considerations of the Flow in Screw Elements of COITSEs

A preliminary analysis of the flow conditions in screw elements of COITSEs considering the flow to be either reactive or non-reactive can be achieved by considering the equations of flow 2.1a and 2.1b, described here as equations 3.35 and 3.36, respectively. Although these equations have been developed for the flow of SSE, the flow in SSE and COITSEs is similar in the sense that flow occurs in both in completely open channels (Meijer and Elemans, 1988). Furthermore, these same relationships are the ones used in the work by Christiano (1994) when performing his scale-up analysis for COITSEs. Also, a relationship equivalent to equation 3.36 is used in the work by Zhu et al. (2005 b), stating that according to Booy (1980) when the leakage flows are neglected, such a relationship can be used to describe the flow in COITSEs.

$$Q = Q_d + Q_p = \frac{1}{2}\pi^2 D^2 NH \sin\phi \cos\phi - \left(\frac{\pi DH^3 \sin^2 \phi P}{12\eta l}\right) \tag{3.35}$$

$$Q = \alpha N - \left(\frac{\beta P}{\eta}\right), \text{ or } P = \frac{\eta}{\beta}(\alpha N - Q) \tag{3.36}$$

Form equation 3.36, it can be appreciated that there exists a relationship between the viscosity and pressure build-up of the system. For the reactive flow conditions analyzed in this work, the viscosity of the system is related to the degree of PP degradation which is a function of both the extent of reaction and the initial peroxide concentration. If, for instance, the total flow rate is kept constant, the pressure build-up, and as a consequence, the pressure-driven back flow will decrease as the degree of degradation increases. The interpretation given above should be taken carefully, given the simplified nature of equations 3.35 and 3.36. For instance, in their work on the PP degradation in SSEs, Tzoganakis et al. (1988 b) associated the increase of the peroxide concentration with the increase in pressure-driven back flow contributions, in contrast to what it is projected here from these equations.

From equation 3.35, it can be appreciated that if there is no pressure-driven back flow contribution to the flow of the system, the maximum flow rate that could be attained would correspond to that of pure drag flow conditions. Another possible scenario that can readily be analyzed from equation 3.35 is the case when there is a pressure-driven back flow contribution to the net flow of the system. In this case, assuming non-reactive conditions and negligible changes in the viscosity, when the flow rate is decreased the pressure of the system will increase according to equation 3.36. In a COITSE, the reduction of the flow rate is usually associated with the use of left-handed conveying screw elements or other type of flow elements that induce a backward flow, or restrict the flow in the forward direction. In the analysis presented in the following chapters, the term “restricted flow” is associated with flow rate values that are lower than the ones corresponding to those obtained under the assumption of a zero or close to zero back flow contribution.

As has been previously discussed, the increase in pressure-driven back flow contributions has been related to improved distributive mixing capabilities (Bravo et al. 2004; Zhu et al. 2005 b). Then, according to the scenarios described in the above paragraphs, for constant flow rate under REX conditions, higher degrees of degradation (lower Mws of the reacted PP) would correspond to poorer distributive mixing capabilities. On the other hand, under non-reactive conditions, a decrease in the flow rate (more restrictive flow conditions) is expected to give rise to better distributive mixing characteristics.

4 SCALE-UP CALCULATIONS: 1D SIMULATIONS

4.1 Proposed Scale-up Analysis

For the 1D simulation approach, the scale-up analysis consists of two steps. Firstly, the reference extruder is simulated for a combination of three different peroxide concentrations and three mass-throughput values, at a constant screw speed. In this case, only two extruder sizes are simulated. In the second step, for a fixed peroxide concentration two different screw speeds are considered, and for each screw speed two different mass-throughput values are implemented. In this latter case, the REX operation is simulated for four different size extruders.

4.1.1 Scale-up Considerations

Following the work of Christiano (1994), in the case of a COITSE system the average residence time ($\bar{t}$), mass throughput (M), and specific energy consumption (SEC) can be expressed as the set of equations 4.1.

$$\bar{t} \propto d^{\,l-1-\nu} \qquad (4.1a)$$

$$M \propto d^{\,2+h+\nu} \qquad (4.1b)$$

$$SEC \propto d^{\,n+n\nu-nh+l-h} \qquad (4.1c)$$

The meaning of the parameters in equations 4.1, and the equations themselves have already been presented in Section 3.4.2.3. The set of equations 4.1 is implemented in this chapter to evaluate the mass throughputs corresponding to scaling-up under constant residence time and specific energy consumption. The first one of these scale-up approaches is mainly used for reference in the calculation procedure to be performed, whereas the second one is used as a performance indicator of the proposed scale-up analysis, as will be discussed below.

In the case of a REX process, two main processing variables are the material temperature and residence time. In a REX operation, these two parameters can be related by means of the thermal time, t_T, whose concept was introduced by Nauman (1977). The thermal time in the case of a first order reaction is calculated as shown in 4.2:

$$t_T = \int_0^t e^{-E/RT(t')} dt' \tag{4.2}$$

where t is the residence time; E is the activation energy of the reaction; and T, and t' are the temperature and residence time, respectively, at a particular point along a path line.

Equation 4.2 applies to individual fluid elements, and it should be integrated over the corresponding path lines. In a simplified 1D flow analysis, one can numerically evaluate equation 4.2 provided that the values of temperature and residence time (along the axial direction of the extruder) are known. It is interesting to note that if hydrodynamic similarity between the reference and scaled-up extruders were to prevail, which is a rather idealized situation, this equation reduces to that one derived by Ganzeveld and Janssen (1990) for the case of homogenous first order reactions.

The proposed scale-up analysis for the REX operation consists of two steps. In the first step, the thermal time for a reference extruder operating under specific processing conditions is evaluated. Secondly, for extruders of different sizes, the corresponding operating conditions for which a similar value of thermal time can be obtained are determined. Additionally to the procedure just described, some simulations are performed considering the scale-up to be performed under similar SEC, as in conventional extrusion. Then, the simulation results, corresponding to the different scale-up criteria (constant thermal time versus constant SEC), are compared in terms of the final Mws and PDIs of the polymer resin.

4.1.2 REX Modeling Considerations

As has been previously stated, the 1D simulations are performed by means of the computer code developed by Strutt (1998). Some modeling considerations with respect to the 1D model presented by this author have already been addressed. However, given its relevance for both the 1D and 3D simulations implemented in this work, more specific information regarding the equations describing the viscosity of the system is addressed here. The equations of reaction kinetics are described by the model proposed by Tzoganakis at al. (1988 a), presented in this work as equations 3.6 and 3.7. It is important to remind the reader that these equations allow for the calculation of the Mw of the reacting polymer. To account for the dependency of both the consistency and power-law indexes on the temperature and Mw of the molten resin, mathematical functions derived from data by Tzoganakis (1988) are implemented (Strutt, 1998; Strutt et al. 2000). In summary, the viscosity of the system is addressed by means of a power-law model, equation 4.3, and the functionality of the parameters of equation 4.3 on both the Mw and temperature is described by equations 4.4 and 4.5.

$$\eta = \begin{cases} \dfrac{K}{\dot{\gamma}_0^{\,1-n}}, & \dot{\gamma} < \dot{\gamma}_0 \\ \dfrac{K}{\dot{\gamma}^{\,1-n}}, & \dot{\gamma} > \dot{\gamma}_0 \end{cases} \tag{4.3}$$

where the consistency index, *K*, and the power-law index, *n*, are expressed as

$$\ln K = -0.6294 \ln M_W - 0.0243T + 0.1364(\ln M_W)^2 \tag{4.4}$$

$$n = 1 - \frac{\chi \sin 2\theta + \sqrt{(\chi \sin 2\theta)^2 + 4(2\sin^2\theta - 1)(0.07\sin\theta)^2}}{2(2\sin^2\theta - 1)} \tag{4.5}$$

where $\theta = \frac{\pi}{2} - \frac{1}{2}\tan^{-1} 0.00106T$ and $\chi = \ln M_W - \frac{0.0154T - 1}{0.00106T}$

and K and n represent the power-law consistency index and the power-law index, respectively (Strutt 1998; Strutt et al. 2000).

4.2 Peroxide Concentration and Mass Throughput Variation

The physical properties of the PP resin used for the simulations performed in this work are given in Table 4.1. In Table 4.2, some parameters regarding the geometry of the two extruders being simulated is presented. Table 4.3 summarizes the processing conditions as well as presents some results of interest corresponding to the scale-up under the constant thermal time approach. As indicated in this table, three different peroxide-feed concentrations were used in

Table 4-1 Material data used for 1D simulations.

Parameter	*Value*
Number-average molecular weight	51,800 g/mol
Weight-average molecular weight	279,700 g/mol
Melt density	750 kg/m^3
Solid density	905 kg/m^3
Bulk solid density	560 kg/m^3
Pellet hydraulic diameter	2 mm
Power law index	0.43*
Melt thermal conductivity	0.185 W/(m ºC)
Melt specific heat capacity	2.428 kJ/(kg ºC)
Melting point	170 ºC
Heat of fusion	133.850 kJ/kg

* used in equation 4.1c (constant SEC).

Table 4-2 Geometrical parameters used for the extruders being considered (data from Leistritz®).

TSE model	Screw outer diameter (mm)	Center line distance (mm)	Flight depth (mm)	Barrel inner diameter (mm)
LSM-30.34	33.70	30.01	3.99	34.00
ZSE-96	95.60	83.90	12.10	96.00

Table 4-3 Simulation results of interest for scaling-up under constant thermal time. E. M. stands for extruder model; M represents the mass throughput; [I], the concentration of initiator; ΔP, the pressure drop in the die; $^{*}T_{AB}$, the average temperature of reaction; R_t, the average residence time of extrusion; Mw and PDI, the final weight-average molecular weight and polydispersity-index, respectively; t_T, the thermal time; and M_{tT}/ M_t is the ratio of the mass throughputs corresponding to constant thermal time and residence time.

E. M.	M (kg/hr)	[I] (wt %)	ΔP (KPa)	R_t (s)	T_{AB} (º C)	Mw x10^{-5} (kg/kmol)	PDI	t_Tx10^{12} (s).	M_{tT}/ M_t
LSM-30.34	4.0	0.01	446	108	204	2.50	4.91	1.04	---
		0.02	374	108	204	2.26	4.53	0.98	---
		0.10	152	104	202	1.36	3.07	0.80	---
	8.0	0.01	617	83	204	2.52	4.94	0.83	---
		0.02	530	83	204	2.30	4.58	0.80	---
		0.10	245	80	202	1.42	3.17	0.65	---
	12.0	0.01	734	84	204	2.49	4.90	1.07	---
		0.02	632	83	203	2.26	4.52	1.01	---
		0.10	299	80	202	1.37	3.08	0.78	---
ZSE-96	97.6	0.01	446	87	209	2.50	4.91	1.04	1.20
		0.02	374	86	208	2.26	4.53	0.99	1.20
		0.10	152	92	205	1.36	3.07	0.80	1.10
	195.2	0.01	617	79	207	2.52	4.94	0.83	1.00
		0.02	530	80	206	2.30	4.58	0.80	0.95
		0.10	245	77	204	1.43	3.18	0.65	1.00
	292.8	0.01	734	93	205	2.49	4.90	1.07	0.8
		0.02	632	93	204	2.26	4.52	1.02	0.80
		0.10	299	87	203	1.37	3.08	0.78	0.83

* Average temperature for the zone of the extruder where the reaction takes place.

the simulations. In all of the analyzed cases, the peroxide injection point was specified at a dimensionless axial distance of 0.45. The diehead pressures for the reference extruder were calculated based upon a two-hole strand die having a length of 12 mm and a diameter of 4 mm. These pressures were specified as fixed values within the set of operating conditions of the REX process being scaled-up. The reference device was a Leistritz® LSM-30.34 COITSE having the screw configuration shown in Figure 4.1. The configuration corresponding to the scaled-up extruder is essentially the same of that shown in Figure 4.1, but the length of the screw conveying elements and kneading blocks has been scaled-up proportionally to d^1.

The mass throughputs shown in Table 4.3 were obtained by using a scale-up index v = 0 in equation 4.1b (which for this equation satisfies the condition of constant residence time according to 4.1a). Such mass throughputs for both the scaled-up and reference extruders were determined from an analysis of the fully-filled capacity of the extruders. This analysis is outlined by making use of Figure 4.2 which corresponds to the variation of the degree-of-fill (DOF) at the center of the screw channel along the axial direction of the extruder. From Figure 4.2a, corresponding to a fixed peroxide concentration of 0.01 wt %, the simulations indicate that for the highest value of the mass throughput (12 kg/hr) the reference extruder operates near at its fully-filled capacity. For this reason, this mass throughput was selected as the upper limit to be simulated for this parameter.

It is interesting to note from Figure 4.2, for both of the presented peroxide concentrations, that the length of the fully-filled sections of both the reference and large extruders is very similar for the case of the lowest mass throughput. However, more significant differences in the length of the fully-filled zones are observed as the mass throughput increases. In principle,

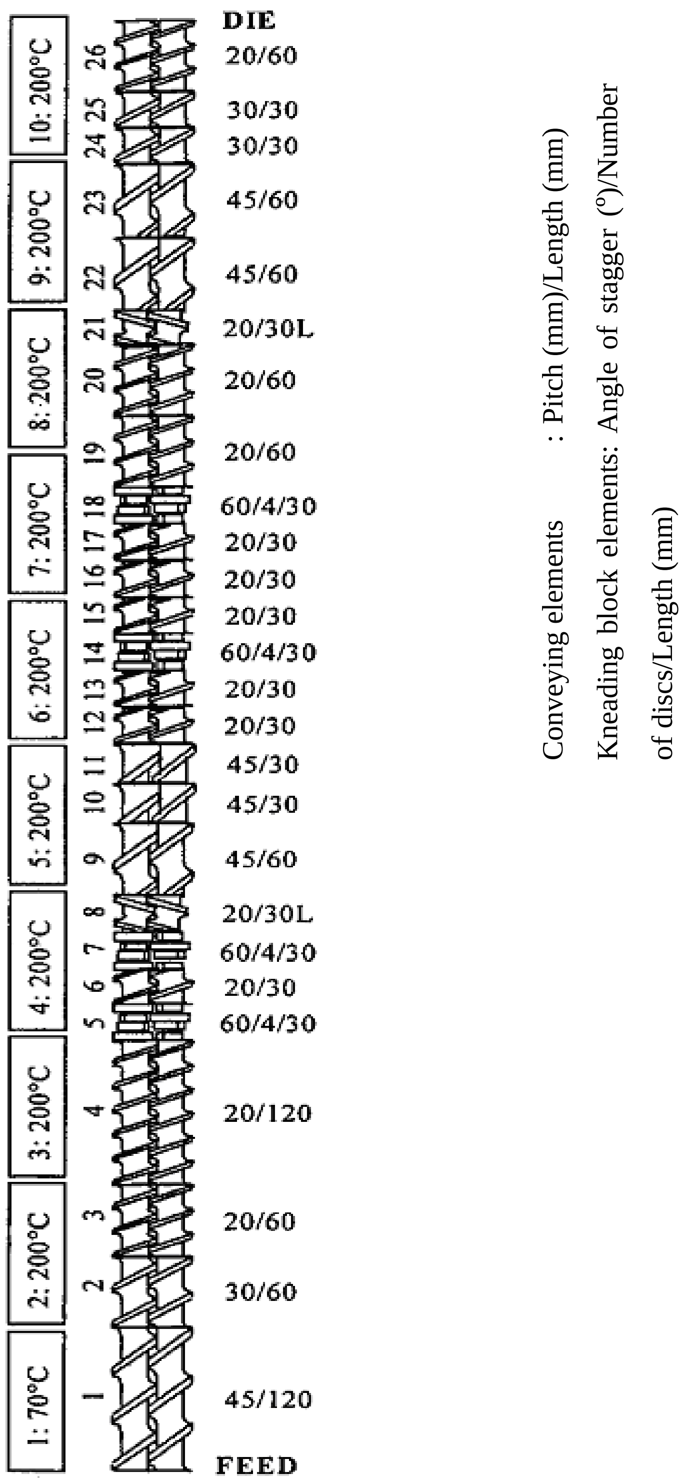

Figure 4-1 Reference-lab Extruder Configuration (Strutt, 1998).

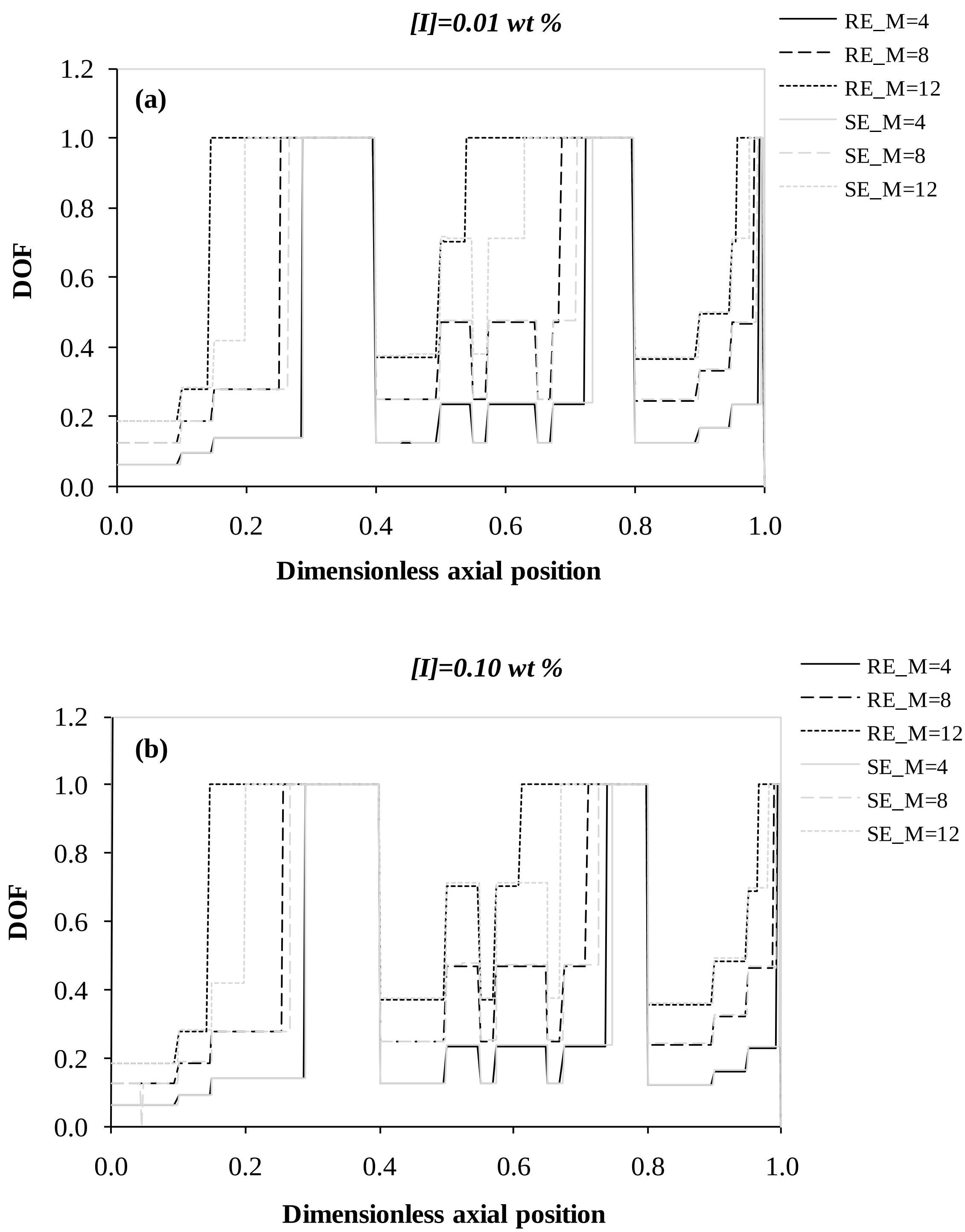

Figure 4-2 DOF variation along the axial distance of the extruder. RE and SE stand for the reference and scaled-up extruders, respectively, and M for the reference mass throughput, in Kg/hr.

with the implementation of the scale-up rule for constant residence time the DOF profiles should be the same for both the small and larger extruders, when the reference and scaled-up mass throughputs, respectively (for the constant residence time approach), are implemented. Therefore, the observed DOF discrepancies may be associated to the simplified approach implied in the implemented scale-up relationship, to the relative difference in screw geometry of the extruders, to differences in processing conditions, i.e., temperature profiles, among other factors. By comparing the information from Figures 4.2a and 4.2b (corresponding to peroxide concentrations of 0.01 and 0.10 wt %, respectively), it can also be observed that the length of the fully-filled zones decreases when the peroxide concentration is increased. This behavior suggests that for the systems with the lower viscosities (related to higher degradation, i.e., higher peroxide concentrations), the less restricted flow conditions, associated to such lower viscosities, are reflected in the reduction of the lengths of the fully-filled sections of the extruders.

For the reference extruder, the calculated values of the thermal time are also shown in Table 4.3. In the case of the ZSE-96 device, to obtain a similar value for this parameter as the one corresponding to the reference extruder, a trial and error procedure was implemented varying both the screw speed and mass throughput of the larger extruder. In such an iterative scheme, the initial mass throughputs are the ones shown in this same table, and the initial screw speed was set to 100 rpm. In order not to cause changes, or to minimize such changes, in the DOF profile of the extruders, both the screw speed and mass throughput were varied simultaneously accordingly to equations 4.1a and 4.1b. It should be stated here that the implementation of the latter equations is equivalent to keeping a constant value for the M/N ratio. The reason to vary the screw speed is clear, since the variation of this parameter causes a modification of the residence time of the extruder (see equation 4.1a), and thus of the thermal time. It was observed in this study that an increase of the screw speed, and therefore of mass throughput (according to equations 4.1a and 4.1b, as previously stated), caused a decrease in the value of the thermal time, and vice versa. This fact was used to improve the convergence of the calculation procedure of the scaled-up mass throughput corresponding to constant thermal time. In all of the simulated cases, the accepted value for the thermal time was set to ± 1 % of the corresponding value of the reference extruder. The procedure just described corresponds to the proposed scale-up approach previously addressed in this work, and this procedure is summarized by means of Figure 4.3. From Table 4.3, it can be seen that the final Mw as well as PDI values for the LSM-30.34 extruder are very close to the ones of the scaled-up machine. As a means of facilitating the reading of this table, the values of these parameters have been shaded for the simulations corresponding to a mass throughput of 8.0 kg/hr and a peroxide concentration of 0.02 wt % (for the reference extruder) and the corresponding scaled-up conditions.

In Figures 4.4 and 4.5, the variation of the average residence time of extrusion and the average temperature of reaction are shown for fixed peroxide concentrations. The temperature corresponds to the average temperature along the axial length of the extruder where the reaction is taking place. This is also the length where equation 4.2 is evaluated, and such length spans from the start of the first fully-filled zone downstream of the peroxide injection point to the entrance of the die. It is important to remind the reader that the extrusion residence time and the temperature of the reaction shown for the ZSE-96 extruder, in Figures 4.4 and 4.5, correspond to points having a similar thermal time to that of the LSM-30.34 extruder operating under the reference screw speed and mass throughput (see Table 4.3). In general

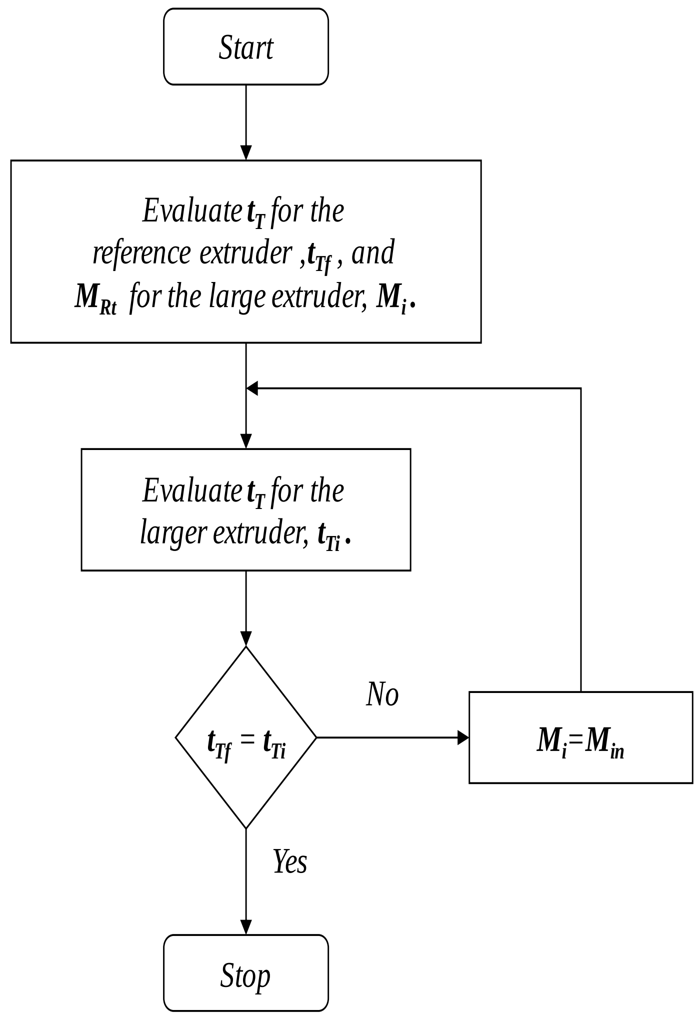

Figure 4-3 Proposed scale-up procedure for the constant thermal time approach. Where t_T stands for thermal time; t_{Tf} is the thermal time of the reference extruder; M_{Rt} represents the scaled mass throughput under constant residence time; M_i, and t_{Ti} are the mass throughput and thermal time values of the larger extruders, respectively, at the calculation step i; and M_{in} is the updated value of the mass throughput calculated accordingly to equations 4.1a and 4.1b.

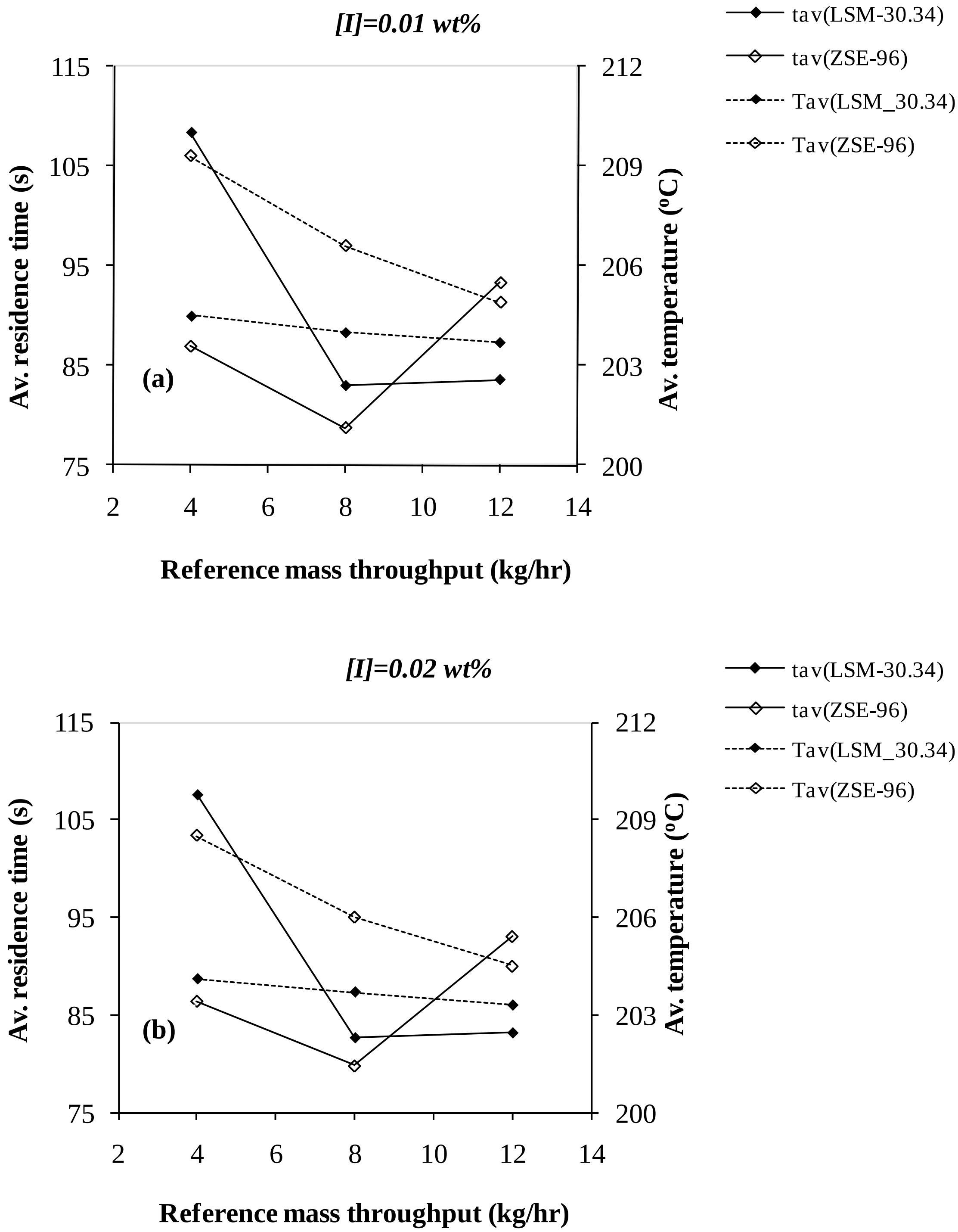

Figure 4-4 Average residence time (tav) and temperature (Tav) of reaction as a function of the mass throughput. The corresponding peroxide concentrations are (a) 0.01 and (b) 0.02 wt %.

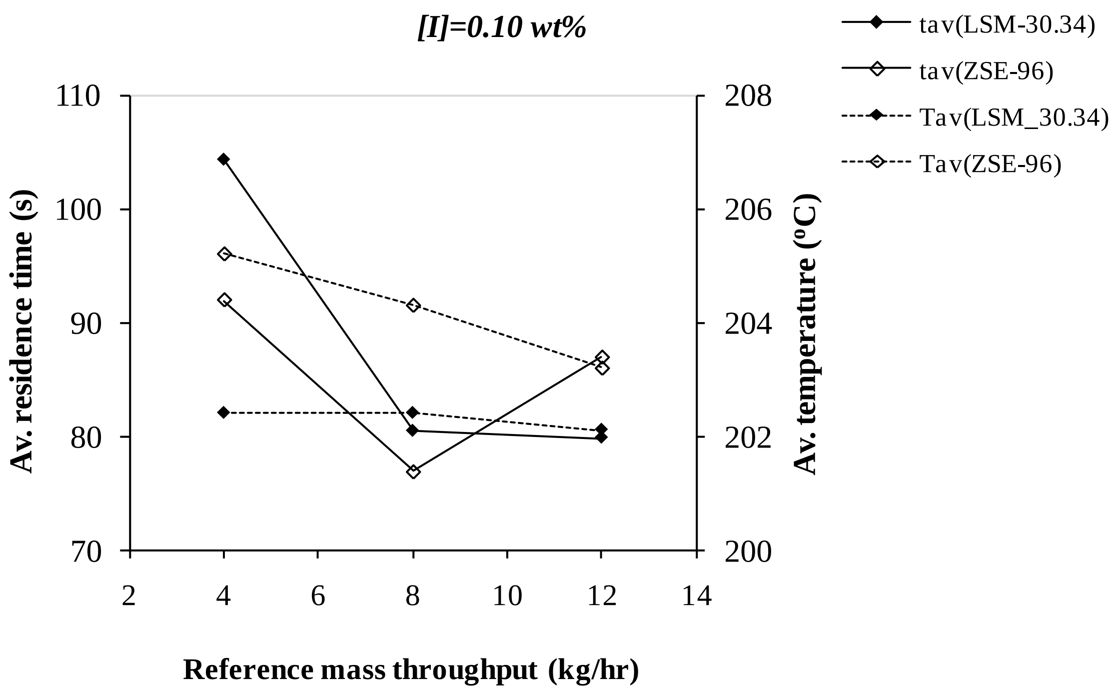

Figure 4-5 Average residence time (tav) and temperature (Tav) of reaction as a function of the mass throughput for a peroxide concentration of 0.10 wt %.

terms, the behavior observed for both the average temperature of reaction and the average extrusion residence time in the reference extruder is very similar for the three different peroxide concentrations being simulated. The observed trend for the temperature is a slight decrease of this variable as the mass throughput increases. In the case of the residence time, still for the reference extruder, this variable significantly decreases when the mass throughput changes from 4 to 8 kg/hr, but remains almost constant when the mass throughout is further increased to its final value. This behavior can be related to the decrease of the pressure-driven back flow in the extruder as the mass throughput increases. The effect of the pressure gradient along the axial distance of the extruder can be explained by means of Figure 4.6. From this figure, it can be appreciated that as the mass throughput increases the pressure gradient per unit length decreases. This in turn gives rise to less restricted flow conditions, which can explain the observed trend in the residence time for the LSM.30.34 extruder.

In the case of the larger extruder (see Figures 4.4 and 4.5), also a very similar trend in the processing parameters being analyzed is observed regardless of the peroxide concentration of the initiator in the feed stream. In this case, the temperature decreases as the mass throughput increases, but the temperature drop is more significant than the one observed for the reference extruder. The variation of the residence time is rather interesting because when the mass throughput increases the residence time decreases, but when the mass throughput further increases a significant increase of the residence time is observed in order to preserve the conditions of similar thermal time. In this latter situation, conversely to what is observed for the reference mass throughputs of 4 and 8 kg/hr, the simulated scaled-up residence time is greater than the one corresponding to the reference extruder.

The fact that for the ZSE-96 extruder and the scaled-up mass-throughput corresponding to 12 kg/hr (in the reference extruder) the residence time is greater than that of the LSM-30.34 device is explained as follows. If the fully-filled length of the reacting-zone in both extruders were the same, then the previously described behavior would be inaccurate. This because the temperature of reaction in the larger extruder should be greater than the one of the smaller extruder, and then its reaction residence time should be lower than the one corresponding to the reference machine. However, this seemingly contradictory situation can be related to the fact that the length of the zone of reaction of the larger extruder is less than that of the reference device, see Figure 4.2. Then, in order to keep a similar conversion of reaction (and

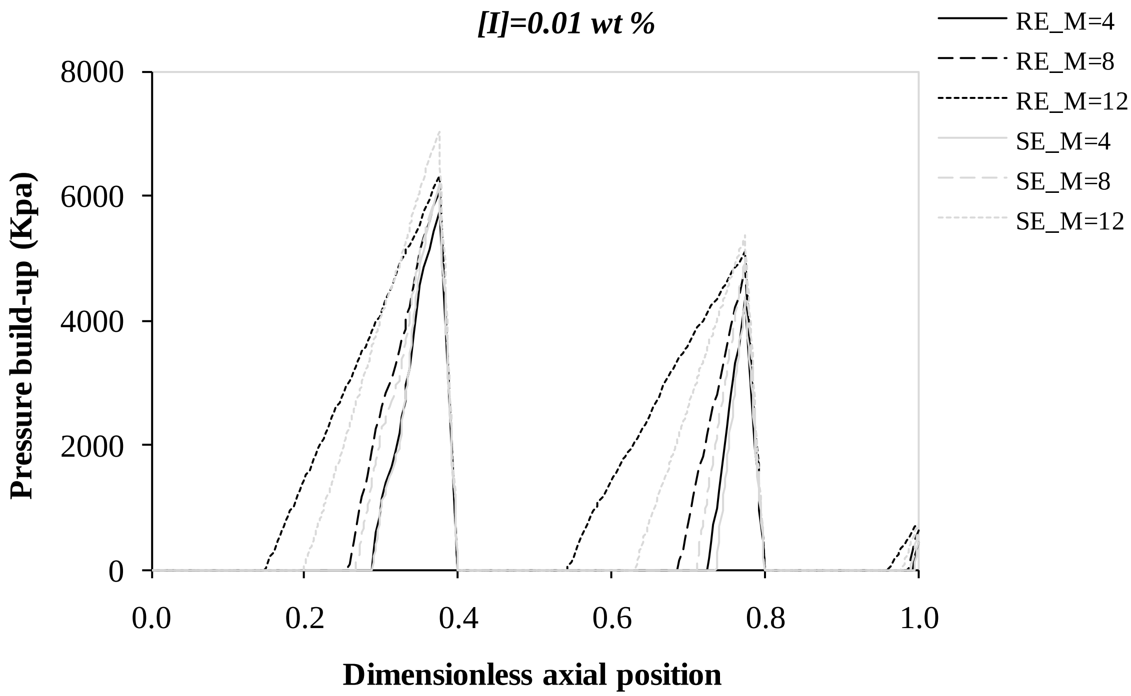

Figure 4-6 Pressure build-up variation along the axial distance of the extruders for the different specified reference and scaled-up mass throughputs. [I] represents the peroxide concentration and M the reference mass throughput, in Kg/hr.

hence, similar values of both Mw and PDI), implied by the similar thermal time scale-up approach, the residence time of the reaction is increased.

In Figure 4.7, the corresponding variations for both the Mw and PDI are presented for the LSM-30.34 extruder. One should be reminded that the values of these variables for the larger extruder are essentially the same to those of Figure 4.7, as previously discussed, because of the assumption of constant thermal time. With respect to the variation of the peroxide concentration (for a constant mass throughput), the general trend for both the Mw and the PDI is as expected, i. e., a slight decrease in both variables when the peroxide concentration varies

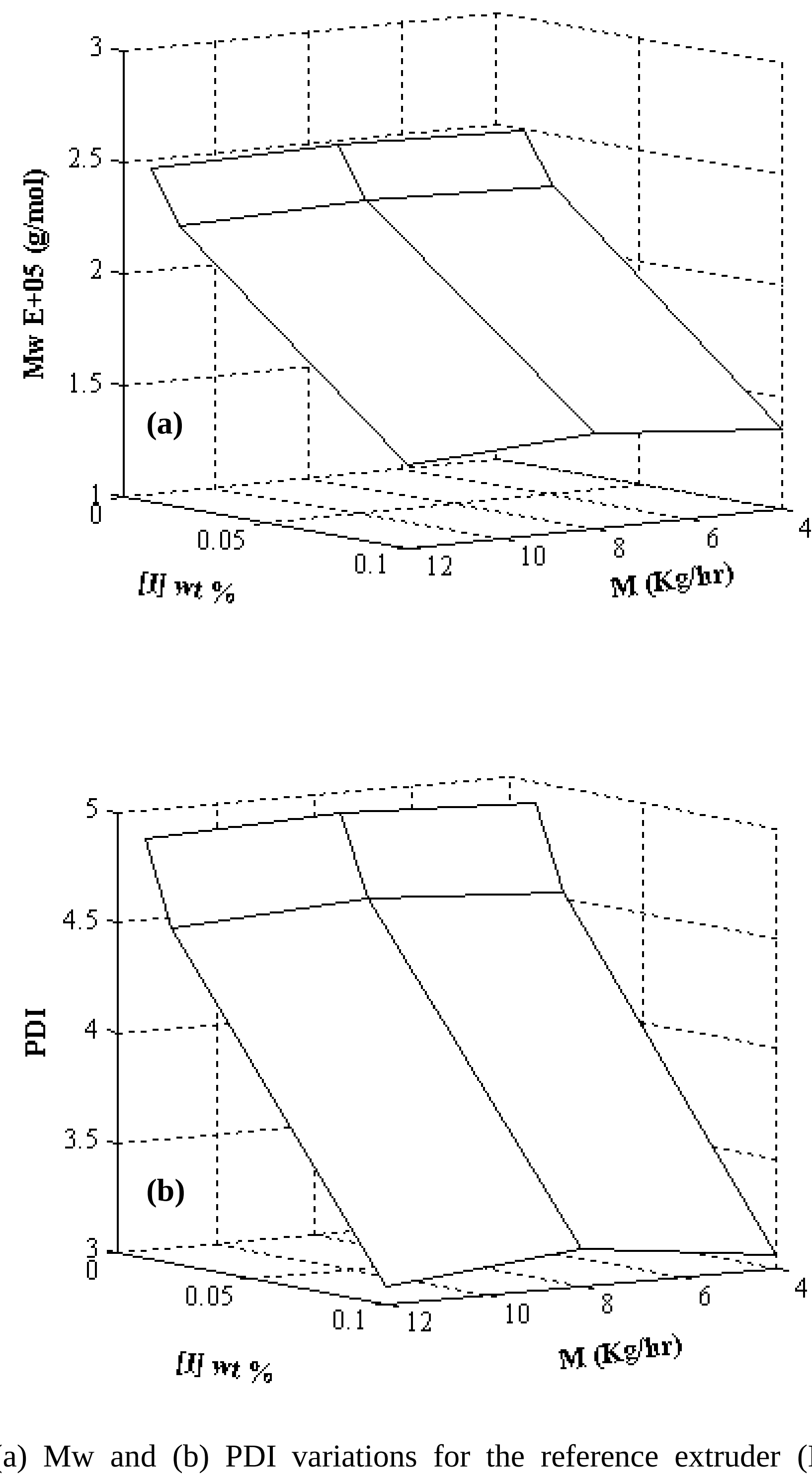

Figure 4-7 (a) Mw and (b) PDI variations for the reference extruder (LSM-40.34) as a function of both the mass throughput and the peroxide concentration.

from 0.01 to 0.02 wt % but a much significant reduction when the value of the peroxide concentration is set to 0.10 wt %. The evolution of these two variables when the mass throughput is varied is very similar regardless of the value of the peroxide concentration. In both cases (Figures 4.7a and 4.7b), when the mass throughput is increased from 4 to 8 kg/hr an increase in the final values of the Mw and PDI is observed. However, when the mass throughput further increases to its upper limit, a reduction in both of the aforementioned processing variables is appreciated. Taking into account that a higher Mw indicates a lower conversion of reaction, the previously referred behavior suggests that although the overall extrusion residence time is approximately the same for the mass throughputs of 8 and 12 kg/hr, the actual residence time of reaction (the residence time in the reaction zone) is greater for the latter mass throughput value. This suggestion is confirmed by performing the calculation of the corresponding residence times of reaction for the aforementioned cases (which in not shown here but can be verified from the complete set of data of the corresponding simulations).

Finally, in Figure 4.8 the ratio between the mass throughputs of the larger extruder calculated from equation 4.1b under the assumption of constant residence time (see Table 4.3) and that corresponding to the scale-up under constant thermal time is presented. The horizontal axis in the plot shown in this figure corresponds to the mass throughput of the reference extruder (the one being scaled-up). In general terms, it can be appreciated that for all of the analyzed peroxide concentrations this ratio decreases as the reference mass throughput increases. Also, it is interesting to note that while for the lowest mass throughput used to simulate the reference extruder the corresponding scaled-up value is greater than the one calculated by equation 4.1b, an opposite situation occurs for the highest value of this

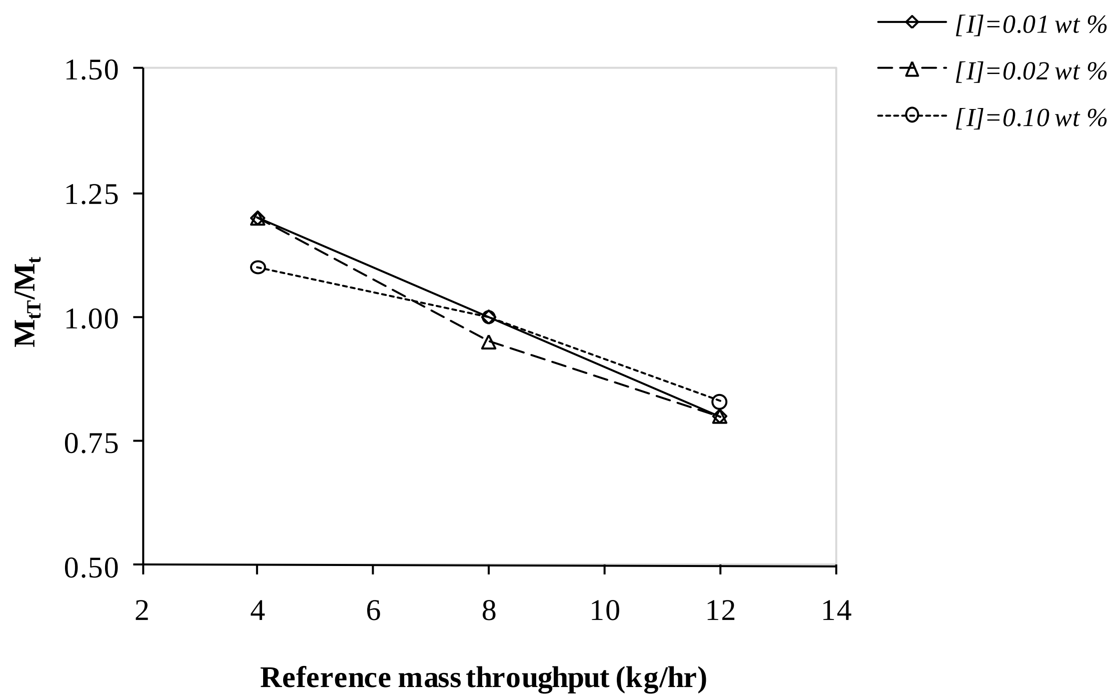

Figure 4-8 Ratio between the mass flow rates scaled-up under the constant thermal time and constant residence time approaches. M_{tT}/M_t represents the ratio of the mass throughputs corresponding to constant thermal time and residence time, respectively.

parameter. The behavior observed for the highest value of the reference mass throughput is similar to the one found in conventional extrusion operations, where the scaling-up index for the mass throughput is usually lower that the one predicted by equation 4.1b (in a conventional extrusion operation this is due to heat transfer constraints).

4.3 Mass Throughput and Screw Speed Analysis

As in the previous analysis, the physical properties of the PP used for simulating the REX operation are given in Table 4.1. In Table 4.4, some parameters related to the geometry of the extruders simulated in this section are presented. In Table 4.5, the processing conditions used to initialize the scale-up procedure under constant thermal time are summarized. Also, in this table some results of interest corresponding to the same scale-up approach are presented. The peroxide concentration for all of the simulations performed in this section was set equal to 0.02 wt %, and the peroxide injection point was specified at a dimensionless axial distance of 0.45. The diehead pressures for the reference extruder were computed considering a two-hole strand die having a length and diameter of 12 mm and 4 mm, respectively. These pressures were specified as fixed values within the set of operating conditions of the REX operation being scaled-up. The reference extruder as well as its configuration is that one presented in the previous section, in Figure 4.1. The length of the screw conveying elements and kneading blocks of the larger extruders has been scaled-up proportionally to d^1.

In the previous section, the effect of both the peroxide concentration and the mass throughput on the REX process scaled-up from a reference extruder operating under constant screw speed was briefly addressed. In what follows, the effect of two different screw speeds, keeping a constant peroxide concentration will be analyzed. From Table 4.5, it can be seen that for the lower value of the screw speed (in the case of the reference extruder), the same mass throughputs considered in the previous section are implemented here, with the exception of the intermediate value of this parameter. The reason for this is that some characteristics of the process under these conditions have already been addressed in this work, at least for the reference and ZSE-96 extruders. The corresponding mass throughputs for the screw speed of 200 rpm were chosen to keep a constant value of the ratio between the mass flow rate and the screw speed (M/N). This later relationship is directly related to the ratio of the volumetric flow rate to the screw speed, Q/N. It should be noticed that maintaining a constant M/N should, in

Table 4-4 Geometrical parameters used for the extruders being simulated (data from Leistritz®). Also the values for some of the parameters used to evaluate the set of equations 4.1 are indicated. The value of the scale-up index v is used only when scaling-up under constant SEC.

TSE model	Screw outer diameter (mm)	Center line distance (mm)	Flight depth (mm)	Barrel inner diameter (mm)	d	h	V
LSM-30.34	33.70	30.01	3.99	34.00	---	---	---
ZSE-50	49.70	42.79	7.21	50.00	1.47	1.52	2.02
ZSE-67	66.70	58.95	8.05	67.00	1.98	1.03	0.11
ZSE-96	95.60	83.90	12.10	96.00	2.84	1.06	0.25

principle, yield a similar DOF profile. Thus, one can assume that this profile for the screw speed of 200 rpm lies within the previously selected working conditions (see Figure 4.2), i. e., it is expected that the limit of fully-filled conditions along the whole axial length of the extruder is avoided. The scaled-up mass throughputs corresponding to the other extruders being simulated are calculated by means of equation 4.1b with the value of v set to 0 (corresponding to the case of scaling-up under constant residence time).

From Figure 4.9a, a similar trend in the evolution of the residence time of extrusion as a function of the size of the extruders when the M/N ratio is kept constant can be appreciated. In general terms, for the lower value of M/N the residence time of extrusion of the larger extruders is less than that one of the LSM-30.34 extruder, and an opposite situation is

Table 4-5 Simulation results of interest for scaling-up under constant thermal time. E. M. stands for extruder model; M represents the mass throughput; ΔP, the pressure drop in the die; T_{AB}, the average temperature of reaction; R_t, the average residence time of extrusion; Mw and PDI, the final weight-average molecular weight and polydispersity-index, respectively; t_T, the thermal time; and M_{tT}/ M_t is the ratio of the mass throughputs corresponding to constant thermal time and residence time.

E. M.	N (rpm)	M (kg/hr)	ΔP (KPa)	R_t (s)	T_{AB} (° C)	Mw $x10^{-5}$ (kg/kmol)	PDI	$t_T x10^{12}$ (s)	M_{tT}/ M_t
LSM-30.34	100	4.0	374	108	204	2.26	4.53	0.98	---
		12.0	632	83	203	2.26	4.52	1.01	---
	200	8.0	517	54	208	2.34	4.65	0.63	---
		24.0	890	42	206	2.35	4.67	0.59	---
ZSE-50	100	15.7	374	108	205	2.26	4.53	0.98	0.97
		47.2	632	100	203	2.26	4.52	1.00	0.75
	200	31.4	517	53	209	2.34	4.65	0.63	0.97
		94.3	890	52	205	2.35	4.67	0.59	0.72
ZSE-67	100	31.6	374	96	207	2.26	4.53	0.95	1.08
		94.8	632	95	204	2.26	4.52	1.02	0.78
	200	63.2	517	40	214	2.34	4.65	0.63	1.26
		189.3	890	47	206	2.35	4.67	0.59	0.78
ZSE-96	100	97.6	374	86	208	2.26	4.53	0.98	1.20
		292.8	632	93	204	2.26	4.52	1.02	0.80
	200	195.2	517	37	216	2.34	4.65	0.63	1.37
		585.7	890	49	206	2.35	4.67	0.59	0.75

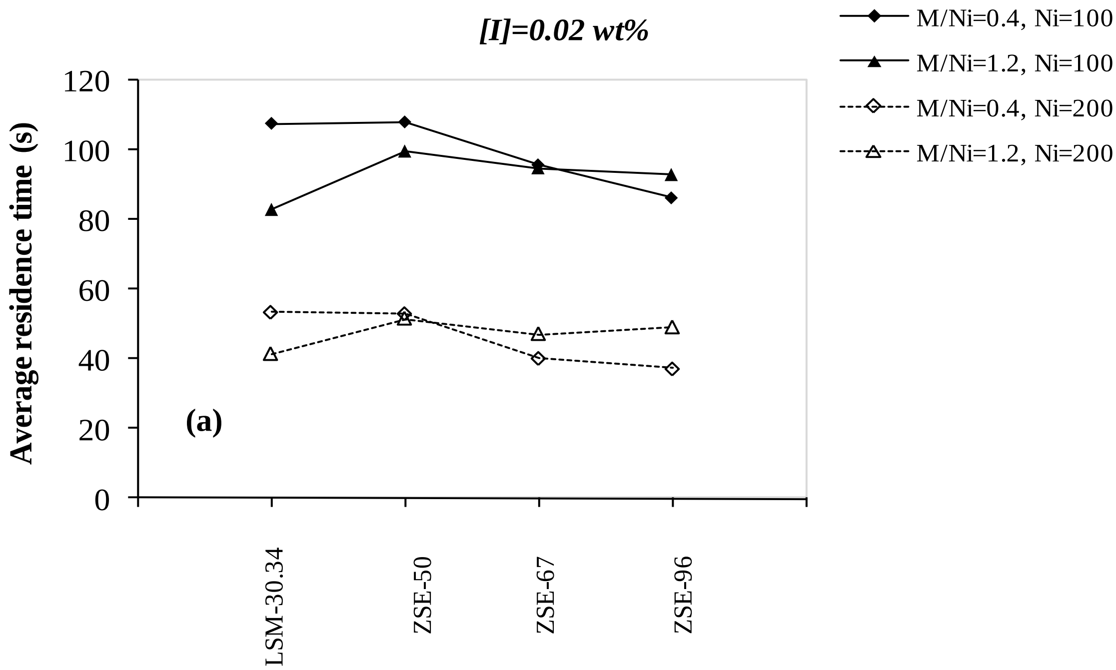

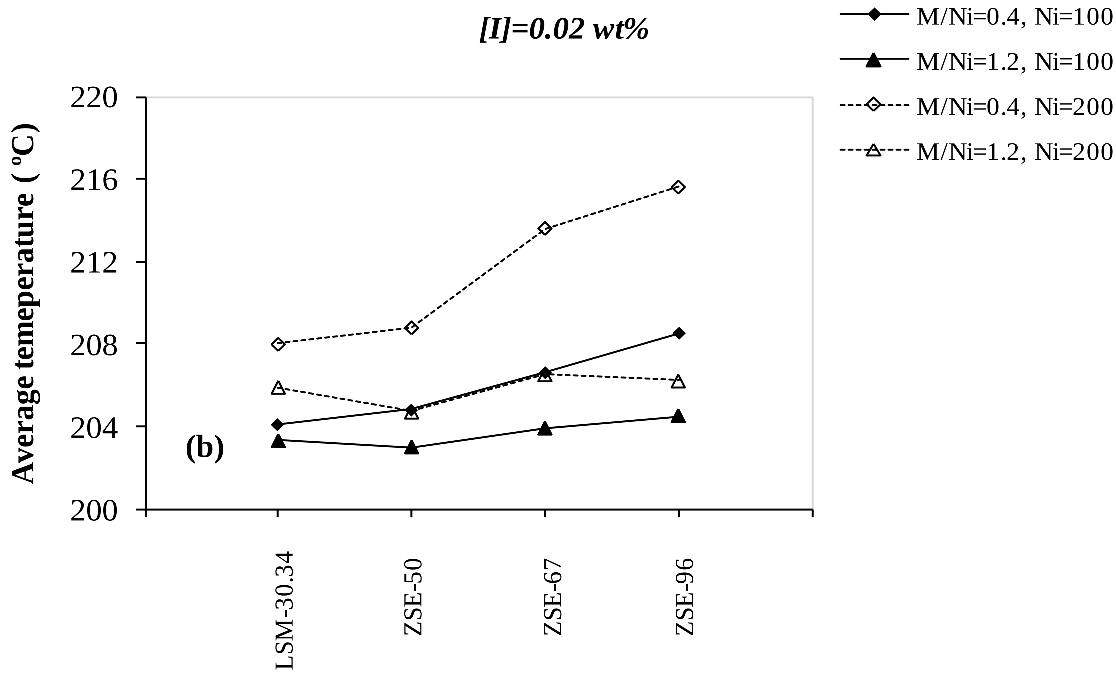

Figure 4-9 (a) Average residence time and (b) temperature of reaction for the scale-up under the constant thermal time approach. The subscript i indicates conditions for the reference extruder.

observed for the higher value of this ratio. It can be also appreciated from Figure 4.9a that for a constant screw speed, in the case of the reference extruder, when the mass throughput increases, the predicted time of extrusion decreases, as expected. With respect to the variation of the average temperature of reaction (Figure 4.9b), when M/N=0.4 an increase of the value of this parameter, for all of the larger extruders, is observed as the size of the extruder increases. When M/N=1.2, there is not a clear trend in the evolution of the temperature of reaction related to the increase of the size of the extruders. However, it can be seen that the temperature of reaction is higher for the larger devices than for the reference extruder, except in the case of the SZE-50 extruder. Overall, it can be noticed that the increase of the temperature of reaction is significantly more important in the case of the lower value of M/N. This can be related to an increase of the viscous dissipation effects as the screw speed is increased or the mass throughput is decreased. The dependence of the viscous dissipation on the screw speed is more obvious since the energy dissipated by viscous effects is proportional to the shear rate to the power $1+n$, n being the power-law index (considering the power-law model to apply). The viscous dissipation effects observed when the mass throughput decreases suggests that at low values of this parameter the flow is more restricted in the fully-filled sections of the extruder than at higher mass throughputs. This is also in agreement with what is observed from Figure 4.6, which indicates that the pressure differential, along the axial direction of the extruder, per unit length is higher for the lower values of the mass throughput. Under these more restricted flow conditions, more energy would be dissipated due to the friction occurring between the polymeric fluid layers.

The just addressed different behavior of the SZE-50 extruder will be briefly explained below in this document, and it is also explained in the work by Ortiz and Tzoganakis (2008).

On the other hand, conversely to what is observed by these authors, the results of this section do not show a clear relation regarding the variation of the temperature of reaction and the average residence time of extrusion, i. e, a decrease of the residence time as the temperature of reaction increases. This is due to the fact that in both this and the previously referred works the average residence time of reaction is not being plotted but the average residence time of extrusion. Furthermore, in the study presented by Ortiz and Tzoganakis (2008), a low value of the mass throughput was used for the calculations, and as can be seen from Figure 4.2 under such conditions, the lengths of the fully-filled zones of the reference and scaled-up extruders are very close to each other. In summary, the results of Figure 4.9a do not follow the expected behavior of a reacting system mainly because of the differences in the fully- and partially-filled conditions prevailing along the extruder for the different devices being analyzed.

In Figure 4.10, the variation of the overall average residence time and temperature of reaction for the constant SEC scale-up approach is presented. In the case of the residence time (Figure 4.10a), a very similar evolution of this parameter is observed regardless of the M/N value or screw speed of the reference extruder. In this case, a decrease of residence time is observed for all of the analyzed extruders. For the ZSE-50 extruder this variation is significantly greater than the one corresponding to the SZE-67 machine. Regarding the variation of the temperature of reaction, for the lower value of M/N a very similar pattern is observed for the two analyzed screw speeds. When M/N=1.2, however, the results do not show a clear trend, and the temperature increase in both cases is significantly lower than the one observed when M/N=0.4, as in the case of the constant thermal time approach. Also, similarly to what is observed for the latter scale-up approach, the behavior exhibited by the SZE-50 extruder is different from the one observed for the larger extruders.

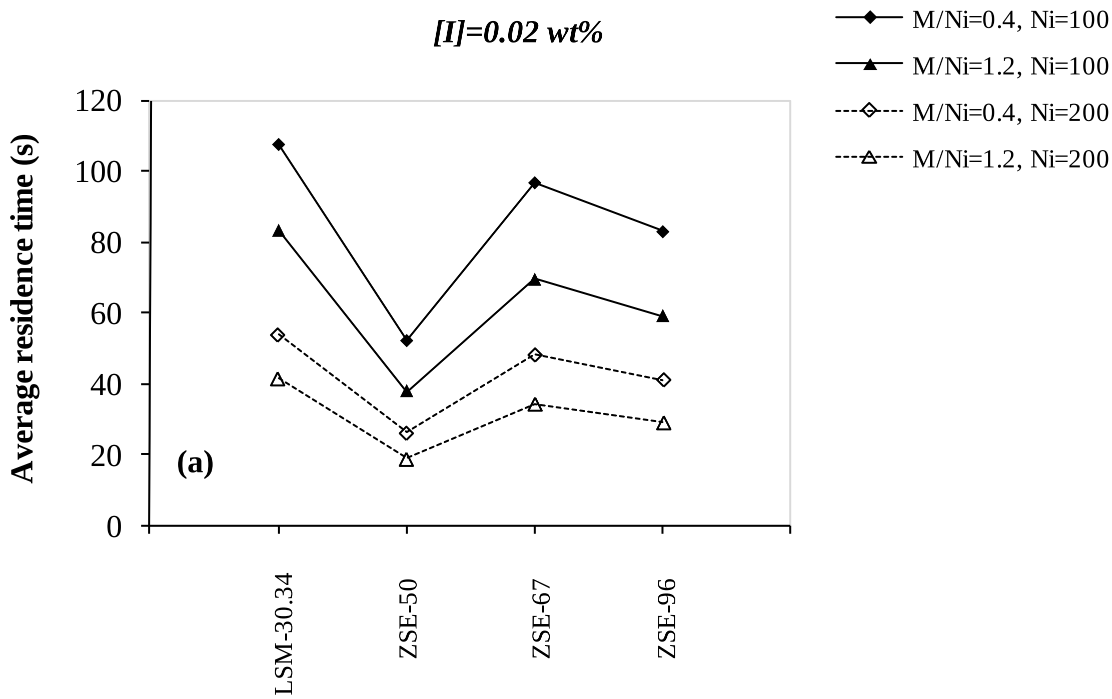

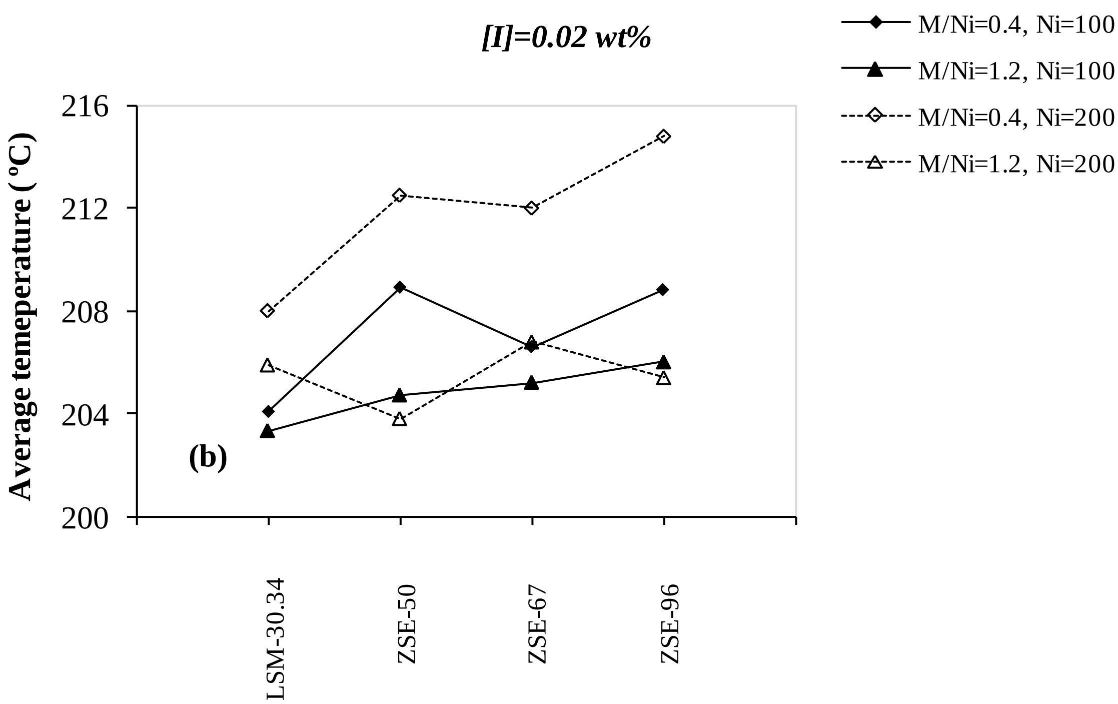

Figure 4-10 (a) Average residence time and (b) temperature of reaction for the scale-up under the constant SEC approach. The subscript i indicates conditions for the reference extruder.

The variation of the thermal time for the constant SEC scale-up approach is presented in Figure 4.11. A very similar trend is observed for the variation of this parameter for the simulations corresponding to the same value of M/N of the reference extruder. With respect to the effect of the screw speed, lower values of thermal time are obtained when this parameter is increased for a constant M/N ratio. It can also be appreciated from Figure 4.11 that for the lower mass throughput of the reference extruder and the lower screw speed (M/N=0.4, N=100 rpm), very similar values of thermal time are obtained for the scaled-up operating conditions corresponding to the larger extruders, except for the ZSE-50 machine.

In Figure 4.12, the variation of the ratio of the mass throughput of the larger extruders calculated by using a constant thermal time and SEC approaches to the one corresponding to constant residence time is presented. The corresponding scale-up index v used to evaluate equation 4.1b in the case of constant SEC is calculated from equation 4.1c, and is presented in Table 4.4 for each one of the analyzed extruders. The power-law index used in all of the cases to calculate v was n=0.43, and it was calculated using a simplified procedure. Under such a procedure, this value of the power-law index was assumed to be representative of both the temperature and weight-average molecular weight effects on the viscosity of the molten polymer under the operating conditions being simulated.

In the case of constant thermal time, it can be seen from Figure 4.12 that, except for the ZSE-50 extruder, for the higher M/N ratio the scaled-up mass throughput is less than that one predicted assuming constant residence time. However, an opposite situation is observed for the lower value of this parameter. In this latter situation, when the screw speed of the reference extruder, Ni, is set equal to 100 rpm, the evolution of the mass throughput ratio in the case of the constant SEC procedure is very close to that one obtained when constant thermal time is

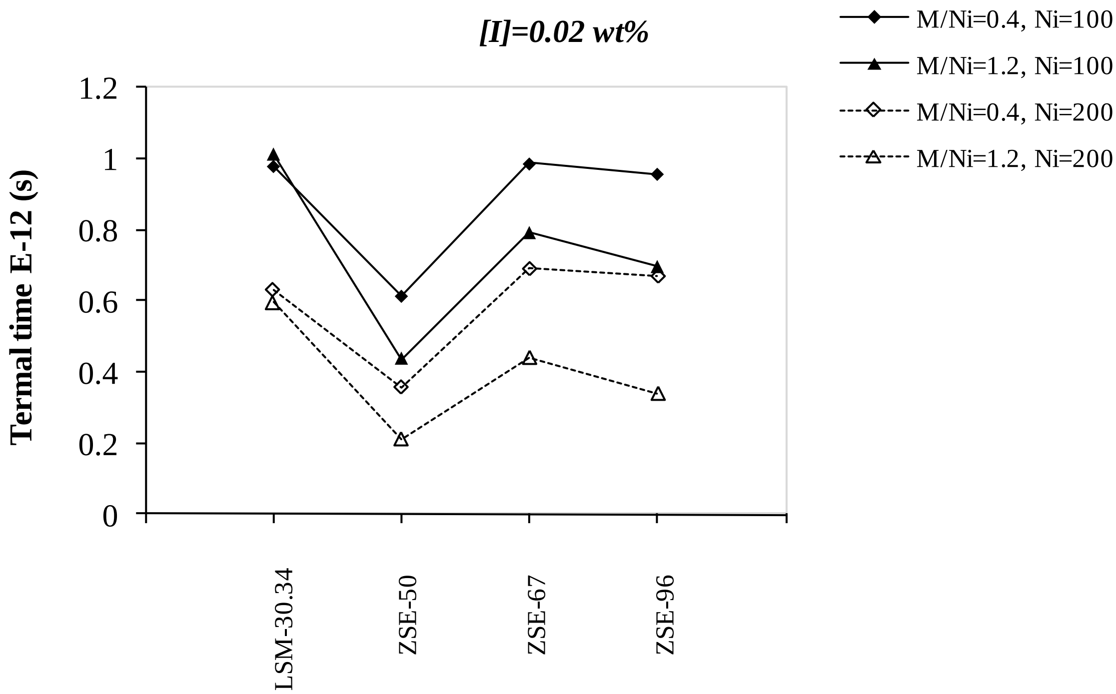

Figure 4-11 Thermal time variation (constant SEC approach). The subscript i indicates conditions for the reference extruder.

assumed (with the exception of the ZSE-50 extruder). Thus, for the aforementioned conditions very similar values of PDI and Mw are expected to be obtained regardless of the scale-up approach being implemented.

The results from Figure 4.12 are essentially in agreement with those of Figure 4.8. In both of these figures, for the lowest value of the reference mass throughput the scaled-up mass throughputs under constant thermal time are lower than the one corresponding to scaling-up under constant residence time and vice versa, again with the exception of the ZSE-50 extruder. These results seem to be mainly related to the differences in the DOF profiles of the reference and scaled-up devices. The explanation for such a behavior can be tracked back to Figure 4.2.

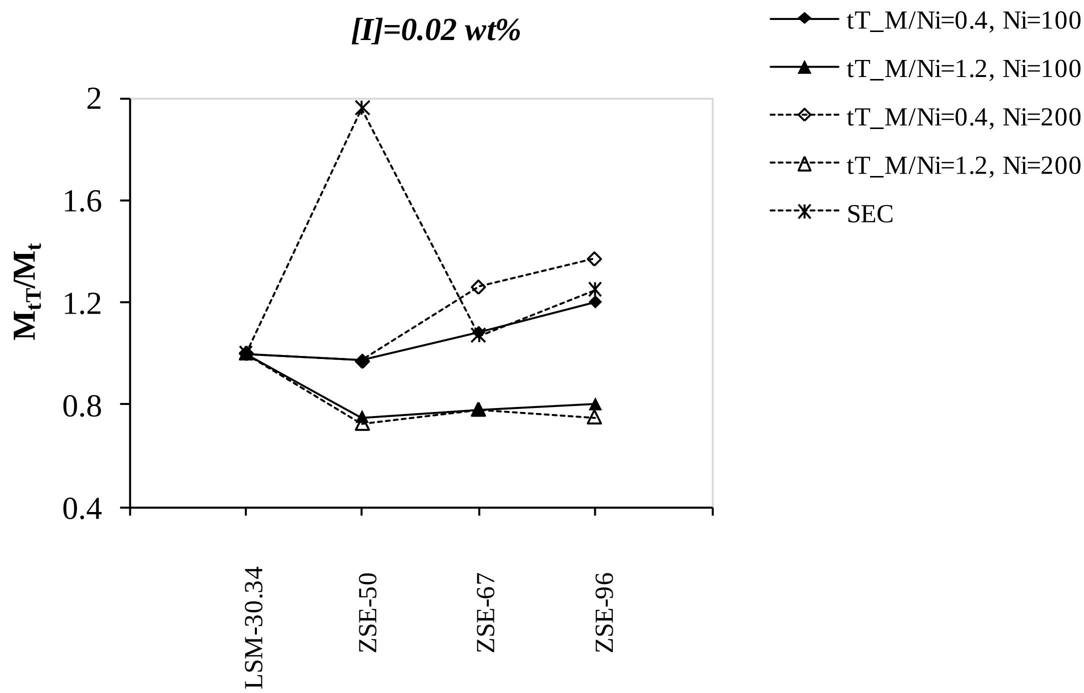

Figure 4-12 Variation of the mass throughput ratio for both the constant thermal time and SEC approaches. Here, the subscript i indicates conditions for the reference extruder.

In this figure, it can be appreciated that the DOF profiles at low mass throughputs are very similar. Therefore, since the temperature of reaction is higher in the larger extruders the residence time decreases in order that similar conversions of reaction can be kept. Then, as a decrease in residence time is associated with an increase in the screw speed, the latter results in a higher mass throughput (according to the proposed calculation procedure of simultaneously varying both the residence time and mass throughput by use of equations 4.1a and 4.1b). For the higher value of the mass throughput, again the temperature of reaction of the larger extruders is higher than the one corresponding to the reference extruder, but the predicted DOF is lower. Then, an increase of the residence time of the larger extruders is needed to compensate for this lower DOF value. Therefore, the screw speed has to be reduced which in turn causes a reduction of the mass throughput, again according to equations 4.1a and 4.1b (which also is translated as a constant M/N value).

In Figure 4.13, a comparison between the predicted Mws and PDIs for the constant thermal time as well as constant SEC scale-up approaches is presented. From this figure it can be appreciated that when the thermal time is kept constant, the scaled-up Mw as well as PDI values corresponding to the larger extruders are essentially the same to those of the LSM-30.34 extruder. For the constant SEC approach, when M/N=0.4, very close values of these parameters to those corresponding to the reference conditions being scaled-up are observed, especially for the lower screw speed (except for the ZSE-50 extruder). For the higher value of M/N, however, there is a more significant variation of these parameters. In this case, the difference between the Mws and PDIs of the reference extruder and the scaled-up values of these parameters are greater for the higher reference screw speed. From Figure 4.13, it can also be noticed that the Mws and PDIs of the reference extruder are dependent upon the initial reference mass throughput and almost independent of the specified screw speed (for a constant mass throughput).

The different trend of behavior observed for the ZSE-50 extruder which has been referred to in this section can be explained in terms of the parameters presented in Table 4.4. From this table, it can be seen from the scale-up indexes *h* and *v* that the extruders ZSE-67 and ZSE-96 are closely geometrically scaled-up versions of the reference device (*h* being close to 1 and *v* being close to 0). However, from these same parameters it can be appreciated that this is not the case for the ZSE-50 extruder. This may result in important differences in the shear rates experienced by the molten polymer in the case of the constant thermal time scale-up approach.

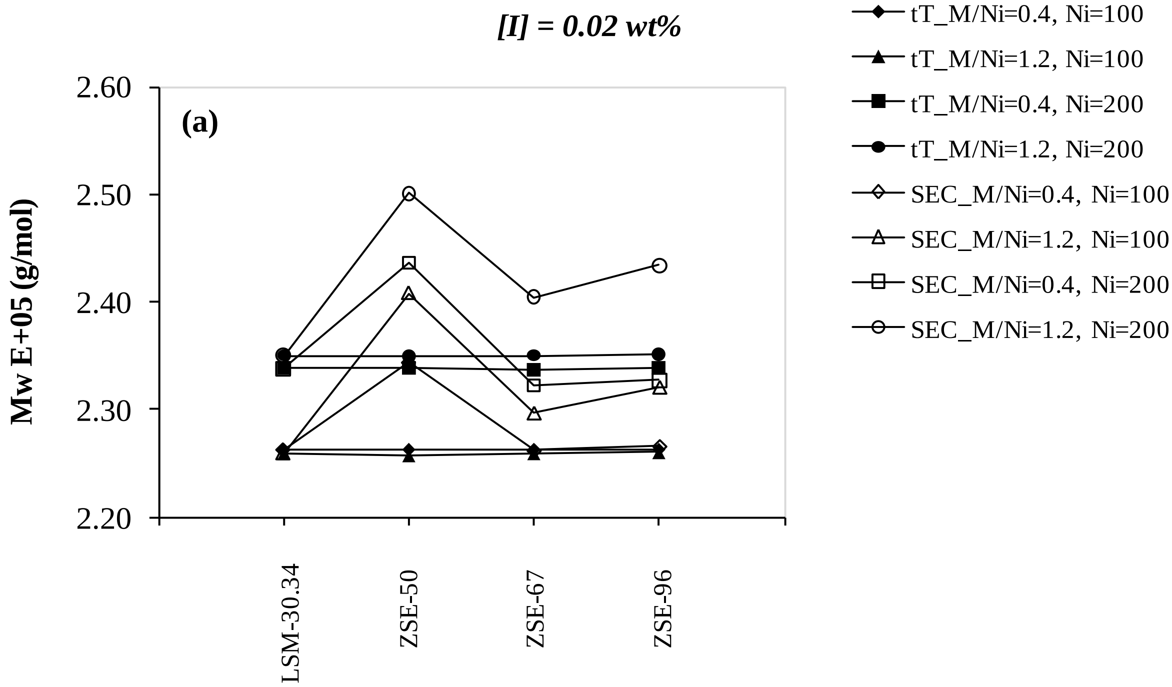

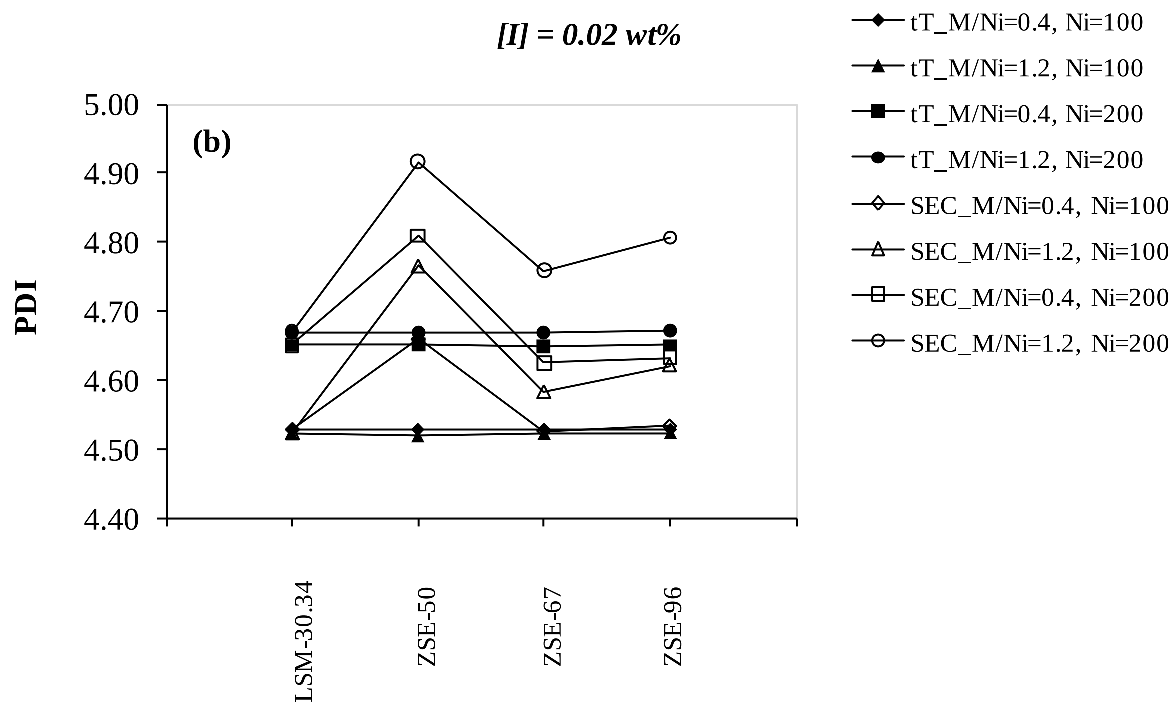

Figure 4-13 (a) Mw and (b) PDI variations for both the constant thermal time and SEC procedures. The subscript i indicates conditions for the reference extruder.

In the case of constant SEC, the screw speed is modified in order to yield similar shear rates. This causes very important differences in the residence time of the extruders, and therefore, in the yielded Mws and PDIs.

5 3D SCALE-UP CALCULATIONS

5.1 Background on the Implemented Simulation Approaches

For the 3D simulations to be presented in this chapter, two simulation approaches have been considered. These two simulation approaches involved a steady-state and a transient-state flow analysis. The implications of these calculation procedures are described below in this section.

5.1.1 Moving Relative System (MRS)

As has been previously stated, a very reasonable approach for describing the flow in COITSE screw elements is to implement transient simulations where the motion of the screws is taken into consideration. A different approach that has been used to simulate this type of flow elements is to consider a moving frame of reference, or moving relative system (MRS) (Böheme and Wünsch, 1997; Pokriefke, 2007; Ortiz-Rodriguez and Tzoganakis, 2009). By making use of this simulation approach, the flow field in the conveying screw elements can be dealt with as a steady-state flow. To illustrate the MRS approach, the reader can imagine an observer who is always moving at the tip of the flights of the screws, moving with the velocity of a moving frame of reference. The assumption of considering a relative system implies that at the screw and barrel surfaces a velocity vector in the axial direction that opposes the actual direction of the flow is imposed. The magnitude of such a vector is nT, n being the rotational speed and T the screw pitch. The previous description of the MRS is illustrated here by means of Figure 5.1.

For a non-reactive system, the assumption of time periodicity (transient analysis) of the flow and related fields is very reasonable. However, this approach does not seem to be appropriate for describing reactive systems where the fields describing the variation of the species concentration due to the reaction are not periodic in time. Therefore, in this study the MRS has been selected for performing the REX simulations of the system being analyzed. For the simulations performed in this work, however, the velocity vector identified as -nT in Figure 5.1 was only imposed on the screw surfaces. This consideration was aimed to keep the conditions of zero velocity at the screw barrel to better account for both the shear rates occurring in the gap between the barrel and the screw tip and the reaction conversions in the regions close to the barrel surface. From the results of the simulations, it is observed that with this modification of the original boundary conditions for the MRS the flow still behaves as a steady state flow, as will be shown below in this chapter.

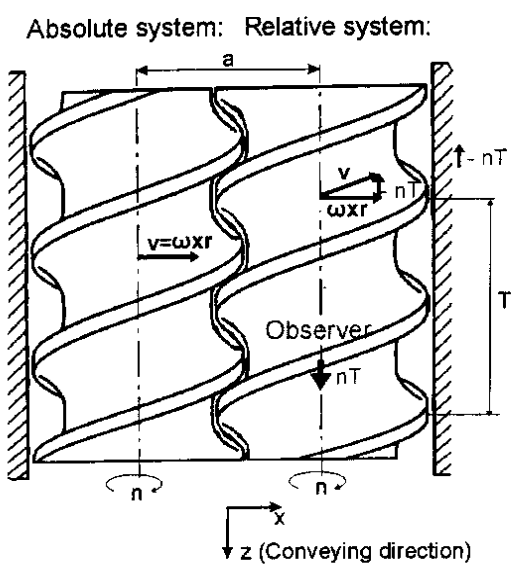

Figure 5-1 Physical interpretation of the MRS [After Pokriefke, 2007].

5.1.2 Transient-State (TS) vs MRS Simulation Analysis

Before proceeding with a further analysis of the REX system under the assumption of the MRS, a comparison between the simulation results obtained from TS analysis and the aforementioned approach is presented. In the case of the transient simulations, the mesh superposition technique (MST) has been implemented for the simulation of a fixed position of the rotating screws. The geometrical specifications for the conveying screw elements to be addressed and the main simulation conditions implemented for the present analysis are shown in Section 5.2.1.2 “Processing Conditions for Simulations”. In the case of the TS approach, some additional information including the mesh of the different implemented computational domains as well as thermal properties for the screws, in the case of the non-isothermal simulation, are included in Appendix B at the end of this thesis.

In Figure 5.2, a comparison between the temperature profile for the MST and the TS is presented. In this case, zero normal and tangential forces are defined both at the entrance and exit of the flow system. Under this consideration, the maximum volumetric flow rate for non-restricted flow conditions is obtained (Q_{100}). A power-law model is assumed, having a consistency index, *K*, and a power-law index, *n*, equal to 7505.2 Pas and 0.397, respectively. These values are obtained from the general power-law model presented in the previous chapter by using a temperature value of 210 ^{o}C. The temperature field in the case of the TS has been obtained for fixed position of the screws (quasi-steady state assumption). A constant temperature equal to 210 ^{o}C has been specified both at the inlet section and on the barrel surface of the flow system. The implemented boundary conditions for the screw surfaces are defined as adiabatic for the MRS, while for the TS a heat conduction problem is defined.

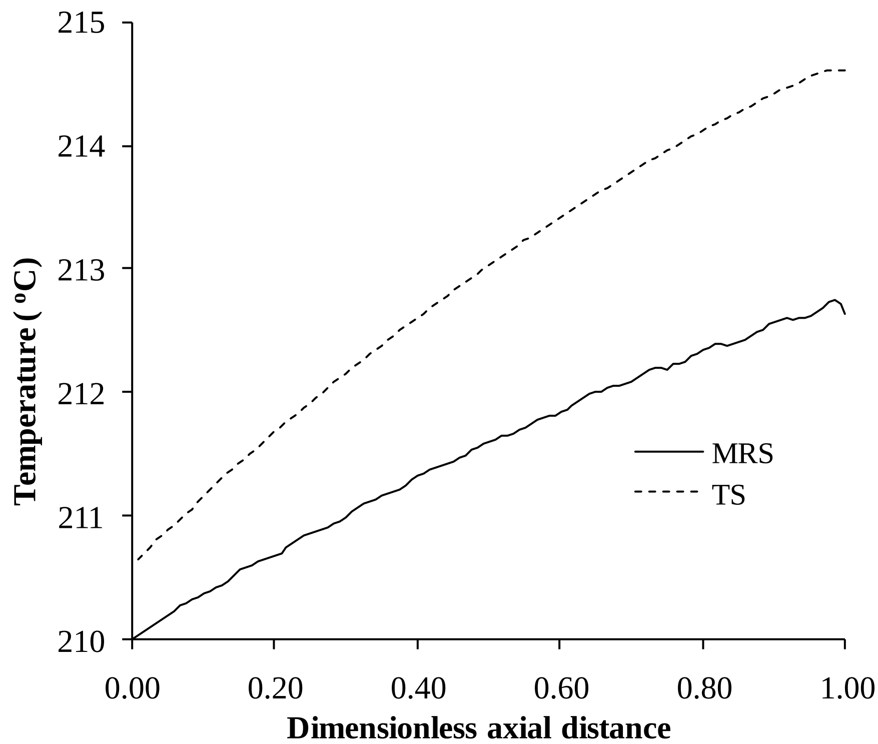

Figure 5-2 Temperature profiles for the TS and MRS simulation approaches. In both cases, non-reactive conditions are specified.

Here, it is important to state that for the TS approach, particularly when the MST is implemented, as the screws are treated as 3D solids which are also discretized for computational purposes, a heat conduction problem can be defined for the computational domains corresponding to the screws (POLYFLOW® examples manual, Avalosse et al., 2000). On the other hand, although for the MRS approach also a heat conduction problem may be defined for the screws of the conveying elements, in this work only the flow domain has been discretized (no computational domains have been defined for the screws). If no computational domains are defined for the screws, adiabatic conditions or constant temperature can be implemented on the surfaces of the screws (Zhu et al. 2005 a and b; Gupta, M., 2008), instead of the already mentioned heat conduction problem. As stated by Zhu et al. (2005 a) implementing adiabatic conditions for the screw surfaces is very reasonable for the case of small diameter extruders. Here, we have indistinctively used this boundary condition for both the reference and the larger screw elements. However, for future calculations, expected to be supported with experimental data, a comparison could be made between simulation results corresponding to the implementation of both adiabatic conditions and a heat conduction problem for the screws of the conveying elements.

The thermal properties of the screws used in the TS simulation are the same ones implemented in the work by Avalosse et al., (2000). It can be noted from Figure 5.2 that the temperature onset does not correspond to the specified boundary conditions (210 ^{o}C) at the inlet of the flow geometry in the case of the TS approach. This is due to the fact that in this case an entry section has to be defined where the flow system consists of the extruder barrel and two inner rotating cylinders. In general terms, it can be appreciated that the trend in the temperature rise is very close between the two analyzed simulation techniques for the given set of boundary conditions. Then, it may be expected that the MRS would yield a reasonable good approximation of the temperature field of the flow system under study.

In Figure 5.3, the pressure profile is presented for restricted flow conditions, i. e., the mass throughput is lower than the calculated Q_{100} value and hence a pressure profile is developed along the axial direction of the flow elements, under isothermal conditions for both the TS and the MRS approaches. In this case, and in what follows of this comparison analysis, Newtonian isothermal conditions, with a constant viscosity equal to 500 Pas, have been assumed for the

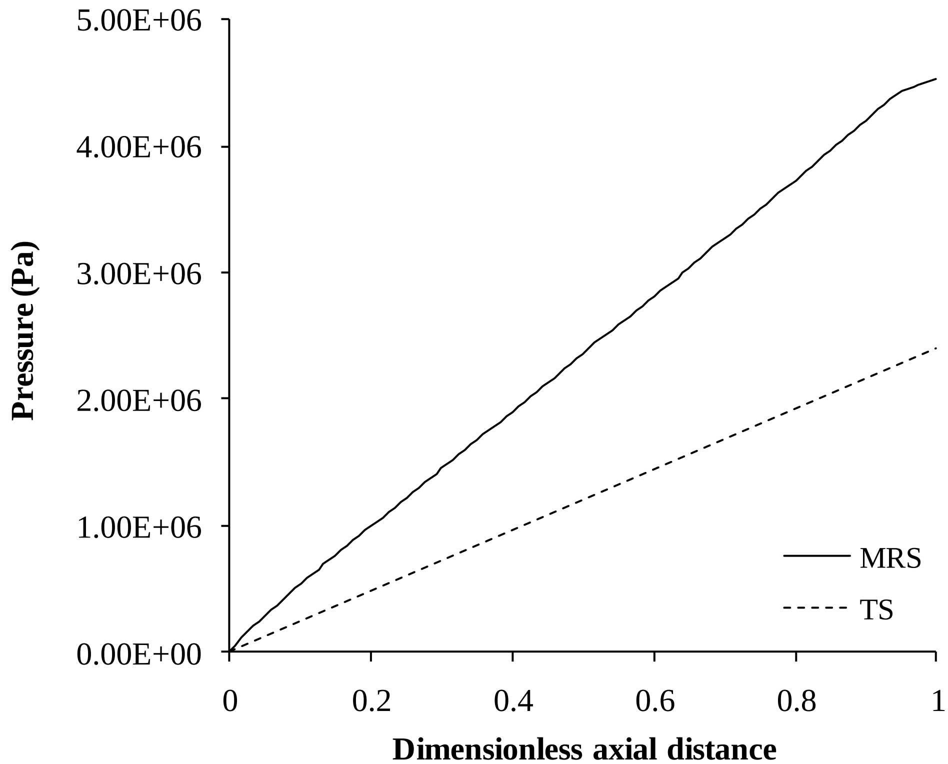

Figure 5-3 Pressure profiles for the TS and MRS simulation approaches.

simulations. In both of the cases being analyzed, the specified flow (Q_{50}) corresponds to half of the value corresponding to non-restricted flow conditions, Q_{100}. The dashed curve in Figure 5.3 (TS case) indicates an estimated trend of the pressure drop, based on the average pressure values at the inlet and outlet sections of the flow geometry. The actual profile for this case has not been calculated due to the fact that in the TS calculation approach the pressure field includes pressure values for the whole flow domain (as a consequence of the implementation of the MST), including the regions lying inside the screw elements. This latter implication means that if averaged cross-sectional values for the pressure profile were to be calculated, such values would be different from the actual ones developed in the conveying screw elements. Overall, it is evident that in the case of the MRS simulation technique the pressure field is not properly described, which may be directly related to the modification of the flow field as a consequence of the superposition of the axial component of the velocity, nT, on the surfaces of the extruder screws. Therefore, for a proper simulation analysis a more accurate description of the pressure field would be obtained from the conventional simulation approach where the flow is simulated for a fixed position of the screws (analysis for non-reactive conditions) and not with the MRS approach.

The evolution of the residence time distribution (RTD) is presented in Figure 5.4 for the same flow conditions described for Figure 5.3. In this case, for the TS analysis 15 positions of the screw elements were simulated to account for half of the rotation of the screws (time periodicity). In both the TS and MRS techniques, around 1000 randomly generated particles were specified (seeded) at the inlet section of the flow domain. Figure 5.4 clearly indicates that the shape of the RTD curves is not the same. However, the height and breath of the curves is relatively similar. For the TS, the RTD spans a wider range along the horizontal axis. One possible explanation for this behavior is the fact that in the MRS calculation the average residence time is approximately 40 % higher than that obtained when implementing the MST calculation procedure. The RTD curves presented in Figure 5.4 show a scattered behavior which has also been reported by Bravo et al. (2004). According to these researchers, such a behavior can be related to the non-diffusive nature of the tracked particles as well as the relatively low number of particles specified for the tracking.

In Figure 5.5, the analysis of the evolution of the area stretch ratio is presented for the simulation approaches being compared. The average values presented for the area stretch ratio

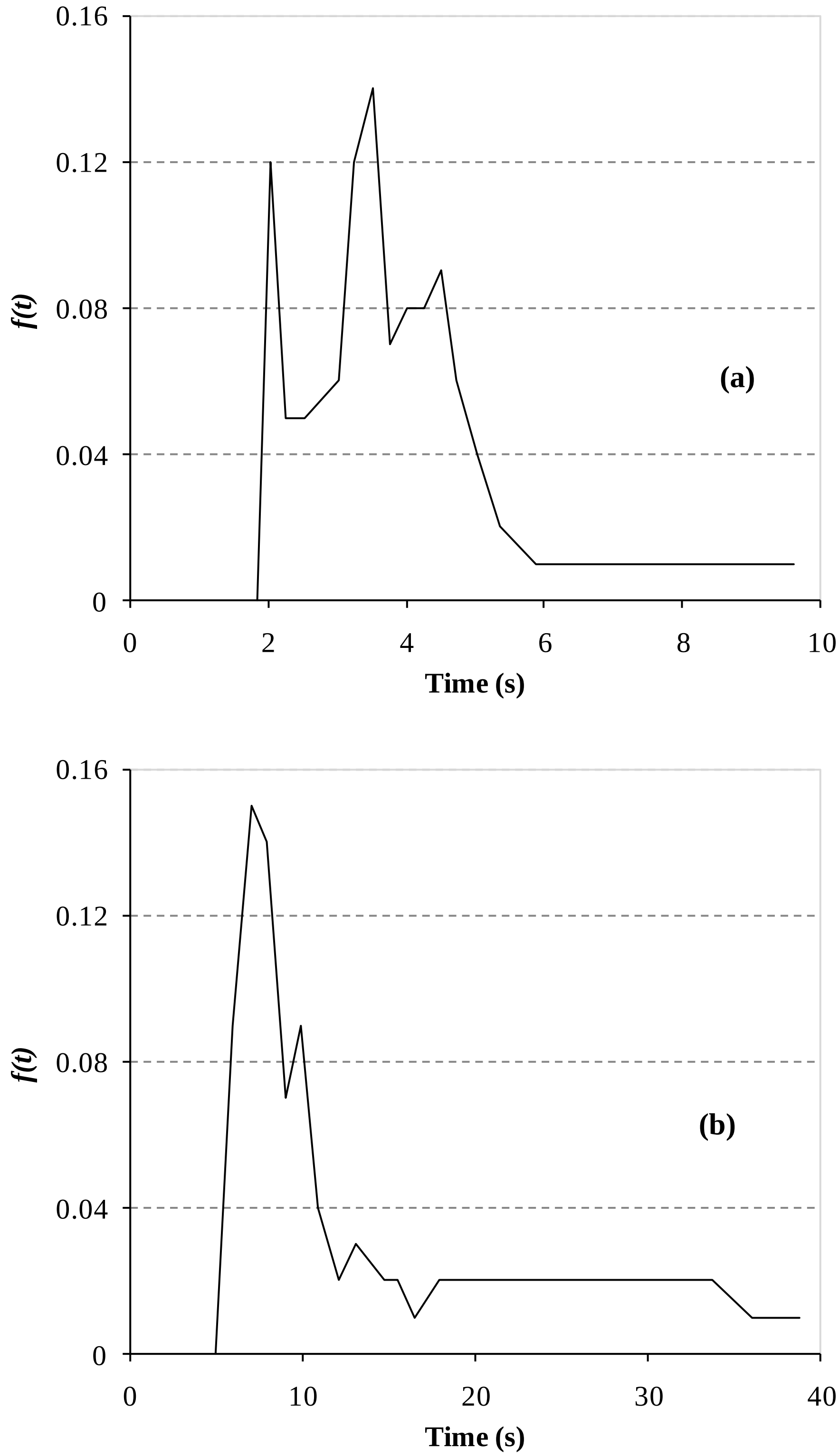

Figure 5-4 RTD curves for (a) the MRS and (b) the TS simulation techniques.

have been obtained by weighting the values of this parameter corresponding to individual tracked particles by the velocity vector, using a weighting of the type normal velocity everywhere (according to the Polystat user's guide, included with the POLYFLOW® documentation files). In this case, and in what follows, the evolution of the area stretch ratio, from information where the MST is used, has been calculated only for the section of the flow geometry where the screws are present, i.e., the entrance and exit sections have been excluded from the calculations. From Figure 5.5, it can be noted that when implementing the TS analysis much higher values of this parameter are obtained than those corresponding to the MRS approach. As indicated by Avalosse and Rubin (2000), ideally, the type of curves presented in this figure should appear as straight lines, indicating an exponential growth of the area elements. This behavior is observed for the TS analysis (Figure 5.5b), where the trend of the curve has been approximated by means of a line of slope I. For the curve obtained under the MRS (Figure 5.5a) approach, however, two regions can be identified. One of such regions, dashed line of slope I, is located close to the entrance of the flow system where a steep slope is observed, and the other one corresponds to the remaining axial length of the flow geometry, dashed line of slope II. The first region of the curve may be related to entrance effects, however, this is not very clear. Then the second part of the curve, dashed line of slope II, can be related to the actual prediction of the area stretch ratio under the MRS approach. The main reason for the observed difference in the magnitude of the area stretch ratio under the two simulation techniques being considered is the non-objectivity of the area stretch ratio, i.e., its value depends upon the frame of reference used for the calculations. The applicability of the MRS in describing the distributive mixing capabilities of the REX flow system of interest will be further addressed in this study when the corresponding simulation results are presented.

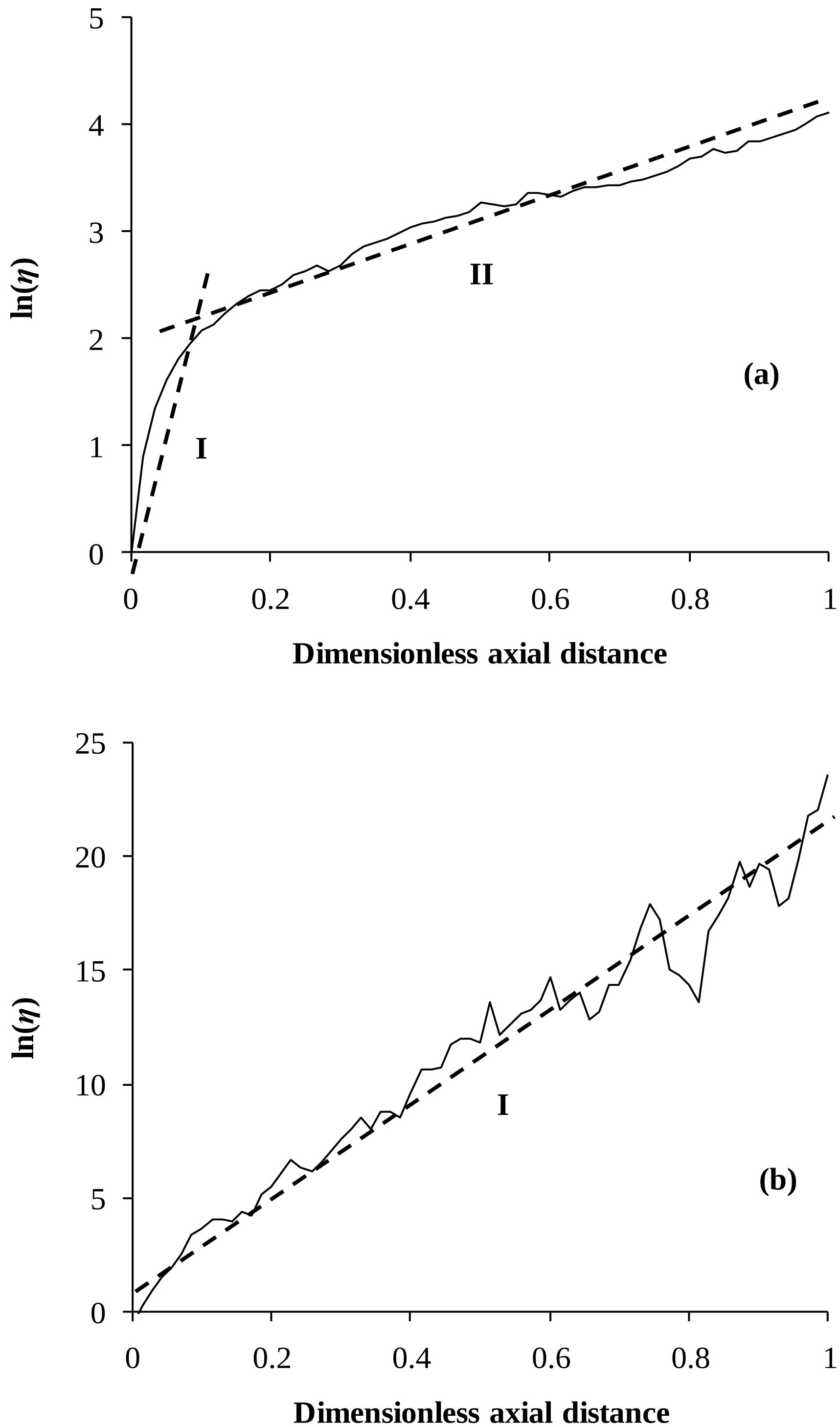

Figure 5-5 Evolution of the area stretch ratio, $\boldsymbol{\eta}$, under the (a) MRS and (b) TS simulation approaches.

In closing this section, it should be said that a simulation analysis where the transient nature of the flow system is taken into account is expected to provide more accurate results for the flow in screw elements of COITSEs than the MRS approach. However, and as previously stated, such analysis is not feasible for reactive systems. Therefore, and in view of the previous discussion, the implementation of the MRS seems to be a reasonable numerical approach for simulating a REX system. As will be later discussed, simultaneous TS and MRS (non-reactive and reactive conditions, respectively) simulations are expected to provide a better insight of the REX system under specific flow conditions.

5.2 3D REX Simulation Results

As in the discussion of the 1D modeling and simulation analysis, the results to be presented in this section are focused on the implications of the scale-up of the peroxide-initiated degradation of PP. The 3D simulations of the reactive system are performed for screw elements corresponding to two of the previously analyzed extruders. The effects of the initial peroxide concentration, mass throughput, and, especially, extruder size on the final weight-average molecular weight and poly-dispersity index of the product of the reaction are studied. In relation to the latter, the temperature of reaction resulting from the specified processing conditions is discussed. Also, some results obtained from particle-tracking analysis for the area stretch ratio and for the RTD are presented and discussed.

The information to be discussed is organized as follows. First, the analysis of the selected processing variables on the REX simulations are discussed for the screw element of the reference extruder. This is aimed to offer a better insight in the analyzed processing variables of the reactive flows being simulated. After that, the simulation results corresponding to the two screw elements being analyzed is presented. In contrast with the scale-up analysis presented for the 1D modeling approach, the discussion to be presented in this section does not intent to evaluate each one of the scale-up rules already addressed. The main reason for proceeding this way is that in the 3D analysis only a small section of the extruder under fully-filled conditions is simulated. Therefore, and taking into consideration the starve-fed operation of a COITSE, a direct comparison between the 1D and 3D results is not appropriate. At the end of this chapter, however, an evaluation of the proposed scale-up approach under constant thermal time is presented.

5.2.1 Set-up of the Simulations

5.2.1.1 Modeling Considerations

In order to describe the reaction kinetics of the REX system under analysis, the model proposed Tzoganakis et al. (1988 a), which has already been used in the case of the 1D simulations, is implemented again. An important consideration, when performing the simulations, is to consider that Q_1 (see equation 3.6) remains constant during the course of the reaction. This essentially means that the density of the system remains constant during the course of the reaction, since Q_1 represents the concentration of monomeric units in the system. By making this consideration, the set of equations given by equation 3.6 reduces from 4 to 3 equations, which reduces both the computational time and the memory requirements for the simulations.

Assumptions implied in the simulations performed in this work are incompressible non-Newtonian flow, steady state conditions, constant thermal properties of the melt flow, heat of reaction, negligible molecular diffusion of peroxide, and non-slip conditions on solid boundaries. The viscosity of the system is modeled by a power-law model, whose parameters have already been defined in the 1D simulation analysis. As previously discussed, according to the proposed model both the consistency and power-law indexes are expressed as mathematical functions of the temperature and Mw of the system.

5.2.1.2 Processing Conditions for Simulations

The simulations are performed by using POLYFLOW®, a commercial computational fluid dynamics (CFD) software based on the finite element method (FEM). Two different screw elements identified as LSM-30.34 and ZSE-96 are used for the simulations. The geometrical specifications for these elements are given in Table 5.1. These geometries are very close to those ones corresponding to two of the already addressed commercial extruders, but both the screw and radial gaps have been slightly increased here. 74852 and 75922 tetrahedral elements are used to discretize the LSM-30.34 and ZSE-96 screw elements, respectively. In Table 5.2, physical properties of interest for the polymer being analyzed are presented. Table 5.3 summarizes the processing conditions used for the simulations. As indicated in this table, a combination of three different peroxide-feed concentrations and two mass flow rates are used for each one of the screw geometries being simulated. The pitch of the ZSE-96 screw element is obtained by scaling-up that of the LSM-30.34 element proportionally to the diameter ratio of these screw elements (i.e., proportionally to d^1).

In Table 5.3, some of the boundary conditions implemented in this work are listed. Additional boundary conditions are non-slip conditions on solid walls, a fully developed velocity field at the inlet section of the screw element, and zero normal and tangential forces

Table 5-1 Geometry specifications of the simulated screw elements. All quantities are expressed in mm or derived units.

Screw element	LSM-30.34	ZSE-96
Screw O. diameter	33.70	95.60
Screw I. diameter	25.72	71.40
Centerline distance	30.51	85.75
Barrel diameter	35.30	100.10
Screw pitch	20.00	56.70
Screw length	60.00	170.1
Flow cross-sectional area	574.94	4827.58

Table 5-2 Physical properties of the molten polymer.

Density	750 kg/m^3
Thermal conductivity	0.185 W/(m °C)
Specific heat capacity	2.248 kJ/(kg °C)
Initial weight-average molecular weight	333000 g/mol
Initial number-average molecular weight	43420 g/mol

Table 5-3 Operating conditions for simulations. Q_{100} and Q_{50} stand for the implemented mass flow rates. Rt stands for the average residence time.

Screw element	LSM 30.34	ZSE 96
Q_{100}(kg/hr)/Rt(s)	26.34/3.54	631.8/3.51
Q_{50}(kg/hr)/Rt(s)	13.17/7.07	315.9/7.02
Screw speed (rpm)	100	
[I] (wt %)	0.01, 0.02, 0.10	
Inlet temperature (°C)	210	
Barrel temperature (°C)	210	

at the outlet section. On the other hand, constant inlet as well as barrel wall temperatures are specified, and at the outlet section of theflow domain a vanishing heat flux is imposed. Also, the screw surfaces are considered to be adiabatic. For the velocity field, an interpolation of the mini-element type (Fortin, 1981) is adopted whereas for the temperature field linear interpolation is implemented. With respect to the reacting species, a fixed concentration is defined at the entrance of the flow geometry, and a zero mass flux is specified at the barrel wall and at the exit section of the flow domain.

The simulations were carried out on a 64 Bit computer with 8 GByte RAM memory and a 2.1 GHz dual-core processor. The computational time for the simulations was dependent on the specified boundary conditions, ranging from around 2 hrs up to more than 6 hrs for each set of implemented REX conditions. In each case, at least two different types of simulations were performed, beginning with a non-reactive system either isothermal or non isothermal. In some cases, an evolutive scheme had to be specified to gradually increase either the viscous dissipation or the gradient of the reacting species. To overcome some problems related to the convergence of the simulations, the gradient of the reacting species was set to zero for a distance of about 3 % of that of the axial length at the end of the flow geometry. This procedure was especially applied to the simulations were the flow was significantly restricted. In all of the final REX simulations the convergence criterion was set to 1e-4.

5.2.2 LSM-30.34 Analysis

The maximum mass throughputs presented in Table 5.3 (Q_{100}) are obtained from simulations corresponding to non-reactive conditions by considering zero normal and tangential forces at the entrance and exit of the flow geometries. In what follows, the Q_{100} values are taken to be representative of scaling-up under constant residence time for the screw elements being analyzed here. In Figure 5.6, the pathlines corresponding to 4 particles seeded at the *z*-plane close to the entrance of the LSM-30.34 screw element for the Q_{50} value are shown. From this figure, it is evident that although no translation velocity for the screw barrel is specified (as in the case of the conventional relative system approach) the flow still behaves as a steady state flow, as indicated previously in Section 5.1.1 “Moving Relative System (MRS)”.

In Figure 5.7a, contour plots for the temperature field for the *z*-plane located at the middle of the axial distance of the screw element for the Q_{50} mass throughput and a peroxide concentration of 0.02 wt % are presented. This figure indicates that the maximum values of the temperature correspond to regions close to the screw surfaces. In Figure 5.7b, the variation of the weight-average molecular weight corresponding to the same *z*-plane shown in the previous figure is presented. In this case, it can be appreciated that some of the zones where the higher

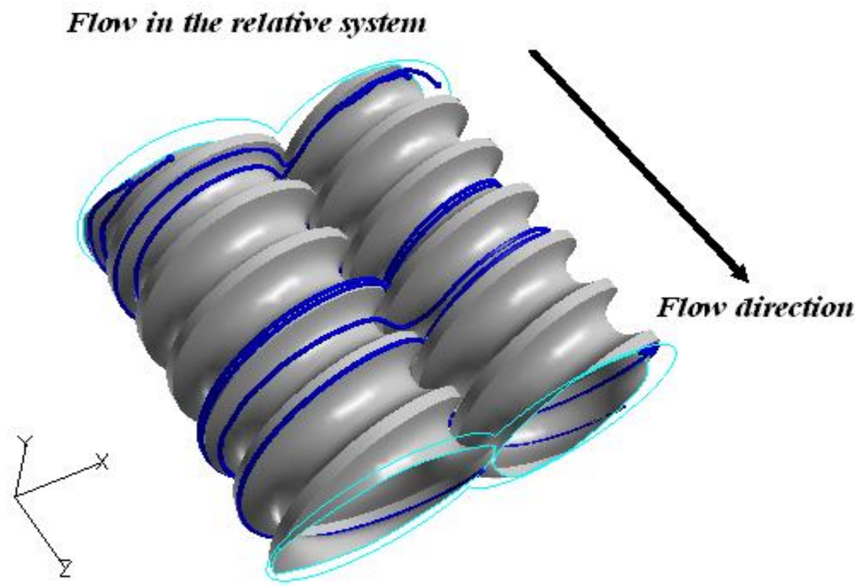

Figure 5-6 Particle paths for 4 particles seeded at the *z* plane, *z*=2.5 mm, for the LSM-30.34 screw element (Q=13.17 kg/hr, non-reactive conditions).

Mws (which can be related to lower conversions of reaction) are found correspond to those same zones where the higher temperatures are detected in Figure 5.7a. These results agree to some extent to those found by Zhu et al. (2005 b) in their study on the polymerization of ε-caprolactone. These researchers reported that for the aforementioned reacting system in the case of screw elements having a small pitch the minimum values of conversion correspond to zones close to the screw surfaces. As higher temperatures are in principle related to higher conversions of reaction, the previously addressed behavior may be explained considering that in these zones of the flow geometry lower values of the residence time prevail. A converse situation to the one just addressed is observed for a region near the surface of the extruder barrel, which again may be related to the residence time. This could be explained considering

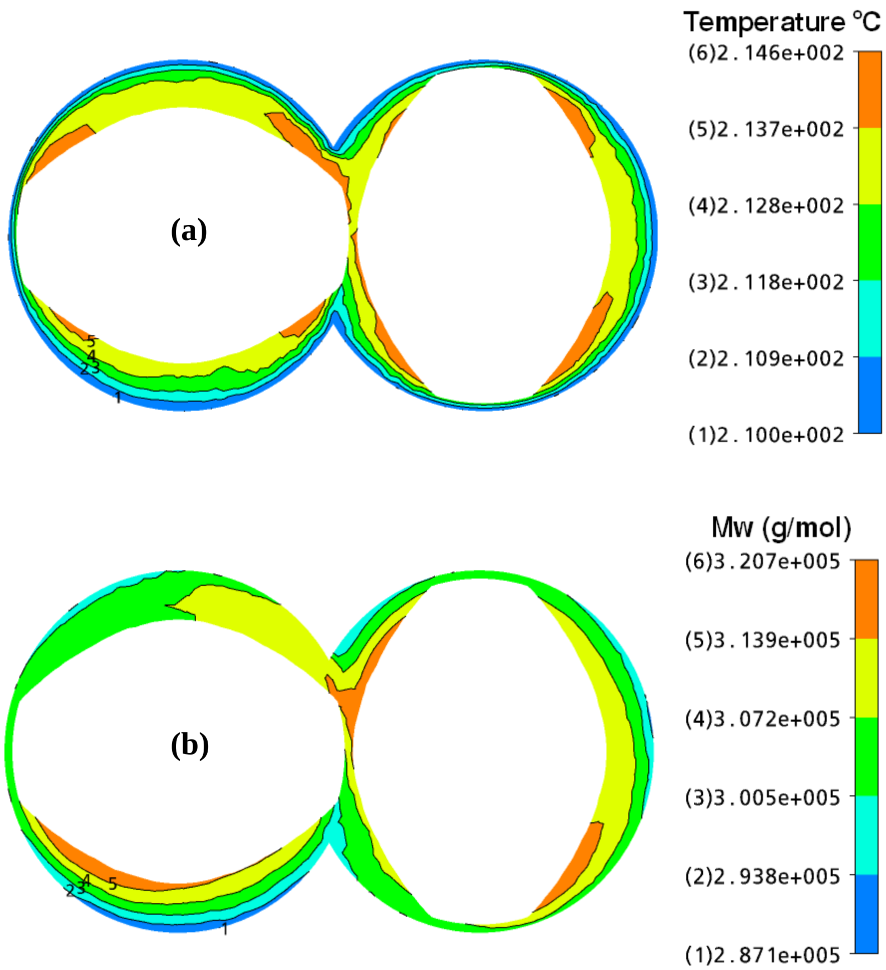

Figure 5-7 Contour plots for (a) the temperature and (b) the Mw. *z*-cut planes at z=30 mm, Q=13.17 kg/hr and [I]=0.02 wt %.

that the particles moving near the barrel are slowed down due to the momentum transfer mechanism occurring near the barrel of the extruder. Under this consideration, these particles are expected to have higher residence times, and, hence higher reaction conversions.

In Figure 5.8, the variation of the average temperature (average cross sectional values) along the axial distance of the screw elements for both the non-reactive and the reactive

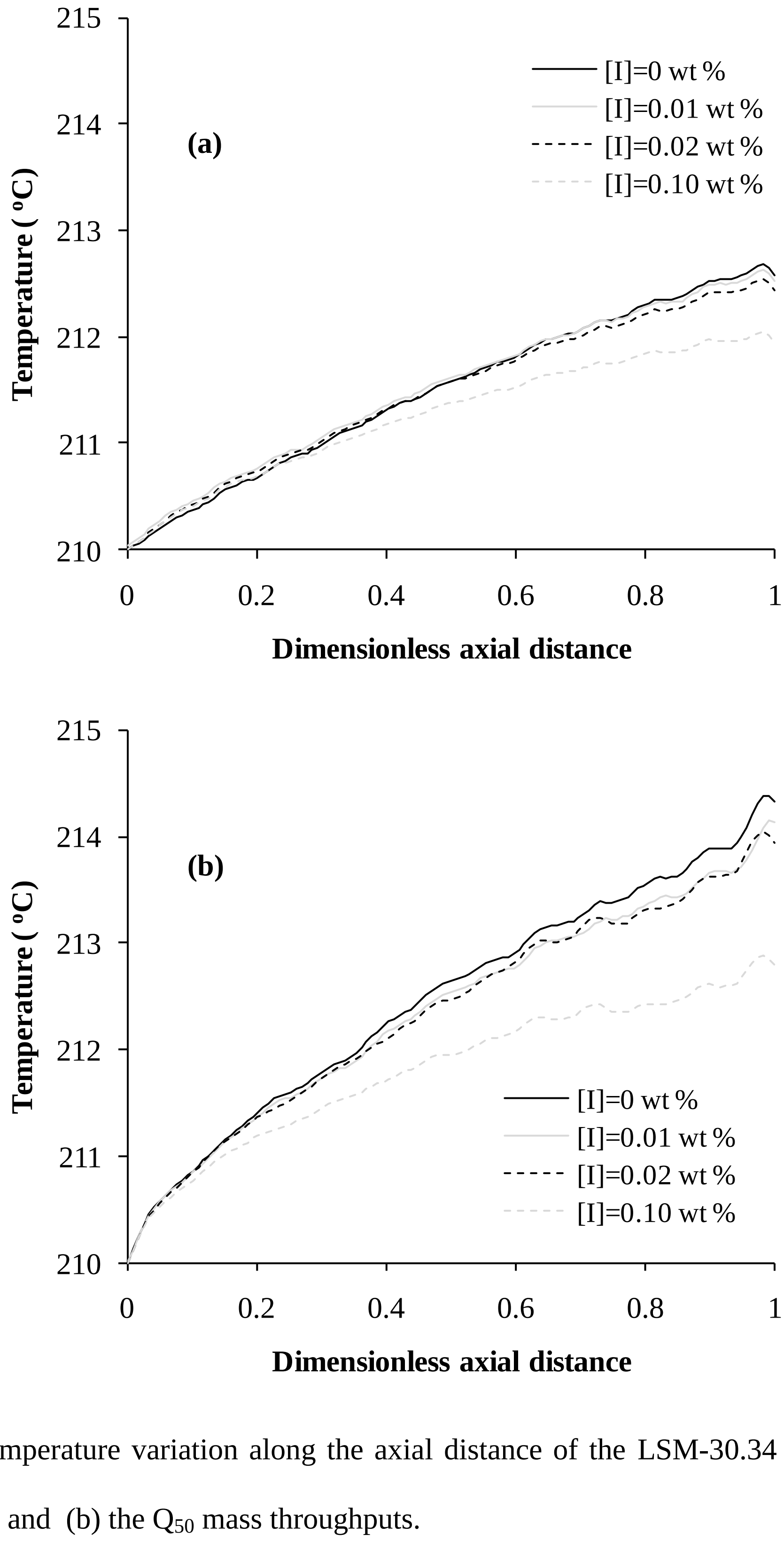

Figure 5-8 Temperature variation along the axial distance of the LSM-30.34 screw element for (a) the Q_{100} and (b) the Q_{50} mass throughputs.

systems is presented. From Figure 5.8a, it can be appreciated that there is no significant difference in the variation of the temperature for the lower values of the peroxide concentration with respect to that of the non-reactive conditions. An opposite behavior, however, can be appreciated for the highest implemented value of the peroxide concentration. When the flow is restricted to 50 % (Q_{50}) of its maximum capacity (Figure 5.8b), a similar trend to the one addressed for the Q_{100} value is observed, but the differences in the final values of the temperature of reaction between the reactive and non-reactive conditions increases.

Two main effects associated to the more restrictive flow conditions influencing the trend in the temperature just described can be identified. Firstly, when the flow rate is decreased the average residence time of the system increases, and, hence a higher reduction of the viscosity is to be expected due to the degradation reaction. This reduction of the viscosity in turn contributes to a decrease of the viscous dissipation effects. Secondly, the more restricted flow conditions contribute to more dissipation effects because of the more friction experienced between the layers of the flowing polymer under such flow conditions. Therefore, the resulting increase of the temperature can be related to the increase of the viscous dissipation effects related to more restrictive flow conditions as well to a reduction of such effects associated with the degradation reaction.

In Figures 5.9 and 5.10, the evolutions of the Mw and PDI of the reacting polymer are presented for both the Q_{100} and Q_{50} mass flow rates. It can be seen that the relative variation of these two parameters is very similar for all of the specified flow boundary conditions and peroxide concentrations. Another important aspect that is evident from Figures 5.9 and 5.10 is that although the molecular weight of the polymer decreases when the average residence time increases (more restricted flow conditions), this decrease is not significantly pronounced. This

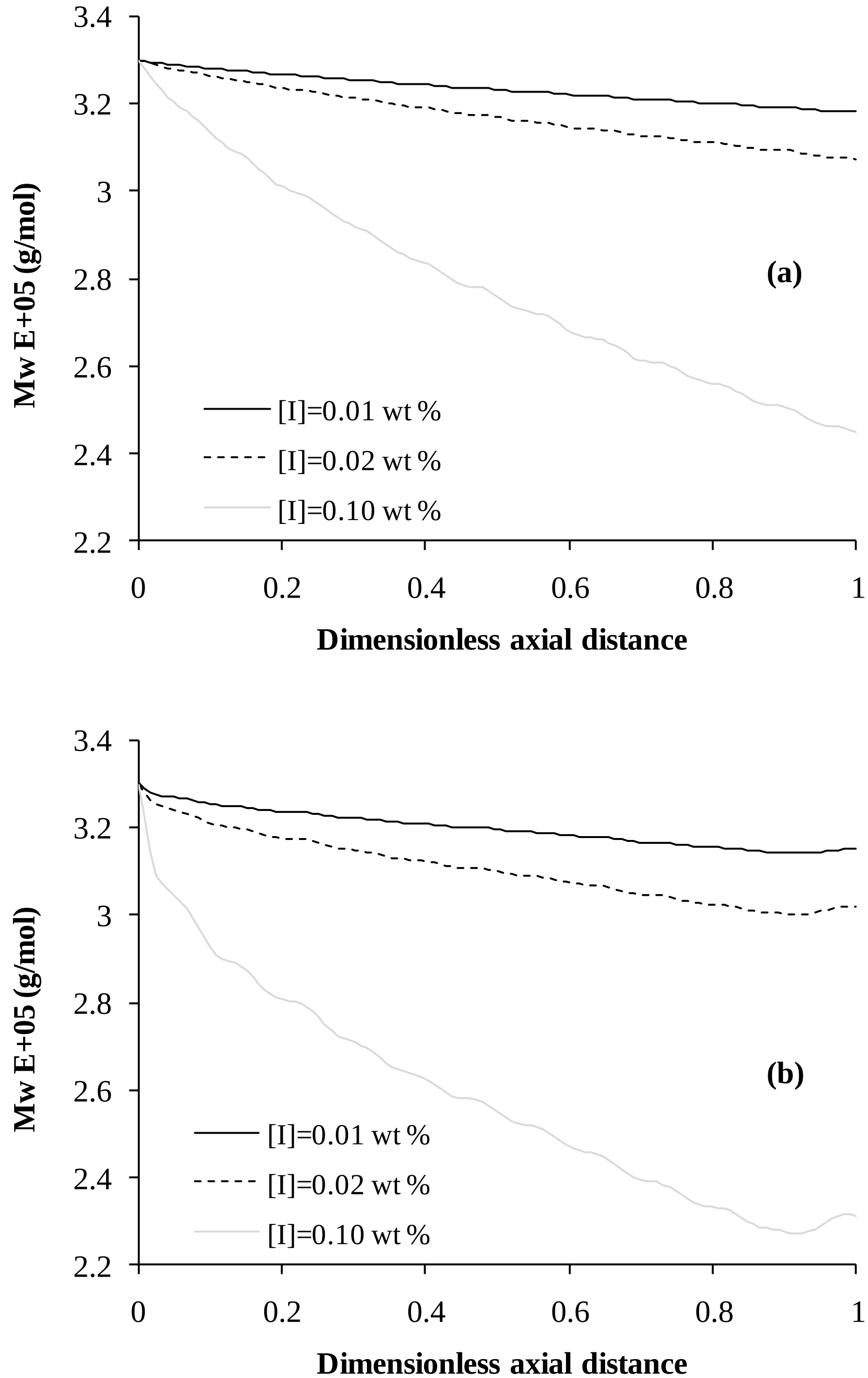

Figure 5-9 Mw variations along the axial distance of the extruder for the LSM-30.34 screw element for (a) the Q_{100} and (b) the Q_{50} mass throughputs.

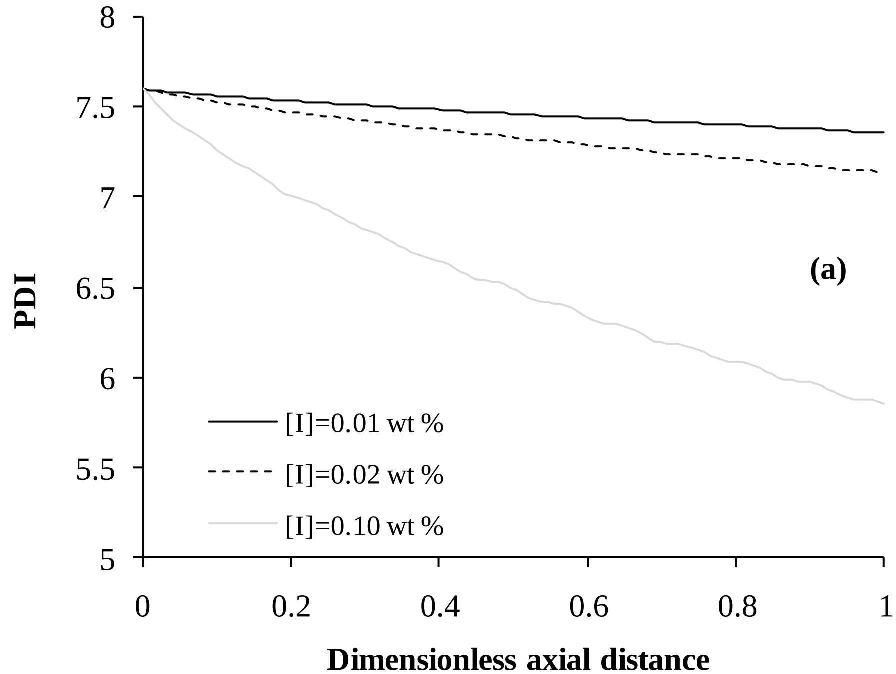

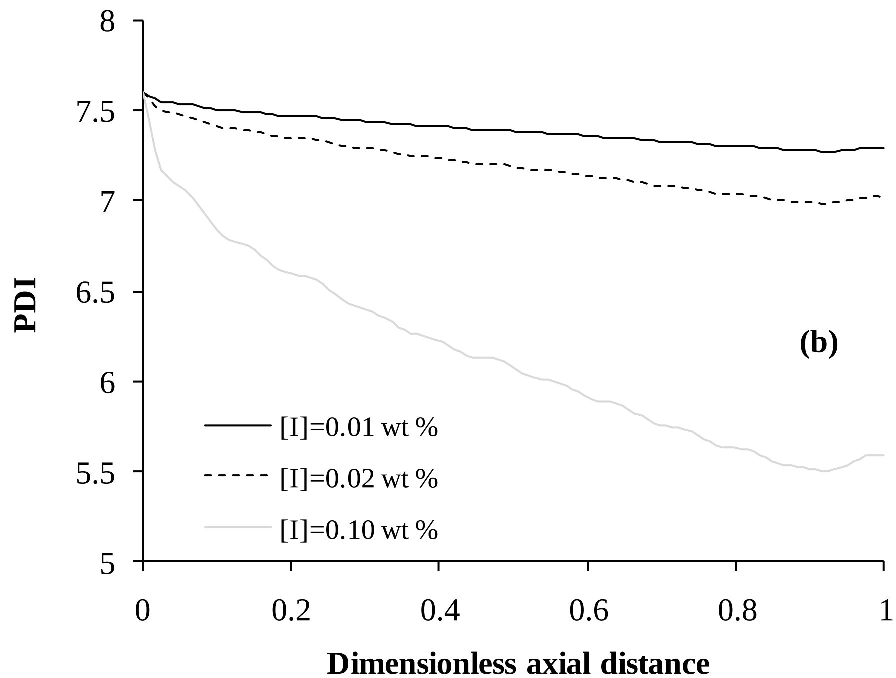

Figure 5-10 PDI variations along the axial distance of the extruder for the LSM-30.34 screw element for (a) the Q_{100} and (b) the Q_{50} mass throughputs.

suggests that the flow rate for a given screw speed does not have a prominent role on the final Mws and PDIs of the reacting polymer resin. These results should be somehow surprising if the variations of these parameters were to be proportional to the decrease of the peroxide concentration during the reaction. However, as can be appreciated from the equations describing the variation of the moments of the molecular weight distribution (see equation 3.6), the reaction kinetics for this system is rather complex. As a reference, in Table 5.4 the peroxide half-lifes are presented for different temperature values. For this information and according to Figure 5.8, it can be seen that the peroxide concentration should be reduced to half of its values in the time period between 9.54 and 5.10 s under the prevailing reacting conditions for the present simulations. When considering the average residence times for the Q_{100} and Q_{50} mass throughputs which are around 7 and 3.5 s, respectively (see Table 5.3), it is evident that the peroxide concentration is only reduced on average to less than half of its initial value in the case of the lower value of the average residence time (Q_{50} mass throughput). Regarding the variations of both the Mw and PDI with respect to the peroxide concentration, it is evident that these variables are very sensitive to the modification of the concentration of the injected peroxide stream.

It can be noticed in Figures 5.9 and 5.10 that some entrance and exit effects are observed. Such effects are manifested as a steep drop of both the Mw and PDI at the entrance of the flow element and as an increase of these variables at the exit of the flow geometry and are more pronounced for the higher implemented value of the peroxide concentration (see Figures 5.9b and 5.10b). This behavior may be related to numerical artifacts which will be discussed in part later on in this chapter. Nevertheless, the general trend of the obtained results can be considered as the one just discussed regardless of such numerical artifacts.

Table 5-4 Peroxide half-life time as a function of the temperature of reaction.

Temperature (^{o}C)	$[\tau]_{1/2}$ (s)
190	36.30
200	18.35
210	9.54
220	5.10

Figure 5.11 corresponds to the RTD of the LSM-30.34 screw element for the different specified flow conditions and for two of the implemented peroxide concentrations, i. e., [I]=0.02 and [I]=10 wt %. The RTD curves were obtained by specifying around 1000 mass-less particles at the entrance of the flow geometry and performing a tracking analysis of such particles. In all of the analyzed cases, the maximum time for the tracking was set to 45 s. The results shown in Figure 5.11 for the different implemented mass throughputs indicate, as expected, that when the mass flow rate is reduced (Figure 5.11b), the RTD curves broaden. On the other hand, no significant broadening of the RTD curves is observed as a function of the peroxide concentration. As a reference to the RTD curves presented in Figure 5.11, the corresponding cumulative RTD curves are presented in Figure 5.12.

To complement the information provided by Figures 5.11 and 5.12, in Table 5.5 presents the average residence times and standard deviations corresponding to the RTD analysis. For reference, the average values of both the residence time and standard deviation have been

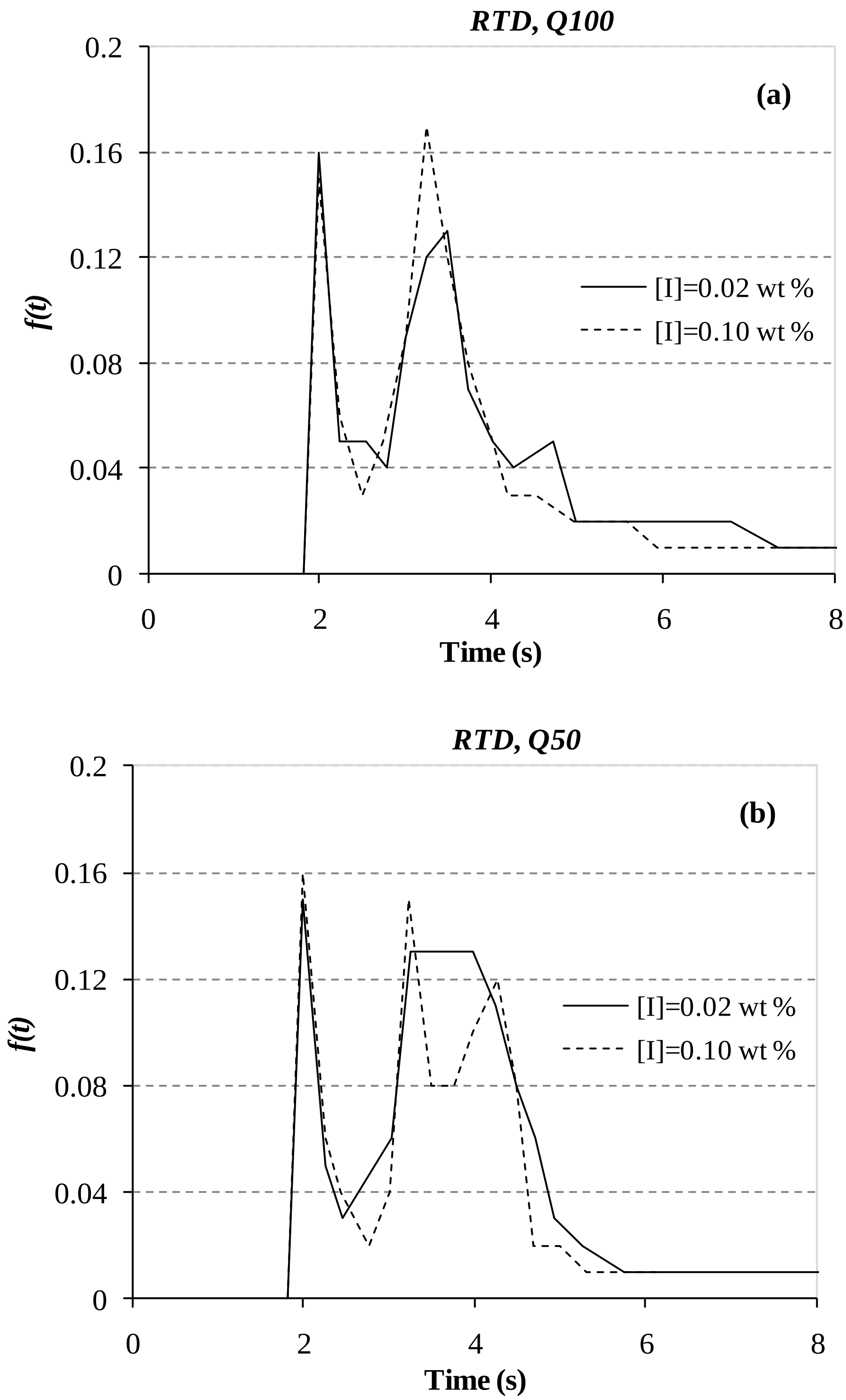

Figure 5-11 RTD in the LSM-30.34 screw element for (a) the Q_{100} and (b) the Q_{50} mass throughputs.

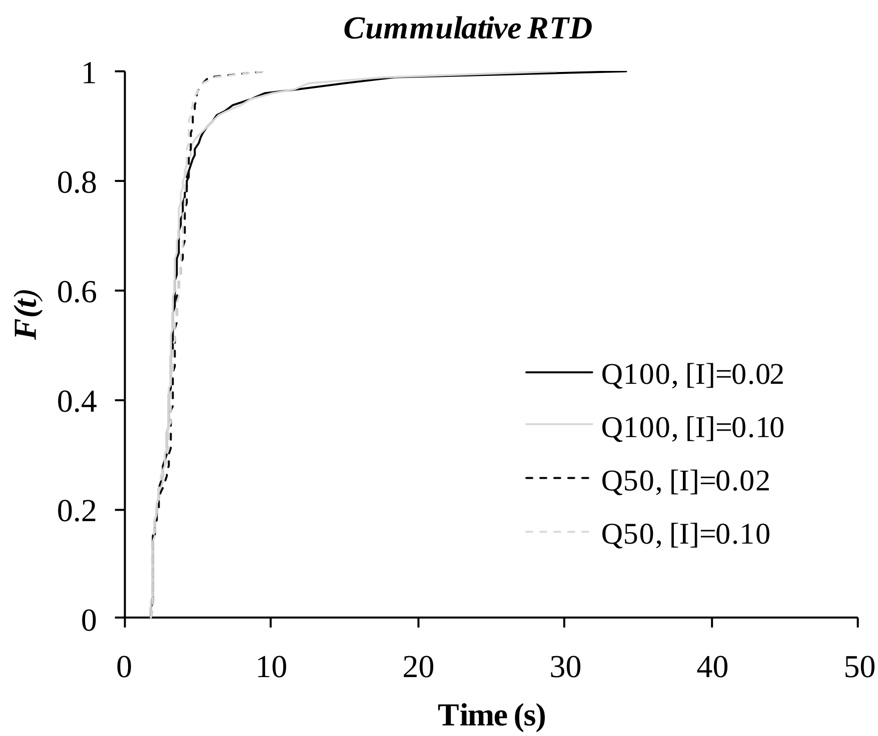

Figure 5-12 Cumulative RTD for the LSM-30.34 screw element.

obtained by weighting the residence times of the individual tracked particles by the velocity vector, using a weighting of the normal velocity type everywhere (according to the Polystat user's guide, included with the POLYFLOW® documentation files). From the results shown in this table, it is interesting to note that for the Q_{100} mass throughput values the predicted average residence times are in very good agreement with the actual average residence times shown in Table 5.3, which are calculated from the volumetric capacity of the screw element and the specified flow rate. On the other hand, in this case high values of the standard deviation are obtained. For the more restricted flow conditions, however, the average residence times are much lower than the actual values presented in Table 5.3, and the values of the standard deviation are significantly lower than those corresponding to the Q_{100} mass

Table 5-5 Average residence times ($\bar{t}$) and standard deviations (STD) for the reactive flow in the LSM 30.34 screw element when the MRS simulation approach is implemented.

Mass throughput and [I] in wt %	$\bar{t}$ (s)	STD (s)
Q100, 0.02	3.88	3.15
Q100, 0.10	3.67	2.79
Q50, 0.02	3.3	1.03
Q50, 0.10	3.22	1.06

throughput.

The behavior just described for both values of the mass throughput can be explained as follows. In the case of the less restricted flow conditions (Q_{100}), at the entrance of the flow domain few particles experience flow in the backward direction. However, in the more restricted flow conditions a significant amount of particles moves in the backward direction at the entrance of the flow elements where the particles are seeded (as it will be later briefly explained, by means of Figures 5.14 and 5.15). This means that for the more restricted flow conditions, in the regions where the flow takes place in the backward direction no particles are considered in the calculations of the particle-tracking analysis. Also, some of the particles initially seeded can leave the computational domain if they are forced to move on the backward direction. This fact can be corroborated from the values of the standard deviation, where lower values indicate that a significant amount of particles having high values of

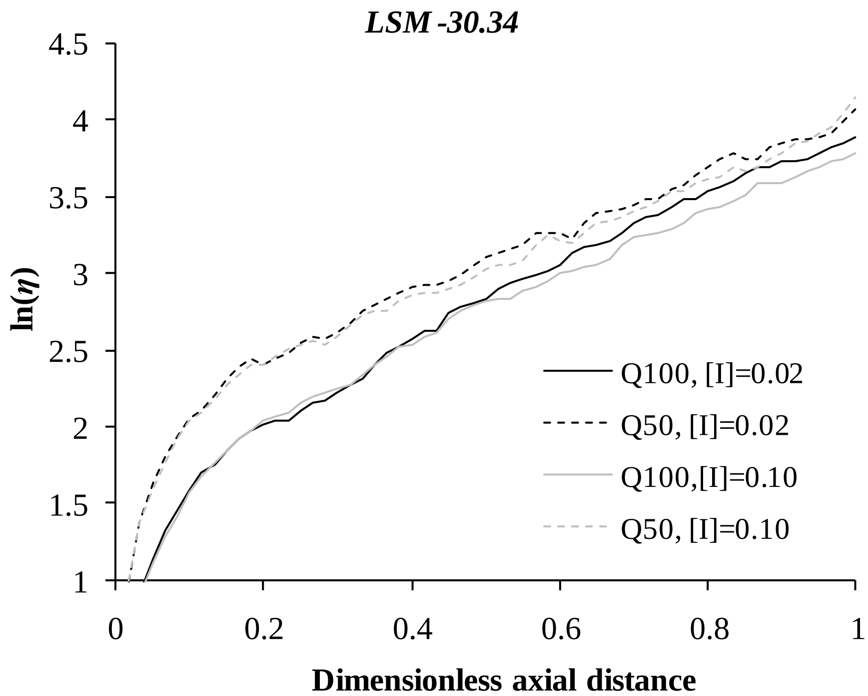

Figure 5-13 Evolution of the area stretch ratio for the LSM-30.34 screw element.

residence time are not considered in the particle-tracking analysis .

Finally, in Figure 5.13 the evolution of the area stretch ratio is presented for the two different specified flow rates and for values of the peroxide concentration of 0.02 and 0.10 wt %, respectively. In this case, the evolution of this parameter is very similar when the same mass throughput is implemented regardless of the implemented peroxide concentration. This behavior is in agreement with what has been found by Strutt et al. (2000) in the sense that the modification of the fluid viscosity by either increasing the shear rate or by the effects of the chemical reaction does not significantly modify the mixing capabilities of the flow field. An additional analysis of the curves presented in Figure 5.13 would indicate that the slope of the curves, in the region spanning from around 0.2 to 1 in the horizontal axis is slightly lower in the case of the more restrictive flow conditions, i.e., for the Q_{50} mass throughput. This may indicate, surprisingly, that the distributive mixing capabilities for the LSM-30.34 screw element decrease as the flow restrictions are increased, which is not expected, according to the discussion presented in Section 3.6 “Additional Considerations of the Flow in Screw Elements of COITSEs”. This behavior, however, can also be explained by the fact that in the particle-tracking analysis particles having high residence time values are not considered for the calculations, as previously described when the RTD curves were analyzed. Then it would be expected that in a more accurate particle-tracking calculation procedure, one could observe that as the flow rate decreases (more restricted flow conditions), better distributive mixing capabilities could be observed as indicated in Section 3.6. On the other hand, conversely with what is expected from the flow analysis presented in that same section, here, no significant effects on the mixing capabilities are found in terms of the implemented peroxide concentration, as previously stated.

5.2.3 LSM-ZSE Analysis

In this section, the analysis of the REX degradation of polypropylene for the screw elements of two of the different size extruders previously addressed is analyzed. The corresponding geometry, physical and operating (boundary) conditions are those presented in Tables 5.1-5.3. The simulation analysis is started here by evaluating the general flow capabilities of the LSM-30.34 and ZSE-96 screw elements. In this context, the flow is simulated for Newtonian, isothermal conditions, assuming the viscosity of 500 Pas. In this case, TS simulations are performed simulating 15 different positions of the screws, by means of the MST, to describe the motion for one half of a revolution (time periodicity).

In Figures 5.14 and 5.15, the initial position of around 1000 particles seeded at the entrance of the flow domain and their predicted positions after 2.5, 5 and 7.5 revolutions (1.5, 3 and 4.5 s, respectively) are shown for both the LSM-30.34 and ZSE-96 screw elements. The specified flow rate for the simulations, Q_{50}, in both of the analyzed cases corresponded to one half of that predicted for non-restrictive flow conditions (Q_{100}). In this case, it can be appreciated that the distribution of the particles is very similar in both of the two simulated cases. This behavior is somehow expected since the geometry of the ZSE-96 element is a closely geometrically scaled-up version of that of the reference extruder, as has been previously addressed. An important characteristic observed in Figures 5.14 and 5.15 is the fact that at the entrance of the flow domain, there are zones where no particles are located. These zones are very similar in both the larger and the reference screw elements. Although the software randomly seeds the particles for the tracking, these particles are only located in zones where the flow is mainly taking place in the forward direction. Therefore, the regions where no particles are found can be related to zones where the flow is mainly taking place in the backward direction. Again, the reader is reminded that these regions are very similar in both of the analyzed cases which may indicate, at least in principle, similar flow characteristics for the two screw elements being investigated.

In what follows, the simulation results generated by implementing the MRS approach will be discussed. In this context, the first variables to be addressed are the maximum mass throughputs presented in Table 5.3 and identified as Q_{100}. Such mass throughput values are obtained from a non-reactive non-isothermal simulation by considering zero normal and

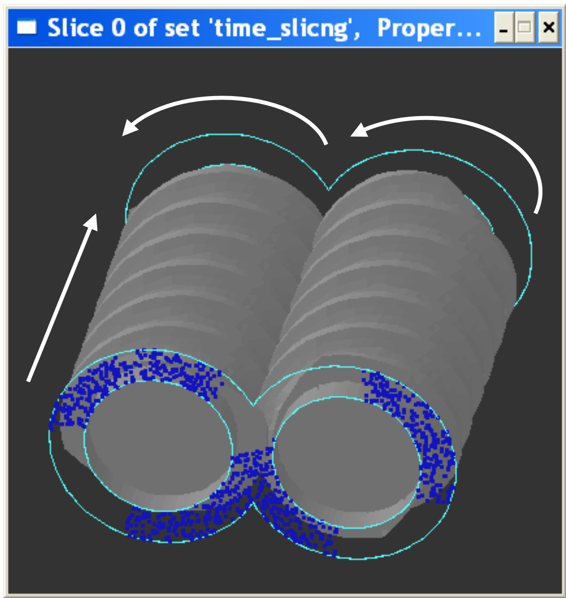

(a)

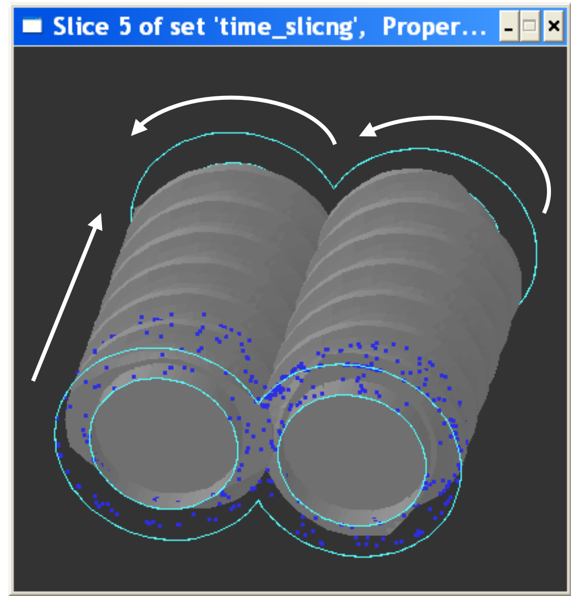

(b)

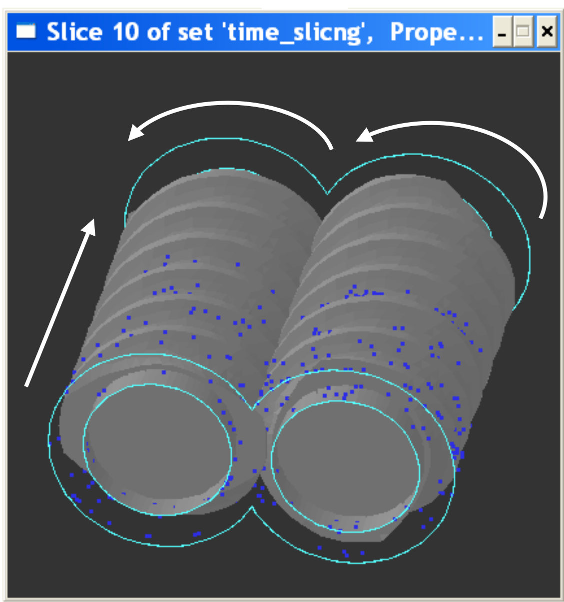

(c)

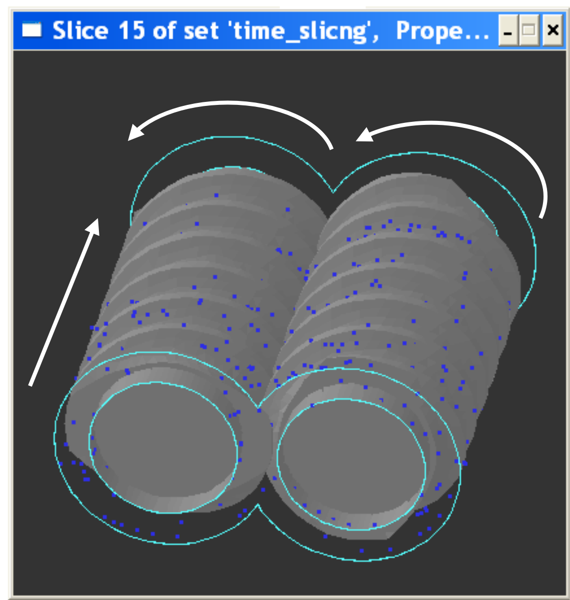

(d)

Figure 5-14 (a) Initially seeded particles and their location after (b) 1.5, (c) 3, and (d) 4.5 seconds for the LSM-30.34 screw element. The conveying and rotation directions are indicated.

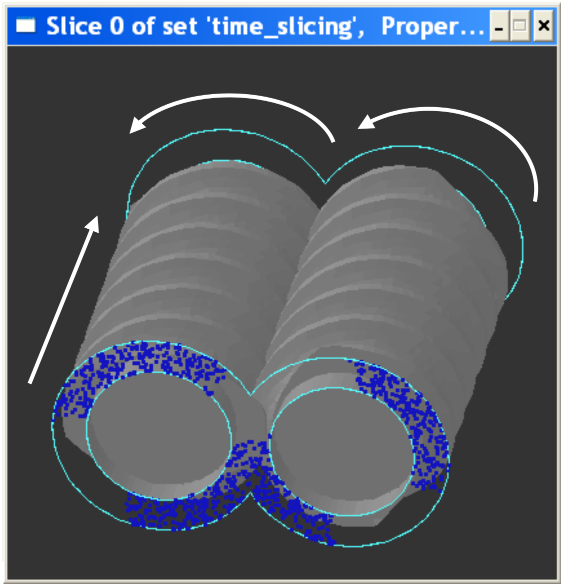

(a)

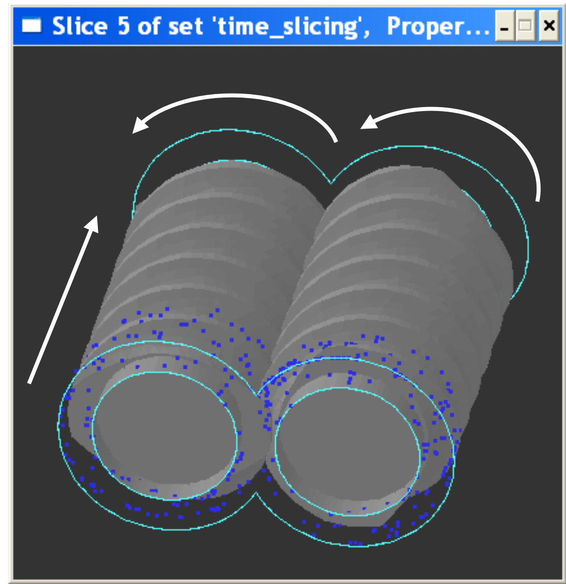

(b)

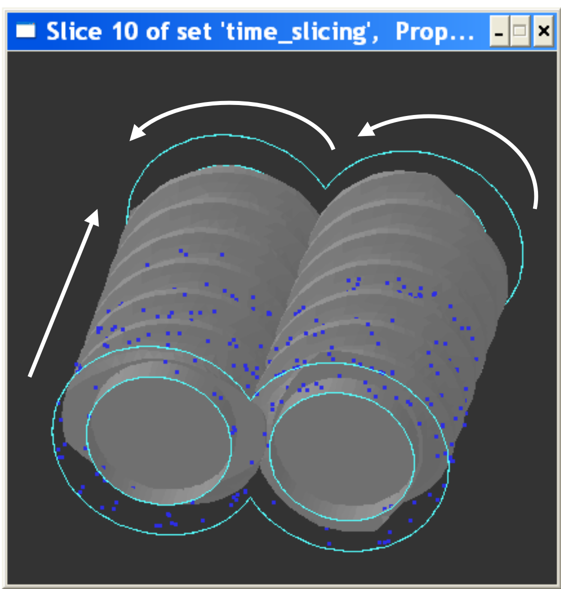

(c)

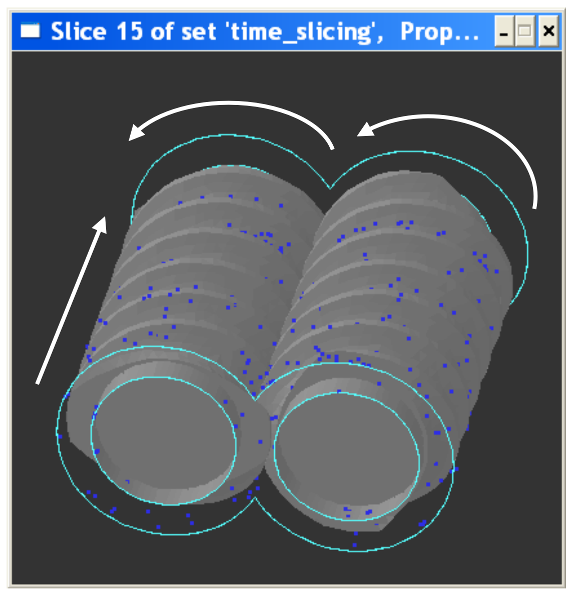

(d)

Figure 5-15 (a) Initially seeded particles and their location after (b) 1.5, (c) 3, and (d) 4.5 seconds for the ZSE-96 screw element. The conveying and rotation directions are indicated.

tangential forces at the entrance and exit of the flow geometries. These throughputs are very similar to those obtained by scaling-up the mass flow rate assuming a constant residence time, as can be seen from Table 5.3. These same Q_{100} values have been kept constant for all of the implemented reactive simulations and are slightly higher than the ones corresponding to reactive flow conditions if zero normal and tangential forces had been specified at the entrance and exit of the flow domain (non-restrictive flow conditions). The mass flow rates identified as Q_{50} in Table 5.3 correspond to half of the Q_{100} value.

In Figure 5.16, the average temperature profiles for non-reactive conditions for the screw elements being studied are presented. For the maximum mass throughput (Q_{100}), in general terms, no difference in the temperature profiles as a function of the size of the screw element can be appreciated. On the other hand, when the flow is restricted to 50 % (Q_{50}) of its maximum capacity a slight increase of the temperature of the larger screw element with respect to that of the smaller one is observed. This may indicate that the viscous dissipation effects are more significant in the case of the larger extruder in this latter case. Overall, the behavior appreciated from Figure 5.16 can be associated to two main heat generation/transfer mechanisms: viscous dissipation and heat transfer at the barrel wall. Recalling that the ZSE-96 screw element is very close to a scaled-up version of the reference screw element, it is expected that the viscous dissipation effects are similar for both screw elements. In this case, this is especially true for the less restricted flow situation. Regarding the heat transfer at the barrel wall, under the specified processing conditions this corresponds to heat losses. Due to the fact that for the present case the temperature differential between the barrel wall and the fluid in close proximity to this wall is relatively small, along with the low value of the thermal

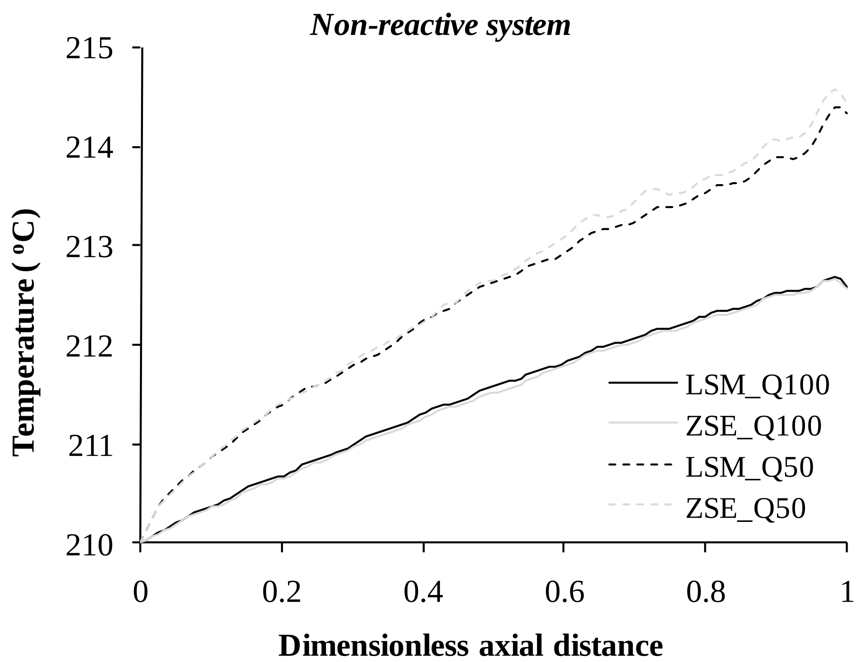

Figure 5-16 Temperature variations for the non-reactive system for both the LSM-30.34 and ZSE-96 screw elements.

conductivity of the molten polymer, this transfer mechanism is expected to have a minor effect on the overall energy balance of the system. Here, it is important to recall that the temperature gradient in the direction perpendicular to the barrel wall times the thermal conductivity defines the heat flux at this physical boundary. Therefore, it should be noticed that as the aforementioned temperature differentials increase the effect of this heat transfer mechanism would become more important. This is especially true taking into account that the heat generated by viscous dissipation would roughly increase proportionally to d^3 while the heat transfer at the barrel wall would only do this proportionally to d^2.

In Figure 5.17, contour plots are presented for the temperature field for the *z*-plane located at the middle of the axial distance of the LSM-30.34 and ZSE-96 screw elements for the Q_{50} mass throughput and a peroxide concentration of 0.02 wt %. It can be seen that the predicted temperature fields are very similar for both of the simulated flow geometries. As previously indicated, for the lower implemented mass flow rates, there are two mechanism involved in the heat generated by viscous dissipation. One of such mechanisms is related to the flow restrictions and the other one to the reduction of the viscosity of the system due the degradation reaction. Then, a preliminary conclusion from the results presented in Figure 5.17 is that the contributions of the aforementioned heat transfer mechanisms are very similar for both the LSM-30.34 and ZSE-96 screw elements. In Figure 5.18, the variation of the weight-average molecular weight corresponding to the same *z*-plane shown in the previous figure is presented. In this case, again, the variation of the Mws for both of the screw elements is very similar. Due to the similitude in the temperature profile shown by means of Figure 5.17, the contour plots for the Mws would suggest that not only similar temperature but also similar flow conditions are developed in the screw elements under the specified processing conditions.

In Figure 5.19, the variation of the average temperature and Mw along the axial distance of the screw elements for both of the implemented flow rates when the peroxide concentration is set to 0.01 wt % is presented. It can be appreciated from Figure 5.19a that the temperature profiles are very similar to those obtained for the non-reactive conditions (see Figure 5.16). However, a slight decrease in the final temperatures can be appreciated with respect to those of the former case. This is not surprising due to the low value specified for the peroxide concentration. The results shown in Figure 5.19b regarding the variation of the Mw show that when the flow is just slightly restricted (Q_{100}) the trend in the variation of this parameter is

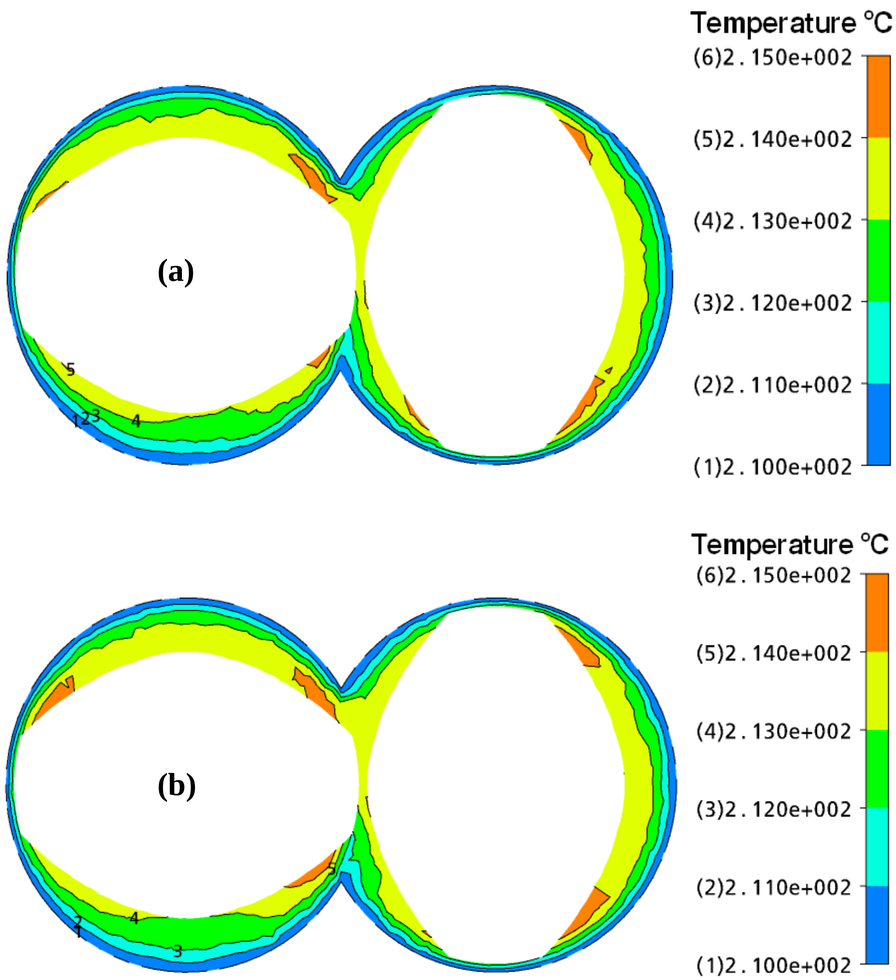

Figure 5-17 Contour plots for the temperature variation in the z-plane located at half of the axial distance of (a) the LSM-30.34 and (b) the ZSE-96 screw elements.

essentially the same for the two flow geometries being analyzed. This information, along with that corresponding to the variation of the temperature for the same specified mass flow rate, suggest that the flow conditions prevailing in the screw elements being analyzed are very similar regardless of their size, for these particular flow conditions. For the flow rates identified as Q_{50}, a more significant decrease in the Mw as well as a slight increase of the

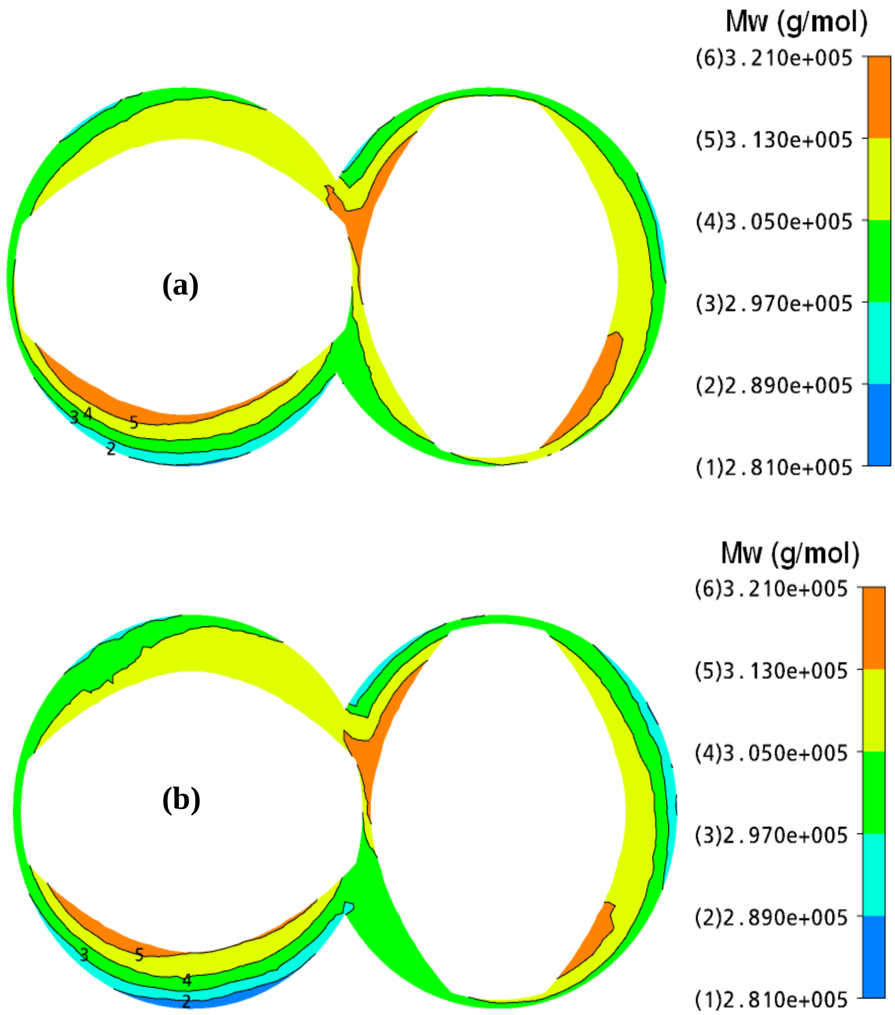

Figure 5-18 Contour plots for the Mw variation in the z-plane located at half of the axial distance of (a) the LSM-30.34 and (b) the ZSE-96 screw elements.

temperature in the SZE-96 screw element with respect to the temperature of the reference screw element is observed (see Figures 5.19a and 5.19b). The fact that more viscous dissipation is observed for the larger screw element is in agreement with results from 1D simulations (Ortiz and Tzoganakis, 2008). On the other hand, the effect of temperature

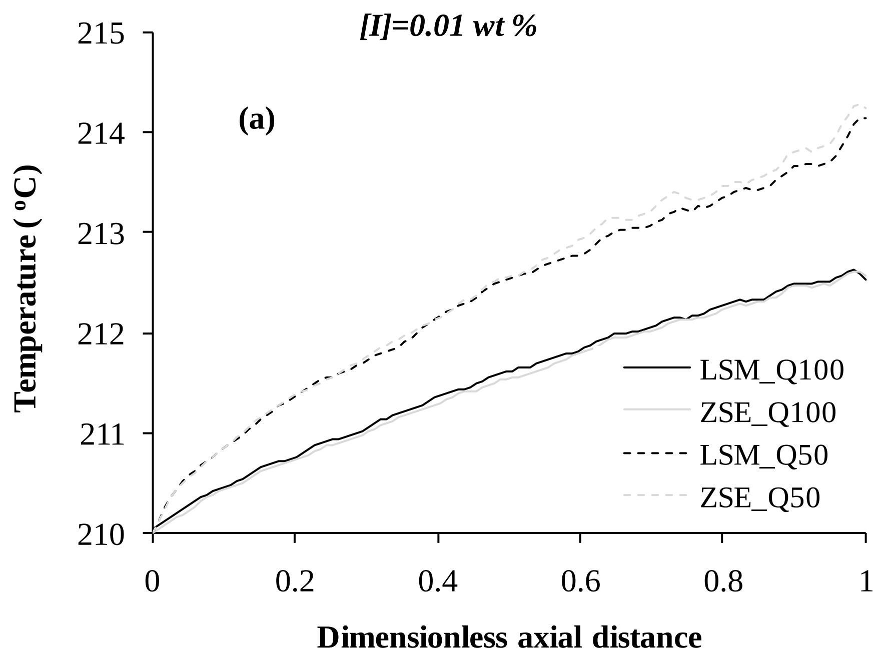

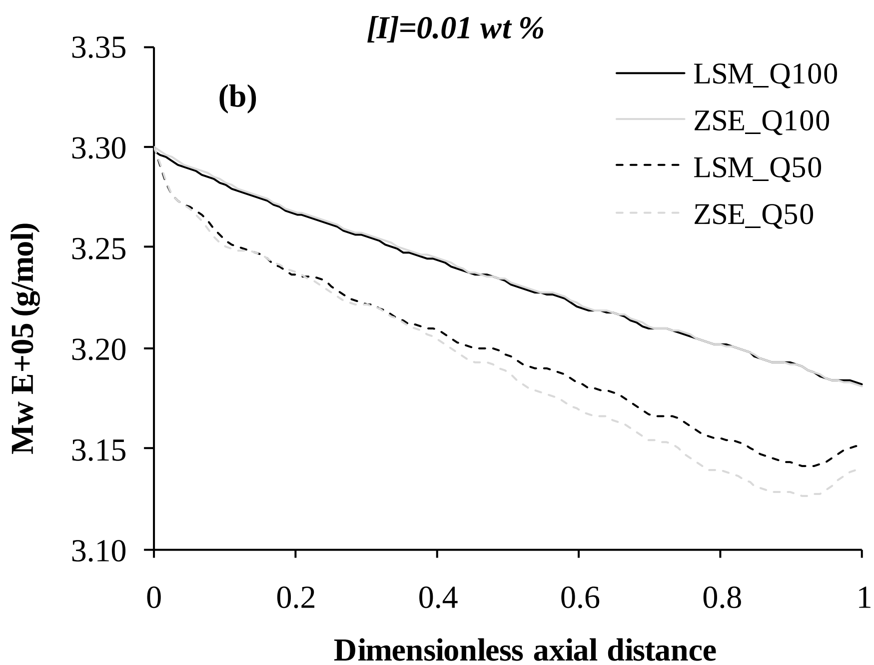

Figure 5-19 (a) Average temperature and (b) Mw variations along the axial distance of the flow geometries for a peroxide concentration equal to 0.01 wt %.

increase on the extent of reaction could be negligible due to the relatively small difference in the temperature profiles for the two different size screw elements being analyzed.

Figure 5.20 corresponds to the variation of the average temperature and Mw along the axial distance of the screw elements for both of the implemented flow rates when the peroxide concentration is set to 0.10 wt %. The trend of the curves shown in this figure is similar to that observed for the lowest implemented peroxide concentration. In this case, however, the final values of the temperature at the end of the flow geometries are lower than the ones corresponding to the former case. Also, it can be appreciated from Figure 5.20 that for the mass flow rates identified as Q_{50}, the evolution of the temperature profiles is slightly different from that corresponding to the lowest specified value of the peroxide concentration. In this case, the final temperature values are essentially the same. Regarding the evolution of the Mw along the axial direction of the screw elements (Figure 5.20b), this is very similar to the one corresponding to the peroxide concentration of 0.01 wt % for all of the implemented mass flow rates. Again, it can be said that because of the very similar evolution of the temperature and Mw, the flow conditions in both the larger and the reference screw elements may be very similar in the case of the mass flow rates identified as Q_{100}.

In Figure 5.21, the RTDs are shown for the LSM-30.34 and ZSE-96 screw elements for all of the implemented flow rates when the peroxide concentration is set to 0.02 wt %. Here, the maximum time for the tracking of the particles was set to 45 and 50 s for the LSM-30.34 and ZSE-96 screw elements, respectively. Although the temperature and Mw profiles have not been presented for this case, the evolution of such parameters can be considered to be very similar to that obtained when the peroxide concentration is set to 0.01 and 0.10 wt %, respectively. The shapes of the curves in the case of the Q_{100} mass flow rate (see Figure 5.21a)

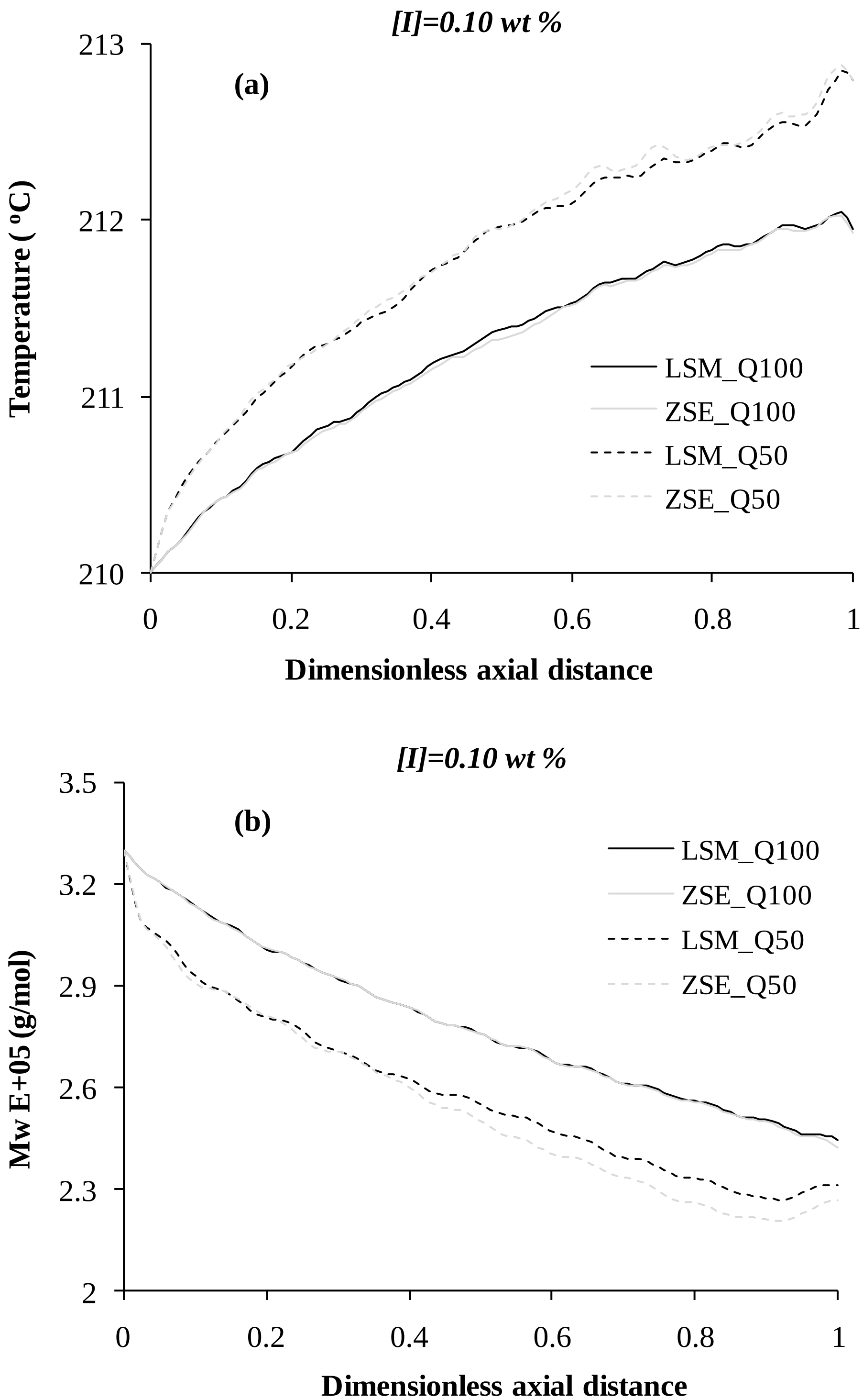

Figure 5-20 (a) Average temperature and (b) Mw variations along the axial distance of the flow geometries for a peroxide concentration equal to 0.10 wt %.

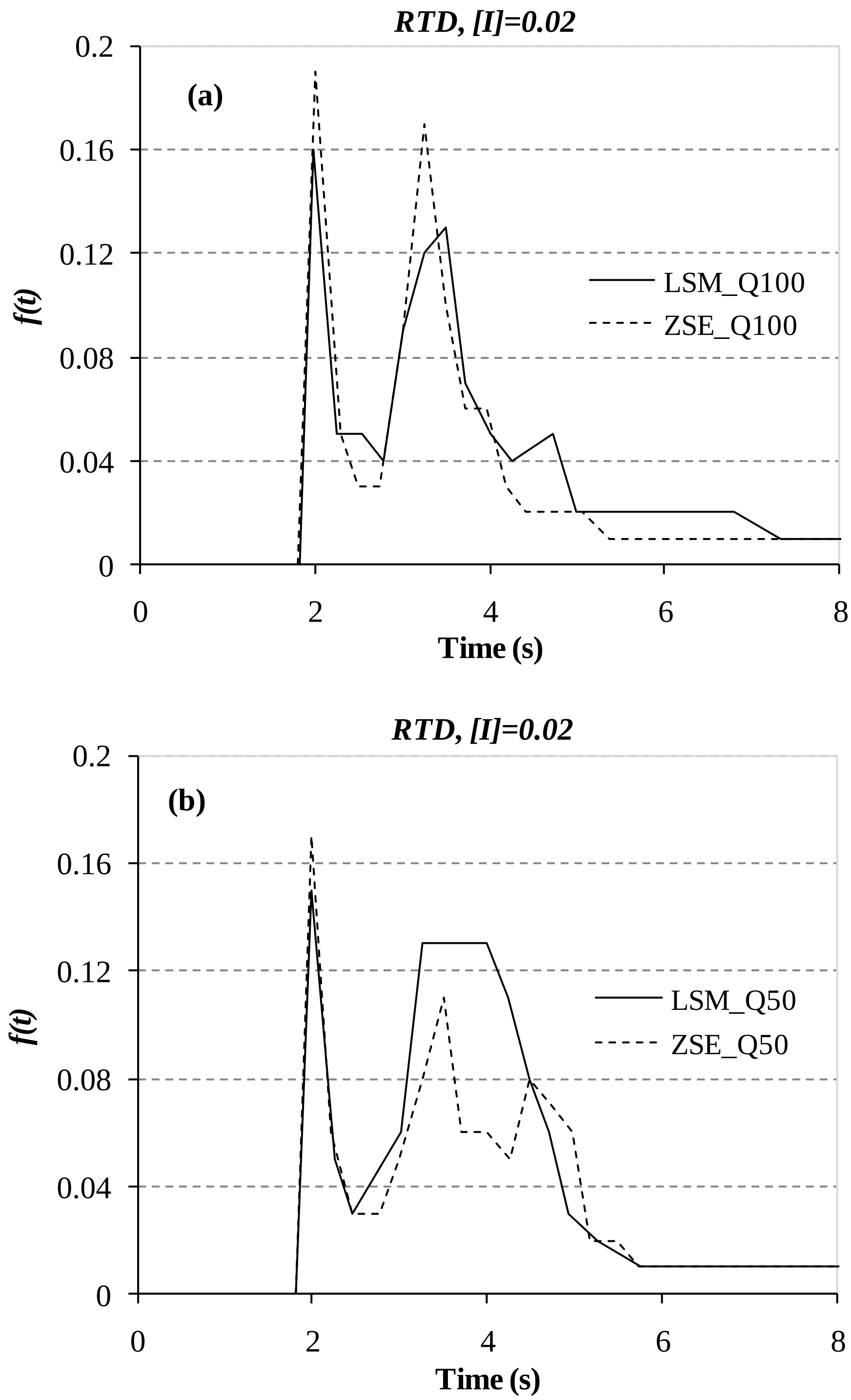

Figure 5-21 RTD variations for (a) the Q_{100} and (b) the Q_{50} mass throughputs for a peroxide concentration equal to 0.02 wt %.

are very similar for both of the two screw elements being analyzed. This behavior along with the fact that the temperature rise is very similar for the less restricted flow conditions, may explain the very similar values of the Mw and PDI for these flow conditions in both the LSM 30.34 and the ZSE screw elements. In the case of the lower mass flow rate, the shape of the curves makes it difficult to establish a difference in terms of their broadness. In this case, similarly to what has been discussed in the previous section, for the more restricted flow conditions (Q_{50} mass throughput values) the fact that few particles with high values of residence time are taken into account in particle-tracking analysis makes it difficult to interpret the latter results. In addition to the RTD curves presented in Figure 5.21, the corresponding cumulative RTDs are shown in Figure 5.22.

In Figure 5.23a, the evolution of the area stretch ratio is presented for all the implemented flow rates when the peroxide concentration is set to 0.02 wt %. When analyzing the results of Figure 5.23a (reacting conditions), it can be seen that regardless of the flow conditions the slopes of the curves in the region around 0.3 to 1 in the horizontal axis are very similar except for the Q_{50} mass throughput value in the LSM-30.34 screw element. This behavior, in principle, indicates poorer distributive mixing for the latter reactive flow conditions in comparison to the former ones. However, these results should be interpreted carefully, since, as previously stated, the fact that few particles with high values of residence time are taken into account in the particle-tracking analysis may influence the predictions of the mixing behavior, especially under the restrictive flow conditions used in the present simulations (Q_{50} mass flow rates). To complement the latter information, in Figure 5.23b TS simulation results corresponding to the non-reactive case obtained under the conditions described in Section 5.1.2 are presented. It is very interesting to note that the predictions in this case imply a

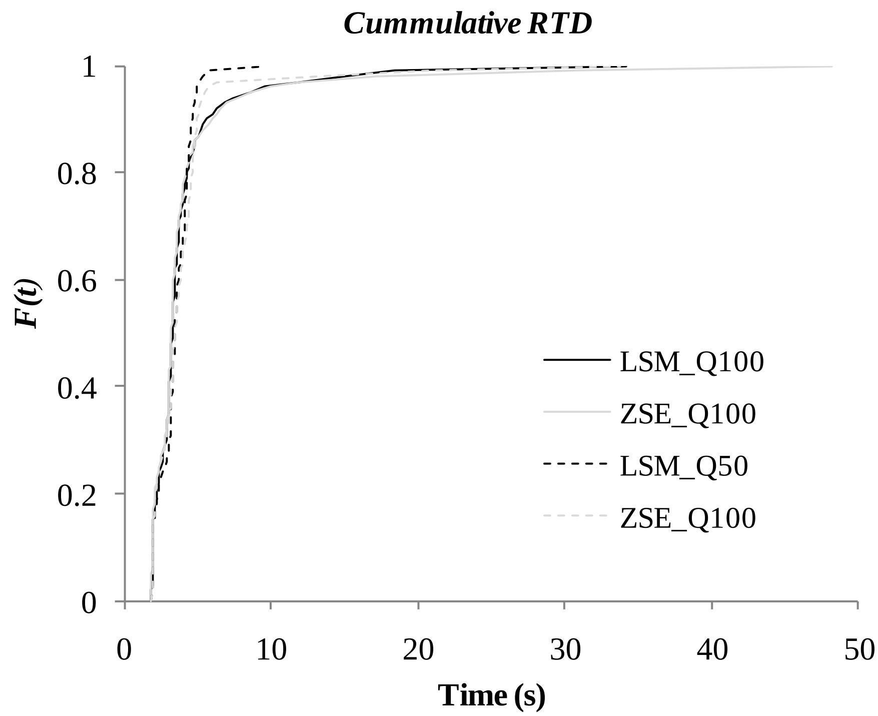

Figure 5-22 Cumulative RTD variations for the Q_{100} and Q_{50} mass throughputs for a peroxide concentration equal to 0.02 wt %.

slightly better mixing performance for the LSM-30.34 screw element than for the SZE-96 screw element. These results differ from those obtained by implementing the MRS simulations for REX conditions, as previously indicated. Considering the findings of the previous section regarding the fact that the peroxide concentration has no significant effect in the mixing capabilities of the REX system, then the results from Figure 5.23b indicate that the LSM 30.34 screw element may present slightly better mixing capabilities than the ZSE-96 screw element both for reactive and non-reactive flow conditions. This behavior could be related to the fact that although the screw elements are very close scaled-up versions of one another, still the LSM-30.34 has relatively shallower screw channels than those of the ZSE-96 element

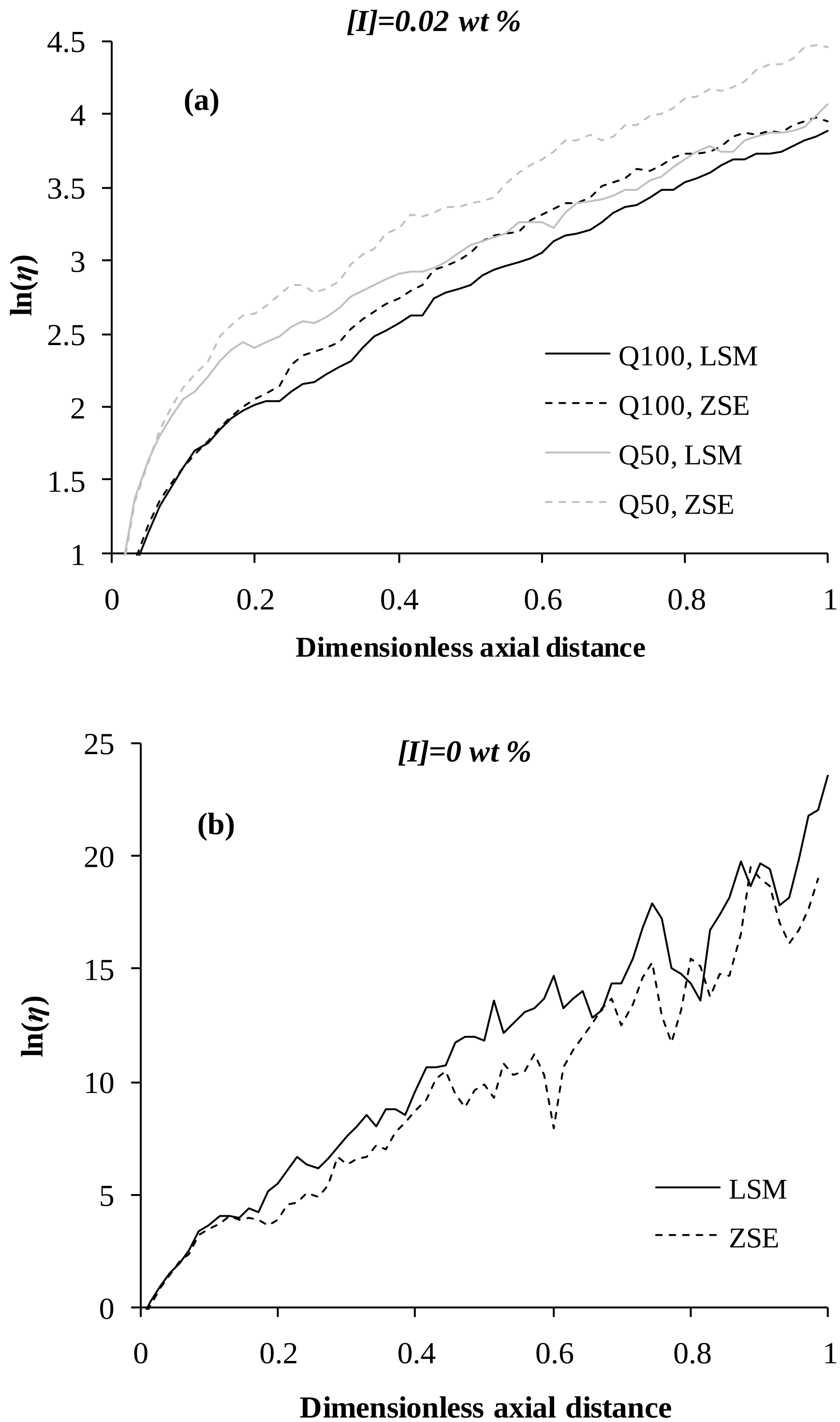

Figure 5-23 Area stretch variations for the (a) reactive conditions (MRS analysis) and (b) non-reactive conditions for the Q_{50} mass throughput (TS analysis).

(recalling the value for the channel depth scale-up index, h=1.06). The latter difference in the relative channel depth may imply that the fluid elements undergo higher deformations in the reference screw element, which can be related to slightly better distributive mixing capabilities.

Since from the information provided by the RTD curves corresponding to the Q_{50} mass throughputs for the MRS simulations it was not possible to infer the differences in the RTDs for the Q_{50} mass flow rate values, an additional flow and particle-tracking analysis is briefly presented here. Firstly, with the aid of Table 5.6 corresponding to the TS non-reactive non-isothermal Newtonian calculations, the average residence times and standard deviations calculated from a particle-tracking analysis are presented. It can be seen from the values of the standard deviation that a slightly broader RTD would correspond to the ZSE-96 screw element. Here, it is also very interesting to note that in contrast with the calculations from the MRS, the values of the average residence time are very close to those calculated from the volumetric capacity of the screw elements and the specified flow rates (see Tables 5.5 and A-5). On the other hand, from Table 5.7, it can be seen that the average pressure drops for both of the analyzed screw elements are very similar in the case of the TS calculations, whereas the value of this parameter is slightly greater for the ZSE-96 screw element when the MRS simulation approach is implemented for reactive non-isothermal Newtonian conditions. From the results from Tables 5.6 and 5.7, the association of higher pressure drops to a broader distribution of the RTD as indicated in the discussion presented in Section 3.6 "Additional Considerations of the Flow in Screw Elements of COITSEs" is not very clear. However, the RTD results (Table 5.6) suggest that the ZSE-96 screw element presents a slightly broader RTD than that of the LSM-30.34 screw element. Then, this consideration would account for

Table 5-6 Average residence time, $\bar{t}$, and STD deviation, STD, for the LSM-30.34 and ZSE-96 screw elements from TS simulations.

Screw element	$\bar{t}$ (s)	STD (s)
LSM-30.34	14.62	10.01
ZSE_96	13.36	10.43

Table 5-7 Average pressure drop, ΔP, for the LSM-30.34 and ZSE-96 screw elements from both TS and MRS calculations.

Screw element	ΔP •1E-6 (Pa)
LSM-30.34_TS	2.468
ZSE_96_TS	2.440
LSM-30.34_MRS*	3.966
ZSE_96_MRS*	4.179

Non-Newtonian reactive conditions, [I]=0.02 wt %.

the lower values of the Mws and PDIs obtained for the ZSE-96 screw element when this Q_{50} mass flow rate is implemented, as has been shown in the discussion of the results presented in this section. Another possible scenario, however, would be the fact even in the case that the RTDs would be very similar for both the LSM-30.34 and ZSE-96 screw elements, the thermal time values could account for the differences observed in the Mws and PDIs when the Q_{50} mass throughput values are implemented in the different screw geometries being analyzed.

5.2.4 Thermal Time Analysis

In this section, the thermal time values for the ZSE-96 and a specific case for the LSM-30.34 screw elements, for simulations where different values of the barrel temperature have been specified, are analyzed. In this case, the Q_{50} mass flow rate and a fixed peroxide concentration of 0.10 wt % are implemented. The aim of the analysis presented below is to evaluate the behavior of the thermal time, and its relationship with the Mws and PDIs of the reacting polymer under different processing conditions. Implications of the generated results to the constant thermal time scale-up approach implemented for the 1D REX simulations will be addressed. It should be stated here that the results to be analyzed are not as accurate as it would be desired due to the problems regarding the particle tacking analysis for the MRS approach when the Q_{50} mass throughput is specified, as discussed in the previous sections.

In Figure 5.24, the evolution of the average temperature along the axial distance corresponding to simulations where different barrel temperatures are specified is presented. The specified temperatures are 200, 210 and 220 ^{o}C. All of the curves shown in this figure correspond to the ZSE-96 screw element, except for that one labeled as 210 C_R. The results in this case correspond to the simulations for the reference element when a barrel temperature equal to 210 ^{o}C (reference temperature) has been specified. From Figure 5.24, it is evident that the temperature profile of the system is substantially modified when different barrel temperatures are implemented. Therefore, significant differences would be expected in the final values of both the Mw and PDI.

The corresponding Mw and PDI variations along the axial distance of the analyzed flow geometries are presented by means of Figure 5.25. As expected, the decrease of the

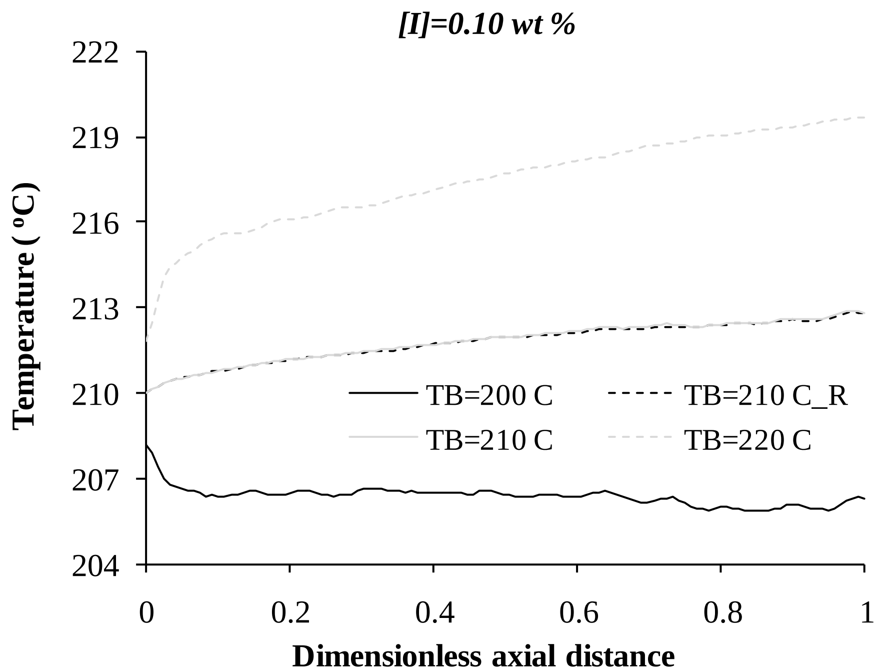

Figure 5-24 Evolution of the average temperature of reaction for different barrel temperatures.

temperature is related to an increase of the final values of the processing parameters being analyzed, whereas a converse situation occurs when the barrel temperature is increased. It is also interesting to note that for the reference temperature the Mw and PDI values of the LSM-30.34 screw element are lower than those of the ZSE-96 screw element. However, the final values of these variables are higher for the latter flow element than those of the reference one when the barrel temperature is set to 200 ^{o}C. Therefore, it would be expected that a decrease (from the reference temperature) by less than 10 ^{o}C, in the barrel temperature of the ZSE-96 screw element, would lead to a matching of the final values of the PDI and Mw in both the reference and larger screw elements.

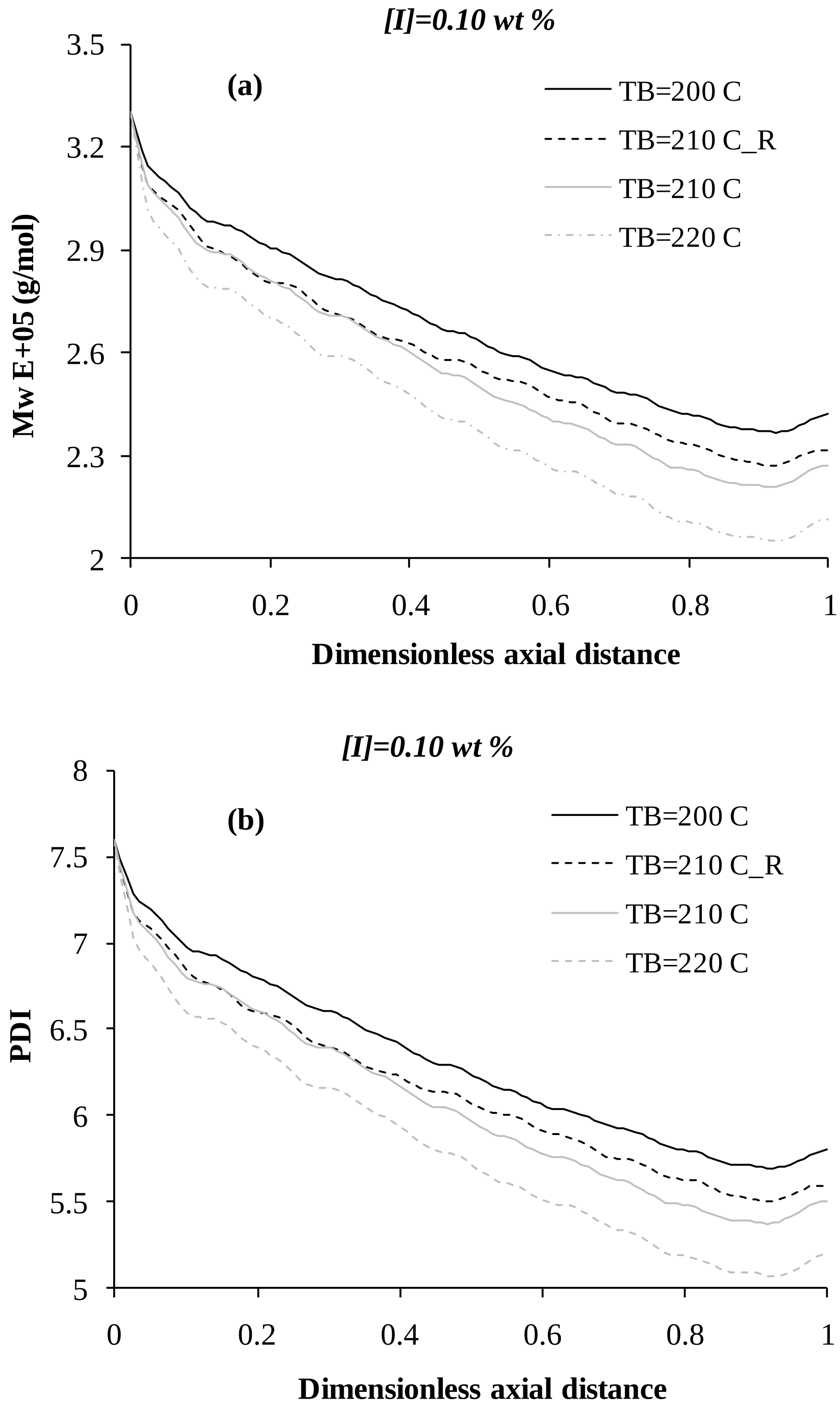

Figure 5-25 (a) Mw and (b) PDI variations of the average temperature of reaction for different barrel temperatures.

In Figure 5.26, the corresponding thermal time distributions (t_TDs) for the simulation results being discussed are shown. In general terms, the shapes of the t_TDs are very similar regardless of the implemented simulation set of boundary conditions except for the ZSE-96 screw element when the barrel temperature is set to 220 ^oC. Particularly, since the onset of the t_TD curves is the same when the same barrel temperature is implemented, a direct comparison of the results shown by means of Figure 5.26a can be made. In this case, it can be appreciated that the curve corresponding to the ZSE-96 screw element is broader than that of the LSM-30.34 screw element. This can be readily related to the lower value of the PDI observed in the case of the larger screw element than that corresponding to the LSM-30.34 screw element when the reference barrel temperature is implemented.

To complement the information regarding the t_TD curves, the average values of the t_T obtained from such curves is shown in Table 5.8. From this table, it can be appreciated that as the temperature of the system increases (for the ZSE-96 screw element) the thermal time increases. Also, it is observed that when the thermal time of the ZSE-96 extruder element is higher than that of the LSM-30.34 screw element a lower value of the Mw is obtained and vice versa. These results confirm the relationship between the final values of Mw and PDI, and the average t_T values of the system. Therefore, this information confirms the validity of the proposed scale-up approach in the case of the 1D REX simulations. From the previous analysis, it is demonstrated that an additional approach (to that described for the 1D simulations) for keeping a constant thermal time during the scale-up procedure may consist in varying the barrel temperature of the larger extruder.

In closing this section, it is important to emphasize that COITSEs generally operate under partially-filled conditions. Then, the extrusion operation may be scaled-up to keep

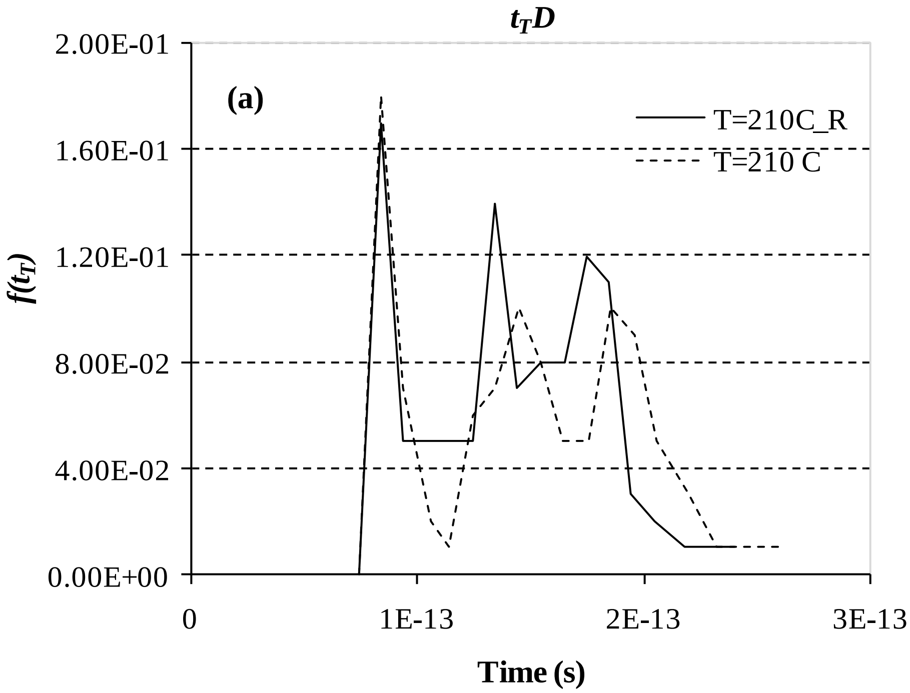

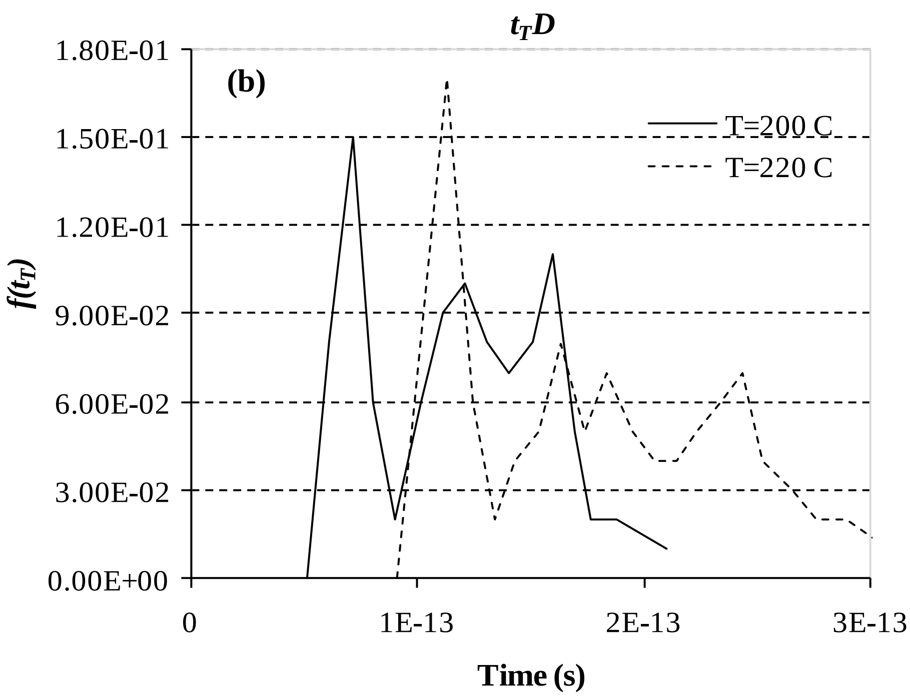

Figure 5-26 Thermal time distribution curves for different values of the barrel temperature. Curves for (a) the LSM-30.34 and ZSE-96 screw elements and (b) the ZSE-96 screw element.

Table 5-8 Average t_T values for the ZSE-96 and LSM-30.34 screw elements when different barrel temperatures are specified. Here, R refers to the LSM-30.34 screw element.

Barrel temperature	t_T mean
200 C	1.06E-13
210 C_R	1.21E-13
210 C	1.50E-13
220 C	1.88E-13

hydrodynamic similarity, that is, to keep a similar profile of the fully- and partially-filled sections of the extruder. If this were to be the case, from the results presented here there might not be important differences in the final values of the Mws, PDIs and temperature of the two extruders corresponding to the screw elements being analyzed. However, if the extrusion operation were to be scaled-up at different hydrodynamic conditions, e.g., from 13.17 to 631.8kg/hr in the LSM-30.34 and ZSE-96 extruders, more important differences in the aforementioned processing parameters would arise. It is also important to note that the type of information presented here should not be interpreted in an isolated fashion but combined with the information generated from the 1D simulations. In this regard, the information provided by 3D results may prove very useful in validating and complementing that corresponding to the 1D simulations.

5.3 Flow Analysis and Possible Improvements of the Simulations

In this section, the results for the evolution of the average cross-section mass flow rate and viscosity along the axial direction of the flow geometry are presented for selected cases. By means of this information, the accuracy of the generated simulation results and some conditions that may be improved regarding the present simulations are briefly addressed.

In Figure 5.27, the evolution of the flow rate for both reactive (for a value of the peroxide concentration equal to 0.02 wt %) and non-reactive conditions is presented. The simulations labeled as Q_{100} and Q_{50} refer to the non-restricted and restricted flow conditions, respectively. In the latter case, the specified flow rate was half of that obtained for the non-restrictive flow case. Although the obtained flow rates at both the inlet and outlet sections of the flow domain are very close to the implemented values of Q_{100} and Q_{50} (usually less than 0.001 % of such values, from simulation results), these results are not constant along the axial distance of the screw elements (for reference, to solve the continuity equation POLYFLOW® makes use of a pressure-velocity coupling). One possible explanation for this could be related to the type of mesh elements implemented to discretize the flow domain. In this case, tetrahedral elements are being used, which are a standard option to discretize complex geometries. However, the use of more regular meshing schemes consisting of brick elements are expected to provide a better description of the flow field (Galaktionov et al., 2002). In fact, the MST computational approach implemented in this work can provide one with a very regular meshing scheme, but while the underlying assumptions implemented in this approach are suitable for describing the momentum and energy equations (Avalosse et al., 2000), these same considerations do not apply to reactive systems.

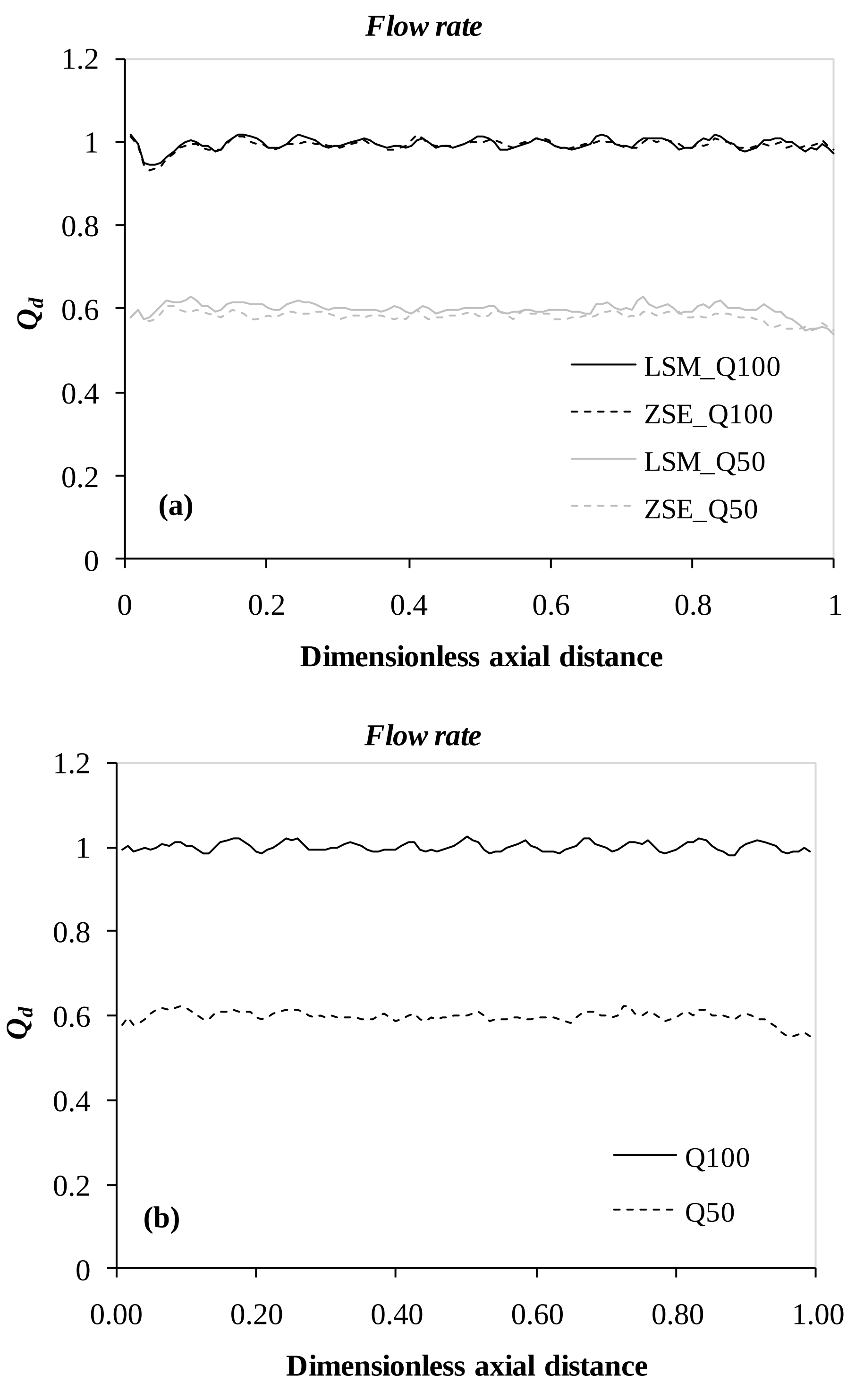

Figure 5-27 Dimensionless flow rate variation for (a) reactive conditions in the ZSE-96 and LSM-30.34 screw elemnts and (b) non-reactive conditions in the LSM-30.34 screw element.

Another drawback regarding the numerical computations presented in this work is related to the relatively low number of tetrahedral elements used when discretizing the flow domain. This is in part related to the increase in both the computational time and memory associated to the reaction kinetics describing the flow system. It was observed that the memory requirements increased almost by a factor of three when going from the non-reactive system to the reactive one. This relatively high increase in memory cost is related not only to the number of variables represented by the reaction species but also to the fact that an up- winding scheme had to be specified for the transport of species, which further contributes to the behavior being discussed.

In Figure 5.28, the results for the evolution of the cross-section average viscosity along the axial direction of the flow geometry are presented for the same conditions corresponding to Figure 5.27. From this figure, it can be appreciated that the trend of the viscosity profile presents oscillations, similarly to what is observed for the evolution of the volumetric flow rate (Figure 5.27). As it has already been highlighted, this behavior may be related to the type of grid being implemented. From Figure 5.28, also important entrance and exit effects are observed for the variation of the average cross-section viscosity. It is possible that some considerations such as mesh refinement, type of grid, and specification of flow boundary conditions may reduce such effects. In the literature several considerations can be found with respect to the specifications of flow boundary conditions at the entrance and exit of COITSE elements (Kruijt et al., 2001; Bravo et al., 2004; Zhu et al., 2005 a and b). Particularly, the boundary conditions implemented by Zhu et al. (2005 a and b) seem to be a very reasonable approach to be implemented for the type of simulations presented in this work.

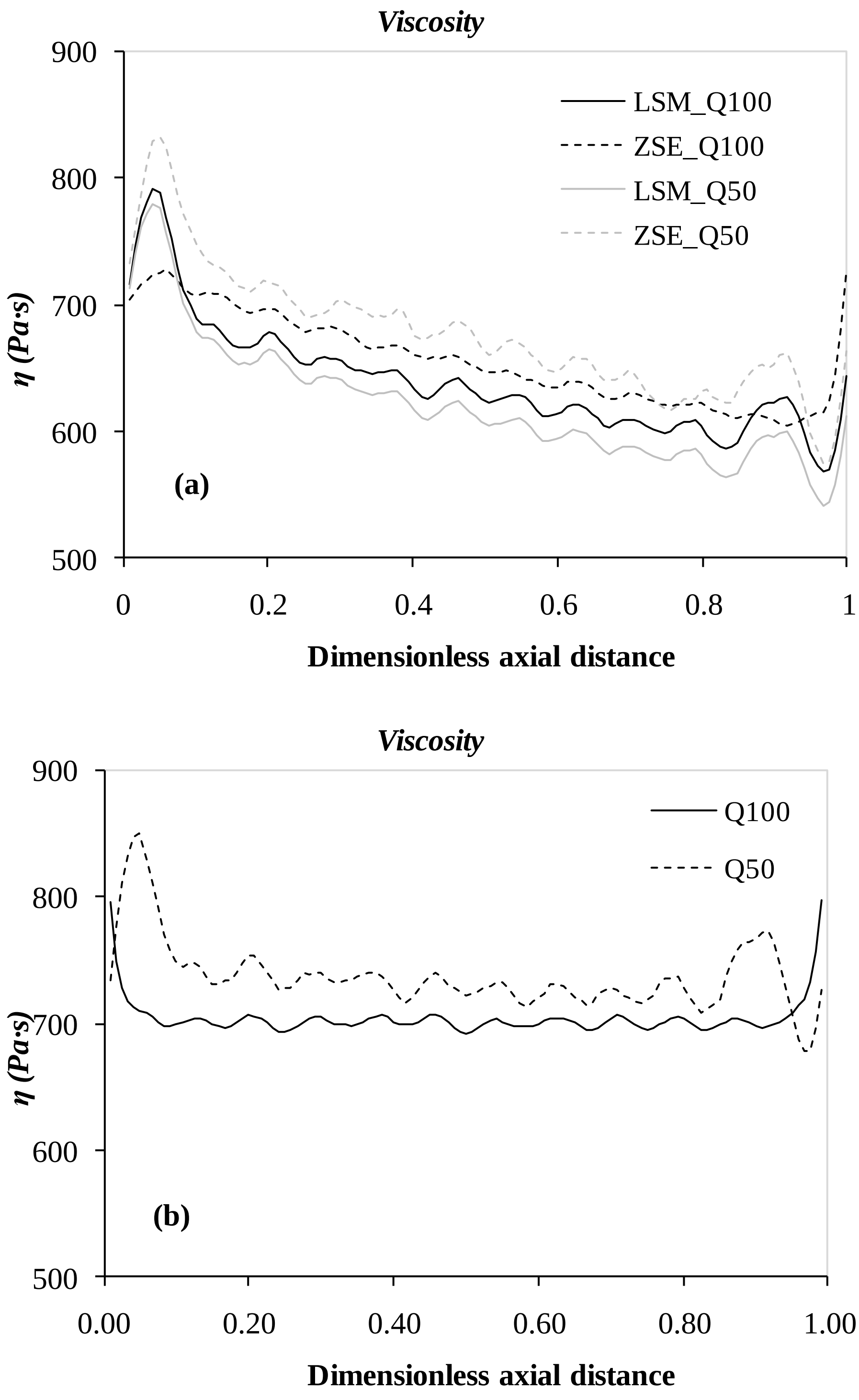

Figure 5-28 Average viscosity evolution for (a) reactive conditions in the ZSE-96 and LSM-30.34 screw elements and (b) non-reactive conditions in the LSM-30.34 screw element.

In the works by Zhu et al. (2005 a and b), the flow boundary conditions at the entrance of the flow geometry are described by a flow field corresponding to a plane perpendicular to the screw axis and located at half of the pitch of the screw elements. Such flow field is calculated by means of considering a non-reactive, Newtonian, and isothermal flow. In the present situation, it seems more appropriate to calculate the flow field corresponding to the entrance of the screw elements by a similar procedure, but considering non-Newtonian, non-reactive and isothermal flow conditions. Regarding the flow conditions at the exit of the screw elements, in the work by these researchers a kneading block section is specified mainly aimed to improve the convergence of the flow calculations. Because adding such an element in the present calculations violates the principle of the MRS, this is not considered as an option here. However, as previously stated, some convergence difficulties were found in some of the performed simulations which were detected to be associated with the variation of the species of reaction at the end of the flow geometry. Such convergence difficulties, however, as already stated, were overcome by specifying, at the end of the flow domain, a length of about 3 % of that of the corresponding screw element where the gradient of the reacting species was set equal to zero. It is expected that in future simulations, the simulation results may be improved by making use of a more regular meshing scheme and performing the type of correction referred to above for the flow boundary condition at the entrance of the flow domain.

6 3D REX ANALYSIS FOR A VARIABLE SPEED EXTRUDER

In this chapter, the analysis of the peroxide initiated degradation of PP is simulated for two different types of screw elements. The first of such elements is a conventional conveying screw element whereas the second one is a special type of conveying element where the cross section of the two screws is different. In Figure 6.1, a schematic corresponding to the screw elements having the same and different cross sections (SGSE and DGSE, respectively) is presented. For the special type of screw element to be addressed, the screw speed of one of the screws is twice of that of its mate. The simulation of this type of elements for non-Newtonian non-isothermal conditions has been recently presented by Zhu et al. (2008). The generation of the corresponding cross sections of both the conventional and special type of screw elements has been performed following the work by Booy (1978).

The information presented in this chapter is organized as follows. First, the general flow characteristics of the two types of screw elements are addressed by performing non-Newtonian simulations, implementing the MST to account for the transient nature of the flow. To complement this analysis and to outline some possible limitations of the MRS approach (the one being used in this work to address the REX taking place in the screw elements of COITSEs), a comparison is made between simulation results from both the MRS and transient approaches. For both of the aforementioned types of simulations, isothermal Newtonian flow conditions are assumed. In the second part of this chapter, the simulation results corresponding to non-Newtonian, non-isothermal REX conditions implementing the MRS technique are presented for both of the screw elements being studied. As in the previous

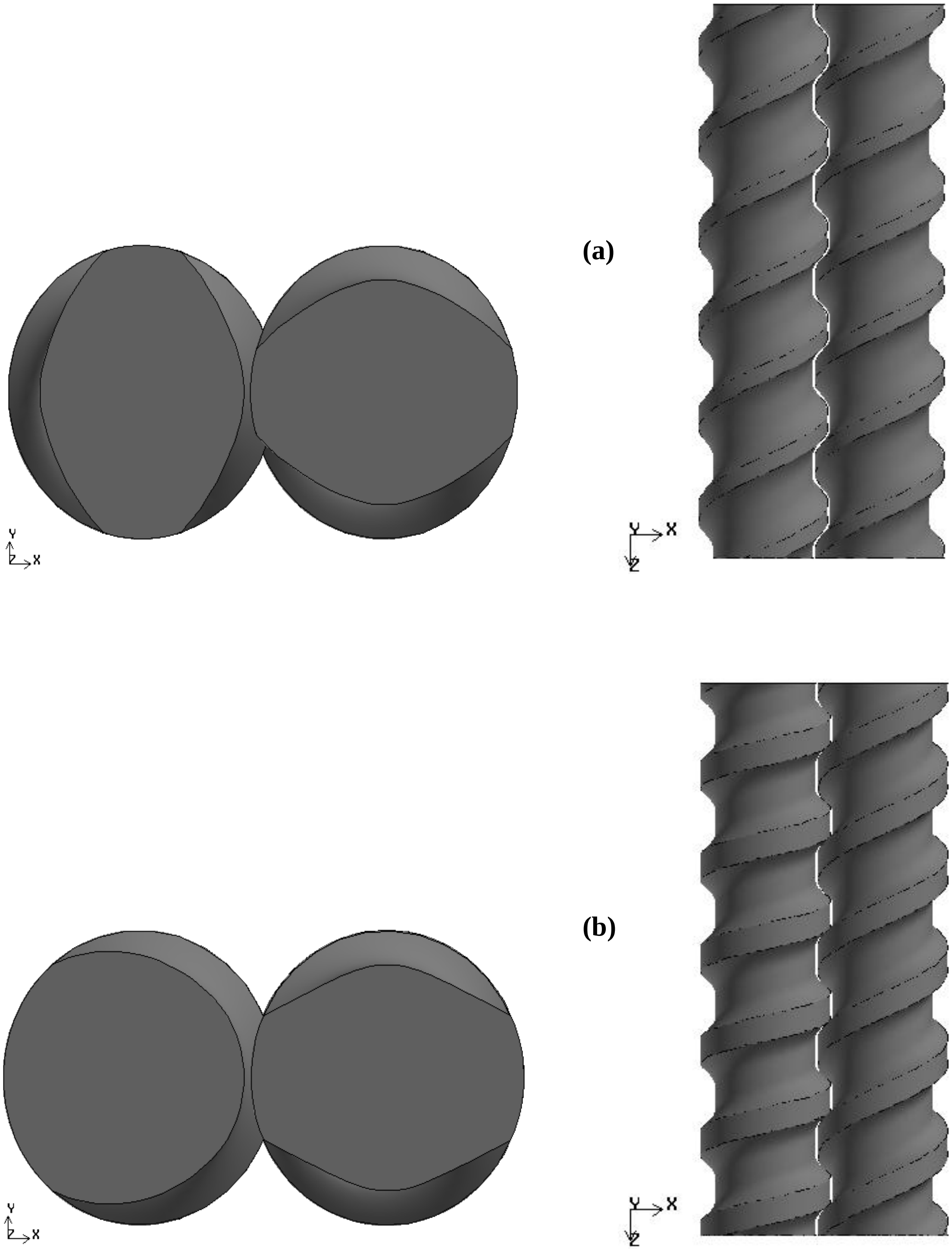

Figure 6-1 Cross sectional and top views for the screws corresponding to the (a) conventional and (b) special type of screw elements, SGSE and DGSE, respectively.

chapter, the effects of the initial peroxide concentration and mass throughput on the final Mw and PDI of the reacted polymer are studied. The temperature of reaction resulting from the specified processing conditions is discussed. Also, results generated from particle-tracking analysis for the rate of area stretch ratio and the RTD are analyzed.

6.1 Comparison Between the Transient-State (TS) and Steady-State (MRS) Simulations

Before proceeding further with the present analysis, it is important to note that the MRS approach previously implemented can also, in principle, be applicable to the special type of conveying element being analyzed here. In this case, two rotational speeds n_1 and n_2 can be defined, for the single- and double-flighted screw elements, respectively. The relationship between the given rotational speeds can be written as $n_1 = 2n_2$, whereas that corresponding to the screw pitches can be written as $2T_1 = T_2$. Therefore, in order to implement the MRS approach (as it is implemented in this work), a translational speed having the magnitude $n_1T_1 = n_2T_2$ is imposed at the surfaces of the screws.

The present discussion is started with the TS for the two different types of screw elements being addressed. The information regarding the mesh of the different specified computational domains are included in Appendix B. For the simulations of both the TS and MRS approaches, isothermal Newtonian flow conditions are implemented (as previously stated), setting the value of the viscosity equal to 500 Pas. To account for the time dependency of the flow, 20 and 15 successive positions of the screws are simulated for the special and conventional types of screw elements, respectively. In the first case, the time periodicity implies a complete revolution of the screw rotating at the higher speed and half of a revolution for the other screw. In the second case, the time periodicity corresponds to half of a revolution of both screws. The mass flow rate specified in this case (TS analysis) is 21.82 kg/hr (Q_{50}). This value corresponds to 50 % of the mass throughput obtained for the conventional screw element under non-restrictive flow conditions, Q_{100} (specification of zero normal and tangential forces at both the entrance and exit sections of the flow system). As a reference, the Q_{100} mass throughput values of the conventional and the special type of screw elements were 43.64 and 44.34 kg/hr, respectively.

In Figure 6.2, the pressure drops along the axial distance of the screw elements are presented for the geometries corresponding to the screw elements having the same and different cross sections (SGSE and DGSE, respectively). The dashed lines correspond to a linear interpolation of the averaged pressures at the entrance and exit sections of the corresponding flow domains. In this case, it can be appreciated that for the specified mass flow rates a significantly higher pressure drop is developed for the DGSE in relation to that of the SGSE. The latter can be readily associated with more restricted flow conditions arising in the former element (according to the discussion of Section 3.6). These results are in agreement with the predictions of the RTD curves which are shown by means of Figure 6.3. From this figure, it can be appreciated that the more restricted flow conditions prevailing in the DGSE are manifested in a significantly broader curve. The trend of the results resembles that obtained by Ishikawa et al. (2002) in their study of the mixing of different types of screw elements, where the element arguably having the best distributive mixing capabilities also presented a significantly broader RTD. With respect to the average residence time, from the information presented in Table 6.2 regarding the available flow cross-sectional area, along with the Q_{100} mass throughputs, it can be seen that the average residence time of the DGSE is approximately 90 % of that of the SGSE.

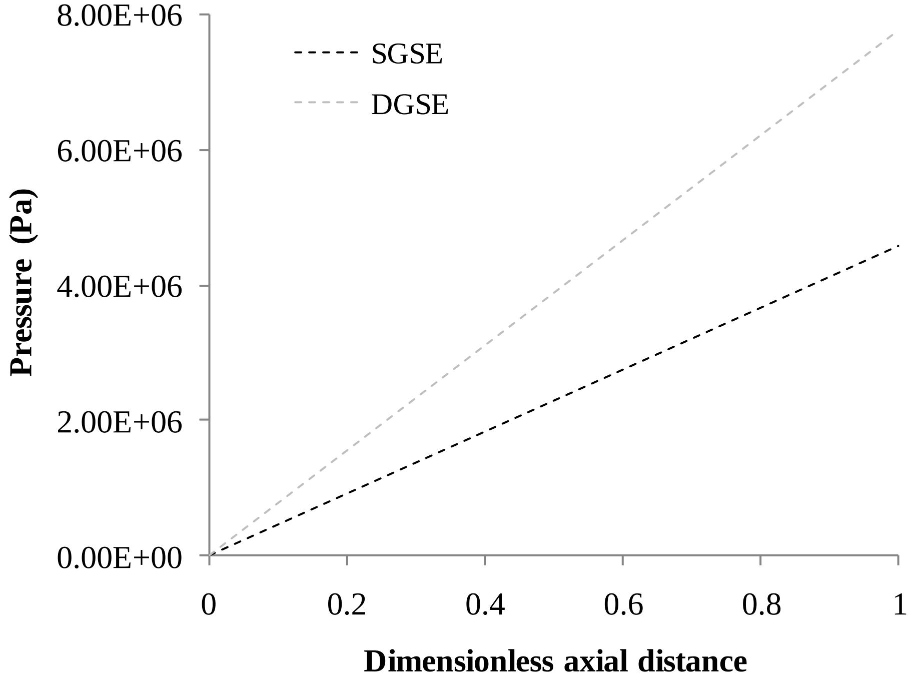

Figure 6-2 Pressure profiles for the SGSE and DGSE from MST simulations.

To have a better insight in the RTD curves just addressed, the initially seeded particles (around 1000 particles) used for the particle-tracking analysis and their positions after 5 revolutions are presented in Figure 6.4 for both the DGSE and SGSE. In the case of the DGSE, the 5 revolutions correspond to the double-flighted screw and therefore the single-flighted one rotates 10 times. As indicated in the previous chapter, although the particles are randomly seeded there are zones where no particles are found. This is mainly due to the fact that in these zones the flow is taking place mainly in the backward direction. It is interesting to note from Figure 6.4 that in the case of the SGSE the particles advancing at the front of the flow almost seem to form a cluster. This may be related to the high peak of the corresponding RTD indicating a more plug-type flow behavior. When analyzing the visualization results

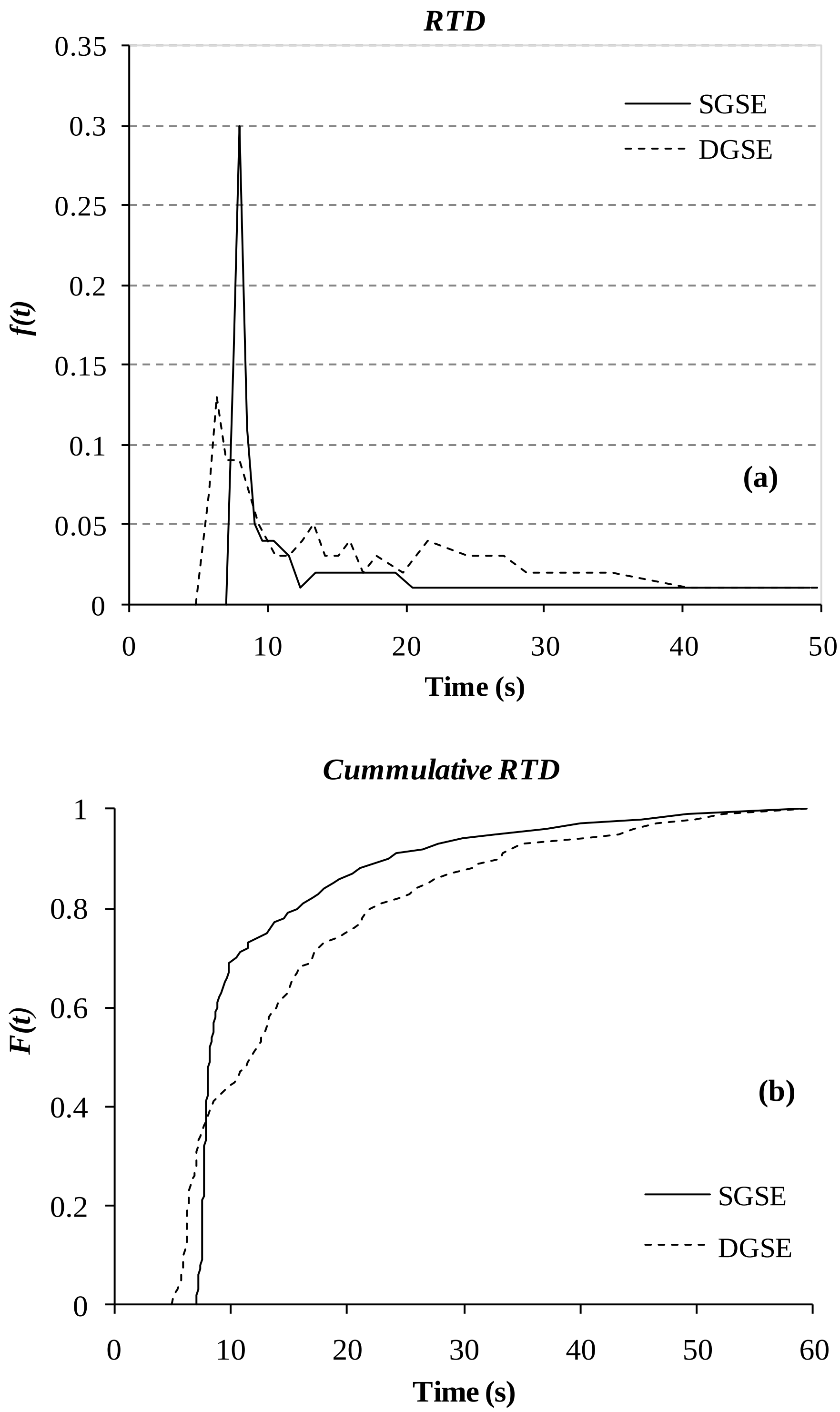

Figure 6-3 (a) RTD and (b) cumulative RTD curves for the DGSE and SGSE from transient simulations.

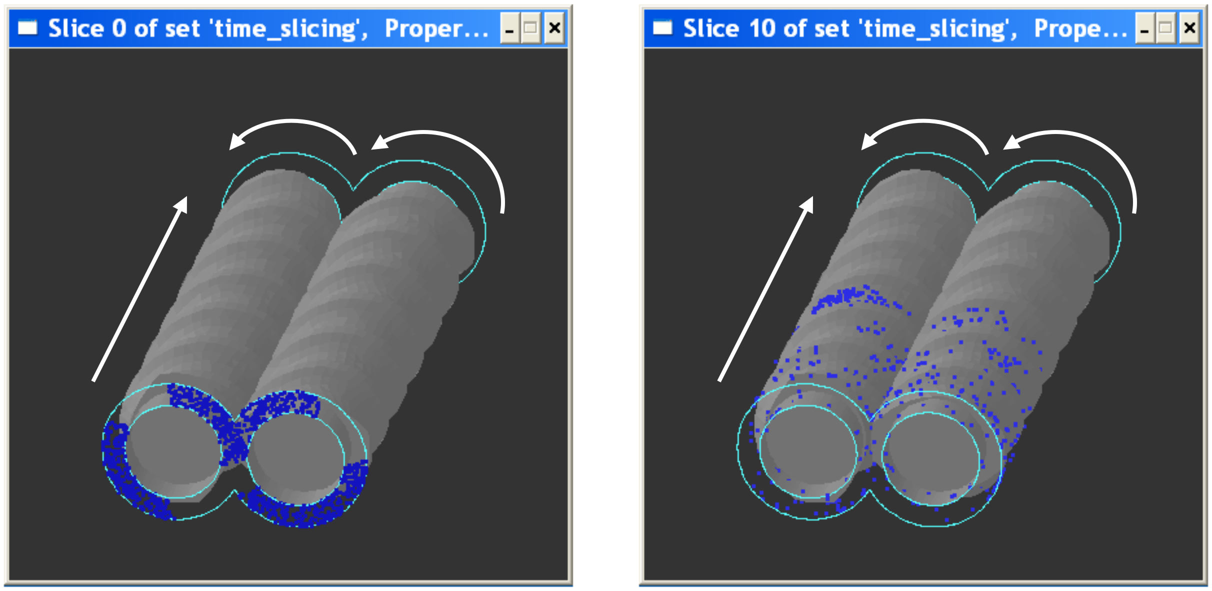

(a)

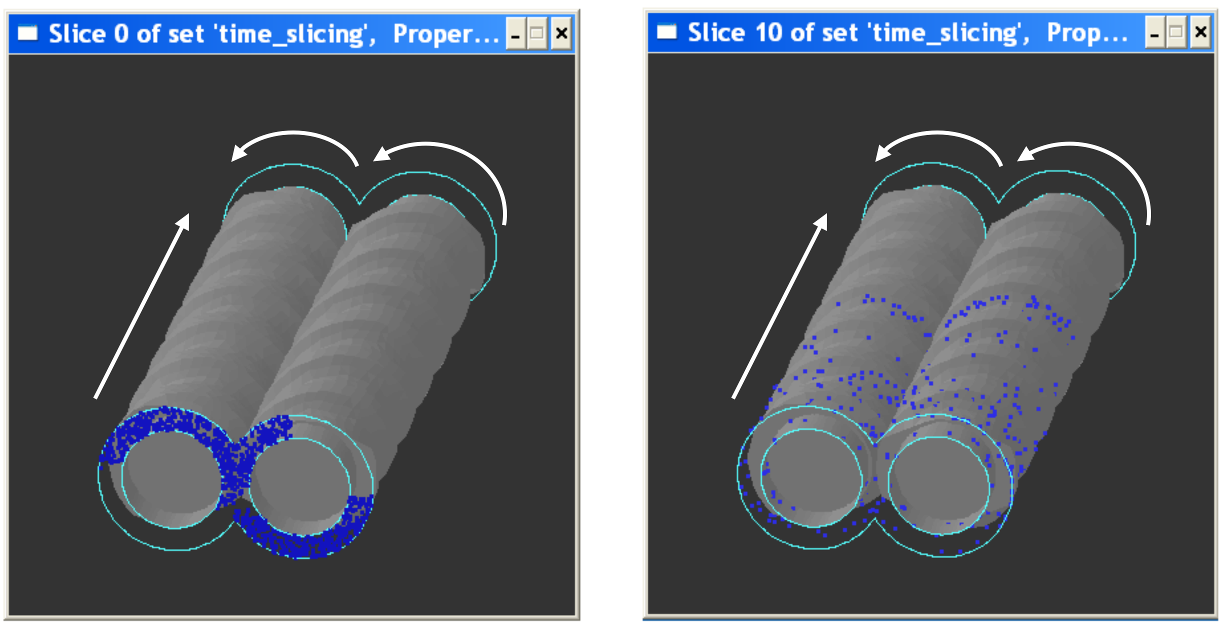

(b)

Figure 6-4 Initially seeded particles and their position after 5 screw revolutions for (a) the SGSE and (b) the DGSE. The conveying and rotation directions are indicated.

for the DGSE, it can be appreciated that in this case the flow conditions lead to a better distribution of the initially seeded particles. In Figures 6.5 and 6.6, a complementary flow analysis is presented for both of the flow geometries being studied. In this case, 500 colored mass-less particles are seeded at the side of each one of the screws of the flow geometry at an axial distance slightly greater (0.1 mm) than that corresponding to the starting of the screws. In this case the advanced positions of the particles are presented for 3, 6 and 9 revolutions (1.8, 3.6, and 5.4 s, respectively). The results from Figures 6.5 and 6.6 indicate on the one hand a more homogeneous mixing of the red and blue particles (better distributive mixing) and on the other hand, as in the case of Figure 6.4, that a cluster of particles (red ones in this case) seems to leave the flow geometry in a relatively close time period (see Figure 6.5d). This behavior, as previously indicated, is related to a more plug-type flow behavior.

In Figure 6.7, the evolution of the area stretch ratio is presented for both the SGSE and DGSE. From this figure, it can be appreciated that the latter element presents better distributive mixing capabilities than the former one. This behavior seems to be related to the relatively broader RTD exhibited by the DGSE, and it is in agreement with the visualization tracking analysis presented by means of Figures 6.5 and 6.6. The just addressed relationship observed between the RTD and the evolution of the area stretch ratio seems to be in agreement with what has been stated by several authors (Bravo et al. 2004; Ishikawa et al. 2002; Zhu et al. 2005 b), in the sense that a broader RTD is related to better distributive mixing capabilities.

The information presented below corresponds to the non-reactive Newtonian isothermal simulation of the flow in both the DGSE and SGSE when the MRS simulation approach is implemented. In this case, except for the flow rate, the same boundary conditions as those specified for the transient approach just described are implemented. The mass flow rate in this

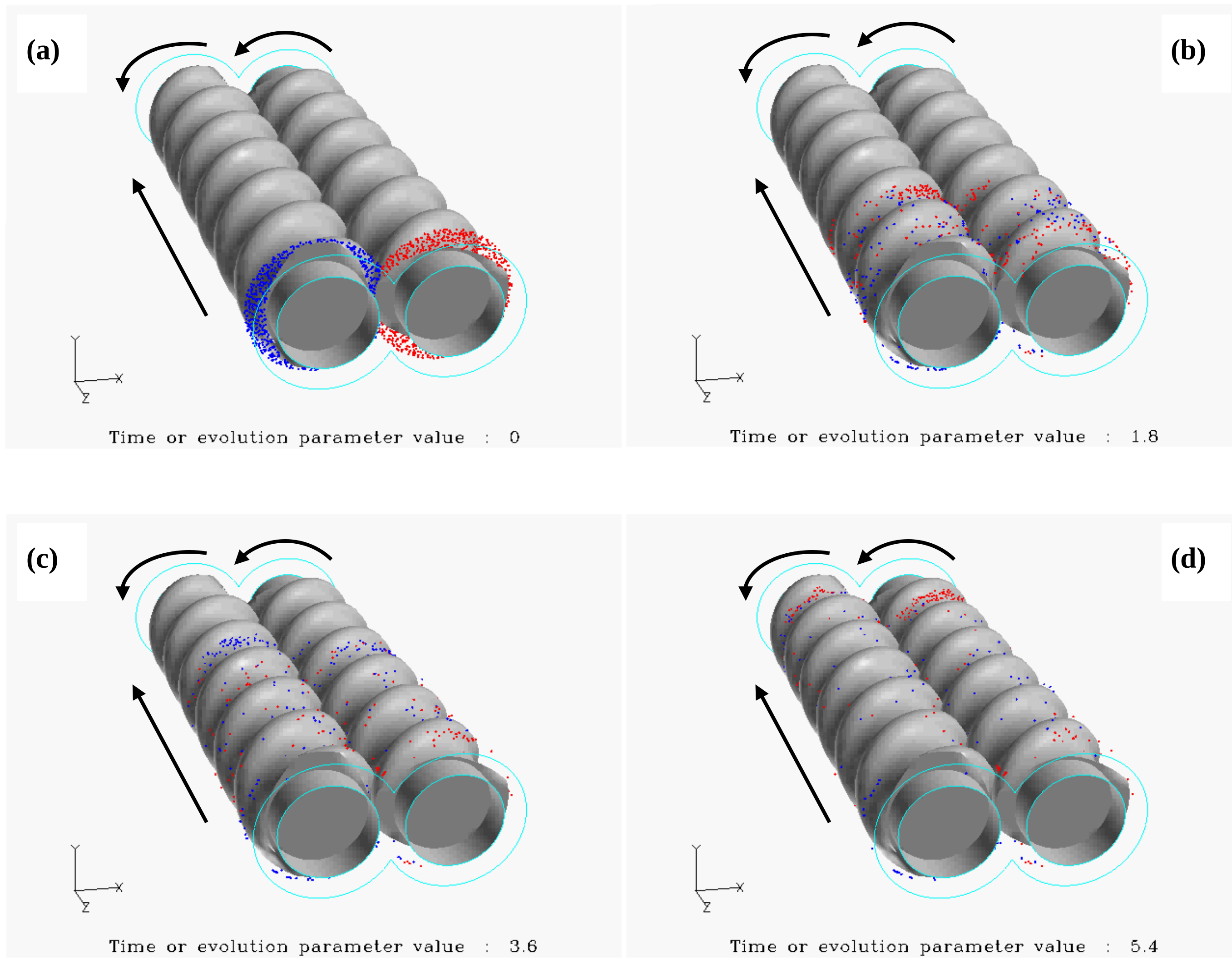

Figure 6-5 (a) Initial position of 500 red and 500 blue tracers and their positions after (b) 3, (c) 6, and (d) 9 screw revolutions in the SGSE. The conveying and rotation directions are indicated.

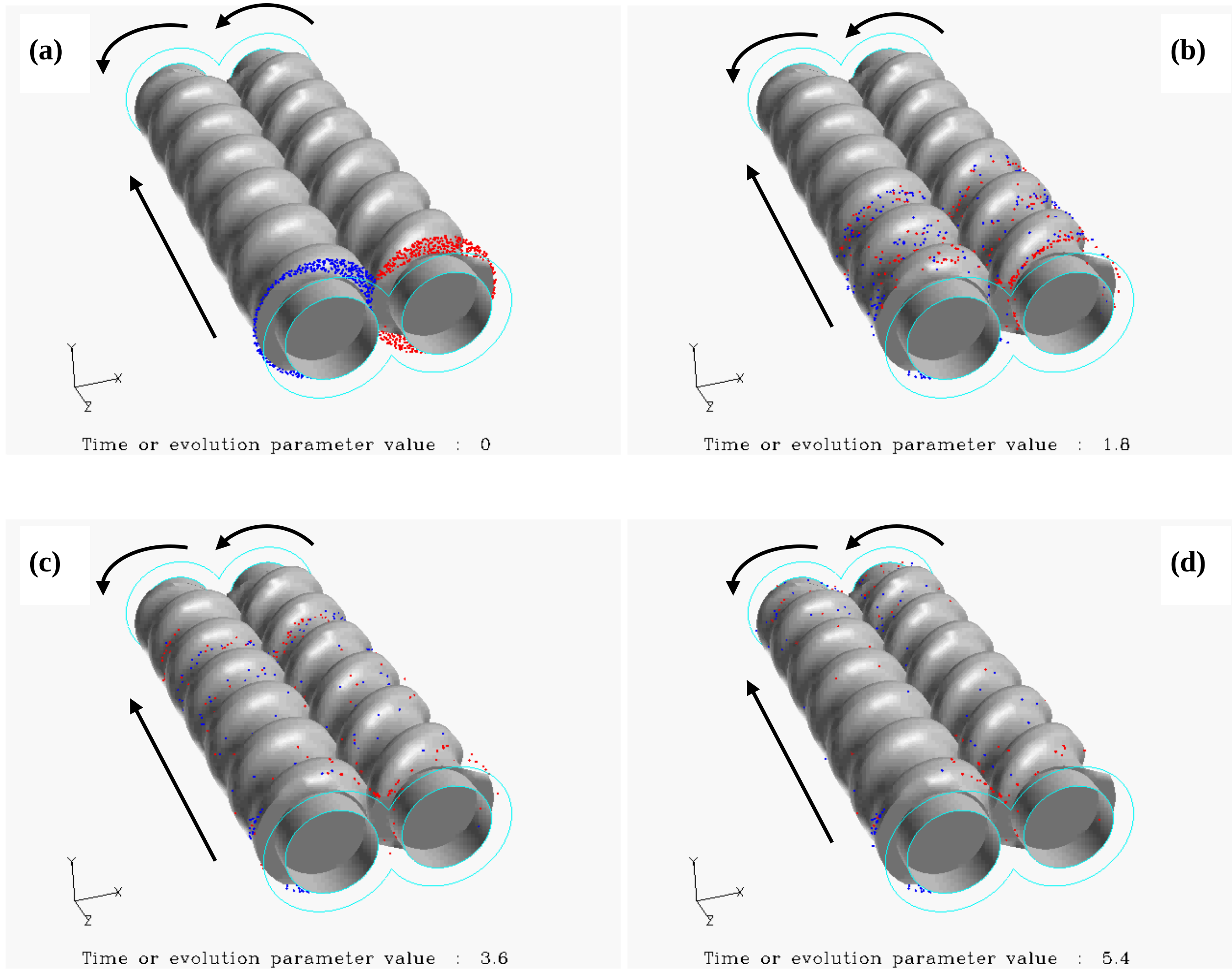

Figure 6-6 (a) Initial position of 500 red and 500 blue tracers and their positions after (b) 3, (c) 6, and (d) 9 screw revolutions of the double-flighted screw in the DGSE. The conveying and rotation directions are indicated.

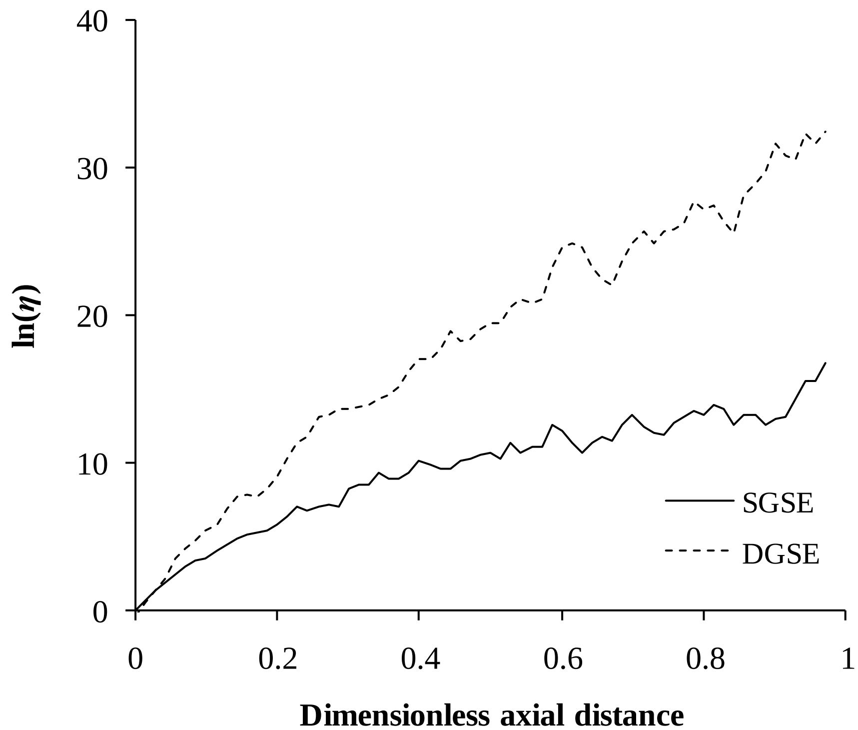

Figure 6-7 Evolution of the area stretch ratio for the SGSE and the DGSE (transient simulations).

case is 33.82 kg/hr (Q_{60}). This value corresponds to 60 % of the mass throughput obtained for the conventional screw element under non-restrictive flow conditions, Q_{100} (specification of zero normal and tangential forces at both the entrance and exit sections of the flow system). As a reference, the Q_{100} mass throughput values of the conventional and the special type of screw elements were 56.36 and 49.91 kg/hr (the corresponding screw speeds are presented in Table 6.4), respectively. Here it is interesting to note that the flow rate corresponding to the DGSE is lower than that corresponding to the SGSE, which is the converse of that observed for the TS simulation approach. This behavior seems to indicate that the capabilities of the MRS approach, in predicting the flow behavior of the conveying DGSE, may be affected by the fact that two different radial velocity vectors are defined for this screw element.

In Figure 6.8, the RTD curves corresponding to the flow elements being considered are presented for the already specified flow rate conditions. In this case, it can be seen that the shapes of the curves are similar, in contrast to what it is observed for the transient simulation approach (Figure 6.3), where the shape of the RTDs is clearly different. As in the results shown in the previous chapter, it is difficult to establish a clear difference in the behavior of the RTD curves when the MRS is implemented for highly restricted flow conditions. Figure 6.9 corresponds to the evolution of the area stretch ratio. From this figure, it can be appreciated that the predicted variation of the area stretch ratio is very similar for both of the flow elements under study. In this case, it is not possible to appreciate better stretching characteristics for the DGSE as in the case of the transient analysis simulations.

To complement the results presented in Figures 6.8 and 6.9, the predicted average residence times and standard deviations, corresponding to the particle-tracking analysis from which the previously discussed RTDs and $\ln(\eta)$ were generated, are presented in Table 6.4. The average residence times presented in this table are significantly lower than those predicted from the volumetric capacity of the screw elements and the implemented flow rates in the case of the MRS (see Q_{50} values in Table 6.2) and considerably more accurate for the TS simulations (see Q_{50} values in Table B.4). The values of the standard deviation in the case of the TS simulations indicate that there are flow particles with high values of residence time that reach the exit of the flow geometry in the particle-tracking analysis. Similarly to the results of the previous chapter, the low values of the average residence time and standard deviation in the case of the MRS approach indicate that for this calculation procedure a significant number

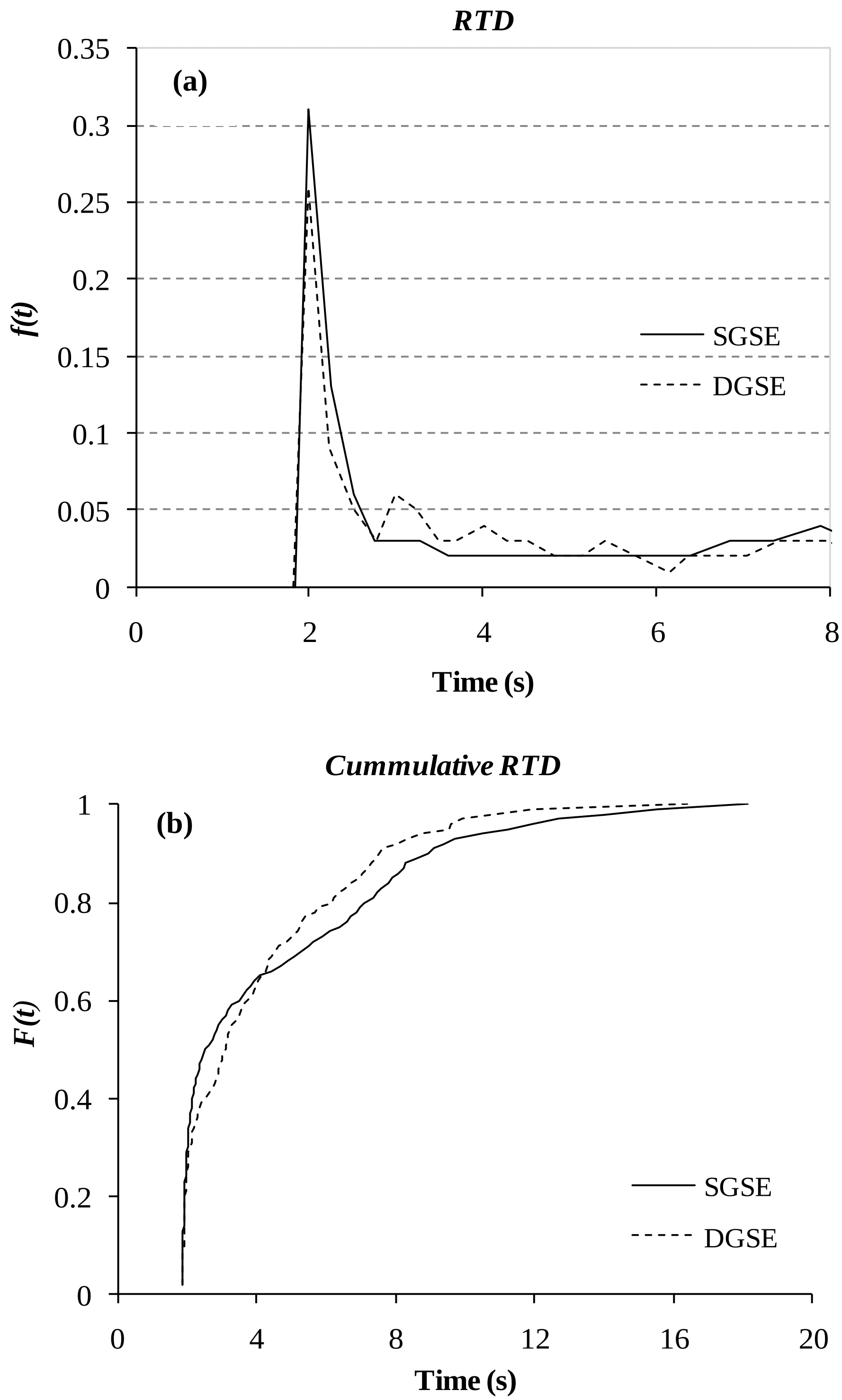

Figure 6-8 (a) RTD and (b) cumulative RTD for the SGSE and DGSE for non-reactive conditions. Calculations from the MRS approach.

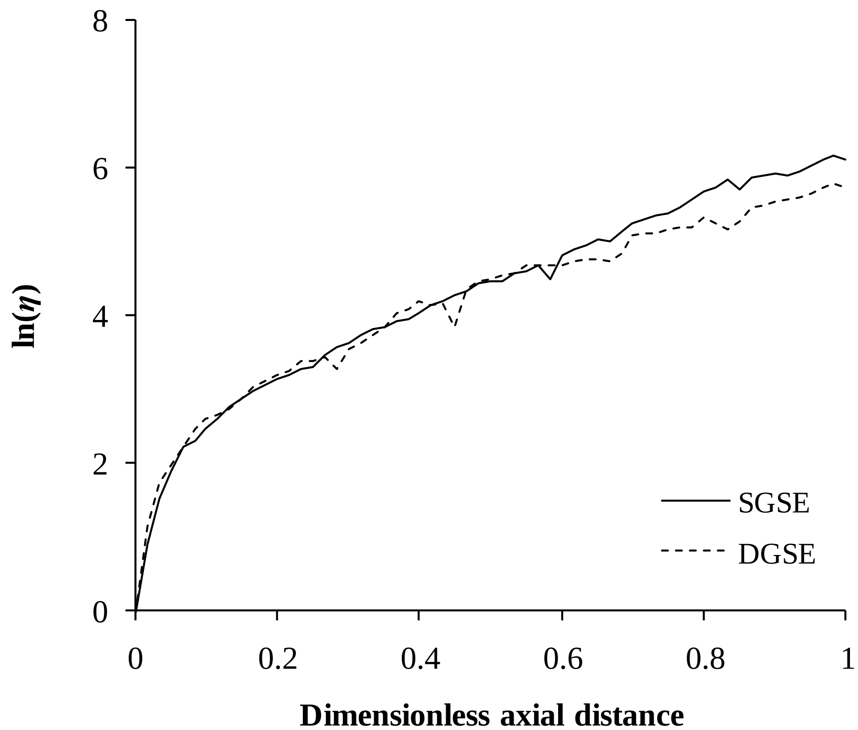

Figure 6-9 Evolution of the area stretch ratio for the SGSE and the DGSE.

Table 6-1 Average residence times ($\bar{t}$) and standard deviations (STD) for the non-reactive flow in the SGSE and DGSE when the TS and MRS simulation approaches, respectively, are implemented.

Screw element	$\bar{t}$ (s)	STD (s)
SGSE_TS	11.71	8.28
DGSE_TS	15.7	12.24
SGSE_MRS	3.9	3.03
DGSE_MRS	3.66	2.28

of flow particles having high values of residence time are not taken into account for the calculations. Therefore, as in the previous chapter, the RTD and distributive mixing behaviors of the analyzed systems are better captured when the TS simulation approach is implemented.

6.2 REX Simulation Analysis

6.2.1 Processing Conditions for Simulations

As previously stated, the simulations are performed in POLYFLOW®. The geometrical specifications for the SGSE and DGSE are given in Table 6.2. 80479 and 80466 tetrahedral elements are used to discretize the former and the latter screw elements, respectively. In Table 6.3, physical parameters of interest for the polymer being analyzed are presented. Table 6.4 summarizes the processing conditions used for the simulations. As indicated in this table, a combination of two different peroxide-feed concentrations and two mass flow rates are used for each one of the screw geometries being simulated. In Table 6.4, some of the boundary conditions implemented in this work are listed. Additional boundary conditions are non-slip conditions on solid walls, a fully developed velocity field at the inlet section of the screw element, and zero normal and tangential forces at the outlet section. On the other hand, constant inlet as well as barrel temperatures are specified, and at the outlet section of the flow domain a vanishing heat flux is imposed. Also, the screw surfaces are considered to be adiabatic. For the velocity field, an interpolation of the mini-element type (Fortin, 1981) is adopted whereas for the temperature field linear interpolation is implemented. With respect to the reacting species, a fixed concentration is defined at the entrance of the flow geometry, and a zero mass flux is specified at the barrel wall and at the exit section of the flow domain.

Table 6-2 Geometry specifications of the simulated screw elements. All quantities are expressed in mm or derived units.

Screw element	SGSE	DGSE
Screw O. diameter	34.00	34.00
Screw I. diameter	26.00	26.00
Centerline distance	30.80	30.80
Barrel diameter	35.60	35.60
Screw pitch	50.00	25.00/50.00*
Screw length	150.00	150.00
Flow-cross-sectional area	585.35	549.07

*Here the two different pitch values refer to the single- and the double-flighted screw elements, respectively.

Table 6-3 Physical properties of the molten polymer.

Density	750 kg/m^3
Thermal conductivity	0.185 W/(m °C)
Specific heat capacity	2.248 kJ/(kg °C)
Initial weight-average molecular weight	333000 g/mol
Initial number-average molecular weight	43420 g/mol

Table 6-4 Operating conditions for simulations. Q_{100} and Q_{60} stand for the implemented mass flow rates. Rt stands for the average residence time and [I] for the peroxide concentration.

Screw element	SGSE	DGSE
Q_{100}(kg/hr)/Rt(s)	55.53/4.27	49.06/4.53
Q_{60}(kg/hr)/Rt(s)	33.31/7.11	33.31/6.67
Screw speed (rpm)	100	100/200*
[I] (wt %)	0.02, 0.10	
Inlet temperature (°C)	210	
Barrel temperature (°C)	210	

*Here the two different values of the screw speed refer to the single- and the double-flighted screw elements, respectively.

The simulations were carried out on a 64 Bit computer with 8 GByte RAM memory and a 2.1 GHz dual-core processor. The computational time for the simulations was dependent on the specified boundary conditions ranging from around 2 hrs up to more than 6 hrs for each set of implemented REX conditions. In each case, at least two different type of simulations were performed, beginning with a non-reactive system either isothermal or non isothermal. In some cases, an evolutive scheme had to be specified to gradually increase either the viscous dissipation, the gradient of the reacting species or both of these factors. To overcome some problems related to the convergence of the simulations, the gradient of the reacting species was set to zero for a distance of about 3 % of that of the axial length at the end of the flow geometry. The latter procedure was especially applied to the simulations where the flow was restricted. In all of the final REX simulations, except for that where the mass flow rate was identified as Q_{60} for the DGSE, the convergence criterion was set to 1e-4. For the DGSE Q_{60}, an oscillatory behavior was observed in the solution; therefore, the convergence was set to 5e-3 in this case.

6.2.2 REX Analysis

The maximum mass throughputs presented in Table 6.4 (Q_{100}) are obtained from the simulations (for non-reactive conditions) by considering zero normal and tangential forces at the entrance and exit sections of the flow geometries. These values are used as reference values to evaluate the effect of the mass throughput in the REX for both the DGSE and SGSE. As in the case of the non-reactive flow simulations presented in the previous section, the Q_{60} mass throughput value is obtained from the Q_{100} value corresponding to the SGSE. The same considerations regarding the rheology of the system implemented in the previous chapter were considered here.

In Figure 6.10a, the temperature field for the *z*-plane located at the middle of the axial distance of the SGSE for the Q_{60} mass throughput and for the lower value of the peroxide concentration is presented. This figure indicates that the maximum values of the temperature correspond to the regions in contact with the screw surface. In Figure 6.10b, the variation of the Mw corresponding to the same *z*-plane shown in the previous figure is presented for the lower implemented value of the peroxide concentration. In this case, it can be appreciated that some of the zones where the higher Mws (which can be related to lower conversions of reaction) are found correspond to those same zones where the higher temperatures are observed in Figure 6.10a. These results agree to some extent to those found by Zhu et al (2005 b) for the polymerization of ε-caprolactone. These researchers reported that for their recating

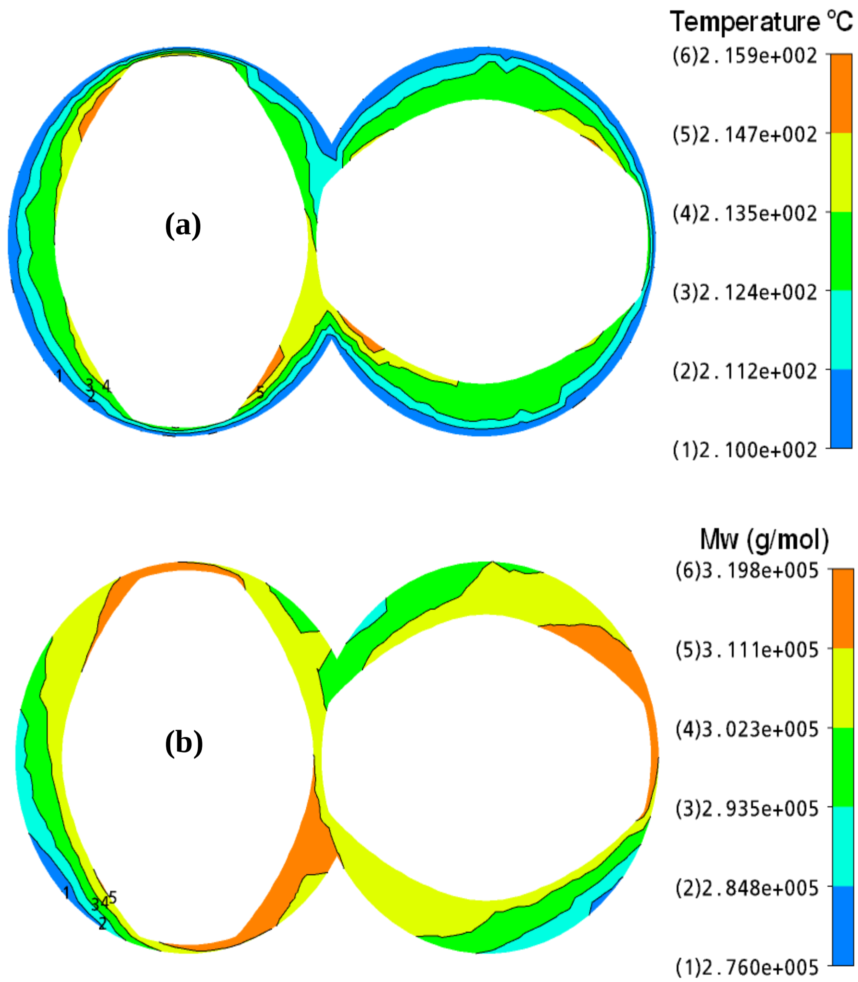

Figure 6-10 Contour plots for (a) the temperature and (b) the Mw for the SGSE. *z*-cut planes at z=75 mm, Q=33.31 kg/hr and [I]=0.02 wt %.

system the minimum values of conversion for screw elements having a relatively small pitch corresponded to zones close to the screw surfaces. As higher temperatures are in principle related to higher conversions of reaction, the previously addressed behavior may be explained considering that in the zones where high temperatures are found lower values of the residence time prevail. A converse situation to the one just addressed is observed for the region near the surface of the extruder barrel which again can be related to the residence time. In this case, because the particles moving near the barrel are slowed down due the momentum transfer mechanism occurring near the barrel of the extruder, these particles may experience higher residence times, and hence, higher conversions of reaction.

In Figure 6.11, the same type of plots as those presented in Figure 6.10 are shown, but in this case the results correspond to the higher simulated value of the peroxide concentration. The information that can be obtained from both Figures 6.10 and 6.11 is very similar. For instance, the zones of higher temperatures and lower Mws are located essentially in the same positions as it can be seen in the contour plots. An important difference, however, between the information yielded by both of the aforementioned figures if the fact that the values of the temperature are lower in the latter case.

In Figure 6.12a, the temperature field for the *z*-plane located at the middle of the axial distance of the DGSE is presented for the Q_{60} mass throughput when the value of the peroxide concentration is set to 0.02 wt %. In this case, the maximum values of the temperature field are found close to the screw having the higher rotational speed in a region where the molten polymer is being compressed by the rotating action of the screw flight. In Figure 6.12b, the variation of the Mw corresponding to the same *z*-plane shown in figure 6.12a is presented. It is very interesting to note from this figure that the regions of lower reaction conversion (higher values of the Mw) are found close to the single-flighted screw. The former observation is in good agreement with the fact that the flow elements are moving faster in this region of the conveying element, and therefore the time available for the reaction is reduced in this region of the flow system. In Figure 6.13, contour plots for the temperature and Mw fields for a *z*-plane located at the middle of the axial distance of the DGSE are presented for the higher

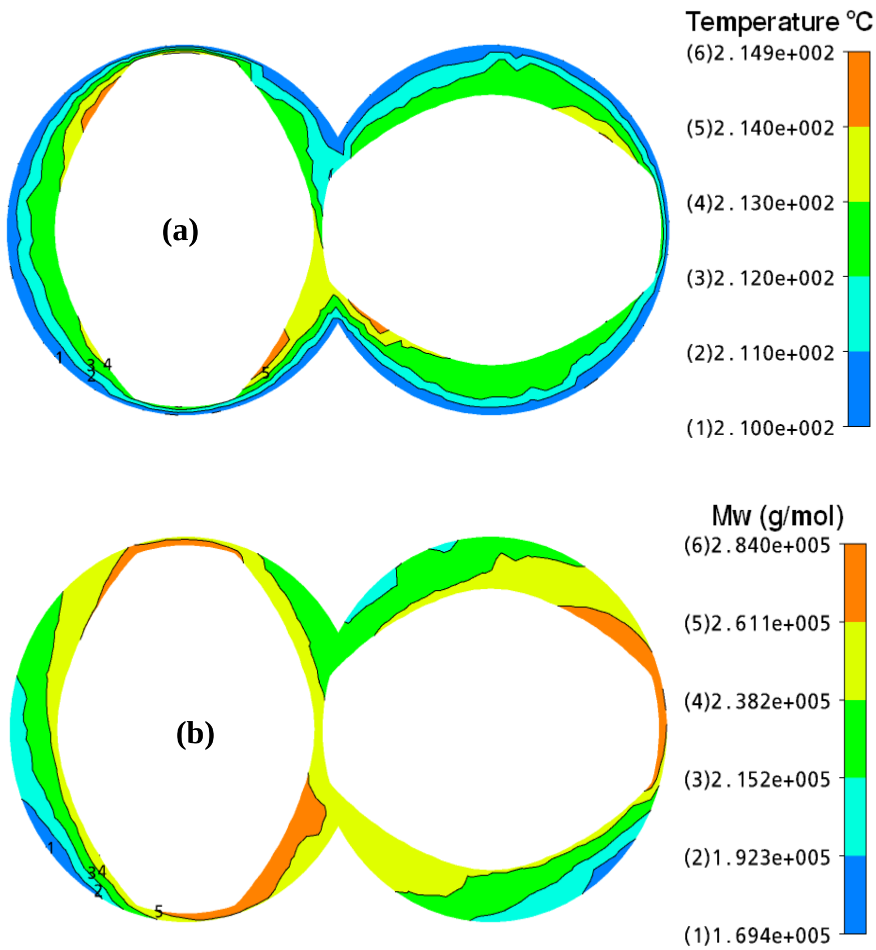

Figure 6-11 Contour plots for (a) the temperature and (b) the Mw for the SGSE. *z*-cut planes at z=75 mm, Q=33.31 kg/hr and [I]=0.10 wt %.

simulated value of the peroxide concentration. The information provided by this figure is very similar to that of Figure 6.12. As in the case of the SGSE, the values of the temperature are lower in the case of the higher implemented peroxide concentration.

In Figure 6.14, the variation of the temperature along the axial distance of the screw elements for both the DGSE and SGSE for the two implemented values of the peroxide

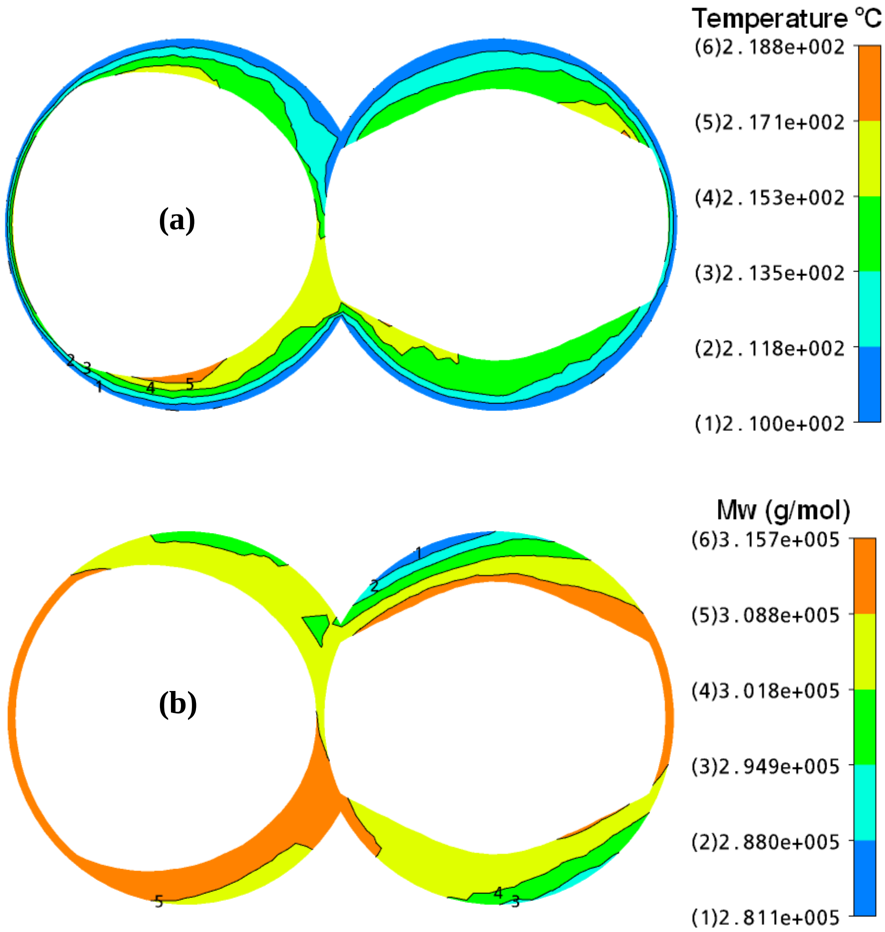

Figure 6-12 Contour plots for (a) the temperature and (b) the Mw for the DGSE. *z*-cut planes at z=75 mm, Q=33.31 kg/hr and [I]=0.02 wt %.

concentration and mass flow rate is presented. From Figure 6.14a, an important difference between the temperature profiles corresponding to the two simulated screw elements is observed when the same mass flow rate is implemented. The results shown in Figure 6.14b corresponding to the higher simulated value of the peroxide concentration are very similar to those of Figure 6.14a. In the latter case, however, slightly lower values of the temperature are

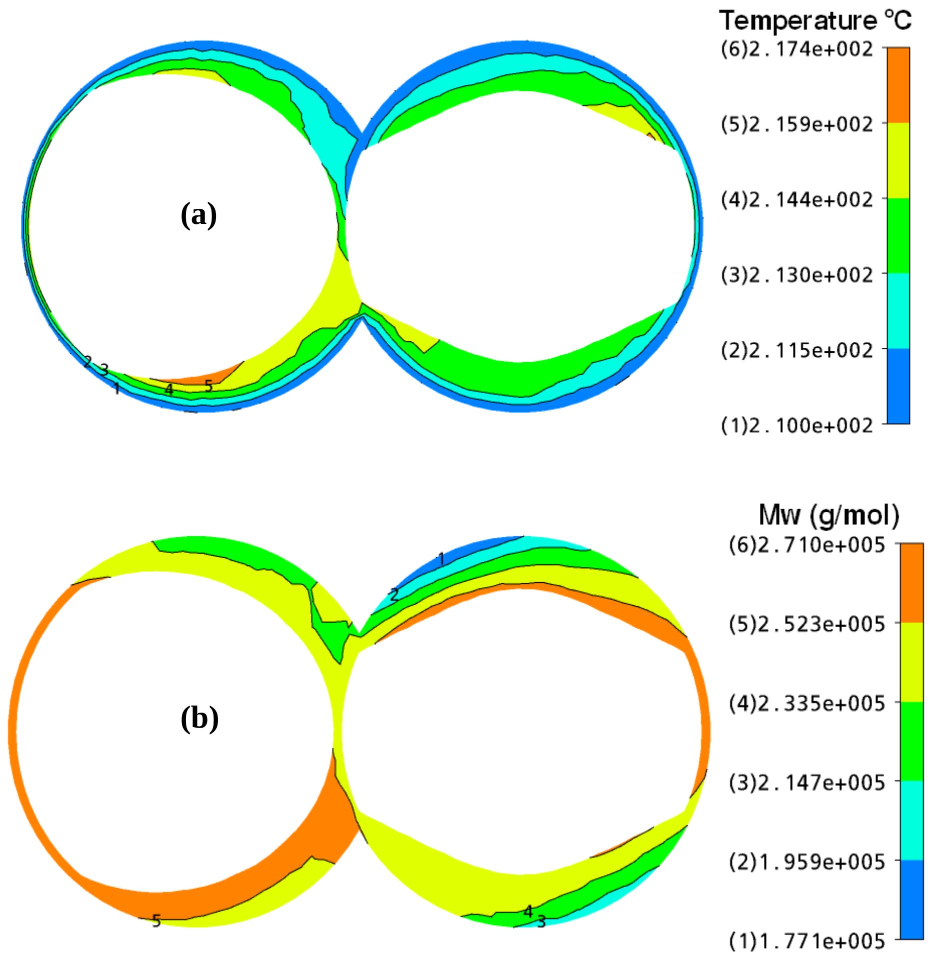

Figure 6-13 Contour plots for (a) the temperature and (b) the Mw for the DGSE. *z*-cut planes at z=75 mm, Q=33.31 kg/hr and [I]=0.10 wt %.

predicted than in the former. This is in agreement with the fact that although the viscous dissipation effects increase when the flow is more restricted, these same effects are also reduced as a consequence of the reduction of the Mw associated to the degradation reaction. Another general trend observed form Figure 6.14 is that for a particular combination of mass flow rate and peroxide concentration, a higher increase of temperature is predicted for the

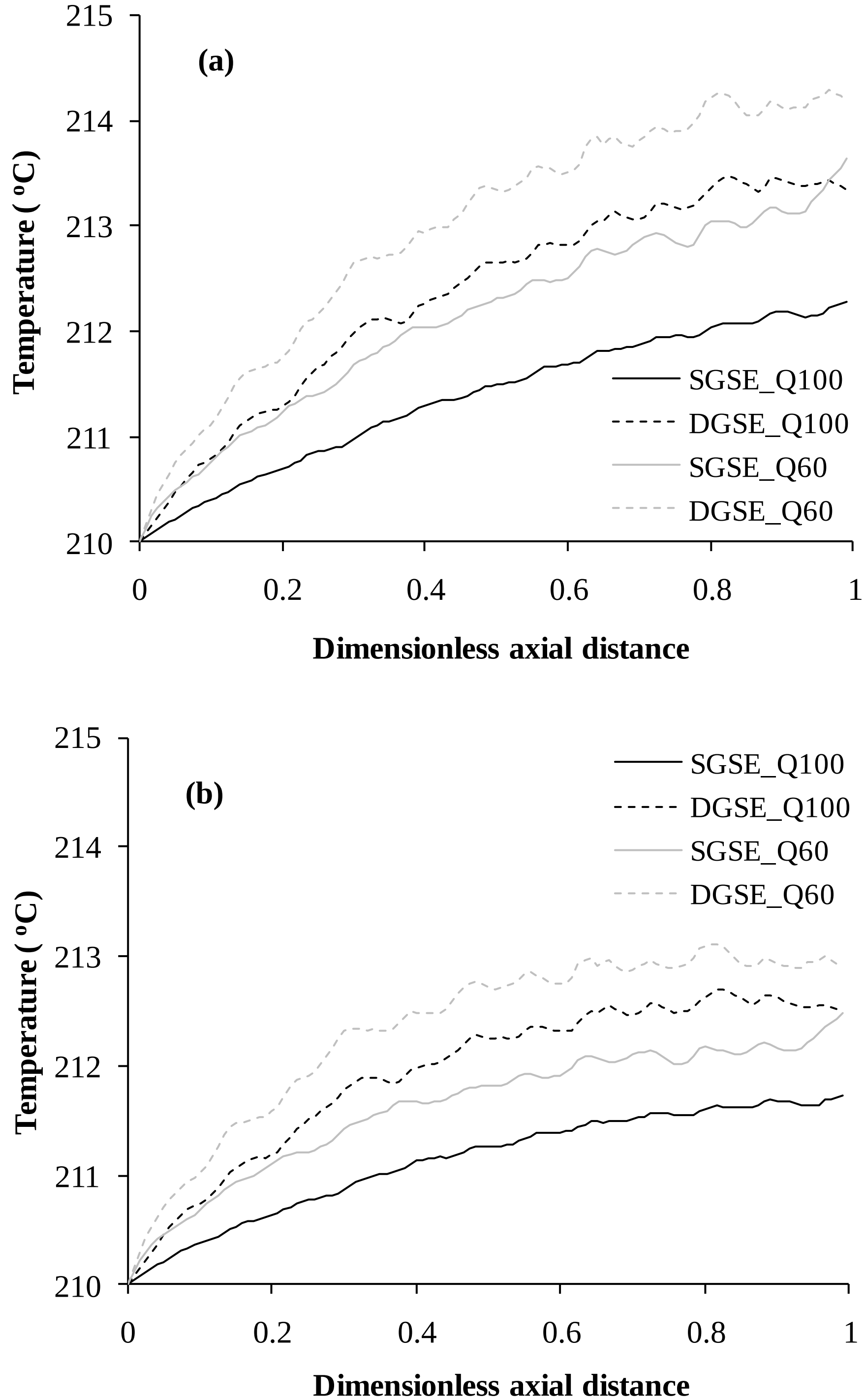

Figure 6-14 Average melt temperature variation. The corresponding peroxide concentrations are (a) 0.02 and (b) 0.10 wt %, respectively.

DGSE. The explanation for this behavior can be readily related to more viscous dissipation generated in the DGSE due to the higher shear rates experienced on the side of the screw that rotates at the higher speed (see Figures 6.12a and 6.13a).

In Figure 6.15, the variations of both the PDI and Mw along the axial distance of the screw elements being analyzed is presented for the lower implemented peroxide concentration. In these figures, the same trend is observed for the variation of these two variables. Also, it is interesting to note that the variation as well as the final value of these two processing parameters is very similar for both the SGSE and DGSE when a specific mass flow rate is implemented. In Figure 6.16, the corresponding variations of the temperature and Mw for both of the analyzed flow systems are presented for the higher implemented value of the peroxide concentration. The trend of the results in this case is very similar to that observed in Figure6.15, when the peroxide concentration is set to 0.02 wt %, but the reductions on both the Mw and PDI are significantly greater accordingly to the relatively higher value of the peroxide concentration. From the information provided by both Figures 6.15 and 6.16, it is evident that modifying the flow rate is not a determinant factor in the final Mw and PDI values when a fixed peroxide concentration and screw speed are implemented. On the other hand, the final values of these processing parameters are very sensitive to the specified peroxide concentration.

In Figure 6.17, the RTDs are shown for the SGSE and DGSE corresponding to both of the implemented flow rates for the higher implemented value of the peroxide concentration. The maximum time for the tracking of the particles was set to 50 s. These results indicate that when the less restricted flow conditions are specified (Figure 6.17a) the shape of the RTDs is

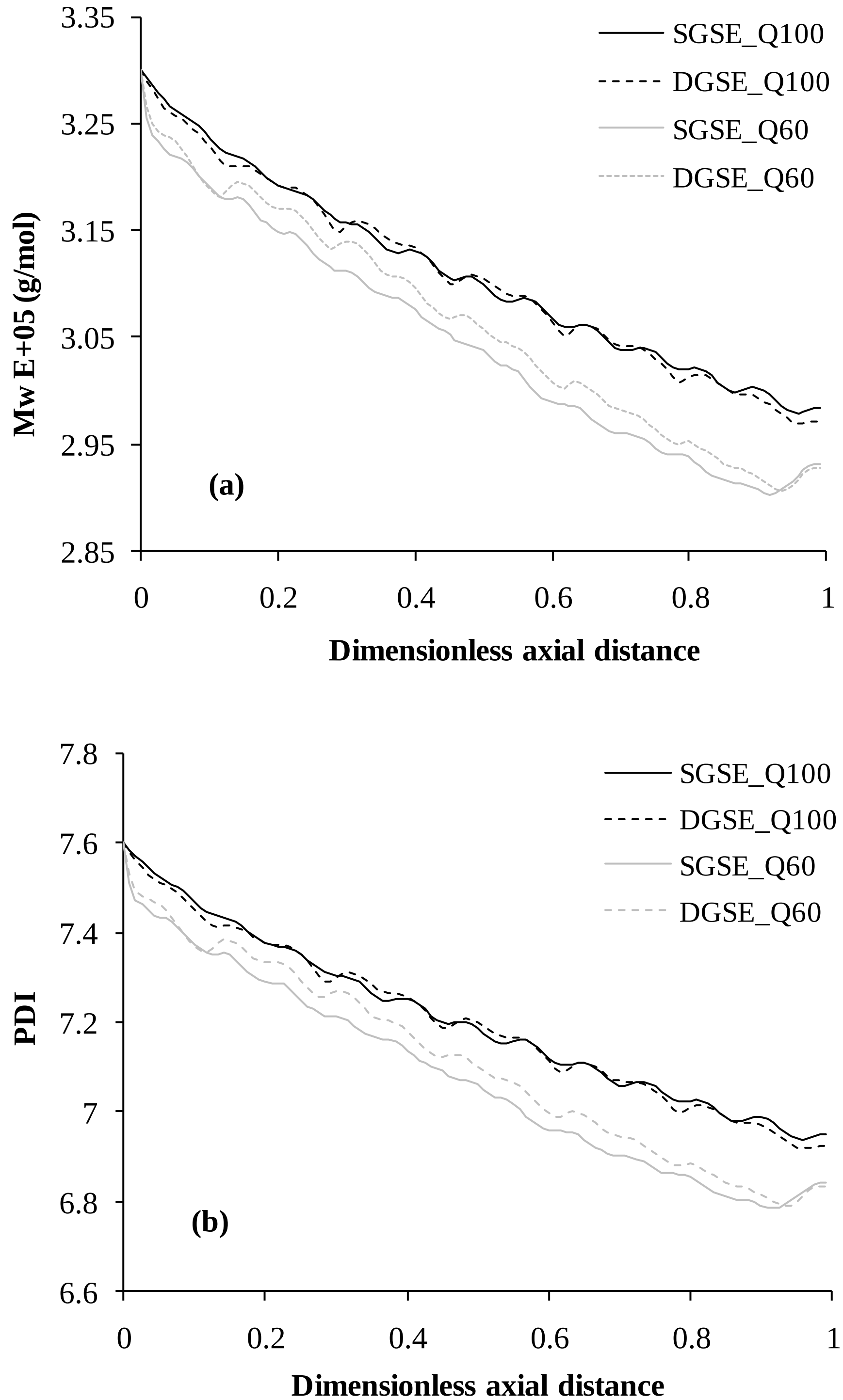

Figure 6-15 Average (a) Mw and (b) PDI variations for the SGSE and DGSE .The corresponding peroxide is 0.02 wt %.

very similar, and even some overlapping between this two curves is observed. As both the average residence time and the RTD corresponding to both of the simulated screw elements are very close to one another (see Table 6.2), and considering the fact that the temperature rise is more significant in the case of the DGSE a higher reduction on the Mw and PDI may be expected for this element to that shown in Figure 6.15a. However, as it has been previously noted by means of Figure 6.13, for the DGSE the higher values of temperature and the regions of lower residence time are both located on the side of the screw element having the higher rotational speed. The latter consideration may imply that the final values of the thermal time for the SGSE may be very similar to that of the DGSE, which can explain the similar evolution and final value observed for the Mw as well as the PDI.

The shapes of the RTDs corresponding to the lower implemented value of the mass flow rate shown by means of Figure 6.17b are again similar for both of the analyzed screw geometries. Again, this consideration, along with the predicted temperature rise for this element may suggest a lower value of the Mw than that observed in Figure 6.16b for this element. The latter when the slightly lower value of residence time in the DGSE, compared to that of the SGSE (see Table 6.4) for the lower value of the mass throughput, is neglected. The explanation for the apparently unexpected values of the Mw is the same as that provided when discussing the results of Figure 6.17a. The cumulative RTDs corresponding to the RTD curves shown in Figure 6.17 are presented in Figure 6.18. The information contained in the latter figure is only presented as reference information and will not be discussed further. The RTD results will be further reexamined since, as previously discussed, a better description of the flow in the analyzed scenarios can be provided from the TS simulation analysis.

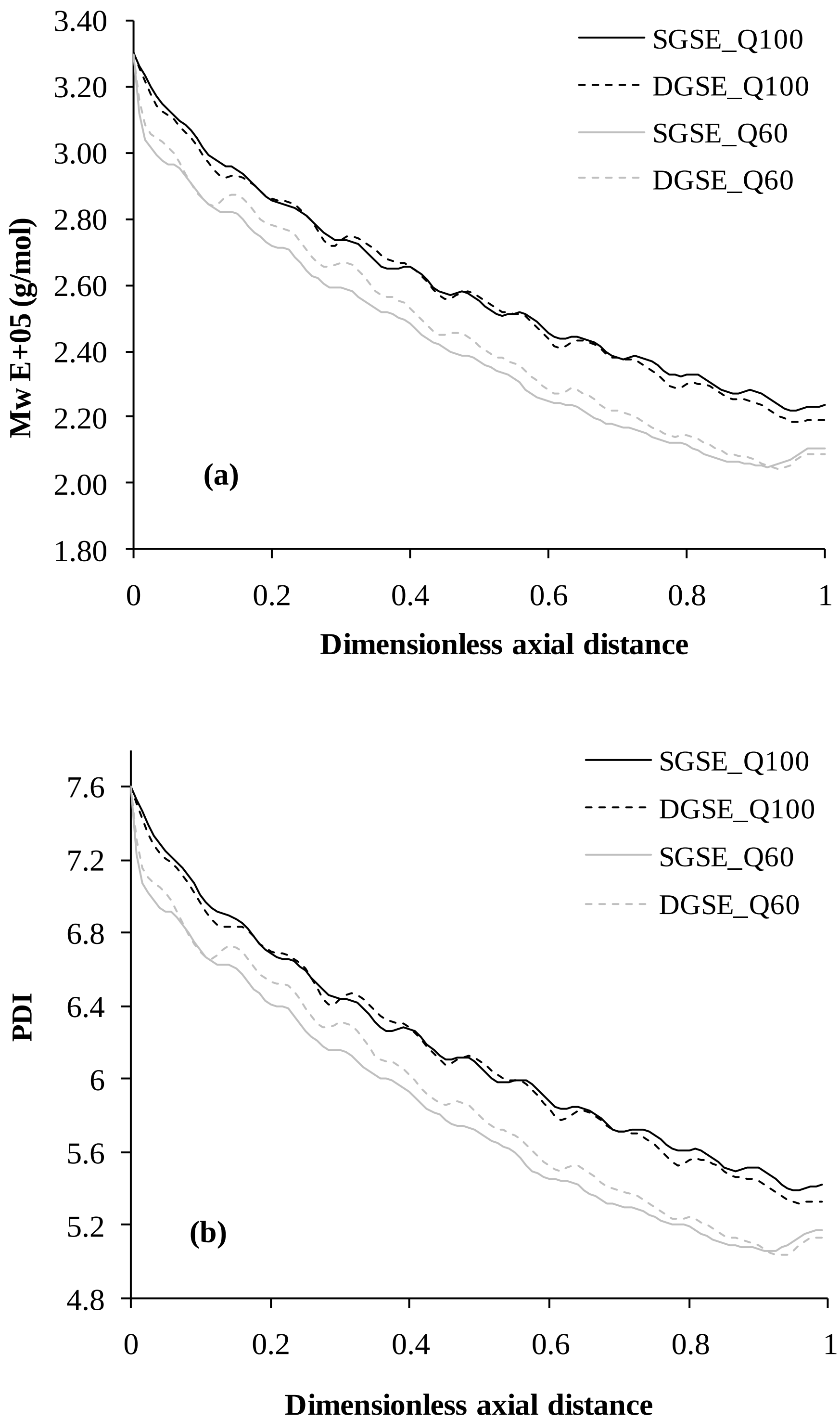

Figure 6-16 Average (a) Mw and (b) PDI variations for the SGSE and DGSE .The corresponding peroxide is 0.10 wt %.

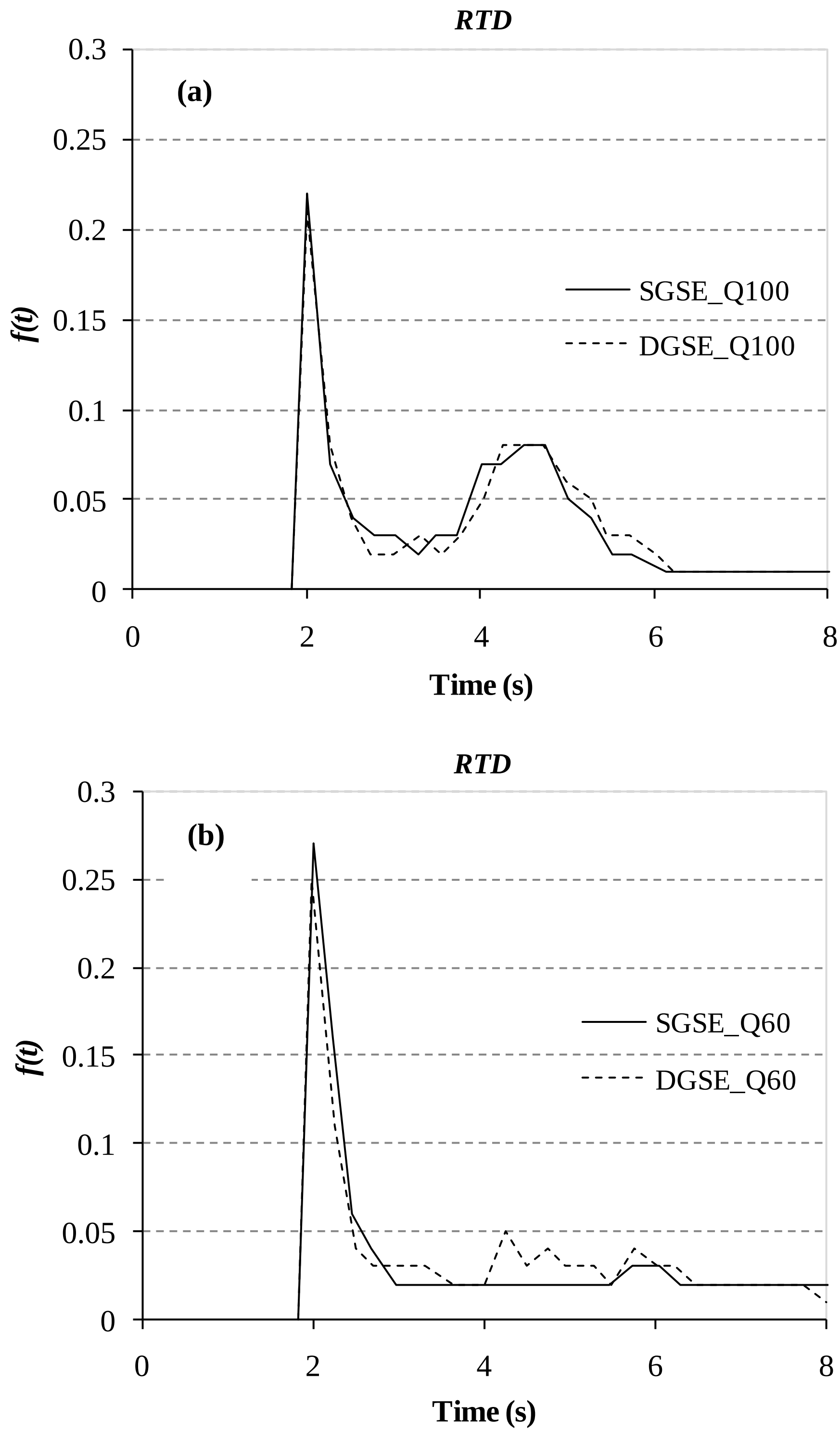

Figure 6-17 RTD variations for the (a) Q_{100} and (b) the Q_{60} mass throughputs. The implemented peroxide concentration is 0.02 wt %.

In Figure 6.19, the evolution of the area stretch ratio is presented for the two implemented flow rates when the peroxide concentration is set to 0.02 wt %. In general terms, it can be appreciated, from the region of the curves around 0.2 to 1 in the horizontal axis that the evolution of this parameter is very similar when similar flow restrictions are implemented especially for the mass flow rate identified as Q_{60}. From Figure 6.19 it can also be appreciated that for a particular flow geometry, when the mass flow rate is decreased (i.e., the flow restrictions increase), an improvement of the mixing capabilities of the screw element is observed. In this case, despite the already discussed drawbacks of the particle-tracking analysis when the MRS is implemented, the results show the expected behavior in the sense that when the mass flow rate is decreased (increase of flow restrictions), the distributive mixing capabilities of the flow system are improved, which is in agreement with what has been discussed in this thesis in Section 3.6.

A comparison of the results of Figure 6.9 (Newtonian non reactive isothermal conditions) with those of Figure 6.19b shows that the trend of the evolution of the area stretch ratio is very similar when similar flow restrictions are implemented. This may indicate that neither the non-Newtonian nor the reacting conditions do significantly modify the mixing capabilities of the flow system when similar flow conditions are specified. The latter is in agreement with what has been found by Strutt et al. (2000) who found out that the modification of the fluid viscosity by either increasing the shear rate or by the effects of the chemical reaction does not significantly modify the mixing capabilities of the flow field. The consideration previously stated in the sense that for similar flow restrictions the non-Newtonian conditions do not significantly modify the mixing capabilities of the flow system is relevant to this study. This, because, in general terms, it has been found here that for the present system when

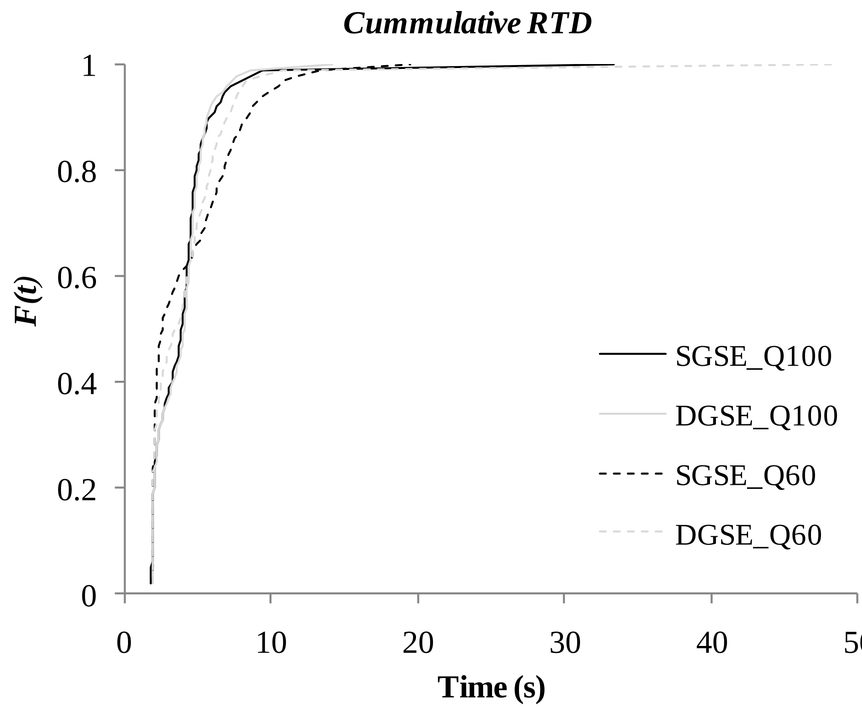

Figure 6-18 RTD variations for the (a) Q_{100} and (b) the Q_{60} mass throughputs. The implemented peroxide concentration is 0.02 wt %.

implementing the MRS analysis the differences in the mixing capabilities of the conveying screw elements are more difficult to address than with the more sophisticated TS analysis. This is especially true considering that the results from the TS simulations predicts significantly better mixing capabilities for the DGSE than for the SGSE, while the MRS does not account for such difference (see Figures 6.7 and 6.9). Therefore, in order to perform a more accurate analysis of the mixing performance of a given set of screw elements the system under non-reactive conditions should be simulated by means of the time-dependent approach, which in this case has been performed specifying Newtonian isothermal flow conditions.

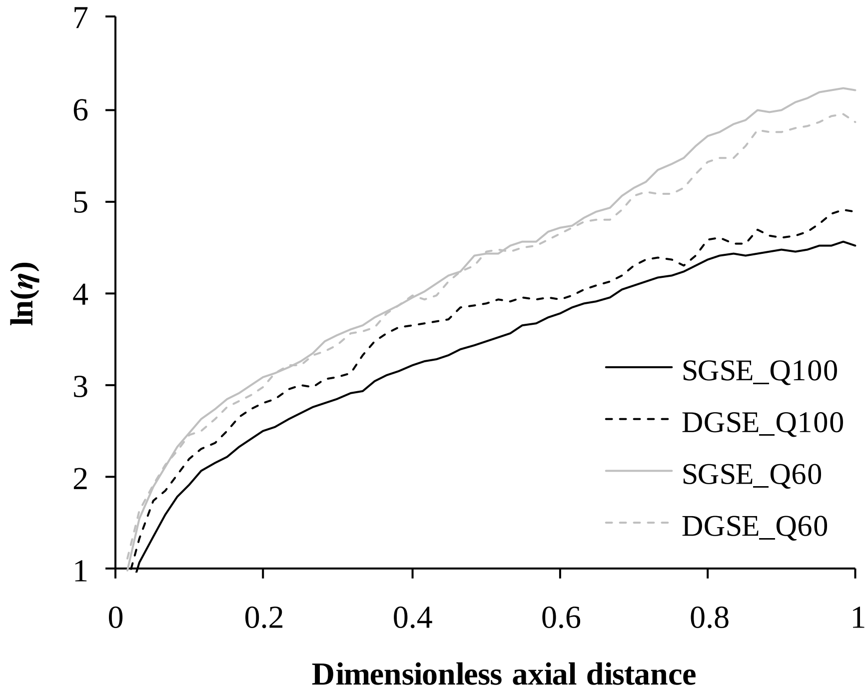

Figure 6-19 Area stretch variations for a peroxide concentration of 0.02 wt %.

Finally, it is important to highlight the fact that according to the TS calculations the RTD curve corresponding to the DGSE is significantly broader than that of the SGSE (see Figure 6.3a). However, the shapes of RTD curves of the SGSE and DGSE are very similar to one another according to Figure 6.17 when the MRS simulation approach is implemented. Under these considerations, it is expected that the actual final values of both the PDI and Mw for the DGSE element would be lower than those predicted with the MRS approach. Therefore, as the MRS predicts similar values of these parameters for the analyzed flow geometries, in a more realistic scenario, it may be expected than when operating under similar processing conditions to those considered in this work, the DGSE would yield lower final values of both the PDI and the Mw.

7 CONCLUSIONS AND RECOMMENDATIONS

7.1 Conclusions

In this work, the peroxide-initiated degradation of PP in COITSEs has been analyzed from a numerical perspective implementing 1D as well as 3D simulation modeling approaches. The main goal of this work was to evaluate scale-up implications of this REX operation in the type of extruders being analyzed. In this context, 1D simulations were performed to evaluate a proposed scale-up rule aimed to find the processing conditions for which similar final values of both PDI and Mw would be obtained for a reference size extruder and larger devices. In the case of the 3D simulation analysis, simulations for two case studies were performed for fully-filled screw elements of COITSEs. In the first case, scale-up implications on the REX operation were considered by analyzing the flow in the conveying elements of two different size extruders. In the second case, the flow was analyzed in conveying elements of extruders having the same size but different screw designs. In this case, the REX operation was addressed in terms of the screw design of the analyzed conveying elements.

In Chapter 4, the scale-up of a REX process in COITSEs was analyzed using the 1D simulation approach. In this case, two scale-up procedures –constant thermal time and SEC– were implemented. The first one of these approaches was proposed in this work under the assumption that systems having similar thermal times would present similar extent of reactions and, in the present case study, would yield similar values of Mw and PDI. The constant SEC approach is generally used in scaling-up non-reactive extrusion operations, and in the present work it was implemented to evaluate the predictions of the proposed constant thermal time scale-up procedure.

Under the specified processing conditions and extruder configuration specified in this work, a very good agreement between the final values of both the PDI and Mw of the polymer being studied, between the reference and scaled-up extruders, was obtained when scaling-up under constant thermal time. For the SEC approach, more significant differences in the values of the PDI and Mw in the reference and scale-up extruders were found, and such differences were related to the geometry of the extruders where the REX operation was being scaled-up and to the specified processing conditions. For the thermal time scale-up procedure, the highest increase of the temperature of reaction corresponded to the lower mass throughputs and higher screw speeds specified, which can be associated with viscous dissipation effects. When the screw speed was kept constant, the scaled-up time of extrusion increased when the reference mass throughput was increased. As in principle the converse to the latter behavior would be expected, such a behavior was mainly related to differences in the DOF profiles in the extruders.

In Chapter 5, the PP reactive flow was analyzed in conveying elements of two different size extruders, by means of 3D simulations. In this case, a steady-state analysis was adopted to address the reaction taking place in the studied flow geometries. A complementary analysis was performed considering non-reactive conditions to account for the time-dependent periodic flow behavior of the system. A combination of two flow rates and three peroxide concentrations, while keeping a constant screw rotating speed, were analyzed in this case. When the same peroxide concentration was implemented, the analysis of the reactive flow indicated that when the implemented flow rate was close to the maximum conveying capacity of the screw elements no significant differences were observed in the final values of the Mw and PDI of both the reference and larger extruders. On the other hand, when the flow was significantly restricted (the mass flow rate was decreased to around half of the maximum conveying capacity of the screw elements) the final values of the Mw and PDI were lower in the case of the larger extruder. The simulation results indicated that this behavior could be related to more viscous dissipation effects occurring in the larger extruder as well to a broader distribution of the RTD curve in the case of this screw element.

The mixing capacity and the RTD behavior of the flow systems were analyzed by means of the results from both the steady- and transient-state flow analysis. Although the steady-state analysis provided useful qualitative information, it was found that the transient-state analysis provided more reliable results. The overall results of the mixing analysis indicated that a broader RTD could be associated to the larger screw element and that that a slightly better mixing capacity would correspond to the smaller screw element, which presented a slightly shallower screw channel. Also, the simulation results indicated that no significant modification of the distributive mixing capabilities of the screw elements could be related to the modification of the rheology of the system associated to the degradation reaction. Finally, a 3D simulation analysis was performed to indirectly evaluate the proposed constant thermal time scale-up procedure presented for the 1D simulations. The results of the simulations indicated that there is relationship between the final Mw and PDI values of the system and the thermal time value. The latter confirmed the assumption in which the proposed constant thermal time scale-up approach is based, i. e., that systems having similar thermal times would yield similar values of Mw and PDI

In Chapter 6 the PP reactive flow is analyzed for screw elements of the same axial length and screw diameter having a conventional and a special design. The special design consisted of an extruder being single-flighted and the other one double-filghted. In this case, the former extruder screw rotates at a speed twice than that of the latter one. As in the results of the previous chapter, here both steady- and transient-state flow analysis were conducted for reactive and non-reactive conditions, respectively. In this case, the flow analysis under reactive conditions indicated that higher temperatures are developed in the case of the special design screw element. This behavior can be associated to the higher screw speeds occurring on the side of the single-flighted screw. The latter, however, was not reflected in the final values of the Mw and PDI obtained for these elements which were slightly lower than those corresponding to the conventional screw element. This behavior was in part explained by the fact that although along their journey through the flow geometry the flow elements pass through regions of high temperature, in the case of the special design screw element, in general terms, these regions are located on the side of the screw element where higher velocities prevail and thus less time is available for the reaction to take place.

Regarding the RTD and mixing analysis of the REX flow in the conventional and special design screw elements, the transient-state analysis showed that under the specified processing conditions a broader RTD as well as better dispersive mixing capabilities corresponded to the special design screw element. When analyzing the effect of the peroxide concentration on the mixing behavior of the reactive flow, it was found that no significant modification of the distributive mixing capabilities of the screw elements could be related to the modification of the rheology of the system associated to the degradation reaction (as in the case study of the previous chapter). As in the case of the steady-state analysis no significant differences in the RTD were found, the observed broader RTD curve predicted by the transient-state analysis was taken as an indication that in a more realistic scenario the yielded Mw and PDI of the analyzed systems would correspond to the screw element having the special design.

7.2 Recommendations

In what follows, a list of recommendations considered for future work is presented.

1. To make a direct comparison of the predictions of the 1D to those of the 3D model to evaluate the possible deviations in the predictions of the 1D model under specific processing conditions. In this case, the 1D computer code should be modified for only applying to a specific section of the COITSE. For both types of simulations, experimental work is necessary to evaluate and validate the simulation results.
2. As indicated in this work, when the steady-state flow analysis (MRS simulation approach) is implemented, the maximum flow capacity of the system is modified. As the flow rate is directly related to the residence time of the system, a relationship may be established to relate these modified flow rate conditions to the actual values of the PDI and Mw.
3. It is expected that in future work, a more regular meshing scheme could be implemented for the MRS simulations, as indicated in Section 5.3 "Flow Analysis and Possible Improvements of the Simulations". If a better meshing scheme is adopted, a more accurate description of the screw clearances may be attempted, since in the present case the screw and radial clearances were increased to avoid numerical difficulties during the simulations.
4. In the case of the scale-up analysis, to evaluate by means of the 3D simulations the effects on the reactive flow and heat transfer behaviors resulting from the implementation of temperature values at the barrel wall different than the temperature value specified at the inlet of the flow geometry. Also, and especially if experimental data are available, to compare the predictions from implementing adiabatic conditions on the surfaces of the screws to those obtained by defining a heat conduction problem for the screws. In this

context, also the boundary conditions on the barrel surface may be changed to define heat flux at this physical boundary (instead of the constant temperature value on the barrel wall considered in this work). In this case, the approaches indicated in the work by Avalosse at al. (2000) and Gupta et al. (2009) may be evaluated.

APPENDIX A: 3D Sample Simulation

In this appendix, the implementation of a 3D simulation for non-reactive flow conditions in a COITSE screw element in which the transient nature of the flow is taken into account is presented. The information to be addressed is aimed to illustrate the steps involved in the setting-up of the simulation and to present typical results for this type of simulations. The transient-state flow condition refers to the time dependency of the flow field due to the rotation of the screws. To deal with the former situation, it is a common practice to simulate a series of instantaneous positions of the screws and to recombine them, to describe the overall effect of the screws motion. Some of the earliest published works included the complete remeshing of the system for each individual position of the screws elements being simulated (Yang and Manas-Zloczower, 1992; Bravo et al., 2000). A more efficient way to deal with the later issue is the implementation of the so called "mesh superposition technique (MST)" (Avalosse and Rubin, 2000). In this technique, a fixed FEM mesh is generated for the inner part of the screw barrel (flow mesh) and one moving mesh for each one of the screws. At each time step, the screw meshes are updated to their actual position and superimposed into the flow mesh. Then, for all nodes of the flow mesh laying within the screws a penalty formulation is applied to impose a velocity value matching the rotation speed of the screws (Avalosse and Rubin, 2000; POLYFLOW® user's guide, 2008).

The general procedure involved in a 3D simulation involves three main steps which are a pre-processing, a solving and a post-processing step. The corresponding computer packages, in the case of the CFD application being implemented in this work are Gambit (the preprocessor), Polyflow (the solver) and Fieldview or cfx-post (the post-processor). In general terms, the implementation of a simulation consist of the importation, or generation, of the geometry of the system to be modeled, by means of the pre-processsing software. Still in this application, a grid (or mesh) is generated for the computational domain. After that, the meshed computational domain is imported into the solver, where the corresponding boundary conditions are specified, and the problem is solved, i. e., the results of interest, i.e., velocity and pressure fields (among others), are generated. Finally, the generated results are visualized by means of the post-processing software.

The sample simulation to be discussed corresponds to the description of the flow a COITSE screw element whose length is set equal to one pitch. The corresponding boundary conditions and geometry of the system are those of example 38 of the Polyflow examples manual (POLYFLOW® documentation files, 2008). The geometry of the screw elements was generated following the work by Booy (1978).The geometrical parameters of these elements are summarized in Table A.1, and in Table A.2 the main considerations taken into account for the simulation are addressed. In Figure A.1, the corresponding meshed geometries for the flow and the screws subdomains are presented. An important consideration when generating the flow subdomain is that the geometry of this subdomain should present a mappable topology. In this case, such a mappable topology was generated by dividing the flow subdomain in four connected volumes. This was achieved by using two planes two split the volume corresponding to the flow subdomain. The first one of these planes was coincident with the axis of the two screws and the other was plane parallel to the axis of the screws and located at an intermediate distance between the two axes of the screws.

A rough evaluation of the sample simulation was achieved, by comparing results obtained from such a simulation to those corresponding to example 38 of the Polyflow examples manual. In Figure A.2, the evolution of the pressure along the axial distance of the conveying elements, for a line located at the geometrical center of the computational domain, is presented for both of the previously addressed cases. Here, Figure A.2a corresponds to the reference simulation and Figure A.2b to the sample simulation. It can be noticed that, although there are differences in the numerical values of both simulations, the trend of the results is the same.

Table A-1 Geometry specifications of the twin screw elements for the 3D sample simulation.

Axial length of the computational domain	50 mm
Screw pitch	40 mm
Center distance of screws	33.9 mm
Barrel bore diameter	42 mm
Flight depth	7.3 mm
Axial barrel clearance	1 mm

Table A-2 Relevant considerations for the implementation of the 3D simulation.

Assumptions	Steady state flow Newtonian and isothermal fluid.
Boundary conditions	Screw rotating speed=10 rpm Gravity and inertial forces neglected Non slip conditions on solid boundaries.
Model	Generalized Newtonian isothermal flow. Viscosity=5X10^4 Pa·s

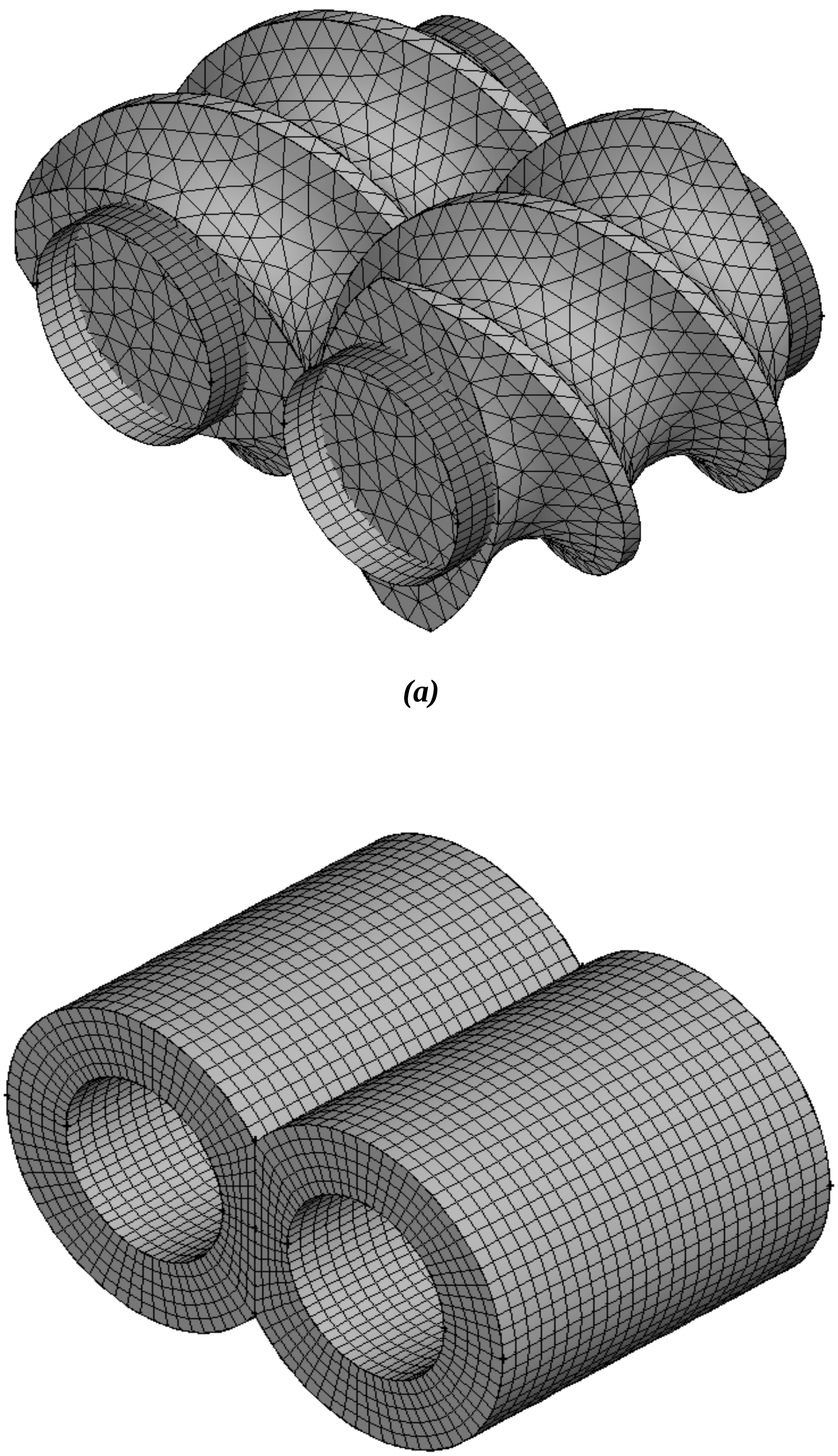

(a)

(b)

Figure A-1 (a) Screws and (b) flow field meshed computational subdomains.

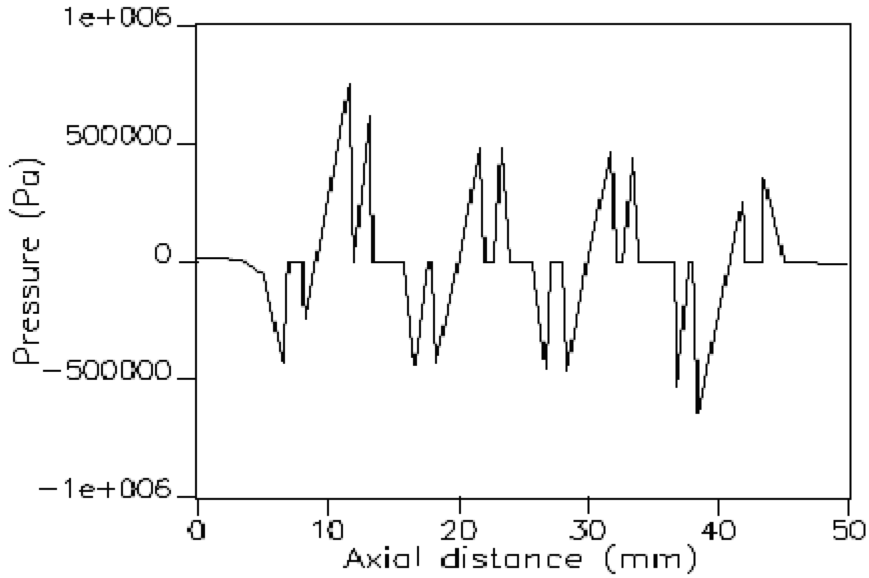

(a)

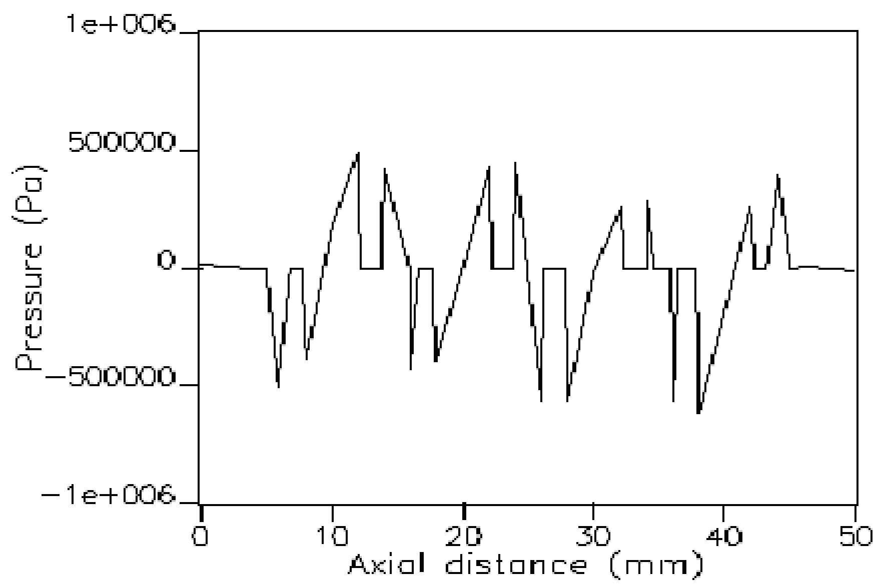

(b)

Figure A-2 Pressure evolution along the axial distance (for a line located at the geometrical center of the computational domain). (a) Reference and (b) sample simulation.

The numerical differences observed in Figure A.2 can be briefly explained by the fact that the meshing strategies are different in each case, as it is evident from the data of Table A.3. Other illustrative results for the sample simulation are presented in Figures A.3 and A.4. The results of Figure A.3 correspond to the vector description of a velocity field for a *"y plane"* located 14 cm away from axes of both screw elements; while Figure A.4 is a contour plot showing the variation of the shear rate at a *"z cutting plane"* located at center of the axial axes of the conveying elements.

Table A-3 Summary of data for comparison of the reference and sample simulations.

	Reference simulation	*Sample Simulation*
Flow subdomain (N)	24120	16000
Screws subdomain (N)	13573	14071
Totals (N)	37693	30071
Computational time	871.0 sec	263.0 sec

* In all cases, N represents the number of 3D elements. The corresponding grids, in the case of the sample simulation, for the screws subdomain and the flow subdomain consisted of 4-node tetrahedral and 8-node hexahedral elements, respectively.

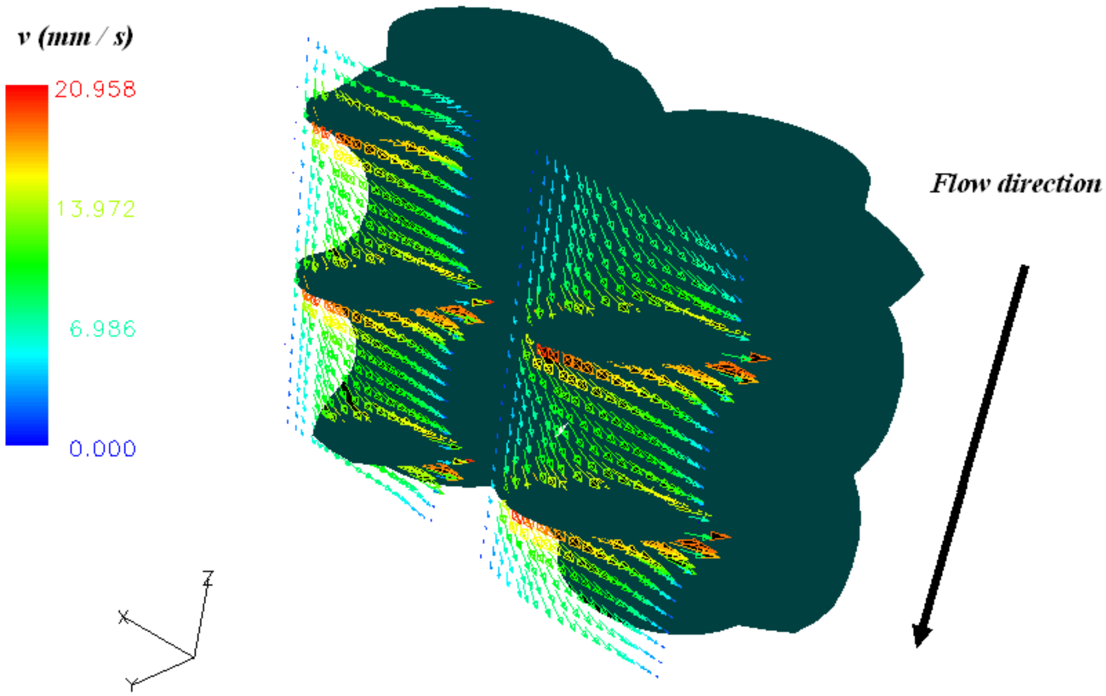

Figure A-3 Velocity field for a cutting plane *y* = 16 mm.

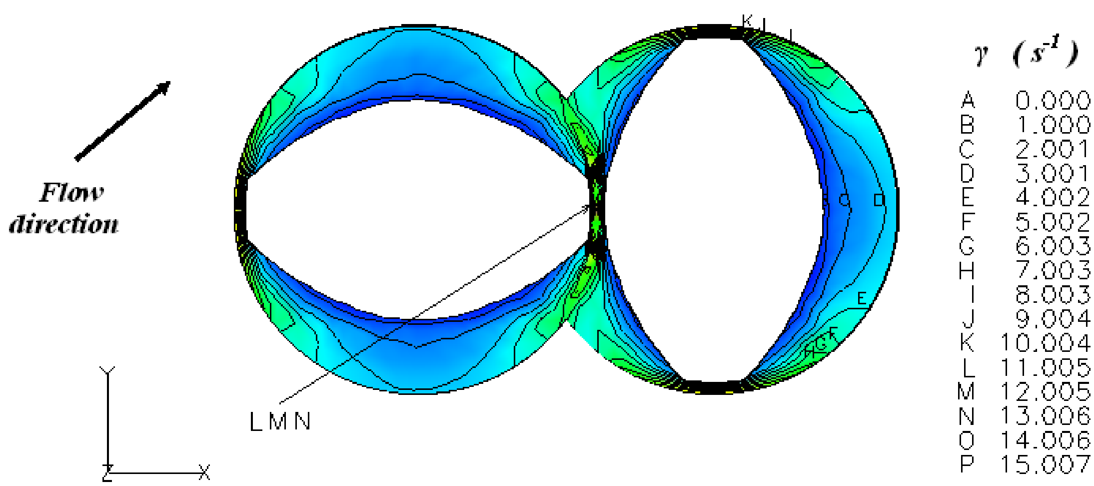

Figure A-4 Contour plot for the shear rate at a *z* cutting plane located at half of the length of the flow element.

A further step in the analysis of the sample system consisted in the simulation of different positions of the rotating screw elements. The results of such simulations were later recombined, by means of the post-processor software, to account for the transient flow field of the system. Due to the periodicity of the flow, the different relative positions of the screw elements (10 in total) covered only a range of 180°. The time step for advancing the position of the screws was then set equal to 0.3 s, taking into account that the specified rotating speed of the screws was set equal to 10 rpm (see Table A.2). Results corresponding to these calculations are presented by means of Figures A.5 and A.6, both of them corresponding to particle-tracking analysis. In the first one of these figures the path lines of 4 particles

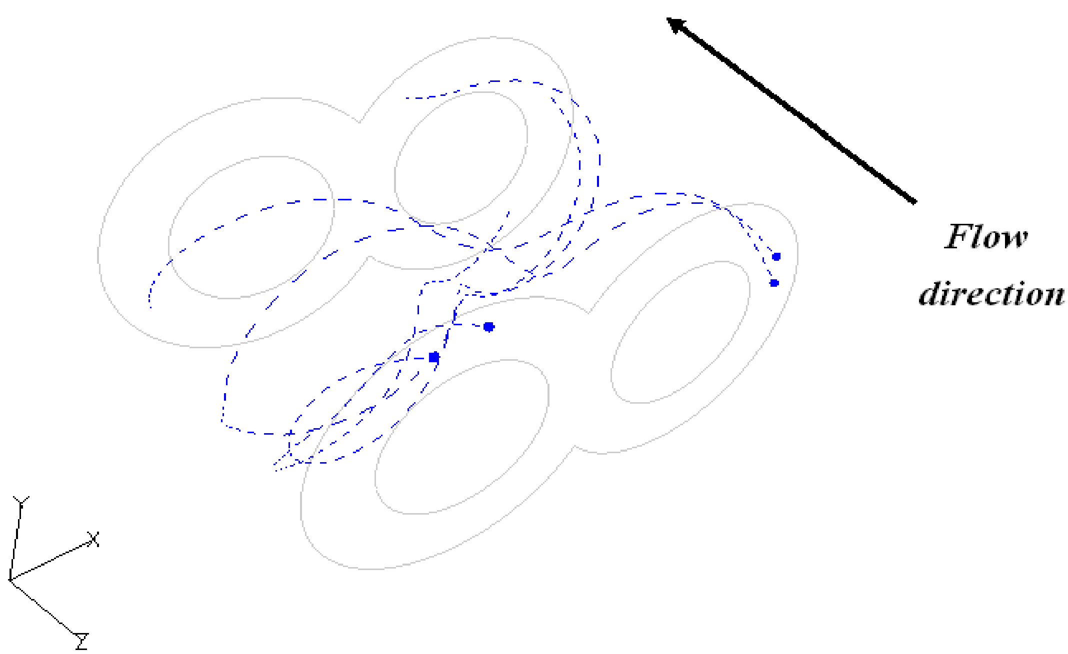

Figure A-5 Path lines for 4 particles seeded at the entrance of the flow element.

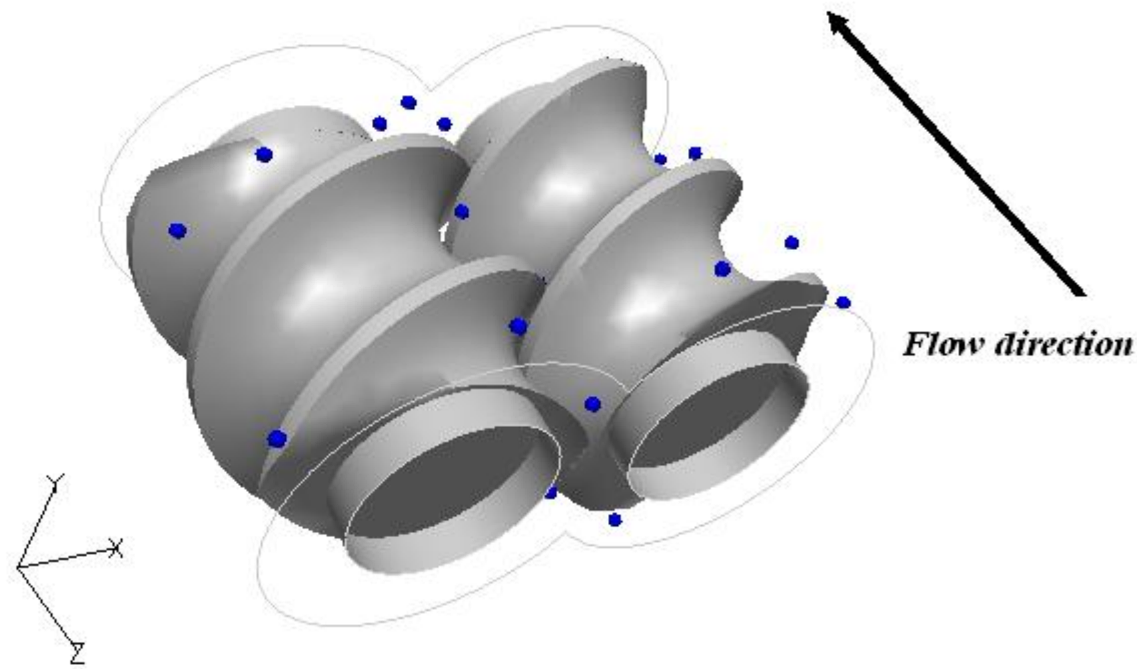

Figure A-6 Position, after 2 revolutions, of 50 particles randomly seeded at the entrance of the flow system.

originally located at the entrance of the flow system is shown, where the characteristic "figure eight" flow pattern, which has been discussed elsewhere (White, 1990), can be appreciated. In the second figure, the advanced position of 50 particles, originally randomly located at the entrance of the flow domain, after 2 revolutions is depicted.

APPENDIX B: Complementary Information for the TS Simulations of Chapters 5 and 6

In this appendix, additional information regarding the meshing of the flow geometries and the flow rates corresponding to the simulation results of Chapters 5 and 6 is presented. All of the information presented here, unless otherwise indicated, corresponds to the TS analysis, where the MST was implemented. Also, average residence time values for the TS simulations, which have been calculated using the information corresponding to the implemented flow rate and the volumetric capacity of the flow geometry (including the entrance and exit sections where no screws are present), are presented. The physical parameters specified for the extruder screws in the non-isothermal simulation of the LSM 30.34 screw element, presented in Section 5.1.2, are also indicated (see Table B.3).

Table B-1 Mesh geometry information of interest for the screw elements of Chapter 5. B and T stand for brick and tetrahedral elements, respectively.

No. of elements	LSM-30.34	ZSE-96
Flow subdomain (B)	72520	72520
Screw 1 (T)	41176	41646
Screw 2 (T)	41540	41259

Table B-2 Simulation results of interest for both the LSM-30.64 and ZSE-96 screw elements. Rt stands for the average residence time.

Extruder	LSM-30.34	ZSE-96
Screw speed (rpm)	100	100
Flow cross section area (mm^2)	574.94	4827.58
Q_{100}(kg/hr)/Rt(s)	16.50/6.58	400.37/6.46
Q_{50}(kg/hr)/Rt(s)	8.25/13.17	200.18/12.92
Q_{50}(kg/hr)/Rt(s)*	14.09/7.71	---

*Non-isohermal simulation where the MRS is implemented.

Table B-3 Physical properties used for the screws of the LSM-30.34 implemented for the TS simulations. The values were taken from the example on non-isothermal flow in a COITSE in the polyflow users guide (POLYFLOW®). These values were also used in the work presented by Avalosse at al. in 2000.

Physical property	Value
Density (g/mm^3)	7.87 e-03
Conductivity (g mm/s^3 ^oC)	4 e+07
Heat capacity (mm^2/s^2 ^oC)	4 e+08

Table B-4 Mesh geometry information of interest for the screw elements of Chapter 6. B and T stand for brick and tetrahedral elements, respectively.

No. of elements	SGSE	DGSE
Flow subdomain (B)	70448	70488
Screw 1 (T)	35823	34966
Screw 2 (T)	35269	31140

Table B-5 Simulation results of interest for both the SGSE and DGSE.

Extruder	SGSE	DGSE
Screw speed (rpm)	100	100/200
Flow cross section area (mm^2)	585.35	549.07
Q_{100}(kg/hr)/Rt(s)	43.64/6.97	44.34/6.53
Q_{50}(kg/hr)/Rt(s)	21.82/13.95	21.82/13.27

APPENDIX C: Experimental Verification of Simulation Results

In order to verify the capability of POLYFLOW® to yield reliable results, the work presented by Ishikawa et al. (2002) was selected to assess the predictions of a typical simulation implemented with this commercial software. In the study presented by the previously addressed researchers, three different types of elements of a COITSE were analyzed in terms of their mixing behavior. As part of the study being addressed, an experimental validation of the simulation results was performed in terms of the pressure drop and the temperature increase between two points separated by a distance of 24 mm in the axial direction of the flow elements. For the verification implemented in this thesis, simulations corresponding to a conventional conveying screw element and a kneading block are presented for similar processing conditions and geometrical specifications to those used in the work of Ishikawa et al. (2002). The simulation results presented in this appendix were obtained by implementing the mesh superposition technique (MST), and only one position of the screws was simulated.

The geometries of the flow elements used to generate the simulation results of this appendix were adapted from schematics shown in the reference paper (in the reference paper, the geometry of these elements is not presented in detail). The corresponding geometrical parameters of the flow elements simulated in this thesis are shown in Table C.1. The information corresponding to the discretization of the computational domains is presented in Table C.2. With respect to the viscosity of the system, the same model (a Cross model with an Arrhenius-type dependence on the temperature) and model parameters used in the work by Ishikawa et al. (2002) are implemented in this thesis. The boundary conditions used for the

Table C-1 Geometrical specifications of the flow elements simulated in Appendix C.

Axial length of the computational domain	36 mm
Screw pitch	30 mm
Center distance of screws	24 mm
Barrel bore diameter	30 mm
Flight depth	4.5 mm
Axial barrel clearance	1.5 mm

In the case of the kneading block element, 8 kneading discs, each one having a length of 3.75 mm (in the axial direction of the flow element), were specified.

Table C-2 Mesh geometry information of interest for the simulations of Appendix C (CS) and the reference simulations (RS). FF and KB refer to the simulated conveying screw elements and kneading block elements, respectively.

Number of nodes	FF_CS	FF_RS	KB_CS	KB_RS
Flow domain	60569	42470	60569	---
Screw 1	4580	---	12726	---
Screw 2	4642	---	12835	---

simulations of this appendix are the same ones as those implemented in the reference paper, except that for the screws and kneading blocks of the flow elements a heat conduction problem was defined instead of the adiabatic conditions at the surfaces of these moving parts, as defined in the reference paper. The physical parameters used for this heat conduction problem are the ones presented in Table B.3. At the end of the flow geometries, in the simulation of this appendix, zero normal and tangential forces were specified. On the other hand, an interpolation of the mini-element type (Fortin, 1981) was specified for the velocity field and a linear interpolation was implemented for the temperature field.

In Figure C.1, the pressure build-up along the axial distance of the simulated flow elements is presented. In Figure C.1a, both the simulated and experimental results presented in the reference paper are shown. In this figure, the conventional screw element is identified as FF and the kneading block element as KB. For the experimental results, as already mentioned, the axial distance corresponding to the measured pressure drop is 24 mm, and the pressure build-up for the simulation results is approximately of the length of the simulated flow element (30 mm). It can be seen that the experimental results are very close to the ones calculated from the simulations. From the results presented for the simulations of this appendix (Figure C.1b), the pressure drop corresponding to the difference between average cross-sectional pressure values at 0.5 mm before and after the starting and ending points, respectively, of the flow elements along their axial distance is presented. When comparing the results from Figures C.1a and C.1b, it can be appreciated that the pressure drops predicted for both the kneading block and the conveying screw elements from the reference simulations are not exactly the same than those values predicted in the simulations performed as part of this appendix. However, the same trend is observed in the results, i.e., a higher pressure drop for the screw elements and a lower pressure drop for the kneading block elements. The observed differences between the results of Figures C.1a and C.1b may be related in part to differences in the geometrical specifications of the simulated flow geometries.

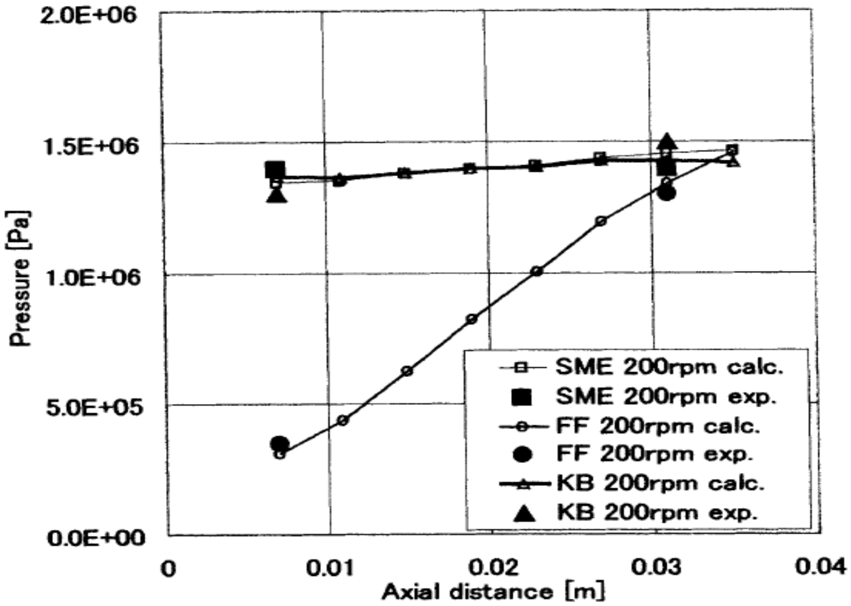

[After Ishikawa et al., 2002]

(a)

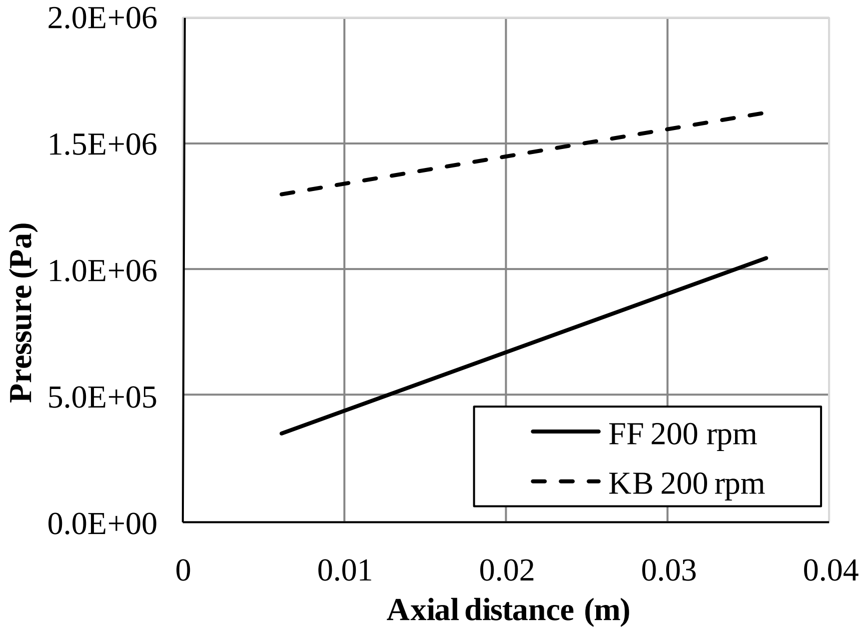

(b)

Figure C-1 Pressure variation for (a) the flow elements analyzed by Ishikawa et al. (2002) and (b) the flow elements simulated in Appendix C.

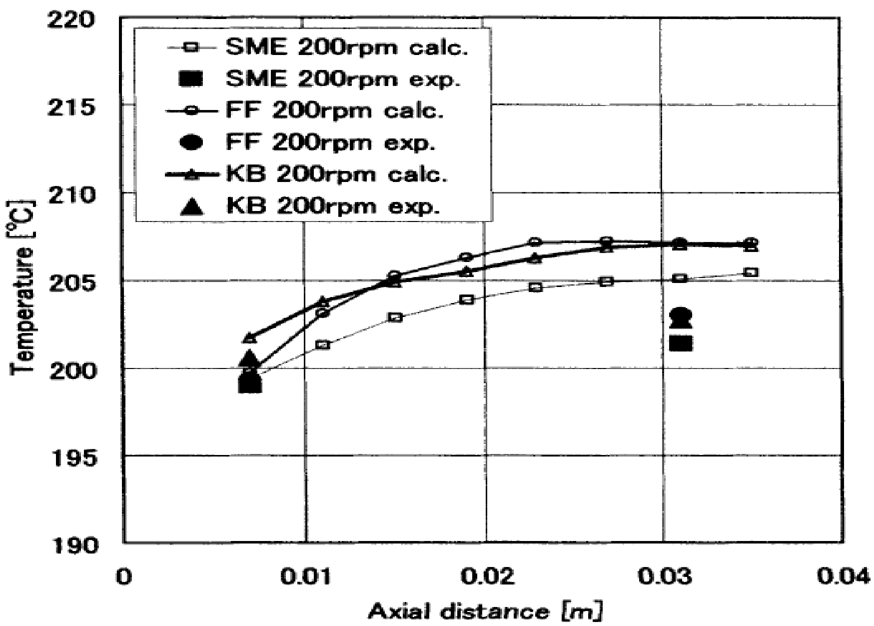

[After Ishikawa et al., 2002]

(a)

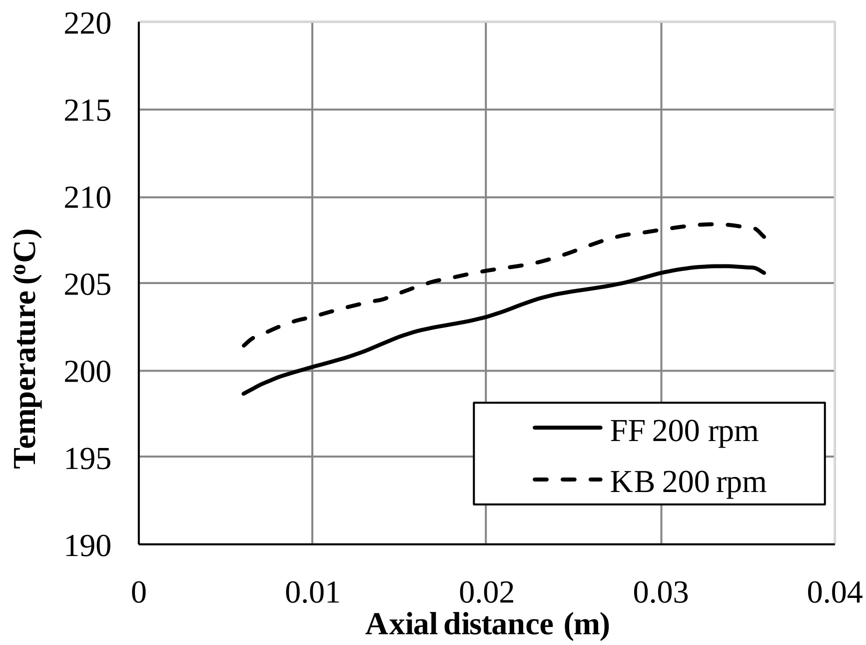

(b)

Figure C-2 Temperature variation for (a) the flow elements analyzed by Ishikawa et al. (2002) and (b) the flow elements simulated in Appendix C.

In Figure C.2, the evolution of the average temperature along the axial distance of the simulated flow geometries is presented. In Figure C.2a, the experimental and simulation results for the conveying element and kneading block element presented in the reference paper are shown. It can be noticed that the predicted values of the temperature increase are significantly higher than the experimental ones. According to Ishikawa et al. (2002), this behavior may be related to assumptions implied in the simulations as well as to the way in which the experimental results were obtained. When comparing Figures C.2a and C.2b, it can be seen that the final values of the temperature predicted for each one of the simulated flow geometries is very similar for both the reference simulations and the simulations performed as part of this appendix. Finally, in the case of Figure C.2b some exit effects are observed for the evolution of the temperature of the system. This seems to be related to a relatively short length (3 mm) defined for the exit section of the flow geometry.

In summary, it has been shown that the predictions of the simulations implemented with the commercial software used in this thesis follow the trend of results that have been experimentally validated. It is important to keep in mind, however, that in order that a simulation could be more reliable, an experimental verification should be performed with the specific experimental system of interest. That is, it is desirable that in future work the type of simulations presented in this thesis be complemented with experimental work.

NOMENCLATURE

a	Infinitesimal area element in its deformed state
A	Heat transfer area of the extruder barrel (m^2)
A	Infinitesimal area element in its reference state
b	Channel width (m)
C_L	Center line distance (m)
C_P	Heat capacity ($J\ K^{-1}\ Kg^{-1}$)
d	Scaling-up diameter ratio (m)
D	Rate of deformation tensor
D_S	External screw diameter (m)
D_R	Screw root diameter (m)
D	Extruder diameter (m)
e	Flight thickness (m)
E	Drive motor energy (J), activation energy (J/mol)
E_a	Reaction activation energy (J/mol)
$f(t)$	Residence time distribution function
f_p	Peroxide decomposition efficiency
F	Deformation tensor
$F(t)$	Cumulative residence time distribution
h	Scaling factor for the channel depth
H	Maximum channel depth (m)
ΔH_t	Latent heat of melting (J)

$[I]$ Peroxide concentration (mol/m^3), peroxide concentration at time t (mol/m^3)

$[I]_0$ Peroxide concentration at time (mol/m^3)

k Constant of reaction kinetics (m^3/s)

k_d Rate constant of peroxide decomposition (m^3/s)

l Length of the metering section (m), scaling factor for the channel length

L Screw length (m), die length (m)

m Mass (Kg)

$\mathbf{m}$ Orientation vector of a material filament in its deformed state

m_0 Monomer molecular weight (Kg/mol)

M Mass throughput (Kg/s), monomer concentration (Kg/mol)

$\mathbf{M}$ Orientation vector of a material filament in its reference state

Mw Weight-average molecular weight (Kg/mol)

M_n Number-average molecular weight (Kg/mol)

M_w Weight-average molecular weight (Kg/mol)

M_z, z- average molecular weight (Kg/mol)

$\mathbf{n}$ Orientation vector, orientation vector of an area element in its deformed state

n Power-law index, number of screw tips

$\mathbf{n}_3$ Minimum eigenventor of the rate of deformation tensor

N Screw rotational speed (rad/s)

$\mathbf{N}$ Orientation vector of an area element in its reference state

P Pressure (Pa), Pressure build-up (Pa)

p^i Pressure at present iteration (Pa)

p^{i-1} Pressure at previous iteration (Pa)

p'	Pressure gradient or pressure correction (Pa)
$[P_n]_I$	Concentration of polymer molecules with chain length n at times t_i (mol/m^3)
q_b	Heat transferred through the extruder barrel (J)
q_r	Heat of reaction (J)
Q	Volumetric flow rate (m^3/s)
$\mathrm{Q_P}$	Pressure component of the flow rate (m^3/s)
$\mathrm{Q_D}$	Drag component of the flow rate (m^3/s)
Q_i	*ith* moment of the molecular weight distribution
R	Die diameter (m), universal gas constant (J mol^{-1} K^{-1})
S_R	Radial flight clearance (m)
t	Screw pitch (m), time (s)
t_i	Reaction time at time step I (s)
t_T	Thermal time (s)
t'	Time at a particular point along a path line (s)
$\bar{t}$	Average residence time (s)
T	Temperature at a particular point along a path line (^{o}C)
T_f	Feed temperature (^{o}C)
T_p	Product temperature (^{o}C)
$\mathbf{v}$	Instantaneous velocity vector
$\mathbf{V}(t)$	Velocity vector of a particle
$\bar{v}$	Instantaneous velocity vector
W	z-component of velocity (m)

x Vector of position of a particle **x** at a time t

X Vector of initial position of particle **x**

$\mathbf{X}(t)$ Position of a particle at time t

$\mathbf{X}(t_0)$ Position of a particle at time 0

Subscripts

1 Refers to the reference lab extruder

2 Refers to the scaled-up extruders

Greek symbols

α Under-relaxation factor

α_i Intermeshing angle (rad)

α_t Tip angle (rad)

β Scaling factor for the helix angle (rad)

γ Rate of strain tensor, strain rate (s^{-1})

$\dot{\gamma}$ Strain rate (s^{-1})

η Area stretch ratio, viscosity (Pas)

η_{Fa} Energy efficiency index

η_{La} Areal growth efficiency index

η_0 Zero shear viscosity (Pas)

$\dot{\eta}$ Instantaneous area growth

λ	Line stretch ratio, mixing efficiency index
λ_3	Minimum eigenvalue of the rate of deformation tensor
ρ	Polymer density (Kg/m^3)
τ	Shear stress
$\overline{\overline{\tau}}$	Shear stress tensor
ϕ	Helix angle (rad)
ϕ_S	Helix angle (rad)
υ	Scaling factor for the screw rotational speed
ω	Vorticity tensor

Abbreviations

CFD	Computational fluid dynamics
COITSE:	Closely intermeshing self-wiping co-rotating twin screw extruder
CRPP:	Controlled-rheology polypropylene
CRTSE :	Counter-rotating twin screw extruders
CSTR	Continuous stirred tank reactor
DGSE:	Conveying screw element with special design
DOF:	Degree-of-fill along axial direction of the extruder
FEM:	Finite element method
FVM:	Finite volume method
MMA :	Methyl methacrylate
MST:	Mesh superposition technique

MRS:	Moving relative system, refers to steady-state flow simulations
MWD:	Molecular weigh distribution
PDI:	Polydispersity index
PSM :	Position of the start of melting, refers to the one-dimensional model
PP:	Polypropylene
RE:	Reference extruder
REX:	Reactive extrusion
RTD:	Residence time distribution
SE:	Scaled-up extruder
SEC:	Specific energy consumption
SGSE:	Conveying screw element with conventional design
SSE:	Single screw extruder
TS:	Transient state, refers to transient-state flow simulations
tTD:	Thermal time distribution
1D:	One-dimesional, refers to a model or simulation
3D:	Three-dimensional, refers to a model or simulation

REFERENCES

1. Agassant, J.-F.; Avenas, P.; Sergent, J. Ph.; Carreau, P. J., *"Polymer Processing: Principles and Modeling"*, Hanser, 1991

2. Aulagner, P.; Ainser, A.; Carrot, C.; Gillet, J., "Free Radical Degradation of Polypropylene in the Bulk: Coupling of Kinetic and Rheological Models", J. Polym. Eng. Sci., 2000, **20**, 381

3. Avalosse, T.; Rubin, Y., "Analysis of Mixing in Corotating Twin Screw Extruders through Numerical Simulation", Intern. Polym. Process., 2000, **XV**, 117

4. Avalosse, T.; Rubin, Y.; Fondin, L., "Non-Isothermal Modeling of Co-Rotating and Counter-Rotating Twin Screw Extruders", SPE ANTEC, 2000, 19

5. Balke, S. T.; Hamielec, A. E., "Bulk Polymerization of Methyl Methacrylate", J. Appl. Polym. Sci., 1973, **17**, 905

6. Balke, S. T.; Suwanda, D.; Lew, R., "A Kinetic Model for the Degradation of Polypropylene", J. Polym. Sci.: Part C: Polym. Let., 1987, **25**, 313

7. Bertrand, F.; Tanguy, Pa.; Thibault, F., "A Three Dimensional Fictitious Domain Method for Incompressible Fluid Flow Problems", Int. J. Num. Meth. Fluids, 1997, **25**, 719

8. Berzin, F.; Vergnes, B.; Canevarolo, S. V.; Machado, A. V.; Covas, J. A., "Evolution of the Peroxide-Induced Degradation of Polypropylebe along a Twin-Screw Extruder: Experimental Data and Theoretical Predictions", J. Appl. Polym. Sci., 2006, **99**, 2082

9. Biesenberger, J. A., "Principles of Reaction Engineering", in *"Reactive Extusion: Principles and Practice"*, Xanthos M. (editor) , Hanser Publishers, 1992

10. Bigio, D. I.; Conner, J. H., “Principal Directions as a Basis for the Evaluation of Mixing”, Polym. Eng. Sci., 1995, **35**, 1527

11. Bird, R. B; Stewart, W. E.; Lightfoot, N. E., “*Transport Phenomena”*, Willey, 1960

12. Booy, M. L., “Geometry of Fully Wiped Twin Screw Equipment”, Polym. Eng. Sci., 1978, **18**, 984

13. Booy, M. L., “Isothermal Flow of Viscous Liquids in Corotating Twin Screw Devices”, Polym. Eng. Sci., 1980, **20**, 1220

14. Bravo, V. L.; Hrymak, A. N.; Wright, J. D., “Numerical Simulation of Pressure and Velocity Profiles in Kneading Elements of a Co-Rotating Twin Screw Extruder”, Polym. Eng. Sci., 2000, **40**, 525

15. Bravo, V. L.; Hrymak. A. N.; Wright D., “Study of Particle Trajectories, Residence Times and Flow Behavior in Kneading Discs of Intermeshing Co-rotating Twin Screw Extruders”, Polym. Eng. Sci., 2004, **44**, 779

16. Brodkey, R. S., *"The Phenomena of Fluid Motions"*, Addison-Wesley, 1967

17. Brown, S. B., “Reactive Extrusion: A Survey of Chemical Reactions of Monomers and Polymers during Extrusion Processing”, in “*Reactive Extrusion: Principles and Practice*”, Xanthos M. (editor) , Hanser Publishers, 1992

18. Carley, J. F.; McKelvey, J. M., “Extruder Scale-up Theory and Experiments”, Ind. Eng. Chem., **45**, 989 (1953)

19. Chapra, S. C., “*Applied Numerical Methods with Matlab for Engineers and Scientists*”, 2nd Ed., McGrawHill, 2008

20. Chen, Z.; White, J. L., "Dimensionless Non-Newtonian Isothermal Simulation and Scale-up Considerations for Modular Intermeshing Twin Screw Extruders", Int. Polym. Process., 1991, **VI**, 309

21. Christiano, J. P., "Scale-up Study of Co-Rotating Fully Intermeshing Twin Screw Extruders using 47mm, 69mm, and 96.5mm Diameters", SPE ANTEC, 1994, 239

22. Chung, C. I., "On the Scale-up of Plasticating Extruder Screws", Polym. Eng. Sci., 1984, **24**, 626

23. Colbert, J. A., "Scale up of Extruders, Practicalities and Pitfalls", Polymer Processing International Conference, 1997, 192

24. Davis, W. M., "Heat Transfer in Extruder Reactors", in *"Reactive Extusion: Principles and Practice"*, Xanthos M. (editor), Hanser Publishers, 1992

25. Dickson, S. B.; Tzoganakis, C.; Budman, H., "Reactive Extrusion of Polypropylene with Pulsed Peroxide Addition: Process and Control Aspects", Ind. Eng. Chem. Res., 1997, **36**, 1067

26. Dreiblatt, A.; Eise, K., "Intermeshing Corotating Twin-Screw Extruders", in *"Mixing in Polymer Processing"*, Rauwendaal, C. R. (editor), Dekker, New York, 1991.

27. Erdmenger, R., "Mehrwellen-Schnecken in der Verfahrenstechnik", Chem. Ing. Tech., 1964, **36**, 175

28. Fortin, M., "Old and New Finite Elements for Incompressible Flows", Int. J. Num. Meth. Fluids, 1981, **I**, 347

29. Ferziger, J. H.; Peric, M., *"Computational Methods for Fluid Mechanics"*, 3rd Ed., Springer, 2002

30. Fukouka, T., “Numerical Analysis of a Reactive Extrusion Part II: Simulations and Verifications the Twin Screw Extrusion”, Polym. Eng. Sci., 2000, **40**, 2524

31. Ganzeveld, K. J.; Janssen, L. P. B. M., “Scale-up of Counter-Rotating Twin Screw Extruders without and with Reactions”, Polym. Eng. Sci., 1990, **30**, 1529

32. Gao, J.; Walsh, G. C.; Bigio, D.; Briber, R. M.; Wetzel, M. D., “Residence-Time Distribution Model for Twin-Screw Extruders”, AIChE J., 1999, **45**, 2541

33. Goffart, D.; Van Der Wal, D. J.; Klomp, E. M.; Hoogstraten, H. W.; Janssen L. P. B. M; Breysse, L.; Trolez, Y., “Three-Dimensional Flow Modeling of a Self-wiping Corotating Twin-Screw Extruder. Part I: The Transporting Section”, J. Polym. Eng. Sci., 1996, **36**, 901

34. Gupta, M., “Non-Isothermal Simulation of the Flow in Co-Rotating and Counter-Rotating Twin-Screw Extruders using Mesh Partitioning Technique”, SPE ANTEC, 2008, 316

35. Gupta, M.; Rohatgi, V.; Kuehn, R, “Estimation of the Temperature Increase in a a Zsk-90 Co-Rotating Twin Screw Extruder using Mesh Partitioning Technique”, SPE ANTEC, 2009, 2350

36. Ishikawa, T.; Amano, T.; Kihara, S.-I.; Funatsu, K., “Flow Patterns and Mixing Mechanisms in the Screw Mixing Element of a Co-Rotating Twin-Screw Extruder”, Polym. Eng. Sci., 2002, **42**, 925

37. Kajiwara, T.; Tomiyama, H.; Uotani, A.; Inoue, S.; Funatsu, K., “Finite Element Analysis of Melt Mixing Zone in Twin Screw Extruders with Special Geometries”, Seikei-Kakou, 2006, **18**, 819

38. Kruijt, P. G. M.; Galaktionov, O. S.; Peters, G. W. M.; Meijer, H. E. M., “The Mapping Method for Mixing Optimization”, Int. Polym. Process., 2001, **XVI**, 161

39. Lee, C.-C.; Castro, J. M., “Model Simplification”, in *“Fundamentals of Computer Modeling for Polymer Processing”*, Tucker III, C. L. (editor), Hanser Publishers, 1989

40. Lindt, J. T, “Transport Interactions in Reactive Processing”, in Preprints of the 3rd International Conference on Reactive Processing of Polymers, Strasbourg, France, 1984, 83

41. Meijer, H. E. H.; Elemans, “The Modeling of Continuous Mixers. Part I: The Corotating Twin-Screw Extruder”, P. H. M., Polym. Eng. Sci., 1988, **28**, 275

42. Michaeli, W.; Grefenstein, A.; Berghaus, U., “Twin-Screw Extruders for Reactive Extrusion”, Polym. Eng. Sci., 1995, **35**, 1485

43. Michaeli, W., Grefenstein, A., “Engineering Analysis and Design of Twin-Screw Extruders for Reactive Extrusion”, Adv. Polym. Tech., 1995, **14**, 263

44. Markarian, J., “Compounders Look to Simulation Software to Save in Time and Costs”, Plastics Additives and Compounding, 2005, **March/April**, 34

45. Middleman, S., *“Fundamentals of Polymer Processing”*, McGraw Hill, New York, 1977

46. Morton-Jones, D. H., *“Polymer Processing”*, Chapman and Hall, 1989

47. Nauman E. B., “Non Isothermal Reactors Theory and Application of Thermal Time Distributions”, Chem. Eng. Sci., 1977, **32**, 359

48. Oliveira, J. A.; Biscaia, Jr., E. C.; Pinto, J. C., “Analysis of Kinetic Models Proposed for the Controlled Degradation of Poly(propylene)-Presentation of a General Analytical Solution”, Macromol. Theor. Simul., 2003, **12**, 696

49. Ortiz, E.; Tzoganakis, C., “Scale Up Calculations for Reactive Extrusion Operations”, SPE ANTEC 2008, 305

50. Ortiz-Rodriguez, E.; Tzoganakis, C., "3D Simulations of a Reactive Flow in Screw Elements of Closely-Intermeshing Twin Screw Extruders: A Scale-up Analysis", SPE ANTEC 2009, 171

51. Ottino, J. M., *"The kinematics of Mixing: Stretching, Chaos, and Transport"*, Cambridge University Press, 1989

52. Ottino, J. M.; Ranz, W. E.; Macosko, C. W., "A Framework for Description of Mechanical Mixing of Fluids", AIChE J., 1981, **27**, 565

53. Pinto, G.; Tadmor, Z., "Mixing and Residence Time Distribution in Melt Screw Extruders", Polym. Eng. Sci., 1970, **10**, 279

54. Pokriefke, G., "Numerical Simulation of Viscous Flow in a Partially Filled Co-Rotating Twin Screw Extruder", Intern. Polym. Process., 2007, **XXII**, 11

55. POLYFLOW® version 3.12.2, by ANSYS Inc., documentation files, 2008

56. Potente, H., "Scaling up of Twin Screw Extruders", Polymer Extrusion Conference II, The Plastics and Rubber Institute, London, 1981

57. Potente, H., "Existing Scale-up Rules for Single-Screw Plasticating Extruders", Intern. Polym. Process., 1991, **VI**, 267

58. Potente, H.; Ansahl, J.; Klarholz, B., "Design of Tightly Intermeshing Co-rotating Twin Screw Extruders", Intern. Polym. Process., 1994, **IX**, 11

59. Potente, H.; Flecke, J., "Analysis and Modeling of the Residence Time Distribution in Intermeshing Twin-Screw Extruders", J. Reinf. Polym. & Compos., 1998, **17**, 1047

60. Rauwendaal, C., "Scale-up of Single Screw Extruders", SPE ANTEC, 1986, 968

61. Rauwendaal, C., "Scale-up of Single Screw Extruders", Polym. Eng. Sci., 1987, **27**, 1059

62. Rauwendaal, C., *"Polymer Extrusion"*, Hanser Publisher, 2001

63. Shah, A.; Gupta, M., "Simulation of Polymeric Flow in a Twin Screw Extruder: An Analysis of Elongational Viscosity Effects", SPE ANTEC, 2003, 322

64. Sherrington, D. C., "Reactive Extrusion", in *"Encyclopedia of Polymer Science and Engineering"*, Kroschwitz, J. I. (editor), Wiley-Interscience, 1985

65. Strutt, D.; Tzoganakis, C.; Duever, T. A., "Response Surface Analysis of Average Residence Times in a Co-Rotating Twin Screw Extruder", J Mater. Process. Manuf. Sci., 1997 **6**, 19

66. Strutt, D. B., 1998, "A Study of Reactive Flow of Polypropylene in Single- and Twin-Screw Extruders", PhD Dissertation, University of Waterloo, Ontario, Canada

67. Strutt, D.; Tzoganakis, C.; Duever, T. A., "Mixing Analysis of Reactive Polymer Flow in Conveying Elements of a Co-Rotating Twin Screw Extruder", Adv. Polym. Tech., 2000, **19**, 22

68. Suwanda, D.; Lew, R; Balke, S. T., "Reactive Extrusion of Polypropylene II: Degradation Kinetic Modeling", J. Appl. Polym. Sci., 1988, **35**, 1033

69. Tadmor, Z.; Gogos, C. G., *"Principles of Polymer Processing"*, Wiley-Interscience, 1979

70. Triacca, V. J.; Gloor, P. E.; Zhu, S.; Hrymak, A. N.; Hamielec, A. E., "Free Radical Degradation of Polypropylene: Random Chains Scission", Polym. Eng. Sci., 1993, **33**, 445

71. Tzoganakis, C., "Peroxide Degradation of Polypropylene During Reactive Extrusion", PhD Dissertation, McMaster University, Hamilton, Ontario, Canada, 1988

72. Tzoganakis, C.; Vlachopoulos, J.; Hamielec, A. E., "Production of Controlled-Rheology Polypropylene Resins by Peroxide Promoted Degradation during Extrusion", Polym. Eng. Sci., 1988 a, **28**, 170

73. Tzoganakis, C.; Vlachopoulos, J.; Hamielec, A. E., “Modelling of the Peroxide Degradation of Polypropylene”, Int. Polym. Process., 1988 b, **III**, 141

74. Tzoganakis, C., “Reactive Extrusion of Polymers: A Review”, Adv. Polym. Tech., 1989, **9**, 321

75. Valentas, K. J.; Levine, L; Clarck, J. P., *“Food Processing Operations and Scale-up”*, Marcel Decker, Inc., 1991

76. Vergnes, B.; Valle, D. G.; Delamare, L., “A Global Computer Software for Polymer Flows in Corotating Twin Screw Extruders”, Polym. Eng. Sci., 1998, **38**, 1781

77. Vergnes, B.; Berzin, F., Plastics, “Modelling of Flow and Chemistry in Twin Screw Extruders”, Plastics, Rubbers and Composites, 2004, **33**, 409

78. Wang, X. C., 1996, *“*Branching of Polypropylene Through Reactive Extrusion”, PhD Dissertation, University of Waterloo, Ontario, Canada

79. White, J. L., *“Twin Screw Extrusion”*, Hanser Publishers, 1991

80. White, J. L.; Chen, Z., “Simulation of Non-Isothermal Flow in Modular Co-rotating Twin Screw-Extruders”, Polym. Eng. Sci., 1994, **34**, 229

81. Wünsch, O.; Kühn, R.; Heidemeyer, P., “Simulation of the Fluid Flow of Deeper Screw Flights for Co-Rotating Twin Screw Extruders”, SPE ANTEC, 2003, 338

82. Xanthos M., “Process Analysis from Reactor Fundamentals: Examples of Polymerization and Controlled Degradation in Extruders”, in *“Reactive Extrusion: Principles and Practice”*, Xanthos M., Hanser Publishers, 1992

83. Yang, H.-H.; Manas-Zloczower, I., “Flow Field Analysis of the Kneading Disc Region in a Co-rotating Twin Screw Extruder”, Polym. Eng. Sci., 1992, **32**, 1411

84. Yao, C.-H.; Manas-Zloczower, I., “Influence of Design of Mixing Efficiency in a Variable Intermeshing Clearance Mixer”, Int. Polym. Process.,1997, **XII**, 92

85. Yoshinaga, M.; Katsuki, S.; Miyazaki, M.; Lui, L.; Kihara, S-I.; Funatzu, K., “Mixing Mechanism of Three-Tip Kneading Block in Twin Screw Extruders”, Polym. Eng. Sci., 2000, **40**, 168

86. Zagal, A.; Vivaldo-Lima, E.; Manero, O., “A Mathematical Model for the Reactive Extrusion of Methyl Methacrylate in a Co-Rotating Twin Screw Extruder”, Ind. Eng. Chem. Res., 2005, **44**, 9805

87. Zerafati, S.; Bigio, D., “Area Deformation as a Basis for Mixing Prediction”, SPE ANTEC, 1994, 310

88. Zhu, L.; Narh, K. A.; Hyun, K. S., “Scale up Consideration for Polymerization in Twin-Screw Extruder using 3-D Numerical Simulation”, SPE ANTEC, 2004, 340

89. Zhu, L.; Narh, K. A.; Hyun, K. S., “Evaluation of Numerical Simulation Methods in Reactive Extrusion”, Adv. Polym. Tech., 2005 a, **24**, 183

90. Zhu, L.; Narh, K. A.; Hyun, K. S., “Investigation of Mixing Mechanisms and Energy Balance in Reactive Extrusion using Three Dimensional Numerical Simulation Method”, Int. J. of Heat and Mass Transfer, 2005 b, **48**, 3411

91. Zhu, S.; Tzoganakis, C.; Shigeishi, T.; Chikara, T., “Analysis of Mixing in a Variable Speed Co-Rotating Twin-Screw Extruder”, SPE ANTEC, 2008, 1437

92. Zlokarnick, M, *“Dimensional Analysis and Scale-up in Chemical Engineering”*, Springer-Verlag, 1991